Analysis of the mechanisms controlling septum cleavage in *Enterococcus faecalis* and the impact of cell chain formation on pathogenesis

By

Bartłomiej Salamaga, BSc MSc

(Jagiellonian University)

A thesis submitted for the degree of Doctor of Philosophy

July 2017

Department of Molecular Biology and Biotechnology, University of Sheffield, Firth Court, Western Bank, Sheffield, S10 2TN

Summary

Bacterial cell growth and division rely on a vast number of proteins including peptidoglycan hydrolases (PGHs). Previous studies have shown that in the opportunistic pathogen *Enterococcus faecalis*, the *N*-acetylglucosaminidase AtlA is dedicated to septum cleavage at the end of the division cycle to release daughter cells. Deletion of the *atlA* gene leads to formation of long cell chains. AtlA is a modular enzyme consisting of (i) an N-terminal domain rich in threonine, proline and glutamic acid residues, (ii) a catalytic domain with an *N*-acetylglucosaminidase activity and (iii) a LysM domain responsible for non-covalent binding to peptidoglycan. In this study, we investigated the mechanisms controlling the septum cleavage activity of AtlA and explored the contribution of the cell separation process to pathogenesis.

Using flow cytometry we showed that post-translational modifications of the N-terminal domain of AtlA modulate the activity of this enzyme. *O*-glycosylation inhibits the cells separation, whereas proteolytic cleavage of this domain promotes it. AtlA C-terminal domain, which consists of six LysM peptidoglycan binding modules, is required for an optimal septum cleavage. The truncation or replacement of AtlA LysM modules with modules from AtlB, another *E. faecalis* PGH, leads to formation of long cell chains. These changes in the LysM domain abolish AtlA surface display and targeting to the septum, resulting in an accumulation of the enzyme inside the cell. A protein called AdmA (AtlA display mutant A) required for AtlA surface display was identified. An in-frame deletion of *admA* in *E. faecalis* JH2-2 leads to the formation of long cell chains and abolishes the septal and polar targeting of AtlA. The impaired septum cleavage in the *atlA* mutant was shown to promote an increased uptake by phagocytes resulting in a reduced virulence in the zebrafish model of infection.

Publications arising from this work

Salamaga, B., Prajsnar, T.K., Jareño-Martinez, A., Willemse, J., Bewley, M.A., Chau, F., Belkacem, T.B., Meijer, A.H., Dockrell, D.H., Renshaw, S.A. and Mesnage S. (2017). Bacterial size matters: Multiple mechanisms controlling septum cleavage and diplococcus formation are critical for the virulence of the opportunistic pathogen *Enterococcus faecalis*. PLoS Pathog. *13*, e1006526

Acknowledgements

First, I would like to thank my supervisor Dr Stéphane Mesnage for giving me the opportunity to carry out my PhD. His guidance and support throughout the project helped me to develop myself and allow me to make another step towards being a better scientist.

There are many people who have helped me throughout my PhD. I am especially indebted to Dr Bob Turner, Dr Christa Walther and Dr Darren Robinson for their help with microscopy data acquisition and analysis. For the last four years I was privileged to work with fantastic people who not only create an intellectually stimulating environment but also were true friends. At this point I would like to particularly thank Joe on whom I could always count on.

I would like to express the particular thanks to my supportive family.

Finally, I would like to thank Kasia, who always supports me and never loses the faith that I am capable of achieving whatever I dream of.

Abbreviations

°C	Degree Celsius
~	Approximately
3D	Three dimensional
a.u.	Arbitral units
aa	Amino acid
AF647	AlexaFluor647
Ami	Amidase
Amp	Ampicillin
APS	Ammonium persulphate
AS	aggregation substance
ATc	anhydrotetracycline
ATP	Adenosine triphosphate
ATPase	Adenosine triphosphate hydrolase
BF	bright field
BHI	Brain heart infusion
bp	base pair
BSA	Bovine serum albumin
CBD	Choline binding domain
CFU	Colony forming units
cm^2	Centimetre squered
CP	Carboxypeptidases
Cps	Capsule
CWBM	Cell wall binding modules
D-Ala	D-alanine
D-Glu	D-glutamic acid
DAA	Diamino acid
dH_2O	Distilled water
DMSO	Dimethyl sulphoxide
dpf	Days post fertilisation
DTT	Dithiothreitol
eDNA	extracellular DNA
EDTA	Ethylenediamine tetra-acetic acid
EfaA	*Enterococcus faecalis* antigen A
ELISA	Enzyme-linked immunosorbent assay

epa	Enterococcal polysaccharide antigen
EPase	Endopeptidase
Ery	Erythromycin
Esp	Enterococcal surface protein
FITC	Fluorescein isothiocyanate
FM4-64	(*N*-(3-Triethylammoniumpropyl)-4-(6-(4-(Diethylamino) Phenyl) Hexatrienyl) Pyridinium Dibromide)
FSC	Forward scattered light
g	Gram
GFP	Green fluorescence protein
GI	gastro-intestinal
Glc*N*Ac	*N*-acetyl glucosamine
Glc*N*Acase	*N*-acetyl glucosaminidase
HADA	Hydroxycoumarin 3-amino-D-alanine
HLGR	High level gentamicine resistance
hpf	Hours post fertilisation
hpi	Hours post infection
HRP	Horseradish peroxidase
IAA	Iodoacetamide
ITC	Isothermal titration calorimetry
Kan	Kanamycin
kb	Kilobase pair
kDa	Kilodalton
kV	Kilovolt
l	Litre
L-Ala	L-alanine
L-Lys	L-lysine
LD$_{50}$	Time leading to 50% mortality of the animals infected
LTA	Lipoteichoic acid
LWT	London wild type zebrafish
lysM	Lysin motif
min	Minute
ml	Millilitre
mm	Millimetre
mM	Millimolar
MSCRAMM	Microbial surface components recognising adhesive matrix molecule
Mur*N*Ac	*N*-acetyl muramic acid

Mur*N*Acase	*N*-acetyl muramidase
MWM	molecular weight marker
nfH$_2$O	Nuclase free water
ng	Nanogram
nl	Nanolitre
nm	Nanometre
NMR	Nuclear magnetic resonance
ns	Not statistically important
nt	Nucleotide
OD$_{600}$	Optical density measure at 600 nm
ORF	Open reading frame
PASTA	Penicillin binding protein and serine/threonine kinase associated domain
PBS	Phosphate buffered saline
PBS-TD	PBS supplemented with TritonX-100 and DMSO
PCR	Polymerase chain reaction
PFA	Paraformaldehyde
PG	Peptidoglycan
PGH	Peptidoglycan hydrolases
PMF	Proton motive force
PTMs	Posttranslational modification
rcf	Relative Centrifugal Force
rpm	Revolutions per min
SDS	Sodium dodecyl sulphate
SDS-PAGE	Sodium dodecyl sulphate polyacrylamide gel electrophoresis
SEM	Scanning electro microscopy
SIM	Structured illumination microscopy
SLH	S-layer homology domain
SOB	Super optimal broth
SOC	Super optimal broth with catabolite repression
Sec	General secretory pathway
SP	Signal peptide
SRP	Signal recognition particle
STORM	Stochastic optical reconstruction microscopy
TAE	Tris-acetate EDTA
Taq	Thermostable DNA polymerase derived from *Thermus aquaticus*
TA	Teichoic acid
Tat	Twin arginine translocate system

TBS	Tris buffered saline
TBST	Tris buffered saline tween
TCA	Trichloroacetic acid
TEMED	N,N,N'N'-tetramethyl-ethylenediamine
Tet	Tetracycline
tricaine	3-amino benzoic acid
Tris	Tris (hydroxymethyl) aminomethane
U	Units (of enzyme activity)
UDP	Uridine diphosphate
UPEC	Uropathogenic *E. coli*
UTI	Urinary tract infection
UV	Ultra violet
V	Volts
v/v	Volume for volume
VRE	Vancomycin resistance enterococci
w/v	Weight for volume
WT	Wild type
WTA	Wall teichoic acid
μF	Microfarad
μg	Microgram
μl	Microlitre
μm	Micrometre
μM	Micromolar
Ω	Ohms

Table of contents

List of figures

List of tables

CHAPTER 1

Introduction

1.1   Enterococci

1.1.1   Historical background

According to the literature, enterococci were first described by a French researcher, Thiercelin at the end on the 19th century. In his report, Thiercelin named this microbe 'Enterocoque' (from French e*ntero-* meaning 'intestine' and *-coque,* 'granule') to highlight the intestinal origin and morphology of this organism (Thiercelin, 1899). Work on the new microbe revealed its virulence in mice, becoming the first report on enterococci pathogenesis. A later observation of a patient suffering from diarrhoea disclosed the ability of enterococci to translocate from the gastro-intestinal tract to blood, causing sepsis (Thiercelin, 1899). The same year, MacCallum and Hasting reported a presence of *Enterococcus faecalis* in the blood of a patient with endocarditis. The bacterium was then named *Micrococcus zymogenes* due to its fermentative properties (MacCallum and Hasting, 1899). Seven years later, in 1906 Andrewes and Horder described a microbe with similar biochemical properties to the ones observed by MacCallum and Hasting (Andrewes and Horder, 1906). They emphasised the human intestine origin of the microorganism by naming it *Streptococcus faecalis* (from Latin *faex* meaning dregs, sediment or feces). Several years later (in 1919), Orla-Jensen described *Streptococcus faecium*, whilst in 1935 Sherman and Wing discovered *Streptococcus durans*. All described bacteria varied in the fermentation profiles (Orla-Jensen, 1919; Sherman and Wing, 1935). In 1933 Lancefield developed a serological test by which enterococci where classified as group D streptococci (Lancefield, 1933). Four years later Sherman suggested a new classification, dividing streptococci into four groups: pyogenic, viridans, lactic and enterococcus, based on cells ability to grow in different conditions (Sherman, 1937). Although Kalina proposed to create a new taxon *Enterococcus* in 1970 (Kalina, 1970), it was only officially accepted in 1984 when Schleifer and Kilpper-Bälz proved that *S. faecalis* and *S. faecium* were genetically distant from the *Streptococcus* genus using molecular tools (Schleifer and Kilpper-Balz, 1984). Following this work, *S. faecalis* and *S. faecium* species were renamed *Enterococcus faecalis* and *Enterococcus faecium*, respectively (Schleifer and Kilpper-

Balz, 1984). The first v̲ancomycin r̲esistant e̲nterococci (VRE), *Enterococcus faecalis* and *Enterococcus faecium* were isolated in the United Kingdom in 1988 (Uttley et al., 1989). Nowadays, enterococci are the second most common group of bacteria isolated from patients suffering from nosocomial infections (Sievert et al., 2013).

1.1.2   The *Enterococcus* genus

According to the Oxford dictionary 'genus' is a taxonomic category that ranks above species and below family. The classification of enterococci has changed many times over the past decades, making it difficult to follow the literature. Genetic tools allowed for performing experiments showing that *S. faecalis* and *S. faecium* are phylogenetically distant from other microbes belonging to the *Streptococcus* genus (Schleifer and Kilpper-Balz, 1984). Based on the analysis of 16S rRNA, the *Enterococcus* genus showed higher similarities to the *Carnobacterium*, *Tetragenococcus* and *Vagococcus* genera than to the *Streptococcus* or *Lactococcus* ones (Facklam et al., 2002). Sequencing of a 438 bp long amplification product of the *sodA* gene is a more discriminative target sequence as compared to 16S rRNA one and was therefore proposed as an alternative method to identify enterococci (Poyart et al., 2002). As of 2017, there are 58 species decribed in the *Enterococcus* genus (http://www.bacterio.net/enterococcus.html#r). Most of them were either discovered or reclassified due to the progressive development of the whole genome analyses. In 'History, taxonomy, biochemical characteristics, and antibiotic susceptibility testing of enterococci' Facklam *et al*. proposed the phenotypic segregation of the *Enterococcus* genus into five groups based on the capacity to ferment mannitol and sorbitol and the ability to degrade arginine. Enterococci of Group I can perform fermentation in the presence of both mannitol and sorbitol, but are not able to hydrolyse arginine (arginine negative). Members of Group II are able to produce acid only in the presence of mannitol and to hydrolyse arginine (arginine positive). Representatives of Group III and IV can ferment neither sorbitol nor mannitol and are arginine positive and negative, respectively. Enterococci in Group V are able to produce acid only from mannitol broth and are arginine negative (Facklam et al., 2002). Despite these metabolic differences, enterococci share several morphological and physiological properties.
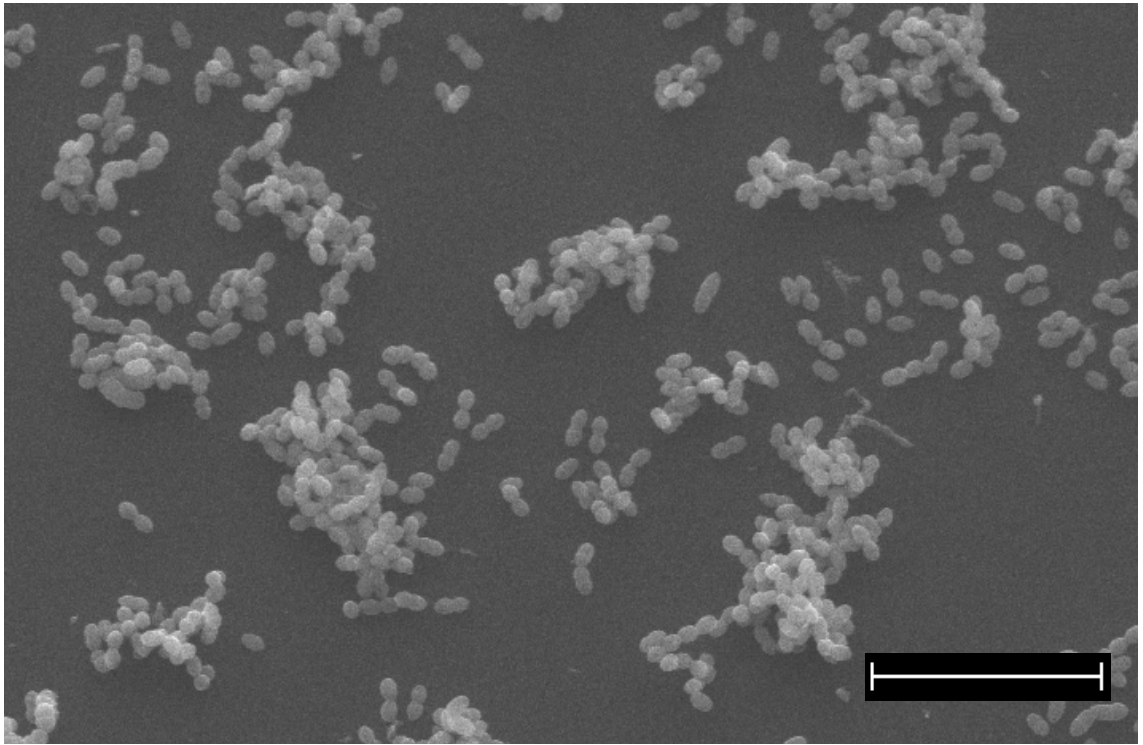
Figure 1.1 *E. faecalis* occurs as a diplococci or short chains

A scanning electron microscopy (SEM) image showing *E. faecalis* JH2-2. Scale bar is 10 μm. Courtesy of Roberth Smith.

1.1.3   Morphology and physiology of enterococci

Enterococci are Gram-positive spherical or ovoid shaped cells (ovococci) that occur as diplococci as well as they can arrange into short chains made up of 4 to 8 cells (Figure 1.1; Murray, 1990). They are anaerobe, non-sporulating bacteria and obligatory fermentative chemoorganotrophs (Murray, 1990). It was shown that enterococci could grow in a range of temperatures from 10 to 45°C with optimal 35°C (Sherman, 1937) and in different pHs raging from 4.0 to 10.0. Moreover, enterococci show a high resistance to various stresses. They are able to grow under a wide range of harsh conditions, including high concentrations of bile salts, ethanol treatment, exposure to heavy metals and sodium dodecyl sulphate (up to 0.01%) (Bradley and Fraise, 1996; Rince et al., 2000). This resistance explains why enterococci can colonise a wide variety of environments, including animals, plants, soil, wastewater and food waste (Murray, 1990). In animals, enterococci are mostly isolated from gastro-intestinal (GI) tracts and faeces of mammals, reptiles, birds and insects (Mundt, 1963; Martin and Mundt; 1972). Although enterococci are mostly found in the GI tract in humans, they can also be isolated from skin, the upper respiratory tract, the oral cavity and vagina dwelling as part of larger microbial communities (Murray, 1990). Moreover, enterococci are one of the first bacteria to colonise the gut of newborns (Adlerberth and Wold, 2009). Most of the bacteria classified to the *Enterococcus* genus are commensal (Murray, 1990). However, in elderly and immunocompromised patients or after the antibiotic treatment perturbing the natural microbiota, enterococci can cause opportunistic infections such as urinary tract infections, bacteraemia or endocarditis (Murray, 1990). Over the past few decades enterococci have been recognised as a problem in a hospital environment due to their intrinsic resistance to a broad range of antibiotic agents, causing more than 10% of all nosocomial infections (Vincent, 2003)

1.1.4   Bacterial cell division

In prokaryotes cell division is performed by binary fission. During this process, a parental cell replicates and separates the genetic information without formation of spindles, while membrane invagination and synthesis of new cell wall leads to the

4

formation of two daughter cells. The whole process is highly regulated, both temporally and spatially (Errington et al., 2003).

It is well known that bacterial cell size and growth is adjusted to nutrient availability. In *E. coli* and *B. subtilis* cells have to reach a critical ratio of DNA content to the cell length to be able to divide. This suggests presence of components sensing bacterial size in order to control a cell cycle. *Enterococcus hirae* divides at a constant cell volume regardless of chromosome replication and cell growth rate (Donachie, 1968; Gibson etal., 1983; Donachie and Begg, 1989; Sharpe et al., 1998; Robert et al., 2014) So far, no bacterial receptor(s) sensing size have been found. The size and growth of *B. subtilis* is highly regulated by presence of UDP-glucose. A *pgcA* and *gtaB* double mutant of *B. subtilis* unable to synthesise UDP-glucose forms cells 30% reduced in length (Weart et al., 2007). The depletion of UDP-glucose alters functionality of UgtP, a glucosyltransferase that utilises UDP-glucose in glucolipid synthesis. In nutrient rich conditions, UgtP inhibits FtsZ in a UDP-glucose dependent manner. This inhibition prevents the FtsZ oligomerisation and thus allows cells to increase their sizes (Weart et al., 2007). Not only timing but also selection of the division site is crucial. The polymerization of FtsZ to form the Z-ring represents the first stage of bacterial cell division. FtsZ localises to the division site as the first protein and initiates recruitment of other cell division components and thus the Z-ring formation must be spatially controlled (Adams and Errington, 2009). The Z-ring marks the septal position at midcell with a high precision of around 99% in rod-shaped bacteria such as *E. coli* and *B. subtilis* (Trueba, 1982; Yu and Margolin, 1999; Migocki et al., 2002). In these organisms the Min system and nucleoid occlusion are the two major systems involved in the Z-ring positioning. In the absence of the Min system proteins cells form multiple septa including polar septa that often lead to formation of minicells without a nucleus (de Boer et al., 1989). A deletion of nucleic occlusion genes causes a bisection of the chromosome as a result of formation of a septum over an unsegregated chromosome (de Boer et al., 1989; Wu and Errington, 2004; Bernhardt and de Boer, 2005). By contrast, overproduction of the Min system and nucleic occlusion components leads to inhibition of cell division (de Boer et al., 1992; Wu and Errington, 2004; Bernhardt and de Boer, 2005). Although their deletion impairs cell division, neither the Min system nor nucleic occlusion proteins are essential in either *E. coli* or *B. subtilis* (Wu and Errington, 2004; Bernhardt and de Boer, 6 2005). In *S. pneumoniae* a transmembrane protein MapZ (LocZ) was shown to position FtsZ. MapZ is not essential and cells in its absence are

still viable and able to divide. In the Δ*mapZ* mutant the localization of FtsZ is altered thus the position of the Z-ring is shifted from the midcell (Fleurie et al., 2014; Holečková et al., 2015). Enterococci, lactococci and streptococci have homologues of MapZ, which do not show any sequence similarity to proteins from other organisms. This suggests that the positioning of FtsZ by MapZ is unique to ovococci (Fleurie et al., 2014; Holečková et al., 2015).

1.1.5   Antibiotic resistance

1.1.5.1   Aminoglycoside resistance

Aminoglycosides consist of one or more amino sugars linked by glycosidic bounds to a dibasic cyclitol (Mingeot-Leclercq et al., 1999). The most studied members of this group are gentamicin, kanamycin, tobramycin and streptomycin. Aminoglycosides interact with 16S rRNA impairing a protein synthesis. Due to their large size (1.8 nm by 1 nm by 1 nm, Mingeot-Leclercq et al., 1999) a poor uptake was proposed to explain the moderate intrinsic resistance to aminoglycosides of enterococci (Aslangul et al., 2006). Two additional mechanisms enhancing the intrinsic resistance to aminoglycosides were described in *E. faecium*. The first one is mediated by a 6'-*N*-aminoglycoside acetyltransferase, AAC(6')-Ii which acetylates the amino group in the antibiotic leading to its inactivation (Costa et al., 1993). The second one is mediated by EfmM, an rRNA methyltransfarase. The methylation of 16S rRNA causes a steric hindrance that disables binding of aminoglycosides. The inactivation of *efmM* was associated with increased susceptibility to kanamycin and tobramycin (Galimand et al., 2011).

The first enterococci with high level of gentamicin resistance (HLGR) were discovered in France in 1979 (Courvalin et al., 1980). The HLGR is encoded by an *aac(6')-aph(2")* gene present either on a plasmid or transposon (Woodford et al., 1993; Huycke et al., 1998). A product of this gene is a bifunctional aminoglycoside-modifying enzyme AAC(6')-APH(2") that acetylates and phosphorylates the antibiotic (Ferretti et al., 1986; Mederski-Samoraj and Murray, 1983).

1.1.5.2   Beta-lactam resistance

All antimicrobial agents containing a β-lactam ring are classified as beta-lactam antibiotics. It is a broad range group of antimicrobial agents including penicillins, cephalosporins, carbapenems and monobactams. Due to the large variety in this group of antibiotics enterococci present different levels of resistance to them. β-lactam antibiotics mimic the D-Ala-D-Ala extremity of peptidoglycan precursor used as a substrate during the peptidoglycan synthesis by penicillin binding proteins (PBPs) (Tipper and Strominger, 1965). β-lactam binding to the D,D-transpeptidase (PBP classes A and B) inactivates the enzyme and stops peptidoglycan polymerisation (Tipper and Strominger, 1965). High level intrinsic resistance of *E. faecalis* to some β-lactam antibiotics (in particular the 3rd generation cephalosporines frequently used in hospitals) is caused by a PBP5 which has a low affinity towards β-lactams (Arbeloa et al., 2004). Moreover, *E. faecalis* can develop high levels of resistance to β–lactam antibiotics through several other mechanisms: (i) acquisition of a β-lactamase gene (Murray and Mederski-Samaroj, 1983); (ii) spontaneous mutations in the *pbp5* gene which further decrease the affinity of this enzyme to β-lactams (Ono, et.al., 2005); (iii) mutations in the *pbp5* promoter increasing the expression level of the enzyme; (iv) activation of an alternative peptidoglycan synthesis pathway involving L,D-transpeptidases insensitive to β-lactams.

Production of β-lactamase, an enzyme responsible for the degradation of the β-lactam antibiotics, is rare in enterococci and was described for only one clinical isolate of *E. faecium* (Murray, 1992).

1.1.5.3 Daptomycin resistance

Daptomycin is a cyclic lipopeptide with antimicrobial activity (Alborn et al., 1991). Although the exact mechanism of daptomycin bactericidal activity remains unknown, it was shown that daptomycin interacts with the bacterial membrane in a calcium-dependent manner leading to the membrane depolarisation (Alborn et al., 1991). An analysis of the genomes isolated from daptomycin resistant enterococci revealed that there are several alteration in genes encoding: (i) a three component regulatory system, LiaFSR responsible for a cell envelop stress response pathway; (ii) a cardiolipin synthase, Cls and (iii) a glycerolphospodiesterase, GdpD (Arias et al., 2011; Humphries et al., 2012; Tran et al., 2012). An impact of such mutations on daptomycin interaction with cells remains unknown.

1.1.5.4 Glycopeptide resistance

Glycopeptide antibiotics are glycosylated mono- or polycyclic nonribosomal peptides with a bactericidal activity. Vancomycin is the most common and known member of this antibiotic family. Vancomycin is often the last resort antibiotic used to treat bacterial infections (Boneca and Chiosis, 2003). It inhibits the cell wall synthesis by binding to D-Ala-D-Ala of the C-terminal extremity of the peptidoglycan precursors and inhibiting the activity of peptidoglycan polymerases by steric hindrance (Hollenbeck and Rice, 2012). Vancomycin resistance was described for the first time in *E. faecalis* (Uttley et al., 1989). It involves several enzymes encoded by a complex locus that modify the composition of peptidoglycan precursors. Nowadays, nine *van* clusters are known among which a *vanA* cluster is the most characterised. The *vanA* cluster consists of seven genes encoding: (i) a two-component system, VanRS; (ii) a dehydrogenase, VanH; (iii) a ligase, VanA; (iv) two dipeptidases VanX and VanY, and VanZ of unknown function (Miller et al., 2014). Collectively, the role of the *vanA* cluster components is to replace the C-terminal D-Ala residue of the pentapeptide stem for D-Lac or D-Ser. This modification drastically reduces the affinity of vancomycin for peptidoglycan precursors (Hollenbeck and Rice, 2012). The *E. faecalis van* genes can be transferred to other species, for instance to *S. aureus*, which is an interesting example of horizontal gene transfer (Weigel et al., 2003).

1.1.5.5 Rifampicin resistance

Rifampicin interacts with the β-subunit of RNA polymerase inhibiting the initiation of transcription, thus bacterial growth (Wehrli et al., 1968). The intrinsic resistance of enterococci to rifampicin is associated with polymorphism of an *rpoB* gene encoding the β-subunit of RNA polymerase. Depending on a mutation in *rpoB* the level of the resistance can vary. Around 32% and 95% of all clinical isolates of *E. faecalis* and *E. faecium* in the UK, respectively, showed the resistance to rifampicin at the end of the 20th century (Andrews et al., 2000).

1.1.6 Clinical significance of enterococci

As previously mentioned, enterococci are part of the natural microbiota of healthy humans. It is speculated that this genus represents around 1% of the intestinal bacterial population (Sghir et al., 2000). Enterococci can easily overgrow other gut bacteria after an antibiotic treatment due to their intrinsic and acquired resistance to a broad range of antimicrobial agents. Similarly, these bacteria can cause life-threatening infections in immunocompromised patients due to dysfunction of the innate immune system, which contributes to intestinal microbiota homeostasis. Additionally, enterococci can share the antibiotic resistance and virulence factors within a given species or outside of it (Weigel et al., 2003), as described above.

Enterococci are responsible for 5 to 15% of infective endocarditis (Murdoch et al., 2009) with a mortal rate of 9 to 15% (McDonald et al., 2005). Amongst enterococci, *E. faecalis* is the most frequently isolated from endocarditis. This condition is mostly associated with elderly patients. The initial source of enterococcal endocarditis is bacteremia caused by dissemination form a gastro-intestinal or genito-urinary tract (Anderson et al., 2004). A chance of enterococcal endocarditis is increased in patients undergoing heart surgery when the prostatic valve has been implanted (Rice et al., 1991). The effective treatment of such an infection requires the use of more than one antibiotic (for instance penicillin in combination with gentamicin to obtain a synergistic antimicrobial activity). A surgery to remove an infected valve is only considered in the case of infections caused by strains with high antibiotic resistance levels (Arias and Murray, 2008).

Urinary tract infection (UTI) is the most common infection caused by enterococci and mainly occurs in elderly men (Graninger and Ragette, 1992). Enterococci can infect both lower and upper urinary tracts causing cystitis, prostatitis, and epididymitis. The long hospitalisation increases a chance of UTI and enterococci are responsible for 15% of UTI in an intensive care unit (Hidron et al., 2008). In uncomplicated urinary tract infections a fosfomycin is suggested to use, whereas ampicillin or amoxicillin are used in case of VRE (Arias and Murray, 2008).

Intra-abdominal infections are the second most common cause of bacteremia and largely contribute to morbidity and mortality (Lopez et al., 2011). It is rare for enterococci to cause a monomicrobial infection and hence it occurs only during the

primary peritonitis (translocation throughout intestinal epithelium) (Solà and Soriano, 2002). More often intra-abdominal infections are caused by a polymicrobial population as a result of necrosis or posttraumatic damage of the gastrointestinal tract (secondary peritonitis). Persistence of primary or secondary peritonitis leads to tertiary peritonitis, mostly associated with immunocompromised patients due to an alteration in the host innate immune system (Marshall and Innes, 2003).

Enterococcal bacteremia is the second most common health-associated bacteremia with a relatively high mortality rate, ranging between 26 and 46% (Hidron et al., 2008). This rate is however higher for elderly patients after a surgery, including transplantation and heart disease, and it can reach up to 75%. Interestingly, higher mortality was observed in patients infected with *E. faecium* than with *E. faecalis* (Noskin et al., 1995). Genitourinary tract is the most common source of enterococci bacteremia and the blood infection often occurs with endocarditis (Anderson et al., 2004; Shlaes et al., 1981). The most common treatment is a usage of synergistic antimicrobial agents (Arias and Murray, 2008).

1.1.7 Experimental model to study enterococcal infections

In 1899, MacCallum and Hasting performed the very first experiment showing the virulence of human enterococcal isolates in mice and rabbits (MacCallum and Hasting, 1899). Since then several experimental models of infections have been extensively used to understand enterococci pathogenesis. Rabbit and mouse are the most common organisms used. More recently, new vertebrate models of enterococci infection was established by Prajsnar *et al.* using zebrafish (Prajsnar et al., 2013). Different model organisms are preferred depending on the type of infection studied.

New Zealand white rabbits and Sprague-Dawley rats are extensively used to study enterococci endocarditis. Although, the procedures vary, the damage to heart valve is induced by placing catheter into the carotid artery. Bacteria are injected intravenously 24 hours post catheterisation and rabbits are culled 48 hours post-infection (Thurlow et al., 2010). Alternatively, the catheter is removed two hours post implantation and bacterial infection is generated by ear vein administration 2 hours after the catheter removal. The animal is sacrificed 96 hours post infection (Chuang et al., 2009). The

10

endocarditis development is dose depended and might vary based on used strains and the induction methods. As a result the overall damage to heart valve and formation of vegetation is measured. The endocarditis model of infection has also been used to study the clearance of enterococci following antibiotic treatments (Bravetti et al., 2009)

Murine models are used to study the UTI caused by enterococci. A transurethral catheter is used to introduce bacteria to the bladder of anaesthetised mice. Animals are culled at regular intervals to quantify the bacterial load in urine, bladder and kidneys (Shankar et al., 2001). Recently a model mimicking more closely catheter-associated urinary tract infection caused by enterococci was proposed (Guiton et al., 2010). Silicon catheter pieces are implanted in a mouse bladder followed by an administration of bacteria. In this model the placement of the silicon segments leads to biofilm formation, thus increased bladder and kidneys colonisation (Guiton et al., 2010).

Peritonitis is the most common model in which enterococci are administrated intraperitoneally. The survival of mice or rats is monitored daily. The virulence of tested strains is characterised by the time leading to the death of 50% of the animals infected (LD$_{50}$) (Dupont et al., 1998). The peritonitis model also allows studying the host innate immune response to the pathogen (Leendertse et al., 2008).

In addition to mammalian models of infection, invertebrate models have been developed. *Caenorhabditis elegans* (a roundworm) and *Galleria mellonella* (a greater wax moth caterpillar) are two invertebrate organisms that are associated with limited ethical problems as compared to mammalian models. Moreover, they are relatively cheap and easy to handle in a laboratory environment, which makes it possible to design high-throughput screens to identify virulence factors. Although invertebrates do not have an adaptive immune system, they have an innate immune system that shares similarities with the innate immune systems of mammals (Leclerc and Reichhart., 2004, Schulenburg et al., 2004). A survival percentage of infected animals in a given period of time is used to investigate the virulence of bacteria.

Recently, the zebrafish model of enterococci infection was established by Prajsnar *et al.* (Figure 1.2; Prjasnar et al., 2013). *Danio rerio* is a small, tropical, freshwater fish naturally indwelling waters of India, Pakistan and Bhutan. The advantages of this model

over other vertebrates are a short generation time (3 months) and high number of eggs per mating (100-200 eggs from 1 pair). Additionally, the genetic manipulations are relatively easy to perform. For example, phagocyte depletion can be carried out by injecting *pu.1* morpholino oligonucleotides, which inhibit the expression of the transcription factor involved in macrophage proliferation. In contrast to other models organisms such as *C. elegans* and *G. mellonella*, zebrafish as a vertebrate has an innate immune system closly related to humans. The development of the cellular innate immune system and blood circulation in zebrafish embryos starts 24 hours post fertilisation (hpf) and macrophages start circulating in the bloodstream one hour later (Herbomel et al., 1999). In zebrafish, macrophages are responsible for utilization of apoptotic corpses (Willett et al., 1999) and their ability to phagocyte intravenously administrated bacteria was shown (Herbomel et al., 1999, Davis et al., 2002, van der Sar et al., 2003). Following infection at 30 hpf, zebrafish embryos survival is monitored for 90 hours.
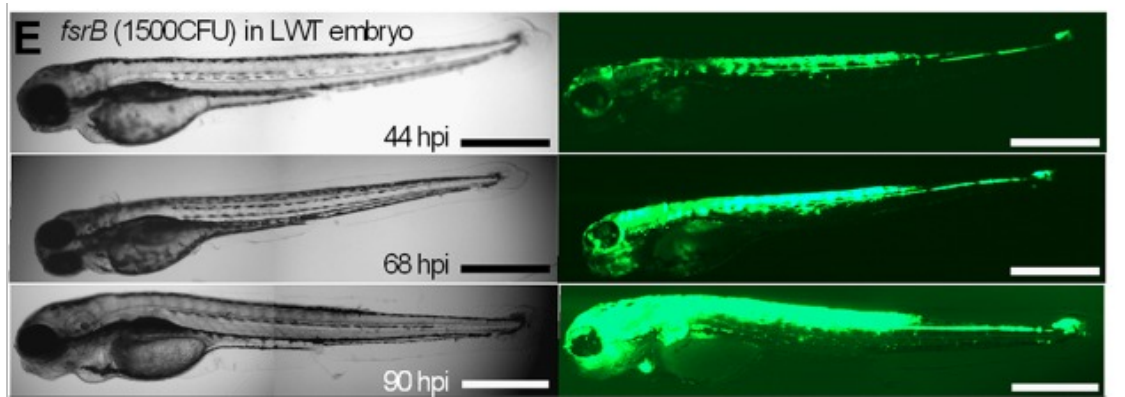
Figure 1.2 Proliferation of *E. faecalis* OG1RF in London Wild Type (LWT) zebrafish larvae.

Microscopy images of zebrafish larvae were taken at 44, 68 and 90 hours post infection. *E. faecalis* producing the green fluorescent protein (GFP) disseminate from the place of injection and proliferate. Reproduced from (Prajsnar et al., 2013).

1.1.8 Virulence factors

Virulence factors allow bacteria to colonise the host, evade and combat the immune system as well as obtain nutrition from the host cells. Enterococci are relatively poorly equipped with virulence factors as compared with other human pathogens such as *Staphylococcus aureus*. The virulence factors produced by *E. faecalis* and *E. faecium* described in this section.

1.1.8.1 Secreted factors

1.1.8.1.1 Cytolysin

Cytolysin is a two-peptide lytic toxin produced mainly by *E. faecalis* strains. It was first described by Todd during studies on haemolytic properties of group D streptococci in 1934 (Todd, 1934). The cytolysin consists of two subunits, $CylL_L$ and $CylL_S$ which are post-translationally modified by proteins encoded in the same gene cluster (Booth et al., 1996; Ike et al., 1990; Cox et al., 2005). The activated subunits are forming pores in the cytoplasmic membrane of target cells and thus cause cell lysis (Van Tyne et al., 2013). Immunity towards the cytolysin activity is conferred by one gene present in the gene cluster; the mechanism by which it protects *E. faecalis* against lysis is not understood. The contribution of cytolysin to *E. faecalis* virulence was investigated both *in vitro* and *in vivo* models of infection. The haemolytic activity of enterococcal cytolysin can be detected using human, horse, rabbit and mouse erythrocytes; sheep and goat erythrocytes are not lysed by the cytolysin (Kobayashi, 1940; Miyazaki et al., 1993). The enterococcal cytolysin was also shown to contribute to *E. faecalis* virulence by targeting mouse polymorphonuclear neutrophils and macrophages (Miyazaki et al., 1993) and human intestinal epithelial cells (Coburn and Gilmore, 2003). The most striking results were observed when a rabbit endophthalmitis model was tested *in vivo*. Cytolysin contributed to a significant increase in retina cells damage during the infection caused by *E. faecalis* as compared to the non-cytolytic isogenic strain (Jett et al., 1992).

Interestingly, enterococcal cytolysin shows bactericidal activity against various Gram-positive strains like *S. aureus*, *Streptococcus pyogenes* or *Clostridium difficile* (Brock et al., 1963).
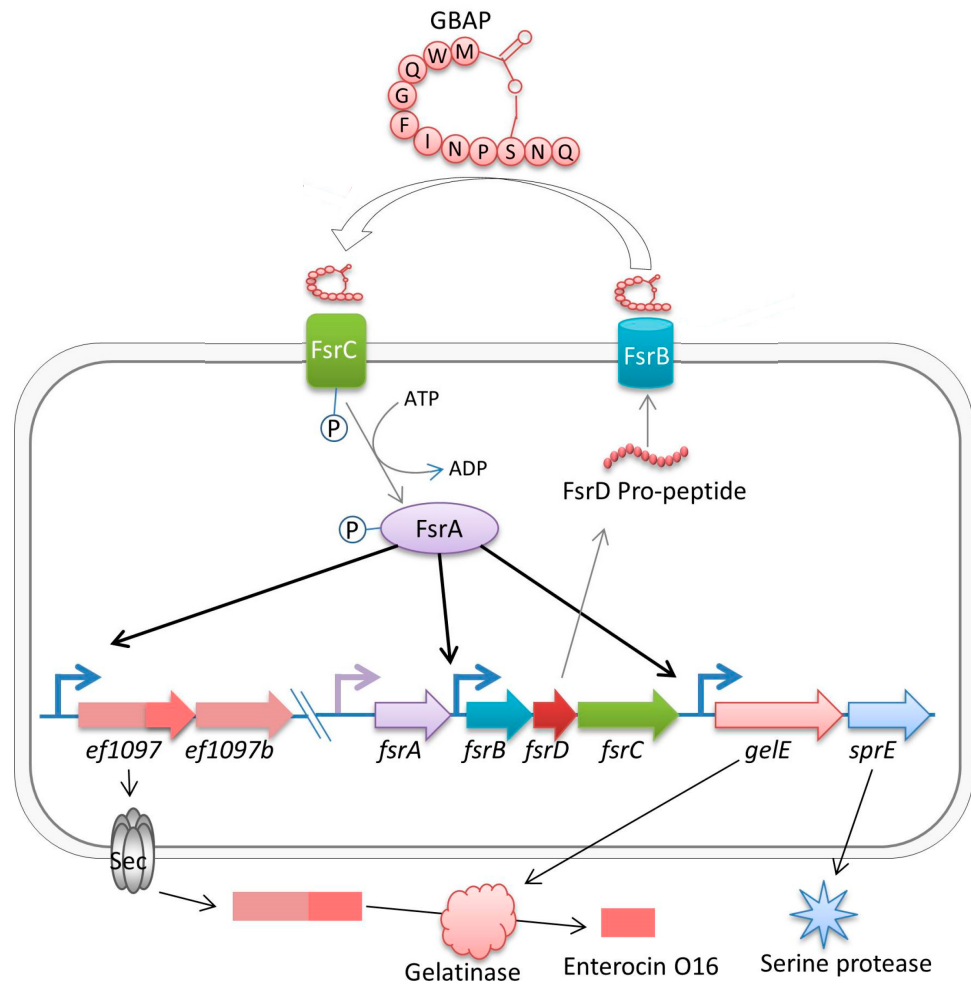
Figure 1.3 Regulation of GelE and SprE production by the quorum sensing *fsr* system.
FsrB exports and processes the product of *fsrD* expression. After secretion, the resulting small
pheromone molecule (GBAP) interacts with the FsrC receptor, a protein involved in a two-
component regulatory system. Activated FsrC phosphorylates FsrA, the intracellular regulatory
protein, which induces expression of *gelE* and *sprE*. Adapted from from (Ali et al., 2017).

1.1.8.1.2 Gelatinase and serine protease

The gelatinase GelE is a zinc metalloprotease. *gelE* is cotranscribed with a downstream gene encoding a serine protease, SprE (Qin et al., 2000). Both enzymes are secreted and their production is controlled by an upstream region called an *fsr* system (Figure 1.3). This system consists of three genes *fsrA*, *fsrB* and *fsrC*, sharing similarities with an *arg* system of *S. aureus* (Qin et al., 2000). The *fsr* system is autoregulated and acts as a quorum-sensing in *E. faecalis* (Qin et al., 2001). It was shown that expression of the *fsrB, fsrC, gelE*, and *sprE* genes increases when cell density increases (Qin et al., 2000; Qin et al., 2001). Using the mouse model of infection, it was shown that a *gelE* mutants are significantly less virulent as compared to the parental strain. A prolonged survival in the mouse model was observed when animals were infected with *fsrA, fsrB* and *sprE* mutants as compared with the parental OG1RF strain (Qin et al., 2001). In the zebrafish model of infection, GelE production is critical for virulence. Rescueing of the *fsr* locus in *E. faecalis* JH2-2 (which lacks *fsr*), restores virulence through GelE production (Prajsnar et al., 2013). Although a higher percentage of gelatinase-positive strains are isolated from a clinical than a community environment, there is no strict correlation between the production of GelE and virulence (Coque et al.,1995)

1.1.8.2 Adhesins

1.1.8.2.1 Enterococcal surface protein

Enterococcal surface protein (Esp) is encoded by an *esp* gene found in both *E. faecalis* and *E. faecium* strains and is located on pathogenic islands (Shankar et al., 2002; Leavis et al., 2004). It is a large cell surface protein of around 202 kDa covalently anchored peptidoglycan by an LPxTG motif (Shankar et al., 1999). In the mouse model of ascending urinary tract infection, the deletion of *esp* leads to a reduction in a number of bacteria isolated from bladder and urine, suggesting that Esp is important for colonisation and persistence of *E. faecalis* in the local infection (Shankar et al., 2001). Moreover, it was shown that an inactivation of *esp* inhibits or alters the biofilm formation in *E. faecalis* clinical isolates (Toledo-Arana et al., 2001). *E. faecalis* strains isolated from patients suffering from enterococcal bacteremia and UTI were found to

produce more Esp than strains isolated from community environment (Shankar et al., 1999).

1.1.8.2.2 Collagen adhesin

Analysis of *E. faecalis* genome revealed the existence of a putative gene encoding an adhesion protein, named *ace*. Ace is a <u>m</u>icrobial <u>s</u>urface <u>c</u>omponent <u>r</u>ecognising <u>a</u>dhesive <u>m</u>atrix <u>m</u>olecules (MSCRAMM). Ace shares similarities with the staphylococcal collagen adhesin Can (Rich et al., 1999). Ace is able to bind collagen type I and IV, and laminin, which are the major components of the extracellular matrix in mammalian cells (Nallapareddy et al., 2000). Expression of *ace* is modulated by the matrix network components leading to an increased abundance of Ace on the cell surface (Nallapareddy and Murray, 2006). The deletion of *ace* in *E. faecalis* leads to an increased susceptibility of the mutant to the immune system of a host in the mouse and insect infection models (Lebreton et al., 2009). Ace contribution to *E. faecalis* virulence was shown in the rat endocarditis model, where the Δ*ace* mutant was severely attenuated as compared to the parental strain (Singh et al., 2010).

1.1.8.2.3 Aggregation substance

There are three well studied proteins belonging to the <u>a</u>ggregation <u>s</u>ubstance (AS) group. Asp1, Asa1 and Asc10 are encoded by pheromone-responsive, conjugative plasmids (Galli et al., 1990; Galli et al., 1992). An induced production of the AS proteins promotes an interaction between a donor cell and a plasmid free recipient cell allowing for a plasmid exchange (Kao et al., 1991). AS proteins are polypeptides covalently anchored to peptidoglycan via a C-terminal LPxTG motif and contain two RGD (Arg-Gly-Asp) motifs (Hendrickx et al., 2009). It was shown that AS proteins enhance the interaction with some of the extracellular matrix components like fibronectin, thrombospondin, vitronectin and collagen type I (Rozdzinski et al., 2001). The contribution of AS proteins to *E. faecalis* virulence was shown using the rabbit model of infective endocarditis. Bacteria carrying the plasmid encoding an AS protein were able to form from 6 to 10 times larger biofilm on heart valves and caused a significantly higher mortality of the host (Chow et al., 1993). Further investigation showed that addition of antibodies specific against AS proteins reduced the severity of

E. faecalis infection (Schlievert et al., 2010). Amino acid substitutions in both RGD motifs of Asc10 significantly reduced the virulence of *E. faecalis,* showing their crucial role in the functionality of AS proteins (Chuang et al., 2009). Enterococcal strains carrying a plasmid encoding an AS protein are more abundant in the clinical isolates than the community ones (Coque et al., 1995).

1.1.8.2.4 *Enterococcus faecalis* antigen A

<u>Enterococcus faecalis</u> <u>a</u>ntigen <u>A</u> (EfaA) was identified in most *E. faecalis* strains and a homologue was also found in *E. faecium* (Eaton and Gasson, 2001). EfaA is encoded in a small operon *efaBCA* along with an ABC-type exporter. Its expression is regulated by a manganese ions concentration. It was proposed that a low level of Mn^{2+} in serum or tissue environment induced a production of EfaA (Low et al., 2003). Using the mouse peritonitis model, it was shown that an interrupted *efaBCA* locus results in a prolonged survival of mice when compared to *E. faecalis* OG1RF, the parental strain (Singh et al., 1998).

1.1.8.2.5 Endocarditis and biofilm-associated pili

The endocarditis and biofilm-associated (Ebp) pili are encoded by a three-gene operon, *ebpABC*. These genes, along with a downstream *bps* gene encoding a sortase, are essential for pili assembly (Nallapareddy et al. 2006). Similarly to other extracellular matrix binding proteins, Ebp production is stimulated by growing cells in the presence of serum. It was shown that the Ebp pili are responsible for binding to fibrinogen in serum and extracellular matrix (Nallapareddy et al., 2011). An analysis of sera from patients with enterococcal endocarditis showed a presence of antibodies against the products of the *ebpABC* operon (Sillanpää et al., 2004). Further investigation of Ebp pili contribution to *E. faecalis* OG1RF virulence in the rat endocarditis model revealed that a non-piliated isogenic derivative was significantly attenuated (Singh et al., 2007). The murine UTI model showed an importance of both the *ebpABC* and *bps* loci for the efficient colonisation of kidneys. Additionally, both *ebpABC* and *bps* mutants were impaired in biofilm formation (Singh et al., 2007; Kemp et al., 2007).

1.1.8.3   Cell wall associated polymers

In addition to protein components enterococci produce non-protein components that contribute to their pathogenesis.

1.1.8.3.1   Enterococcal capsule

Capsular polysaccharides are anionic polymers covalently attached to the cell surface. The proteins involved in a biosynthesis of the capsules are encoded by a complex locus named *cps* (Hancock and Gilmore, 2002). It was proposed that polysaccharides, including capsules are responsible for resistance to opsonisation, which mediates bacterial clearance by neutrophils (Huebner et al., 1999; Rakita et al., 2000). Incubation of capsulated strain with specific anti-capsule antibodies significantly increased killing by neutrophils (Hancock and Gilmore, 2002). A mutant carrying a mutation in the *cpsI* gene disrupting the capsule synthesis was more susceptible to opsonophagocytosis by human neutrophils. The capsule is also involved in hiding epitopes recognised by complement and specific antibodies engaged in the opsonophagocytic killing mediated by macrophages (Thurlow et al., 2009).

1.1.8.3.2   Lipoteichoic acid

The exposure of lipotechic acids (LTA) varies between different strains of *E. faecalis* and it depends on the presence or absence of the polysaccharide capsules. The contribution of LTA to *E. faecalis* virulence was shown by an *in vitro* assay where addition of the anti-LTA antibodies induced killing mediated by opsonisation (Theilacker et al., 2011). Additionally, the protective effect of the anti-LTA antibodies was shown in the mouse model of enterococci infection (Huebner et al., 2000).

1.1.8.3.3   The Enterococcal polysaccharide antigen (Epa)

Epa is a rhamnopolysaccharide produced by all *E. faecalis* strains. Epa is encoded by a complex locus, *epa* (Teng et al., 2009). It contains 18 very conserved genes (*epaA* to *epaR*) and variable downstream region, which was proposed to be responsible for Epa decoration (Rigottier-Gois et al., 2015). It was suggested that Epa is not exposed on the

cell surface but more likely embedded in the cell wall based on inability to detect the polymers via immunodetection (Xu et al., 2000). Deletion of some components of the *epa* locus alters the synthesis of Epa and reduces virulence by increased phagocytosis of the mutants (Xu et al., 2000; Teng et al., 2002). Recent studies focused on the variable upstream region of *epa* and showed an importance of EpaX during the mouse intestine colonisation, since a Δ*epaX* mutant was unable to persist (Rigottier-Gois et al., 2015). Additionally, three other genes *wcaA, rmlB* and *epaOX* from the variable region along with *epaX* are involved in resistance to cationic antimicrobial agents. A transposon insertion in these genes impairs virulence and the mutants are attenuated in the zebrafish model of infection (Smith et al., submitted).

1.2   The cell wall of Gram-positive bacteria

In Gram-positive bacteria, the cell wall surrounds the cytoplasmic membrane and acts as an interface between a cell and its environment. It protects a cell from mechanical stresses and is responsible for bacterial shape (Vollmer and Seligman, 2010). In Gram-positive bacteria the cell wall consist of peptidoglycan (PG), anionic polymers and surface proteins (Figure 1.4).

1.2.1   Peptidoglycan

PG (murein) is the main component of the bacterial cell wall. It is a single, macromolecule made of glycan strands cross-linked by short peptides surrounding the cytoplasmic membrane (Silhavy et al., 2010). Although the composition of PG building blocks (precursors) is invariable in a given species, several modifications can occur after their polymerisation. These modifications (called PG remodelling) can affect both glycan strands and peptide stems. Growth conditions have been reported to have an impact on PG composition and structure (Vollmer et al., 2008b)

1.2.1.1   PG composition and diversity

The PG glycan strands are composed of disaccharide units consisting of *N*-acetylglucosamine (Glc*N*Ac) and *N*-acetylmuramic acid (Mur*N*Ac) linked by β-1,4
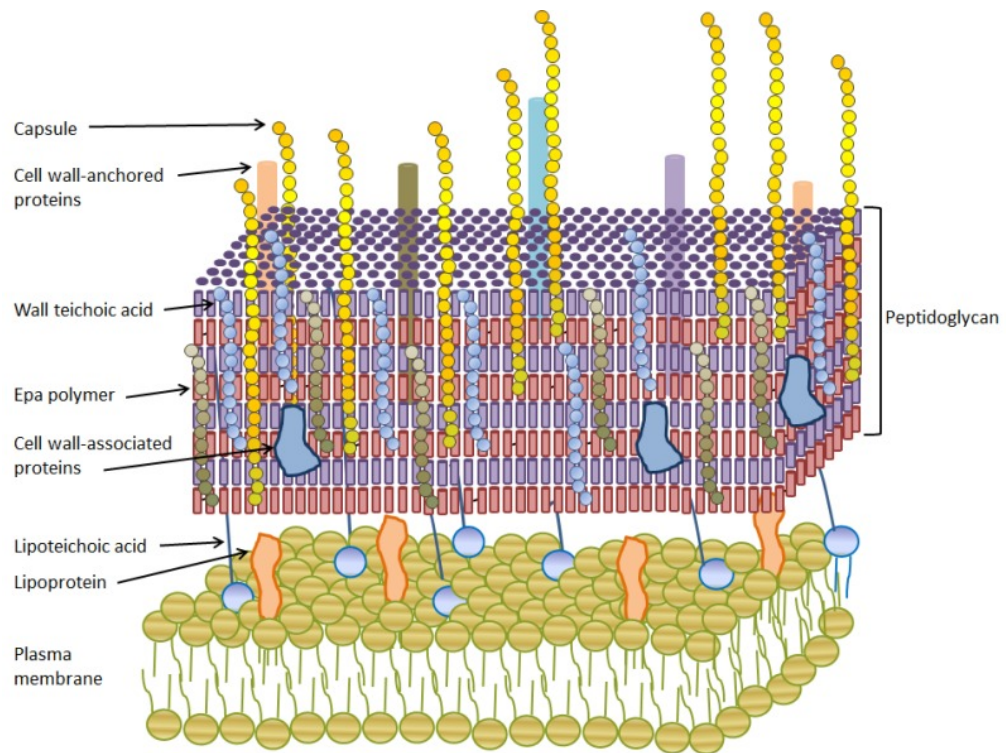
Figure 1.4 Cell envelope of Gram-positive bacteria

The cell envelope of Gram-positive bacteria consists of the cytoplasmic membrane and the cell wall separated by a region which has been proposed to be the equivalent of the periplasm in Gram-negative bacteria. The cell wall contains peptidoglycan and covalently bound proteins and polymers including wall teichoic acids, capsules, secondary cell wall polymers. Lipoproteins and lipoteichoic acids are attached to the membrane and embedded in the cell wall. Reproduced from (Hancock et al., 2014).

bonds. In most Gram-positive bacteria, the lactyl group in the C2 position of Mur*N*Ac is substituted by a stem peptide, which is [L-Ala-γD-Gln-DAA-D-Ala-D-Ala] (Figure 1.5). The diamino acid (DAA) in position 3 is usually a L-Lys or meso-diaminopimelic acid (*m*-DAP) (Schleifer, 1975; Vollmer and Bertsche, 2008).

Even though, the composition of the glycan strands is extremely conserved, there are differences in between different bacterial species due to variations in their length and modifications.

The average length of glycan strands does not correlate with a particular thickness of the PG. Several methods were applied to determine the length of glycan strands including: (i) a gel filtration of radiolabelled glycan strands (Wheeler et al., 2011), (ii) a measurement of a ratio of specifically reduced to non-reduced hexosamine residues (Harz et al., 1990) and (iii) a quantification of radiolabelled galactosamine residues that were enzymatically added to the ends of glycan strands (Schindler et al., 1976). An analysis of glycan strands from different species showed that *S. aureus* has relatively short glycan strands (6 to 20 disaccharides on average), whereas *Bacillus subtilis* has very long glycan strands (>100 disaccharides) (Wheeler et al., 2011; Hayhurst et al., 2008).

After polymerisation, the glycan strands can undergo several modifications such as (i) de-*N*-acetylation of Mur*N*Ac and Glu*N*Ac (Vollmer, 2008), (ii) *N*–glycosylation of peptidoglycan in some mycobacteria (Raymond et al., 2005), (iii) *O*-acetylation of Mur*N*Ac and Glc*N*Ac (Vollmer, 2008) and (iv) an attachment of polysaccharides polymers like teichoic acids (WTA) to C6-hydroxyl of Mur*N*Ac. Some of the modifications have an important role for bacterial lifestyle like *O*-acetylation, which prevents PG hydrolysis by lysozyme (Bera et al., 2005; Hébert et al., 2007).

Variations in a composition of the stem peptide between species are associated with a substrate specificity of the Mur ligases, enzymes responsible for biosynthesis of a peptide moiety of the PG precursor (van Heijenoort, 2001). The major variation occurs in the 3rd position of the stem peptide, where either L-Lysine or m-DAP is found. In many species, including Gram-positive pathogenic cocci, the ε-NH$_2$ group of the L-Lys residue is substituted by a lateral chain. The lateral chain is variable in composition and length. It can contain L- or D-amino acids, and one to five residues (*e.g.,* 5 glycines in *S. aureus,* two L-Ala in *E. faecalis* and one D-Asp in *Enterococcus faecium*
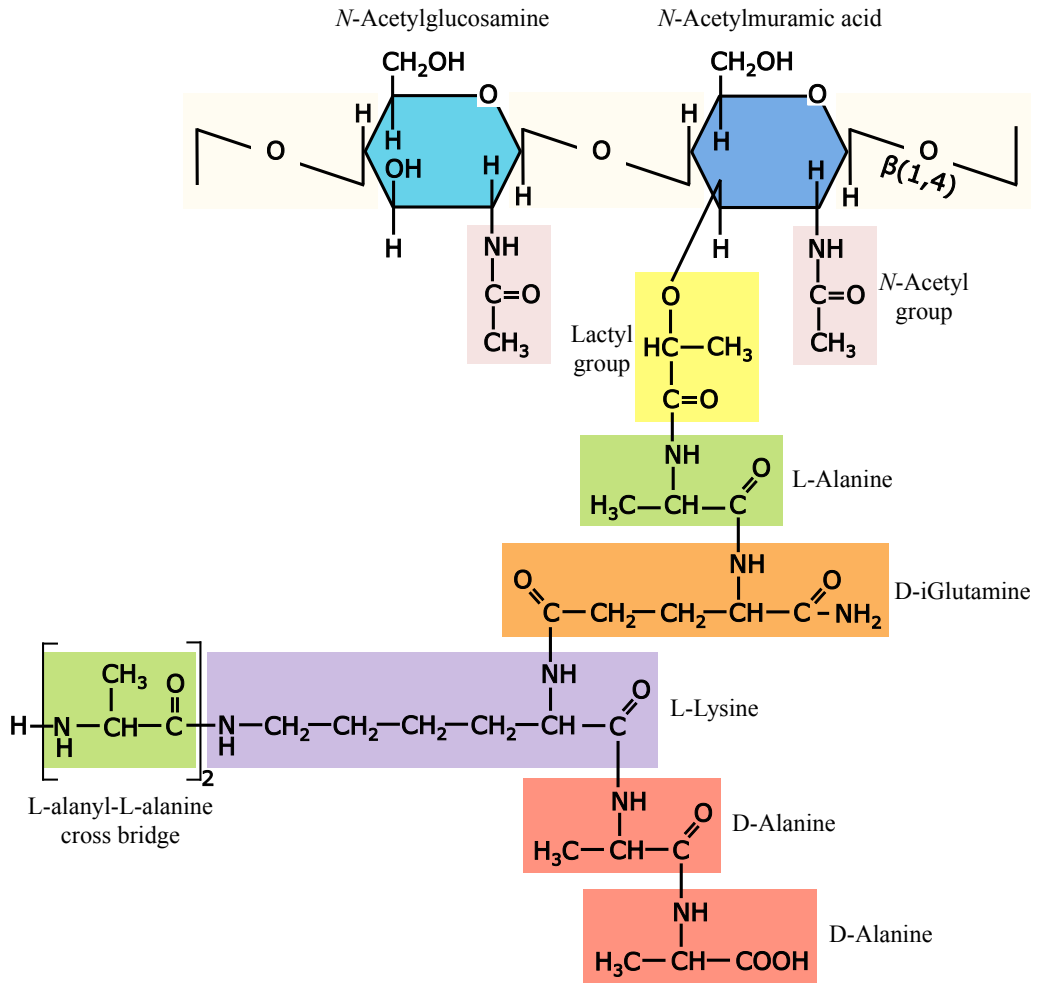
Figure 1.5 Chemical structure of PG building blocks

The PG building blocks consist of a disaccharide unit composed of *N*-acetylglucosamine and *N*-acetylmuramic acid residues with a pentapeptide stem covalently linked via a lactyl group to Mur*N*Ac. In *E. faecalis* an L-alanyl-L-alanine lateral chain is attached to the epsilon group of L-lysine in the position 3 of peptide chain.

(van Heijnoort, 2001). The amino acid in 5th position can vary and D-Ala can be substituted for D-Ser, D-Gly or L-Lac. These substitutions are important modifications determining the resistance to vancomycin (Vollmer and Bertsche, 2008).

1.2.1.2 Synthesis of PG

The first step of PG synthesis occurs in the cytoplasm. Fructose-6-phosphate is converted to glucosamine-6-phosphate by the GlmS synthase. The product is further converted to glucosamine-1-phosphate by of the enzyme GlmM. The bifunctional enzyme GlmU then converts the glucosamine-1-phosphate to uridine 5'-pyrophosphate-*N*-acetylglucosamine (UDP-Glc*N*Ac). Next, MurA mediates the transfer of enolpyruvate to position 3 of the Glc*N*Ac residue. The resulting product, UDP-Glc*N*Ac-enolpyruvate is further reduced to uridine 5'-pyrophosphate-*N*-acetylmuramic acid (UDP-Mur*N*Ac) by MurB. The sequential addition of amino acids to the D-lactoyl group of UDP-Mur*N*Ac is catalysed by Mur synthases (MurC, MurD, MurE and MurF) and results in formation of UDP-Mur*N*Ac-pentapeptide (van Heijenoort, 1998)

The second step of PG synthesis occurs in the membrane, where a phospho-Mur*N*Ac-pentapeptide motif of UDP-MurNac-pentapeptide is transferred onto undecaprenyl phosphate by MurY. The resulting product (lipid I) is further converted to lipid II by addition of *N*-acetylglucosamine by MurG (van Heijenoort, 1998). In some bacteria, addition of a lateral chain occurs at this stage. In *Enterococcus faecalis* two L-Ala are added to the L-Lys residue in the 3rd position of the peptide stem. This addition is catalysed by the tRNA-dependent aminoacyl ligases BppA1 and BppA2 (Bouhss et al., 2002).

In the third and last step of PG synthesis, lipid II is translocated across the membrane by enzymes called flippases. Three proteins: FtsW, MurJ and Amj were reported to play such a role (Mohammadi et al., 2011; Sham et al., 2014; Meeske et al., 2015). The final step of PG polymerisation occurs on the outer face of the cytoplasmic membrane. PBPs are responsible for polymerisation and cross-linking of the glycan strands. PBPs can be divided into three groups: Class A PBPs can carry out both transglycosylation and transpeptidation reactions, for the polymerisation of glycan strands and cross-linking the stem peptides; class B PBPs only have transpeptidase activity; class C PBPs are low molecular weight carboxypeptidase (Figure 1.6; Scheffers and Pinho, 2005; van Heijenoort, 2007).

24
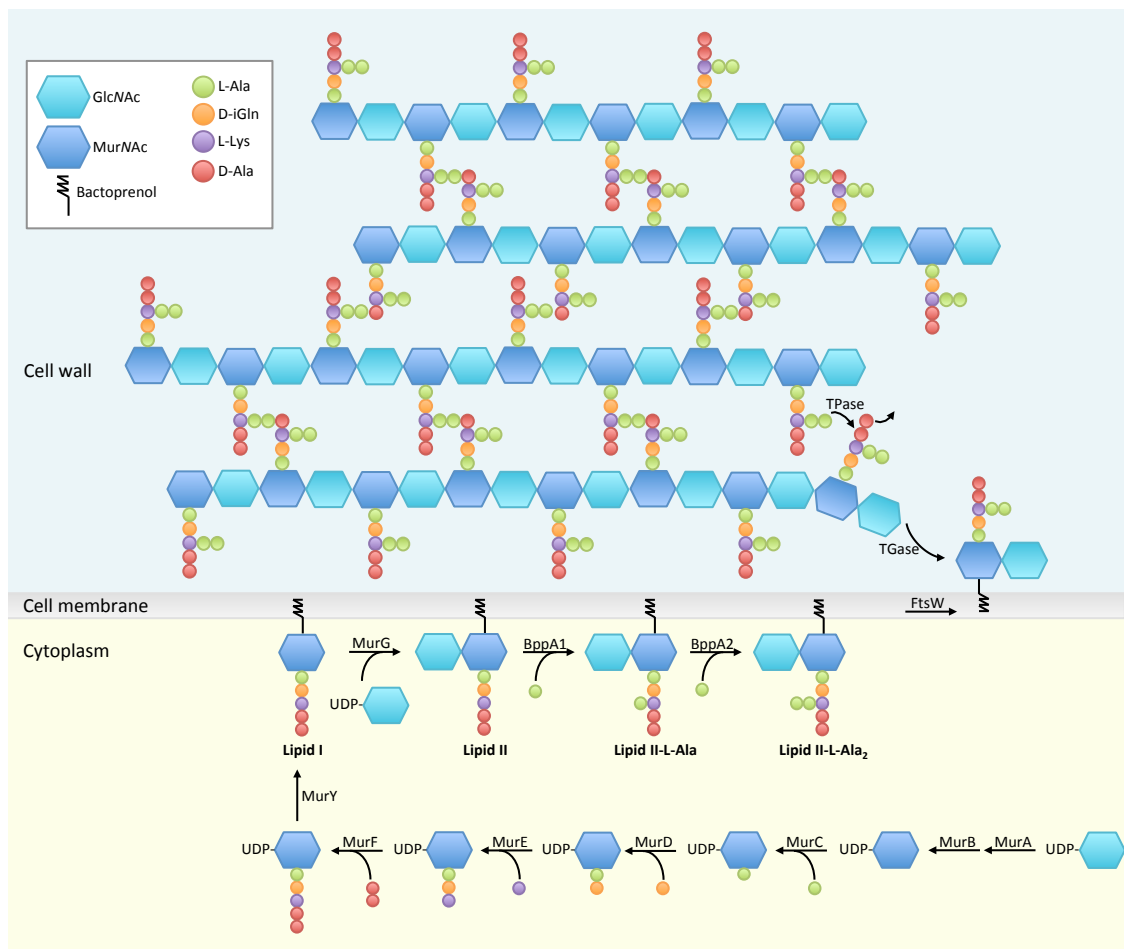
Figure 1.6 Peptidoglycan synthesis in *E. faecalis*

The synthesis of peptidoglycan precursors starts in the cytoplasm where UDP-Mur*N*Ac pentapeptide is produced. It is then transferred on a bactoprenol carrier on the inner side of the cytoplasmic membrane. The resulting lipid I is then converted to lipid II by addition of Glc*N*Ac, which is transported across the cell membrane by a flippase (FtsW/MurJ/Amj). At the external side of the cell membrane PBPs use lipid II as a substrate to produce nascent peptidoglycan as a result of transglycosylation and transpeptidation reactions. Adapted from (Typas et al., 2012; Pinho et al., 2013)

1.2.2   Anionic polymers

Gram-positive bacteria produce a single or several types of anionic polymers. Two major types of anionic polymers have been described: teichoic acids, which are polyphosphate compounds and caspules, made of polysaccharides. In rare cases, like in *Bacillus anthracis,* capsules can be made of polyglutamate (Candela and Fouet, 2006). Anionic polymers are usually covalently attached to C6-hydroxyl of Mur*N*Ac through a phosphodiester linkage except in *S. pneumoniae*, where the capsule has been shown to be linked to the Glc*N*Ac residues (Larson and Yother, 2017). Polypeptidic capsules are covalently anchored to the PG via the steam peptide (Candela and Fouet, 2006).

The composition of anionic polymers often varies and can be strictly strain specific. In *E. faecalis,* three anionic polymers anchored to the PG have been described: teichoic acids (TAs), a rhamnopolysaccharide (Epa) and capsule (Cps).

1.2.2.1   Teichoic acids

In most Gram-positive bacteria TAs play several roles like a control of autolysins activity, surface proteins scaffolding or attachment to environment components. There are two types of TAs: (i) lipoteichoic acids (LTA) anchored in the cytoplasmic membrane and (ii) wall teichoic acids (WTA) covalently attached to PG. TAs create a negatively charged polyanionic matrix on a cell surface via the phosphate groups (Neuhaus and Baddiley, 2003). The structure of *E. faecalis* TAs is unusual and seems to be more complex than that of other Gram-positive bacteria such as *B. subtilis* or *Listeria monocytogenes* which produce polyribitol- or polyglycerolphosphate polymers (Theilacker et al., 2012). TAs from *E. faecalis* are composed of D-glucose, D-galactose, 2-acetamido-2-deoxy-D-galactose, 2-acetamido-2-deoxy-D-glucose, D-ribitol and phosphate in a molar ratio of 1:2:1:1:1:1.

TagO and TarO are two enzymes responsible for the incitation of the WTA synthesis in *B. subtilis* and *S. aureus*, respectively (Soldo et al., 2002; Weidenmaier et al., 2004). They catalyse a transfer of Glu*N*Ac-1-phosphate on to a lipid carrier before TarA/TagA catalyse the addition of *N*-acetylmannosamine. Only these two pairs of genes TarO/TarA and TagO/TagA involved in the early stage of WTA synthesis are dispensable for cell viability and their deletion causes WTA depletion (D'Elia et al.,

2006). Interruption of genes involved in further steps of WTA synthesis is lethal for a bacterial cell. This suggests that the early stage of WTA is reversible, whereas interruption in the later stages leads to formation of non-reversible WTA precursor forms, which deplete the population of the accessible lipid carrier essential for PG synthesis (Swoboda et al., 2009). In *E. faecalis epaA* shears a sequence similarity with *tagO* and *tarO* and a four-gene operon *tagBACD* encodes TagA-like proteins (Rigottier-Gois et al., 2011).

1.2.2.2 Capsule

The second group of anionic polymers associated with the surface of *E. faecalis* corresponds to capsular polysaccharides (CPSs). They contribute to pathogenesis through specific interactions with opsonophagocytic antibodies as previously described (Chapter 1, section 1.1.7.3.1). Different TA compositions have been reported depending on the strain analysed. In *E. faecalis* 12030 and *E. faecium* 838970, TAs consist of repeating units of α-D-glucopyranosyl-(1-2)-α-D-glucopyranose (kojibose) attached to a glycerol diphosphate (Huebner et al., 1999; Wang et al., 1999). In *E. faecalis* FA2-2, TAs contain glycerol, glucose and phosphate in a 1:1:2 ratio. *E. faecalis* produces four serological types of CPSs encoded by a *cps* operon CPS-A, -B, -C and -D. Enterococci of the first two groups, CPS-A and CPS-B have only two genes *cspA* and *cspB*, whereas enterococci of classified to CPS-C and CPS-D serological groups have from 8 to 9 additional genes in the *cps* operon responsible for biosynthesis of capsules. Only the last two serological groups possess CPSs (Hufnagel et al., 2004). Thurlow *et al.,* showed that *cpsF* is present only in enterococci CPS-C group and proposed that this enzyme is responsible for glycosylation of serotype C capsules (Thurlow et al., 2009).

1.2.2.3 Enterococcal polysaccharide antigen (Epa)

In addition to TAs and capsules, some Gram-positive bacteria produce secondary cell wall polymers. They are impotant for cell growth and interaction with the host and some surface proteins bind non-covalently anchored to these polymers (Mesnage et al., 2000). In enterococci, Epa plays role in invasion of host tissues (Zeng et al., 2004) and has been proposed to play a role in biofilm formation (Mohamed et al., 2004). It has been
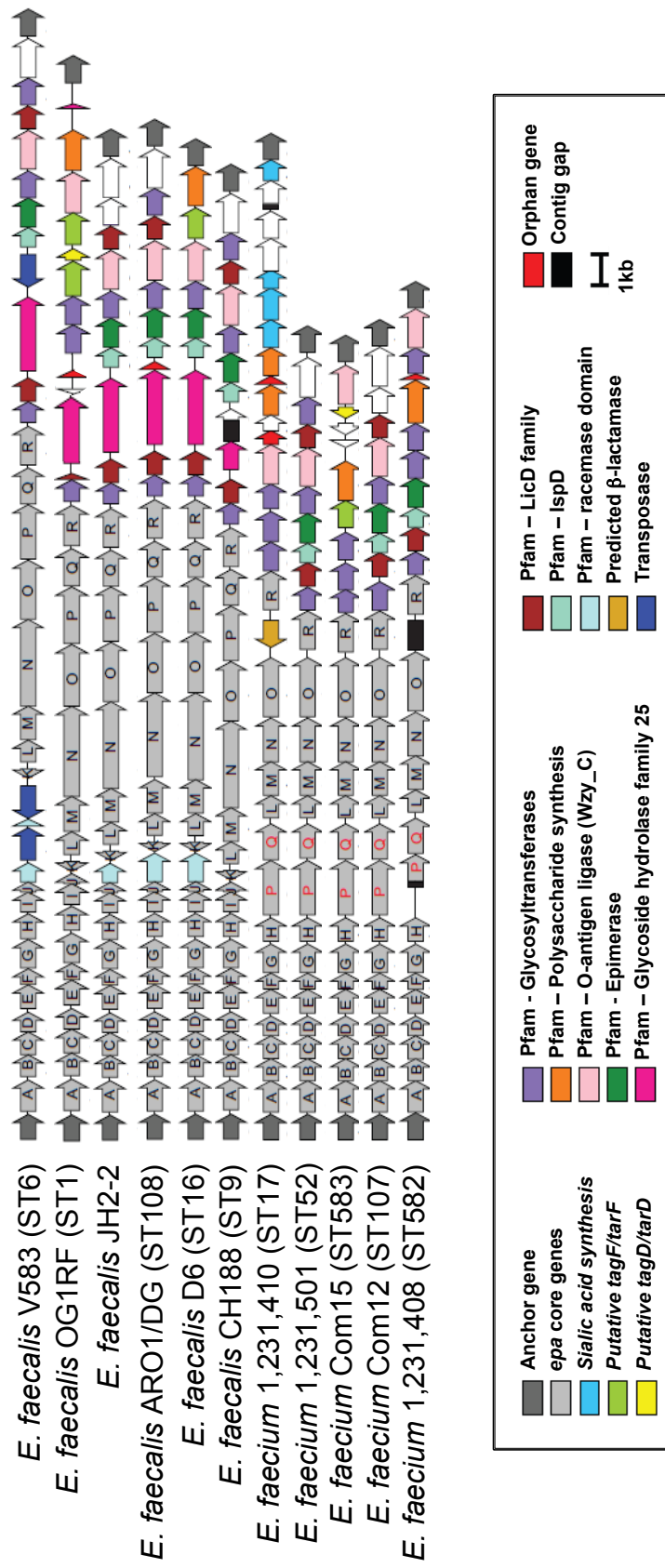
Figure 1.7 Genetic organisation of the *epa* locus in enterococci

Schematic representations of the *epa* loci in *E. faecalis* and *E. faecium* strains. Genes in the conserved *epa* region are in light grey colours. The colour code of the variable downstream region is showed in the legend.

28

recently shown that Epa is important for phagocyte evasion during infection of the host (Prajsnar et al., 2013).

The genes responsible for Epa production are encoded by a complex locus (*epa*) that contains 18 genes (*epaA* to *epaR*; Teng et al., 2009). It was proposed that the variable downstream region is responsible for Epa decoration (Figure 1.7; Rigottier-Gois et al., 2015). The enterococcal Epa is composed of glucose, rhamnose, *N*-acetyl glucosamine, *N*-acetyl galactosamine, and galactose. The biosynthesis starts with addition of a UDP-Glu*N*Ac residue on bactoprenol (lipid carrier) present in the membrane form cytoplasmic side and a further addition of monosaccharides by glycosyltransferase that are not identified yet. Next, the translocation of polysaccharide chains from the cytoplasm to periplasm is supported by a membrane transporter. At this stage polysaccharides are anchored to PG where further modifications may occur (Mistou et al., 2016).

1.2.3 Surface proteins

Bacterial surface proteins play important roles during cell growth and division. PG hydrolases will be described in detail below (Vollmer et al., 2008a). The surface proteins are important for the interaction of a pathogen with a host and host's immune system. For example, MSCRAMM such as *E. faecalis* Ace recognizes and binds to collagen (Liu et al., 2007), facilitating host colonisation. Surface-associated proteins M and H from *Streptococcus pyogenes* have an antiphagocytic function (Kihlberg et al., 1999). Some surface proteins are involved in competition with other bacteria for a niche, such as the lysostaphin produced by *Staphylococcus simulans* (Scott and Barnett, 2006)

1.2.3.1 Posttranslational modification

PTMs were first discovered during studies on eukaryotic cells. For a long time it, was thought that there was no PTMs in prokaryotes. Proteomic studies revealed that PTMs of proteins in bacteria are rather norm than exception. Phosphorylation of proteins plays an important regulatory function. Recent focus on protein-tyrosine kinases allowed for

mapping of the network of phosphatases, kinases with their substrates and processes controlled by them in *B. subtilis* (Shi et al., 2014). It was shown that a protein-tyrosine kinase PtkA can modulate an activity of MinD by a physical interaction and thus regulates the spatial formation of a Z-ring in *B. subtilis* (Shi et al., 2014). Another PTMs of proteins discovered in bacteria are *N*-glycosylation found on asparagine residues and *O*-glycosylation found on serine and threonine residues. *N*-glycosylation is well characterized in *Campylobacter jejuni*, however the biological functions of this modification remain unknown (Nothaft and Szymanski, 2010). The best studied case of *O*-glycosylation are S-layer proteins. Glycoproteins in the S-layer play different roles and are involved in immune response, intracellular targeting, intercellular recognition, and protein folding and stability (Schuter and Sleytr, 2015). Acetylation is another common PTMs of proteins. Recent studies on MreB in *B. subtilis* showed that temporal acetylation of MreB is involved in the cell wall growth and cell diameter regulation during stationary phase of growth (Carabetta et al., 2016).

1.2.3.2 Secretion

Most extracellular proteins in Gram-positive bacteria are traslocated across the cytoplasmic membrane via the general secretory pathway (Sec) along with specific accessory secretion systems SecA2-only and SecA2/SecY2 as well as via the twin arginine translocate (Tat) system (Green and Mecsas, 2016).

The Sec system consists of three main components: a targeting protein (SecB or SRP), a motor protein (SecA) and a protein channel composed of three integral membrane proteins, SecY, SecE and SecG. SecA is a cytosolic ATPase, important for targeting substrates to SecYEG and powering a preprotein transport across the membrane. SecA, SecY and SecE are highly conserved across bacteria and are essential for the Sec secretion (Feltcher and Braunstein, 2012; Murphy et al., 1995) Sec-dependent secretion involves two distinct mechanisms mediated by either a chaperone SecB or SRP. The first mechanism is co-translational. In this case, the <u>s</u>ignal <u>r</u>ecognition <u>p</u>article (SRP) recognises and binds the trans membrane domain of a translated protein. The SRP further interacts with the docking protein, FtsY. The whole complex (SPR-ribosome-protein) is then targeted to the Sec-channel where the protein translocation occurs. (Green and Mecsas, 2016).

The second mechanism is post-translational. When the polypeptide is released from the ribosome, the signal peptide can be either recognised by the chaperone, SecB or directly targeted to the channel by SecA (Figure 1.8 A (i); Feltcher and Braunstein, 2012) A homolog of SecA, called SecA2 was discovered in some Gram-positive bacteria. SecA2 plays the same role (motor protein) in secretion as SecA. Two systems involving SecA2 were described: (i) in SecA2-SecY2 highly glycosylated proteins and accessory Sec system proteins (Asp) are secreted via an alternative channel formed by a SecY homolog (Figure 1.8 A (ii); Sardis and Economou, 2010), (ii) in SecA2-only, a SecA homolog uses the SecYEG channel to secrete proteins (Figure 1.8 A (iii); Rigel et al., 2009). The analysis of *E. faecalis* genome suggests that there is no accessory SecA2 secretion system in this organism.

The Tat system is another system used for secretion of folded proteins (Figure 1.8 B; Natale et al., 2008). *E. faecalis* encodes a Tat system. It is present in cytoplasmic membrane of most bacteria and it is composed of two (TatA and TatC) or three (TatA, TatB and TatC) proteins. The Tat system uses PMF as a source of energy for protein translocation across the cytoplasmic membrane (Natale et al., 2008).

1.2.3.3 Proteins covalently bound to PG

Covalent attachment of proteins to PG is conserved in Gram-positive bacteria and was first studied using protein A from *S. aureus* as a model (Figure 1.9; Schneewind et al., 1992). All proteins covalently anchored to PG have a specific C-terminal targeting signal which consists of (i) an LPxTG motif followed by (ii) a region of 15-22 hydrophobic amino acids and (iii) a charged tail of 5-12 amino acids (Schneewind et al., 1992; Ton-That et al., 2004). The LPxTG signalling sequence is recognised after secretion by a transpeptidases called sortase. Sortase is responsible for the protein cleavage and linkage to the cross-bridge of a PG precursor (Figure 1.9). In *E. faecalis*

A
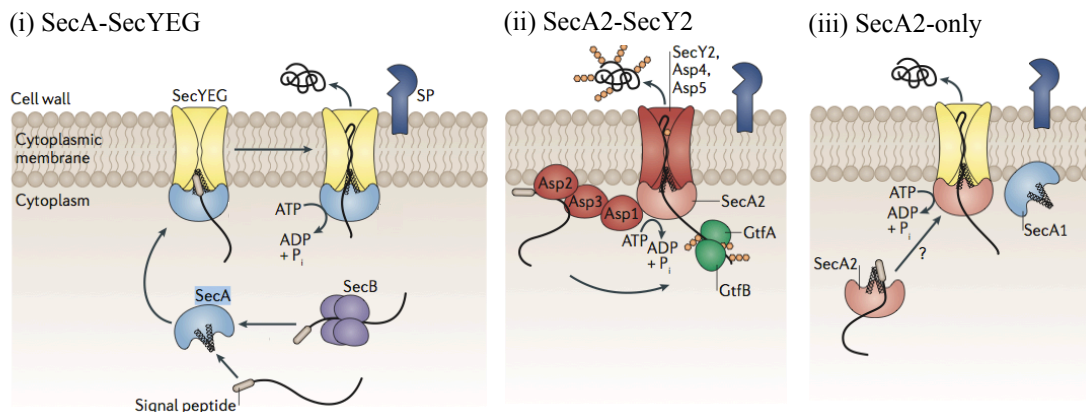
B
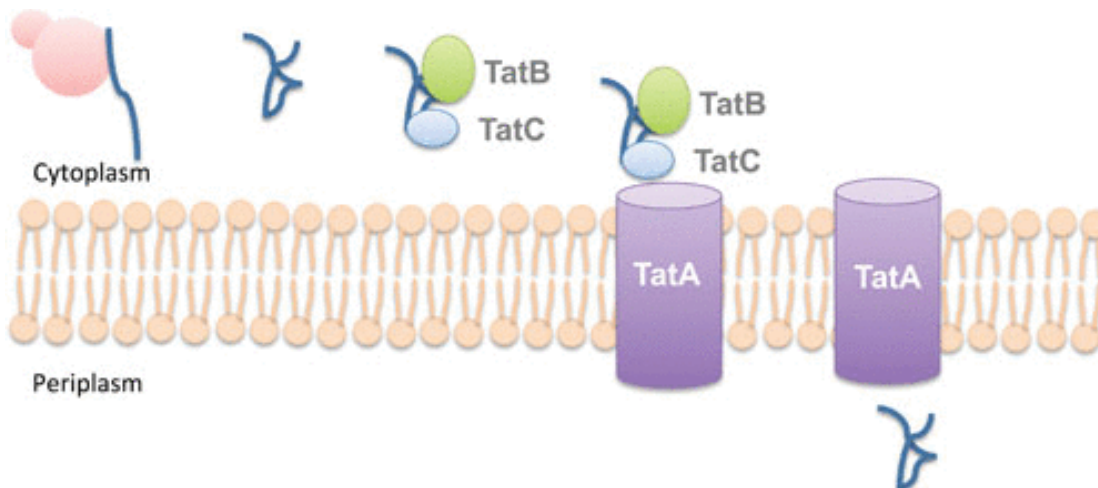
Figure 1.8 Schematic representation of the major secretion systems in Gram-positive bacteria

A. The Sec system transports unfolded or not fully folded proteins. The signal peptide of a translated protein is recognised by SecB or directly targeted to the SecYEG channel by SecA (i). Some preproteins are secreted via a specific accessory system involving a SecA homologue, SecA2 and an alternative channel containing SecY2, a SecY homolog (ii). A third secretion system has been described where SecA2 is required (iii). In this case the canonical SecYEG channel is used. Reproduced from (Feltcher and Braunstein, 2012).

B. The Tat system translocates fully folded proteins. The peptide released from a ribosome, folds in the cytoplasm, where post translational modification may occur. A specific Tat signal peptide is then recognised by TatB and/or TatC, which recruits the protein to the membrane-spanning channel formed by TatA, allowing secretion. Reproduced from (Green and Mecsas, 2016).

32
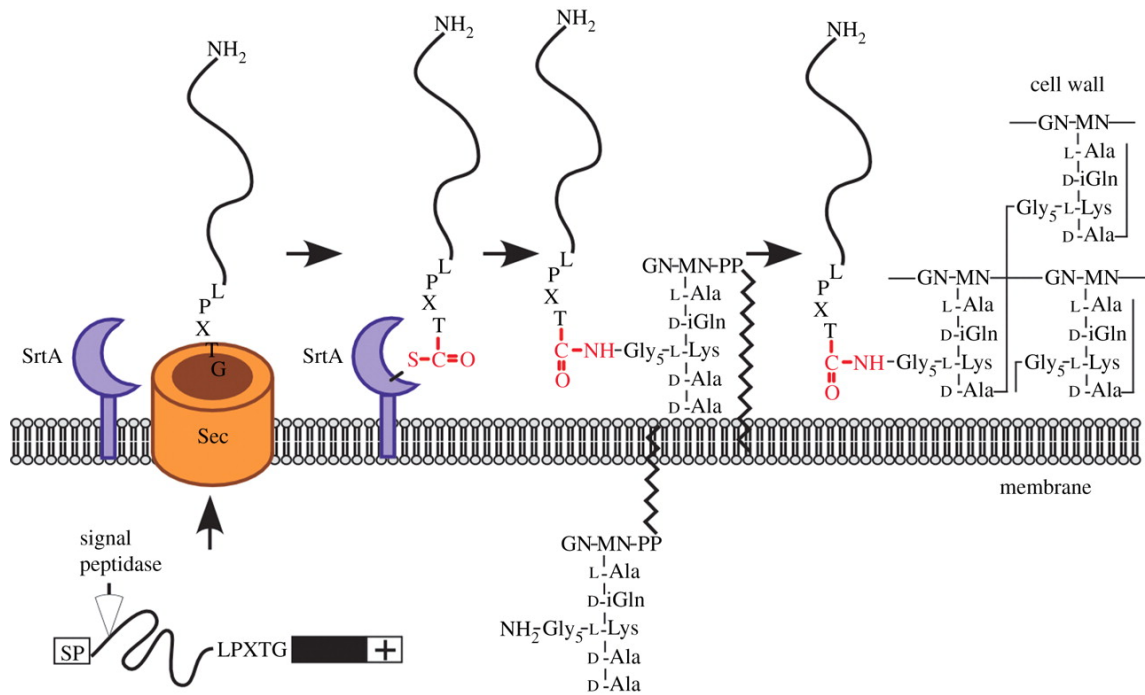
Figure 1.9 Covalent binding of proteins to peptidoglycan by SrtA

Proteins covalently anchored to PG have a specific C-terminal targeting signal containing an LPxTG motif followed by a hydrophobic sequence (black box) and 5-12 charged amino acids. Following secretion, both the hydrophobic region and the charged tail acts as a retention signal that allows recognition of the LPxTG motif by the sortase. This enzyme cleaves the substrate between the threonine and glycine residues to form an acyl-enzyme, in which cysteine from the active site interacts with the carboxyl group of threonine. The carbonyl group of the threonine residue is then attached to the amine group of the last glycine residue of the lateral chain on a lipid II precursor. The protein reaches cell surface as the PG precursors are polymerized into the existing network. Reproduced from (Schneeewind et al., 1992).

proteins involved in the host-pathogen interaction like Ace, Esp and aggregation substance proteins are anchored to the cell surface via the LPxTG signalling sequence (Shankar et al., 1999; Hendrickx et al., 2009).

1.2.3.4 Non-covalently binding proteins

The vast majority of surface proteins in Gram-positive bacteria have a modular organization. In addition to a signal peptide, they usually contain one or more domains determining their activity. Non-covalent binding to the cell wall is mediated by imperfect repeats of 30 to 100 amino acids called cell wall binding modules (CWBM).

1.2.3.4.1 LysM

The lysin motif (LysM) is present in prokaryotic and eukaryotic cells. The bacterial LysM binding modules consist of imperfect repeats of 44 to 50 amino acid residues that can be precededby sequences of low complexity (Buist et al., 2008). LysM motifs adopt a characteristic βααβ fold. LysM binding domains are found either at the N- or C-terminus of proteins and contain from 1 to 12 binding modules. The nature of the LysM domain binding varies and may even require a trimetric structure for some eukaryotic cell (Ohnuma et al., 2008; Liu et al., 2012). The LysM modules from *E. faecalis* AtlA do not form any quaternary structure and bind PG independently of one another. Based on these results, itwas proposed that LysM modules act as 'beads on a string' (Mesnage et al., 2014). Single LysM modules recognise a Glc*N*Ac-X-Glc*N*Ac motif within the PG. Structural studies revealed that LysM binding relies both on two hydrophobic pockets that interact with the acetyl groups in Glc*N*Ac and several amino acids present in a well defined cleft that are responsible for interaction with a sugar backbone (Mesnage, et al., 2014).

LysM proteins often contain additional subcellular targeting signals (Figure 1.10) such as (i) an N-terminal signal peptide for secretion (*e.g. E. faecalis* PG hydrolase AtlA involved in septum cleavage); (ii) an LPxTG motif for covalent binding to PG (*e.g., S. aureus* IgG-binding protein A Spa) or (iii) a hydrophobic membrane anchor (*e.g.,* the conserved teichoic acid transporter TagH or the *B. subtilis* division protein YneA). Interestingly, LysM proteins with a membrane anchor harbor acidic LysM motifs,

whereas proteins displayed at the bacterial cell surface tend to have basic LysM motifs. This observation has led to the hypothesis that the charge of LysM motifs could represent a major determinant for the anchoring of proteins within distinct regions of the cell wall (Buist et al., 2008). LysM domains with low pI have been proposed to bind the cell wall in the vicinity of the outer protonated face of the cytoplasmic membrane representing the 'inner wall zone' (Matias and Beveridge, 2005; Buist et al., 2008); basic LysM motifs have been proposed to interact with the 'outer wall zone', closer to the cell surface where the net charge is essentially anionic.

1.2.3.4.2 PASTA

The PASTA domain (for penicillin-binding protein and serine/threonine kinase associated domain) was first described in *S. pneumoniae* during the structural studies of a complex of PBP2x with cefuroxime. It was proposed that the PASTA domain binds β-lactams (Gordon et al., 2000) and a potential interaction with PG was subsequently suggested (Yeats et al., 2002). The PASTA domain, which usually has 70 amino acids, consists of a variable number of imperfect repeats. Although PASTA domains share a low sequence similarity their structure is conserved (Barthe et al., 2010). An interaction of the PASTA domains with PG was shown by plasmon resonance (Mir et al., 2011) and NMR (Squeglia et al., 2011) revealing that a muramyl tetrapeptide is the minimal recognition motif in the PG for the PASTA domain (Mir et al., 2011). Moreover, the binding studies demonstrated that the PASTA domains of StkP (Serine/threonineprotein kinase of *S. pneumoniae*) bind PG of *S. pneumoniae* but not PG from *S. aureus,* suggesting the specificity of the PASTA domains (Maestro et al., 2011). This confirmed the previously published findings by Shah et al. who showed that germination controlled by the PrkC kinase in *B. subtilis* could be activated in the presence of muroeptides containing m-DAP in their stem peptide (Shah et al., 2008). The specific recognition of the PG motif by the PASTA domain of *S. pneumoniae* StkP plays a crucial role in the localisation of the enzyme. The substitution at the PASTA domains in StkP for the PASTA domains from *B. subtilis* PrkC leads to delocalization of a hybrid protein StkP-PASTAPrkC form septal to membrane and polar localization (Righino et al., 2015).
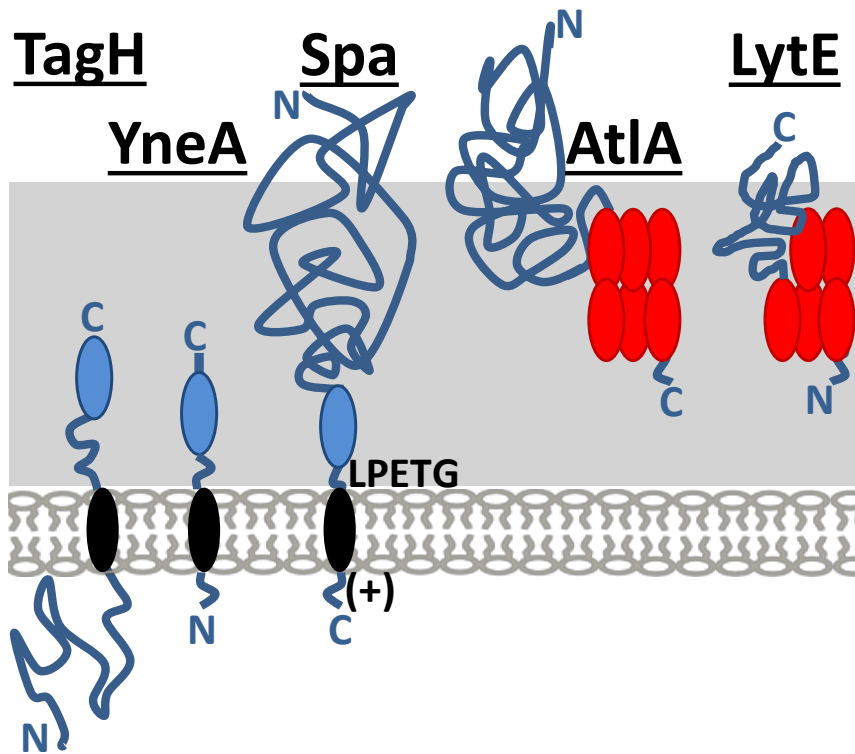
Figure 1.10 Model of subcellular targeting of LysM proteins in the cell wall

TagH, YneA and *S. aureus* protein A contain a hydrophobic membrane anchor (black oval) preceding a single acidic C-terminal LysM motif (pI=4.12, 4.03 and 4.92, respectively, blue oval). Protein A also contains a positively charged C-terminal tail and a LPETG motif for covalent binding to PG. *E. faecalis* AtlA and *B. subtilis* LytE are PG hydrolases involved in septum cleavage. They contain LysM domains made of six (AtlA) and 5 (LytE) basic LysM motifs (pI=10.1 and 10.0, respectively, red oval).

1.2.3.4.3 SH3b

Another PG binding domain is an SH3b domain. The SH3b domain was found in lysostaphin, a staphylolytic enzyme produced by *S. simulans* (Baba and Schneewind, 1996; Thumm and Götz, 1997). The SH3b domain shares a structural similarity with eukaryotic SH3 domains recognising short proline-rich segments in proteins (Pawson, 1995). The binding domain of *S. capitis* ALE-1 that is made of 92 residues was used as a model to study the SH3b binding activity. ELISA results showed that a presence of a glycine pentapeptide crossbridge was required for binding, suggesting that SH3b is specifically recognising this motif (Lu et al., 2006). The SH3b binding domain was found in other species with and without a peptide crossbridge. How different SH3b domains bind to PG remains unknown.

1.2.3.4.4 WxL

The WxL domain was recently discovered based on the sequence analysis of *E. faecalis* secretome. The results showed presence of two WxL motifs separated by 80 to 120 amino acids in 27 proteins mostly encoded in 8 operons (Brinster et al., 2007a). Proteins with the WxL domain are also found in other low GC Gram-positive bacteria including *Listeria monocytogenes*, *Bacillus cereus* and *E. faecium*. Although the ability of the WxL domains to bind PG has been demonstrated, the motif it recognises remains unknown (Brinster et al., 2007a). Some proteins with a WxL domain are involved in pathogenesis. For instance the enterococcal internalin-like protein, ElrA modulates the host inflammatory response (Brinster et al., 2007b).

1.2.3.4.5 SLH and CBD

Additionally to the PG binding domains described above, several cell wall binding domains interacting with anionic polymers were identified. SLH domains recognise a pyruvylated polysaccharide (Mesnage et al., 2000). Choline binding domains (CBD) found in *Streptococcus pneumoniae* surface proteins bind to choline residues present in TA (Fernández-Tornero et al., 2001).

1.3 PG hydrolases

1.3.1 Cleavage specificities of PG hydrolases

Bacteria produce enzymes capable of PG cleave called <u>PG</u> hydrolases (PGHs). A very large number of PGHs has been described. The diversity of these enzymes reflects the complexity of the PG composition previously described. Depending on the PG bond they cleave, three classes of PG hydrolases can be distinguished (Vollmer, 2008a).

Glycosyl hydrolases recognise and cleave PG glycan chains. They are divided in two groups: (i) *N*-acetylglucosaminidase and (ii) *N*-acetylmuramidase. *N*-acetylglucosaminidases cleave between Mur*N*Ac and Glc*N*Ac residues releasing a Glc*N*Ac residue at the reducing end, while an *N*-acetylmuramidases hydrolyse the bond between Glc*N*Ac and Mur*N*Ac residues and release a Mur*N*Ac residue at the reducing end (Figure 1.11; Vollmer, 2008a). Bacteria can also produce lytic transglycosylases. Although they recognise and cleave the same bond as *N*-acetylmuramidase, they do not use a water molecule during cleavage and therefore cannot be classified as glycosyl hydrolases. They do not release a Mur*N*Ac residue at the reducing end but an anhydroMur*N*Ac residue instead. Muropeptides with masses compatible with the presence of anhydroMur*N*Ac residues have been reported in *B. subtilis* (Atrih et al., 1999) and *C. difficile* (Peltier et al., 2011) but the presence of anhydroMur*N*Ac has not been convincingly demonstrated and remain controversial (Bern et al., 2017). No direct evidence is available showing lytic transglycosylase activity in Gram-positive bacteria.

Another class of PGHs is a group of enzymes called *N*-acetylmuramoyl-L-alanine amidases (or amidases). They cleave the bond between Mur*N*Ac and the N-terminal L-Ala residues of the stem peptide (Figure 1.11; Vollmer, 2008a).

Peptidases represent the most diverse group of PGHs. They can be divided in two groups: (i) endopeptidases and (ii) carboxypeptidases. Endopeptidases cleave bonds within the peptide stem or cross bridge. They can be defined by the stereospecificity of the amino acids forming the bond they cleave, and are either L,L-, L,D- or D,L-peptidases. Carboxypeptidases remove C-terminal D-Ala residues of peptide stems(Figure 1.11; Vollmer, 2008a).
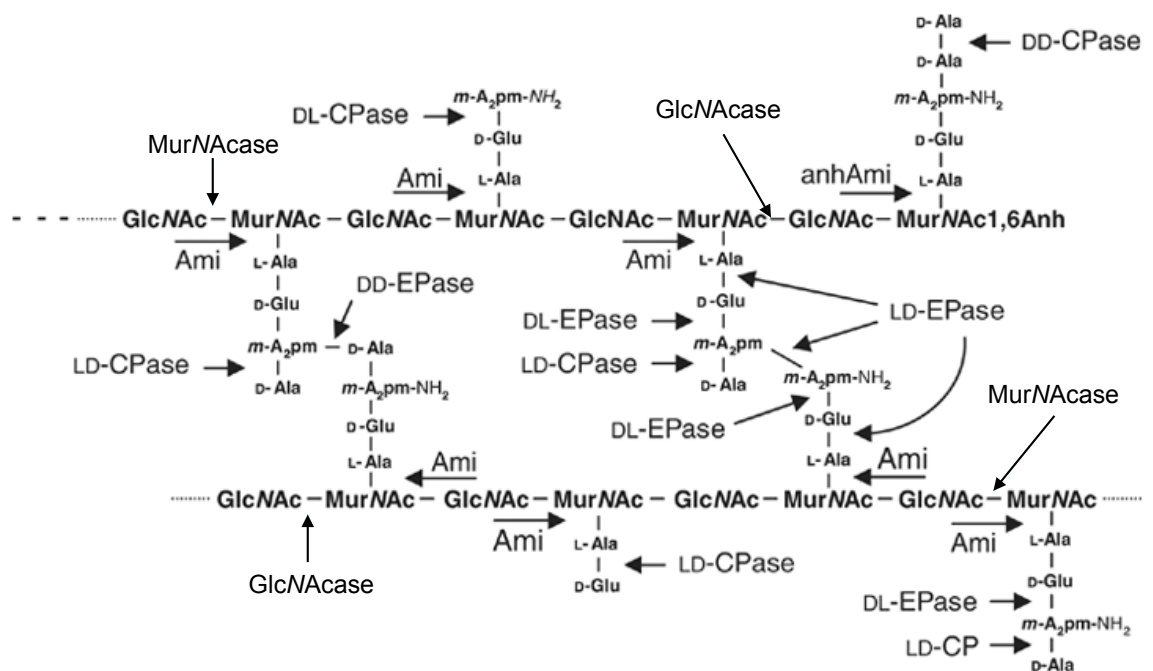
Figure 1.11 Cleavage of PG bonds by peptidoglycan hydrolases

PG is composed of glycan strands and stem peptides that in some bacteria can be linked via cross bridges. *N*-acetylglucosaminidase (Glc*N*Acase) and *N*-acetylmuramidase (Mur*N*Acase) recognise and cleave the bonds between Glc*N*Ac and Mur*N*Ac in glycan chains. *N*-acetylmuramoyl-L-alanine amidases (Ami) cleave bond between Mur*N*Ac and the N-terminal L-Ala residues of the peptide stems. Some of them (anhAmi) release 1,6-anhydroMur*N*Ac residues as a digestion product. The endopeptidases (EPase) and carboxypeptidases (CP) clave the peptide bonds in stem peptide and cross bridges. They can be defined by the stereospecificity of the amino acids forming the bond they cleave, and are either L,L-, L,D- or D,L-peptidases. Adapted from (Vollmer et al., 2008a).

1.3.2 Physiological roles of PGHs

Many PGHs are involved in a regulation of cell growth. It was shown that some are part of the divisome, a protein complex mediating cell division and PG synthesis (den Blaauwen et al., 2008). For instance, D,D–carboxypeptidases can remove of the D-Ala residue in position 5 of the stem pentapeptide . This controls a degree of crosslinking in the nascent PG and contributes to localisation of other proteins involved in cell division (Morlot et al., 2004). In *E. coli* and *B subtilis,* activity of the LytE endopeptidase is required for incorporation of PG precursors to the growing PG molecule (Carballido-López et al., 2006).

PGHs play an important role at the late stages of cell division. They are involved in septum cleavage that leads to separation of daughter cells. One or more enzymes can be involved in this process. In *E. faecalis* a single hydrolase, AtlA is responsible for a cell separation (Mesnage et al., 2008), whereas in *S. aureus* the activity of both Sle1 and Atl are required (Yamada et al., 1996).

Some Gram-positive bacteria can produce spores in unfavourable conditions. This process starts with formation of an asymmetric septum that is further cleaved by the PGH SpoIID (Gutierrez et al., 2010). The spore PG maturation requires an activity of an amidase, CwlD and the deacetylase PdaA, which together produce δ-lactam Mur*N*Ac residues (Vollmer, 2008a). When spore formation is finished, the mother cell is lysed by PGHs (LytC, Cw1C and Cw1H). In favourable environment a spore requires PGHs activity to germinate (Moir, 2006).

Many PGHs are involved in a biofilm formation. This specific bacterial community structure helps cells survive and colonise unique niches like hospital environment or host tissues. For instance, the *Staphylococcus epidermidis* major PGH, AltlE is essential for biofilm formation. Mutations in this gene led to a biofilm negative phenotype (Heilmann et al., 1997). Similarly, *E. faecalis* AtlA and its ortholog AcmA in *Lactococcus lactis* are responsible for the biofilm formation (Mercier et al., 2002). It has been shown that a cell lysis mediated by these enzymes releases extracellular DNA (eDNA), which is an important component involved in the biofilm formation (Thomas et al., 2009).

1.3.3   1.3.3 Control of PGHs activity

The activity of PGHs must be tightly regulated to prevent cell autolysis. Such a control can take place at a transcriptional or posttranslational level.

Transcriptional regulation of autolysins in *B. subtillis* will be described as an example. In this bacterium, an alternative sigma factor (SigD) controls genes involved in motility as well as transcription of genes encoding autolysins, *lytD* and the *lytABC* operon. Two major hydrolases, LytC and LytD, are produced in large amounts, allowing for a release of single cells from chains and the single cells become motile. This transcriptional regulation allows the cell to adjust its response to chemotactic signals (Margot et al., 1994; Kuroda and Sekiguchi, 1993).

Several posttranslational regulations of autolysins have been described. They include: (i) glycosylation; an AcmA2 autolysin from *Lactobacillus plantarum* was recently shown to be substituted by Glc*N*Ac residues. This modification has an inhibitory effect on its enzymatic activity (Rolain et al., 2013); (ii) modulation of PGH binding to PG has been reported to have a major impact on enzymatic activity (Eckert et al., 2006). The affinity of the PG binding domain for PG is therefore expected to be of the major importance for PG cleavage; (iii) some autolysin are produced as inactive or poorly active enzymes due to the presence of a domain preventing access of a substrate to a catalytic site. In such cases, proteolytic cleavage can generate a fully active enzyme (Bublitz et al., 2009). Finally, another example of PGH activity control is given by an *S. pneumoniae* PcsB hydrolase which needs to interact with a transmembrane FtsEX complex from the division machinery for its activity (Bartual et al., 2014).

1.3.4   *E. faecalis* PGHs

A bioinformatics analysis revealed that the genome of *E. faecalis* encodes 21 putative PG hydrolases, only seven of which are ubiquitous. A zymogram analysis of crude extracts and supernatants of *E. faecalis* showed that a limited number of PGH activities can be detected. Bands with hydrolytic activities correspond to three PGHs: AtlA (EF0799), AtlB (EF0355) and AtlC (EF1992) (Mesnage et al., 2008). Additionally, a

hydrolytic activity of prophage encoded EF1473 was shown by studying it in a heterologous system (*E. coli*) (Reste de Roca et al., 2010).

AtlA was first identified during a search for enterococcal antigens expressed in *E. coli* using antisera from patients suffering from endocarditis caused by *E. faecalis* (Xu et al., 1997). The hydrolytic activity of AtlA was identified using a zymogram assay. AtlA was shown to be the only enzyme in OG1RF with autolytic activity as a ΔatlA mutant was not able to lyse in a phosphate buffer as compared to the wild-type strain (Qin et al., 1998). Interestingly, AtlA displays a lower enzymatic activity against the whole sacculi when compared to AtlB (Emirian et al., 2009).

AtlA is a modular enzyme that consists of (i) a signal peptide, (ii) an N-terminal domain, (iii) a catalytic domain and (iv) a multimodular LysM binding domain (Eckert et al., 2006). AtlA has unusually long signal peptide with a cleavage site between Ala53 and Thr54. The signal peptide is composed of (i) a charged N-terminal region, (ii) a hydrophobic region and (iii) a canonical AEA motif with a cleavage site after the second Ala. The N-terminal domain of AtlA is cleaved by secreted proteases (Eckert et al., 2006; Waters et al., 2003) and recent studies showed that it is glycosylated (Salamaga et al., 2017). The AtlA catalytic domain belongs to the CAZy family GH73 and displays *N*-acetylglucosaminidase activity (Eckert et al., 2006). The C-terminal multimodular LysM binding domain is responsible for non-covalent attachment of the enzyme to PG. This domain is composed of six LysM modules preceded by low complexity sequences. The presence of the LysM domain is essential for the optimal activity of AtlA as its truncation led to a 500-fold decrease of the enzymatic activity of the recombinant enzyme (Eckert et al., 2006).

AtlA is responsible for the separation of daughter cells at the end of cell division. The deletion of the *atlA* gene results in formation of long cell chains (Mesnage et al., 2008). The lack of AtlA impairs the biofilm formation. The autolytic activity of AtlA is required for the eDNA release, an important component involved in the biofilm formation (Kristich et al., 2008).

A PGH of 45 kDa called AtlB can be detected in *E. faecalis* extracts (Mesnage et al., 2008). The gene encoding AtlB was identified by reverse genetics by mass spectrometry analysis of tryptic digestion of AtlB purified from culture supernatants. AtlB is a PGH encoded by a prophage and is not present in all *E. faecalis* strains. It is a

modular enzyme composed of (i) a signal peptide of 21 residues followed by (ii) an N-terminal catalytic domain and (iii) a C-terminal binding domain (Mesnage et al., 2008). The catalytic domain of AtlB belongs to CAZy family GH25 and displays *N*-acetylmuramidase activity. The binding domain consists of two LysM repeats, which are not preceded by linkers. The pI of the AtlB LysM domain is slightly acidic (pI=6), whereas pI of AtlA LysM domain is basic (pI=10) (Figure 1.12; Mesnage et al., 2008). In the absence of AtlA, AtlB is able to cleave septum, however with a much lower efficiency, suggesting that this *N*-acetylmuramidase plays a minor role in this process (Mesnage et al., 2008). It was shown that AtlB does not contribute to the polymerisation of the nascent PG but it is involved in PG turnover in a stationary phase of bacterial growth (Mesnage et al., 2008).

AtlC was identified along with AtlB (Mesnage et al., 2008). The gene encoding AtlC was identified by a BLAST search for a hydrolase similar to AtlB. The analysis of a *atlC* mutant and its complemented counterpart confirmed that AtlC is expressed in *E. faecalis*. AtlC displays 69% similarity to AtlB. It is a modular enzyme with a similar domain organization as AtlB displaying the *N*-acetylmuramidase activity (Mesnage et al., 2008). The physiological role of this hydrolase is unknown.

EnpA is encoded by prophage that was identified by genome analysis (Reste de Roca et al., 2010). This large hydrolase is present only in a few strains of *E. faecalis*. The bioinformatics search in the Pfam database revealed the presence of a C-terminal region that belongs to a M23 family of peptidases. EnpA endopeptidase activity was confirmed when its hydrolytic activity was tested against disaccharide peptides (Reste de Roca et al., 2010). The physiological role of this hydrolase remains unknown
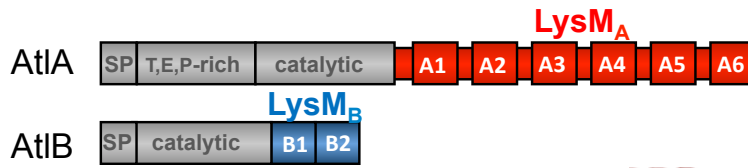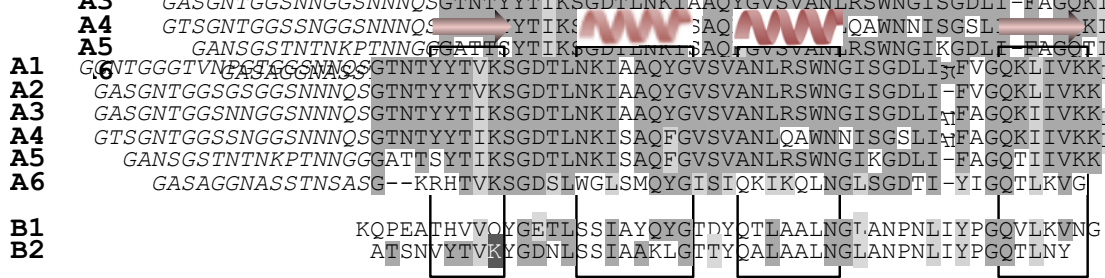
Figure 1.12 Modular organization of *E. faecalis* AtlA and AtlB

A.   Domain organisation of *E. faecalis* AtlA and AtlB. The colour code refers to the isoelectric point of the LysM domains (red, pI=10; blue, pI=6.25). SP-signal peptide; T,E,P-rich domain (present in AtlA); catalytic domain and LysM domain.

B.   Sequence alignment of AtlA and AtlB LysM modules with predicted secondary structures providing the characteristic βααβ fold of the LysM modules.

1.4 Working hypothesis and aim of the thesis

The formation of diplococci and short chains by *E. faecalis* is a distinctive property of this organism. Morphological plasticity was recently reported as a major factor contributing to the pathogenesis of Gram-positive and –negative bacteria. We hypothesised that the strict conservation of the diplococcus morphology could shape the interaction of this bacterium with the host and favour pathogenesis.

In *E. faecalis,* one enzyme named AtlA is dedicated to septum cleavage. The aim of this study was to investigate the mechanism(s) controlling septum cleavage and explore the impact of enterococcal size minimization on the outcome of an experimental infection in zebrafish

CHAPTER 2

Materials and methods

2.1   Chemicals and enzymes

All chemicals and enzymes were of analytical grade quality and were purchased from Sigma, Fisher Scientific, MP Biomedicals or Roche. All restriction enzymes, ligases, polymerases, DNase and appropriate buffers were purchased from New England Biolabs.

2.2   Buffers and solutions

All buffers and solutions were prepared using distilled water (dH$_2$O) and stored at room temperature. If necessary, solutions were sterilised by autoclaving, unless otherwise stated.

2.2.1   Phosphate buffered saline (PBS)

NaCl	8 g l^{-1}
Na$_2$HPO$_4$	1.4 g l^{-1}
KCl	0.2 g l^{-1}
KH$_2$PO$_4$	0.2 g l^{-1}

The pH was adjusted to 7.4 with NaOH.

2.2.2   PBS-TD

The PBS supplemented with TritonX-100 and DMSO at 0.4% (v/v) and 1% (v/v), respectively.

2.2.3   TAE (50x)

Tris	242 g l^{-1}
Glacial acetic acid	5.7% (v/v)
Na$_2$EDTA pH 8.0	0.05 M

50x stock solution was diluted with dH$_2$O to produce a 1x TAE working solution.

2.2.4 DNA loading buffer (10×)

Bromophenol blue   0.25% (w/v)

Glycerol   50% (v/v)

2.2.5 Solutions for sample preparation for microscopy

2.2.5.1 Sodium phosphate buffer

1 M Na_2HPO_4 57.7 ml

1 M NaH_2PO_4 42.3 ml

The final volume was adjusted to 1 l to give a 100 mM solution. The final pH was 7.0.

2.2.5.2 16% (w/v) paraformaldehyde

100 mM sodium phosphate buffer (pH 7.0)   50 ml

Paraformaldehyde   8 g

8 g of paraformaldehyde were added to 40 ml of 100 mM sodium phosphate buffer (pH 7.0). The solution was heated to 60°C while mixed vigorously. 10 M NaOH was added dropwise, until the solution cleared. The solution was stored up to 3 months at 4°C.

2.2.5.3 Fixative solution

16 % (w/v) paraformaldehyde   0.5 ml

PBS   2 ml

2.2.6 SDS-PAGE solutions
2.2.6.1 SDS-PAGE buffer (10x)

Glycine   144 g l^{-1}

Tris   30.3 g l^{-1}

SDS   10 g l^{-1}

A 1:10 dilution with dH_2O was made to give a 1x SDS-PAGE working buffer.

2.2.6.2 SDS-PAGE loading buffer (5x)

Tris-HCl pH 6.8   250 mM

SDS   10% (w/v)

Bromophenol blue   0.5 % (w/v)

Glycerol   50% (v/v)

DTT   0.5 M

2.2.6.3 Coomassie Blue stain

Coomassie Blue R-250   0.25% (w/v)

Methanol   50% (v/v)

Acetic acid glacial   10% (v/v)

Coomassie stain was stored in a foil-wrapped Duran bottle (light sensitive).

2.2.6.4 Coomassie destain

Methanol   5% (v/v)

Glacial acetic acid   10% (v/v)

2.2.6.5 Zymogram renaturing solution

Triton X-100   0.2 %(v/v)

NaCl   50 mM

Buffer   50 mM

Depending on the pH, the following buffers were used:

50 mM Na_2HPO_4 pH 6.25

50 mM Tris-HCl   pH 7.4

2.2.7 Western blotting solutions
2.2.7.1 Blotting buffer

Tris   2.4 g l^{-1}

Glycine   11.26 g l^{-1}

Ethanol   20% (v/v)

2.2.7.2 TBST (20x)

Tris   48.4 g l^{-1}

NaCl   20 g l^{-1}

Tween-20   2% (v/v)

The pH was adjusted to 7.6. A 1:20 dilution with dH_2O was made to give a 1x TBST working solution.

2.2.7.3 Blocking buffer

2% (w/v) dried skimmed milk powder was added to 1x TBST.

2.2.8 Southern blotting solutions

2.2.8.1 Depurination solution

HCl   250 mM

2.2.8.2 Denaturation solution

NaOH   0.5 M
NaCl   1.5M

2.2.8.3 Neutralisation solution

Tris-HCl   0.5 M
NaCl   1.5 M

The pH was adjusted to 7.5 with 12M HCl.

2.2.8.4 20x SSC

NaCl   3 M
Sodium citrate   300 mM

The pH was adjusted to 7.0 with 1 M NaOH. 20x SSC was diluted with dH_2O to make 5x, 2x and 0.5x SSC wash solutions.

2.2.8.5 ECL prehybridisation buffer

Gold hybridisation buffer (GE Healthcare)   1x
NaCl   0.5 M
Blocking reagent (GE Healthcare)   5% (w/v)

2.2.8.6 2x SSC wash solution

SSC   2x
SDS   0.1% (w/v)

2.2.8.7 0.5x SSC wash solution

SSC   0.5x
SDS   0.1% (w/v)

2.2.9 Solutions to prepare electrocompetent *E. coli* and *E. faecalis* cells

2.2.9.1 Washing solution

Glycerol   10%

The solution was sterilised and stored at 4°C.

2.2.9.2 Suc-Gly

Sucrose   0.5 M

Glycerol   10% (v/v)

The pH was adjusted to 7.0 using 1 M HCl before autoclaving.

2.2.10 Pull-down assay solutions

2.2.10.1 Buffer A

1M NaH_2PO4	6.3 ml
1M Na_2HPO4	13.7 ml
NaCl	0.5 M

The final volume was adjusted to 1 l and the pH was adjusted to 7.2.

2.2.10.2 Buffer B

Buffer A supplemented with imidazole at a final concentration of 400 mM.

2.2.10.3 Fixation solution

Methanol	40% (v/v)
Acetic acid glacial	2% (v/v)

2.2.10.4 Colloidal Coomassie solution

Colloidal Coomassie stock (Sigma)	16 ml
Methanol	20 ml
MilliQ water	up to 100 ml

2.2.10.5 DTT 10x

DTT	1.54 mg
dH2O	up to 1 ml

2.2.10.6 IAA 10x

IAA	3.69 mg
dH2O	up to 1 ml

2.2.10.7 Colloidal Coomassie destain

Methanol	25% (v/v)

2.2.10.8 Trypsin solution 10x

Tripsin (Promega)	1 mg
Supplied buffer	up to 1 ml

A 1:10 dilution with 50 mM ammonium bicarbonate pH 8.5 was made to get a working solution of trypsin at a concentration of 0.1 mg ml^{-1}.

.

2.2.11 Immunolabelling solutions

2.2.11.1 PBST

0.1% (v/v) Tween-20 in PBS

2.2.11.2 Blocking solution

2% (w/v) BSA in PBST

2.2.12 STORM buffers

2.2.12.1 STORM dilution buffer

Tris-HCl	50 mM
NaCl	10 mM

pH was adjusted to 8.0 with 12 M HCl. The buffer was stored at 4°C.

2.2.12.2 GLOX MEA

Glucose	10% (w/v)
Catalase	40 μg ml^{-1}
Glucose oxidase	0.5 mg ml^{-1}
β-mercaptoethylamine	100 mM

The buffer was freshly prepared in STORM dilution buffer prior to microscopy imaging (Section 2.12.8).

2.3 Media

All media were prepared in distilled water (dH$_2$O) and sterilised by autoclaving for 20 min at 121°C unless otherwise stated.

2.3.1 Brain heart infusion (BHI)

Brain heart infusion (Oxoid)   37 g l^{-1}

2.3.2 BHI agar

Brain heart infusion (Oxoid)   37 g l^{-1}

Oxoid agar No. 1   1.5 % (w/v) .

2.3.3 Super optimal broth (SOB)

Tryptone (Oxoid)   2% (w/v)

Yeast extract (Oxoid)   0.5% (w/v)

NaCl   10 mM

KCl   2.5 mM

Once autoclaved, filter-sterilized MgCl$_2$ and MgSO$_4$ were added to a final concentration of 10 mM.

2.3.4 Super optimal broth with catabolite repression (SOC)

SOB was supplemented with sterile glucose to a final concentration of 20 mM.

2.3.5 M17-Glu

M17 (Oxoid)   37 g l^{-1}

Sterilised medium was supplemented with filter-sterilised glucose at a final concentration of 0.5% (w/v).

2.3.6 SGM17

M17-Glu was supplemented with 0.5 M sucrose and 2% (w/v) glycine and the pH was adjusted to 7.0.

2.3.7 SM17MC

M17-Glu containing:

Sucrose   0.5 M

MgCl$_2$ 10 mM

52

CaCl$_2$ 10 mM

The pH was adjusted to 6.9 using 1 M HCl before filter-sterilization.

2.4   Antibiotics

Antibiotics used in this study are listed in Table 2.1. Stock solutions were filter-sterilised (0.2 μm pore size) and stored at -20°C.

Antibiotic	Stock concentration (mg ml^{-1})	*Enterococcus faecalis* working concentration (μg ml^{-1})	*Escherichia coli* working concentration (μg ml^{-1})	Solvent
Ampicillin (Amp)	100	-	100	dH$_2$O
Erythromycin (Ery)	30	30	200	95% (v/v) ethanol
Kanamycin (Kan)	50		50	dH$_2$O
Tetracycline (Tet)	10	5	-	50% (v/v) ethanol

Table 2.1 Antibiotic stock solutions and concentrations

2.5   Bacterial strains and plasmids

2.5.1   Bacterial strains

Enterococcus faecalis and *Escherichia coli* strains are listed in Table 2.2. Strains were grown on BHI agar plates containing antibiotics where appropriate to maintain selection of resistance markers. For short-term storage, plates were kept up to two weeks at 4°C. For long-term storage, a dense culture was stocked in BHI supplemented with 20% glycerol and stored at -80°C.

Strains	Relevant properties or genotype[a]	Source
Enterococcus faecalis		
OG1RF	Plasmid-free, virulent laboratory strain isolated from the oral cavity	Dunny *et al*., 1978
OG1RF Δ*atlA*	OG1RF mutant harbouring a deletion of *atlA*	Salamaga et al., 2017
OG1RF GFP	OG1RF carrying pMV158-*gfp*, Tet^R	Prajsnar et al., 2013
OG1RF Δ*atlA* GFP	OG1RF D*atlA* carrying pMV158-*gfp*, Tet^R	This study
JH2-2	Plasmid-free laboratory strain	Jacob and Hobbs, 1974
JH2-2 Δ*atlA*	JH2-2 mutant harbouring an in-frame deletion of *atlA*	Mesnage et al., 2008
JH2-2 P$_{atlA}$::*atlA-his*	JH2-2 producing a C-terminally His-tagged AtlA under the *atlA* promoter	Salamaga et al., 2017

JH2-2 P$_{atlB}$::*atlB-his*	JH2-2 producing a C-terminally His-tagged AtlB under the *atlB* promoter	This study
JH2-2 P$_{atlA}$::*atlB-his*	JH2-2 producing a C-terminally His-tagged AtlB under the *atlA* promoter	This study
JH2-2 *atlA*$_\Delta$$_N$	JH2-2 producing AtlA without its N-terminal domain	Salamaga et al., 2017
JH2-2 *atlA$_{1-4}$*$_\Delta$$_N$	JH2-2 *atlA*D$_N$ derivative producing AtlA lacking the last two C-terminal LysM repeats	This study
JH2-2 Δ*gtfAB*	JH2-2 derivative with an in-frame deletion of the *gtfAB* operon (*EF2890-EF2891*)	Salamaga et al., 2017
JH2-2 Δ*gtfAB atlA$_{1-4}$*	JH2-2 D*gtfAB* derivative producing AtlA lacking the last two C-terminal LysM repeats	This study
JH2-2 *atlA**	JH2-2 producing AtlA with a catalytic domain flanked by NcoI and BamHI sites	Salamaga et al., 2017
JH2-2 *atlA$_{AtlB}$*	JH2-2 *atlA** derivative producing AtlA with *N*-acetylmuramidase activity	Salamaga et al., 2017
JH2-2 *atlA$_{Ami}$*	JH2-2 *atlA** derivative producing AtlA with amidase activity	Salamaga et al., 2017
JH2-2 *atlA$_{Cse}$*	JH2-2 *atlA** derivative producing AtlA with endopeptidase activity	Salamaga et al., 2017
JH2-2 *atlA$_{1-5}$*	JH2-2 producing AtlA with a LysM domain lacking the last C-terminal LysM repeat	This study
JH2-2 *atlA$_{1-4}$*	JH2-2 producing AtlA with a LysM domain lacking the last two C-terminal LysM repeats	This study
JH2-2 *atlA$_{1-3}$*	JH2-2 producing AtlA with a LysM domain lacking the last three C-terminal LysM repeats	This study
JH2-2 *atlA$_{1-2}$*	JH2-2 producing AtlA with a LysM domain lacking the last four C-terminal LysM repeats	This study
JH2-2 *atlA$_1$*	JH2-2 producing AtlA with a LysM domain lacking the last five C-terminal LysM repeats	This study
JH2-2 *atlA*$_{1-6HB}$	JH2-2 producing AtlA with a LysM domain consisting of LysM modules from AtlB	This study
JH2-2 *atlA$_{E212Q}$*	JH2-2 producing AtlA with a point mutation (E212Q) in the catalytic domain	Laboratory collection
JH2-2 *atlA$_{1-6}$-gfp*	JH2-2 producing AtlA fused with GFP via a12 aa linker	This study
JH2-2 *atlA$_{1-5}$-gfp*	JH2-2 *atlA$_{1-5}$* derivative producing AtlA$_{1-5}$ fused with GFP via a12 aa linker	This study
JH2-2 *atlA$_{1-4}$-gfp*	JH2-2 *atlA$_{1-4}$* derivative producing AtlA$_{1-4}$ fused with GFP via a 12 aa linker	This study
JH2-2 *atlA$_{1-3}$-gfp*	JH2-2 *atlA$_{1-3}$* derivative producing AtlA$_{1-3}$ fused with GFP via a 12 aa linker	This study
JH2-2 *atlA$_{1-2}$-gfp*	JH2-2 *atlA$_{1-2}$* derivative producing AtlA$_{1-2}$ fused with GFP via a 12 aa linker	This study
JH2-2 *atlA$_1$-gfp*	JH2-2 *atlA$_1$* derivative producing AtlA$_1$ fused with GFP via a 12 aa linker	This study
JH2-2 *atlA*$_{1-6HB}$-*gfp*	JH2-2 *atlA*$_{1-6HB}$ derivative producing AtlA$_{1-6HB}$ fused with GFP via a 12 aa linker	This study

JH2-2 Δ*admA*	JH2-2 mutant harbouring an in-frame deletion of *atlA*	This study
JH2-2 Δ*admA*/pTetH-*admA*	JH2-2 Δ*admA* carrying pTetH *admA*, Ery^R	This study
Escherichia coli		
TG1 *repA+*	TG1 derivative harbouring *RepA* for pGhost propagation at 37°C	P. Serror

Table 2.2 Bacterial strains used in this study

Ery^R, erythromycin resistant; Tet^R, tetracycline resistant.

2.5.2 Plasmids

Plasmids used in this study are listed in Table 2.3. All plasmid DNAs were purified using the GeneJET Plasmid Mini kit (Thermo Scientific).

Plasmid	Relevant genotype/selection markers	Source
pGhost9	Thermosensitive plasmid for targeted gene replacement in *E. faecalis*; Ery^R. Replicative in *E. coli* and *E. faecalis*	Maguin et al., 1992
pGBBhis	pGhost derivative for expression of His-tagged AtlB in *E. faecalis*; Ery^R	This work
pGABhis	pGhost derivative for the expression of His-tagged AtlB under the control of the *atlA* promoter; Ery^R	This work
pGAtlA$_{1-5}$	pGhost9 derivative used to delete the last C-terminal LysM repeat; Ery^R	This work
pGAtlA$_{1-4}$	pGhost9 derivative used to delete the last two C-terminal LysM repeats; Ery^R	This work
pGAtlA$_{1-3}$	pGhost9 derivative used to delete the last three C-terminal LysM repeats; Ery^R	This work
pGAtlA$_{1-2}$	pGhost9 derivative used to delete the last four C-terminal LysM repeats; Ery^R	This work
pGAtlA$_1$	pGhost9 derivative used to delete the last five C-terminal LysM repeats; Ery^R	This work
pGAtlA$_{1-6HB}$	pGhost9 derivative used to replace AtlA LysM repeats with AtlB LysM modules; Ery^R	This study
pGAtlA$_{1-6}$-GFP	pGhost9 derivative used to introduce an AtlA-GFP fusion; Ery^R	This study
pGAtlA$_{1-5}$-GFP	pGhost9 derivative used to introduce an AtlA$_{1-5}$-GFP fusion; Ery^R	This study
pGAtlA$_{1-4}$-GFP	pGhost9 derivative used to introduce an AtlA$_{1-4}$-GFP fusion; Ery^R	This study
pGAtlA$_{1-3}$-GFP	pGhost9 derivative used to introduce an AtlA$_{1-3}$-GFP fusion; Ery^R	This study
pGAtlA$_{1-2}$-GFP	pGhost9 derivative used to introduce an AtlA$_{1-2}$-GFP fusion; Ery^R	This study
pGAtlA$_1$-GFP	pGhost9 derivative used to introduce an AtlA$_1$-GFP fusion; Ery^R	This study
pGAtlA$_{1-6HB}$-GFP	pGhost9 derivative used to introduce an AtlA$_{1-6HB}$-GFP fusion; Ery^R	This study

pGAdmA	pGhost9 derivative carrying an in frame deletion of *admA*; Ery^R	This study
pGAdmA-GFP	pGhost9 derivative used to introduce an AdmA-GFP fusion; Ery^R	This study
pTetH-*admA*	pTet derivative encoding *admA* under the tet inducible promoter; Ery^R	L. Brown
pMK-RQ-6HB-GFP	pMK derivative encoding 398 bp of the AtlA catalytic domain followed by a 1209 bp fragment encoding three pairs of LysM$_{B1}$ and LysM$_{B2}$ from AtlB preceded by linkers from AtlA and a 717 bp fragment encoding GFP; Kan^R(*E. coli*)	GeneArt
pMK-5LysM	pMK derivative encoding the AtlA catalytic domain (507 bp), five LysM$_A$ modules (1029 bp) and 253 bp downstream of the *atlA* stop codon; Amp^R(*E. coli*)	GeneArt
pMV158-*gfp*	pMV158 derivative encoding GFP; Tet^R (*E. faecalis*)	Nieto and Espinosa, 2003

Table 2.3 Plasmids used in this study

Amp^R, ampicillin resistant; Ery^R, erythromycin resistant; Kan^R, kanamycin resistant; Tet^R, tetracycline resistant.

2.5.3 Growth conditions of *E. faecalis*

Strains were streaked out from glycerol stocks and grown on BHI-agar plates. A single colony from the fresh streak was used to inoculate BHI. Cells were grown in standing cultures overnight at 37°C unless otherwise stated. Exponential cultures were prepared from overnight cultures at a starting OD$_{600}$ of ~0.02 until log phase (OD$_{600}$ 0.5-0.6) was reached, unless otherwise stated.

2.5.4 Growth conditions of *E. coli*

Strains were streaked from glycerol stocks and grown on BHI-agar plates. A single colony from the fresh streak was used to inoculate BHI. The cells were grown overnight with agitation (200 rpm) at 37°C, unless otherwise stated. Growth media contained antibiotics, where appropriate.

2.5.5 Determining bacterial cell density

In order to quantify the optical density of a bacterial culture, spectrophotometric measurements at 600 nm (OD$_{600}$) were performed. If necessary, dilutions of culture samples were made in an appropriate culture medium to give a reading between 0.1 and 0.9.

2.6 *In vitro* DNA manipulation techniques

2.6.1 Primer design

Primers were synthesised by Eurofins MWG Operon. Primers were resuspended in nucleases free H_2O (nfH_2O) and stored as 100 μM master stocks or 10 μM working stocks at -20°C. Primers used in this study are listed in Table 2.4.

Oligonucleotides	Sequence 5'→3'	Enzyme
BBH_H11	AAACTCGAGCAACTGGCGAAGCTATTCCAGATTG	XhoI
BBH_H12	CTTATTTCTTAGTGGTGATGGTGATGATGATAATTCAATGTTTGGCCAGGA	
BBH_H21	GAATTATCATCATCACCATCACCACTAAGAAATAAGTAAAAGACCTACTTCTC	
BBH_H22	AAAGAATTCAGAAGCAATGCCTCTGCCTCTATAG	EcoRI
pGhost_up	GTCACGACGTTGTAAAACGACGG	
pGhost_dn	CTAGCGGACTCTAGAGGATCCCA	
BBH_DCO1	AGCTTCCTTAAATGGGTTGGTAAATC	
BBH_DCO2	GTCTTTTACTTATTTCTTAGTGGTGATG	
ABH_1	CCCCTCGAGTTCGTTCCGTCAATTCAA	XhoI
ABH_2	CAGGAATTCCTTGTCCAGATGGATAGGGAAACATAT	EcoRI
AtlA_up	CCGCTCCCTCTTTCTACACGATTC	
AtlA_dn	CTCTTTGTGATTGTAGCTCATG	
CatH11	CTTAACTCAATATGATACACCATCCATGGGTG	NcoI
AtlA1_H12	ACCAGATCTTTTTTTCACGATAAGTTTTTGACCAACG	BglII
AtlA1-2_H12	AGATCTTTTTTTCACGATGAGTTTTTGACCAACGAAAATTAAATC	BglII
AtlA1-3_H12	ATCAAGATCTTTTTTTCACAATAATTTTTTGACCAGCGAAG	BglII
AtlA_5'	AAGGAAAGTTGGGGACGTATCAATG	
AtlA1-6_H1	CCATCCATGGGTGGAAATACTGGGGGCGGAACAG	NcoI
AtlA1-6_H2	TCCGGATCCACCAACTTTTAAAGTTTGACCAATATAAATTG	BamHI
AdmA_H11	AAACTCGAGTCTAAAATGTGACGAGCAGCAATTTC	XhoI
AdmA_H12	CGCTCCACTTCCTGAACCACCGACGATTACACCGACCATTC	
AdmA_H21	GGTTCAGGAAGTGGAGCGATTAAATAAAAAAAGAACCAGCGT	
AdmA_H22	TATGAATTCGTTTAGCCCGTTTATTTCAACAATATTTGAC	EcoRI
AdmA_up	GTGTCACTGAAGAAGAATTACGTGGATAC	
AdmA_dn	CTTGCTTCTCTTTACTTCAACTACAGCTC	
AdmA-GFP_H11	AAACTCGAGAATGCCTATGAAAAGTATACCTCTTTGGTC	XhoI
AdmA-GFP_H12	TCCTCCACTACCTGATCCTCCTTTAATCGCTTTAAAATAATGAAGTGGTTC	
AdmA-GFP_H21	GGATCAGGTAGTGGAGGAAGCAATAATATGAGTAAAGGAGAAGAACTTTTCAC	
AdmA-GFP_H22	GTACGCTGGTTCTTTTTTTATTTGTATAGTTCATCCATGCCATG	
AdmA-GFP_H31	CAAATAAAAAAAGAACCAGCGTACCCGCT	
AdmA-GFP_H32	GATGAATTCGAATAGTTTAGCCCGTTTATTTCAAC	EcoRI

Table 2.4 Oligos used in this study. Underlined are sites recognised by restriction enzymes.

2.6.2 PCR amplification

2.6.2.1 Phusion polymerase

PCR amplification reactions were performed using Phusion High Fidelity Master Mix (2x) (Thermo Scientific) where 3'-5' proofreading activity was required. A final reaction volume of 50 μl contained:

Phusion High Fidelity Master Mix (2x)	25 μl
Forward primer (10 μM)	2.5 μl

Reverse primer (10 µM)	2.5 µl	
Template DNA	50-100 ng	
Sterile nfH$_2$O	up to 50 µl	

PCR amplification was carried out in a Bio-Rad T100 thermal cycler. The following reaction conditions were used:

Initial denaturation	98°C	30 s
Denaturation	98°C	10 s
Annealing	55-65°C	10 s
Extension	72°C	15-30 s/kb, go to denaturation step, 32x
Final extension	72°C	3-5 min

PCR products were analysed by agarose gel electrophoresis (2.6.5).

2.6.2.2 Taq polymerase

Home-made Taq Master Mix (2x) (provided by Stéphane Mesnage) was used to perform PCR reactions where accurate amplification was not required. A final reaction volume of 50 µl contained:

Home-made Taq Master Mix (2x)	25 µl	
Forward primer (10 µM)	2.5 µl	
Reverse primer (10 µM)	2.5 µl	
Template DNA	50-100 ng	
nfH$_2$O	up to 50 µl	

PCR amplification was carried out in a Bio-Rad T100 thermal cycler. The following reaction conditions were used:

Initial denaturation	95°C	1 min
Denaturation	95°C	30 s
Annealing	50-60°C	30 s
Extension	72°C	1 min/kb, go to denaturation step, 32x
Final extension	72°C	5-7 min

PCR products were analysed by agarose gel electrophoresis (Section 2.6.5)

2.6.2.3 Colony PCR screening of *E. coli*

The PCR reaction mixture was prepared as described in Section 2.6.2.2, without the addition of template DNA. Using a sterile pipette tip, a single colony was transfered into the PCR reaction tube. The PCR reaction was performed as described above.

2.6.2.4 Colony PCR screening of *E. faecalis*

The cells from a single colony were transferred into a PCR tube and heated in a microwave oven for 4 min using low heating settings. The treated cells were resuspended in 50 μl of nfH$_2$O and incubated for 10 min at 98$^{\text{o}}$C. The PCR reaction mixture was prepared as described in Section 2.6.2.1, using 10 μl of the cell lysate as a template. The PCR reaction was performed as described above.

2.6.3 Restriction endonuclease digestion

Digestion of DNA was performed according to the manufacturer's instructions, using the buffers supplied. The reaction mixtures were incubated at 37$^{\text{o}}$C for 60 min. For cloning purpouse the digested DNA was purified (Sections 2.7.3 and 2.7.4).

2.6.4 DNA ligation

After restriction enzyme digestion and purification DNA fragments were mixed as follows:

Vector DNA	30 ng
Insert	3 fold molar excess of vector DNA
T4 DNA ligase	0.5 μl (100 U)
T4 DNA ligase buffer (10x)	1 μl
nfH$_2$O	up to 10 μl

The reaction mix was incubated at room temperature over night. The ligation products were used to transform competent *E. coli* cells (Section 2.11.1).

2.6.5 Agarose gel electrophoresis

DNA samples were resolved in a 1% (w/v) agarose gels stained with 20 ng ml^{-1} SYBR safe (Invitrogen) prepared in DMSO. A 10x DNA loading dye (Thermo Scientific) was added to the DNA samples before loading into the wells of the gel. The DNA fragments were separated for 30 min at 100 V. DNA was visualised using an UV transilluminator at 305 nm. The size of DNA fragments was estimated by comparison with the fragments of a 1kb DNA ladder (New England Biolabs) that was loaded along with the samples.

2.6.6 DNA sequencing

Plasmids were sequenced by GATC Biotech. Sequencing results were analysed using SnapGene v.3.0.3.

2.6.7 Determining DNA concentration

DNA concentrations were determined using a NanoDrop 3300 fluorospectrometer. The blank measurement was taken for 1 μl solution used for DNA elution (nfH$_2$O). 1 μl of the sample was used to measure DNA concentration at 260 nm.

2.7 DNA purification techniques

2.7.1 Genomic DNA purification

Genomic DNA was isolated and purified using a QIAGEN DNeasy Blood & Tissue kit. 2 ml of an overnight culture of *E. faecalis* were spun for 5 min at 17,000 rcf. The cell pellet was resuspended in 195 μl of 50 mM phosphate buffer (pH 6.0). Next, 5 μl of 5 mg ml^{-1} mutanolysin was added and the sample was incubated at 37°C for 1 h. Genomic DNA extraction was then carried out following the manufacturer's instructions.

2.7.2 Plasmid purification

Plasmid purification from *E. coli* was performed using a GeneJET Plasmid Mini kit (Thermo Scientific) using 5 ml of overnight cultures. Manufacturer's instructions were followed except the volume of the overnight culture used for plasmid extraction.

2.7.3 Gel extraction of DNA

UViewer (Bio-Rad) was added to the DNA samples before separation on a 1% (w/v) TAE agarose gel. The required band was excised from the gel using a clean scalpel under UV exposure (305nm). DNA was extracted from the agarose gel slice using a GeneJET Gel extraction kit (Thermo Scientific). Manufacturer's instructions were followed.

2.7.4 Purification of PCR products

PCR products were purified using a GeneJET PCR purification kit (Thermo Scientific) according to manufacturer's instructions.

2.8 Protein analysis

2.8.1 Preparation of whole cell lysates (crude extracts)

E. faecalis cells were grown in 50 ml BHI to an OD_{600} of 0.3 - 0.5, unless otherwise stated. Cells were harvested by centrifugion at 5,000 rcf for 10 minutes at room temperature and washed twice in PBS. Cells were resuspended in 0.5 ml of PBS and transferred to chilled lysing matrix tubes containing 200 µl of glass beads ($\geq$ 106 µm, Sigma). Cells were broken using an MP Biomedicals FastPrep 24 Homogeniser for 6 cycles of 45 seconds, at the maximum speed, with 5 min incubation on ice between each cycle. The lysates were cooled on ice for 15 min and the FastPreap beads were allowed to settle. The supernatant was recovered and stored at -20°C until needed.

2.8.2 Precipitation of proteins form culture supernatants

E. faecalis cells were grown in 50 ml BHI to an OD_{600} of 0.3 - 0.5, unless otherwise stated. Following centrifugation at 5,000 rcf for 10 minutes at room temperature, proteins from supernatants were precipitated with TCA at a final concentration of 10% (w/v) by incubation on ice for 10 min. Samples were centrifuged at 5,000 rcf for 15 min at room temperature and the pellet was washed twice with ice-cold 100% (v/v) acetone. The pellet was air-dried and resuspended in 250 µl SDS-PAGE loading buffer 1x.

2.8.3 SDS-PAGE

Cell lysates, supernatants and co-extraxted proteins were analysed using the Laemmli SDS-PAGE method. A resolving gel was prepared as follows:

SDS-PAGE 10% (w/v) resolving gel:

dH$_2$O	4 ml
1.5 M Tris-HCl pH 8.8	2.5 ml
10% (w/v) SDS	100 µl
30% (w/v) acrylamide/bis (37.5:1)	3.5 ml
10% (w/v) APS	100 µl
TEMED	20 µl

All components were mixed except for N,N,N'N'-tetramethyl-ethylenediamine (TEMED), which was added last to the mixture. After the addition of TEMED the components were mixed gently and immediately poured between the glass plates of a gel casting apparatus (Mini-Protean Tetra cell gel slabs, Bio-Rad). A layer of 100% (v/v) isobutanol was pipetted onto the top of the gel to isolate it from the air. Once the gel had set the isobutanol was drained using filter paper. A stacking gel was prepared as follows:

SDS-PAGE 4% (w/v) stacking gel:

dH$_2$O	3.6 ml
0.5 M Tris-HCl pH 6.8	0.75 ml
10% (w/v) SDS	50 µl
30% (w/v) acrylamide/bis (37.5:1)	0.65 ml
10% (w/v) APS	50 µl
TEMED	20 µl

All components were mixed except for N,N,N'N'-tetramethyl-ethylenediamine (TEMED), which was added last to the mixture. Stacking gel components were mixed and poured gently on top of the resolving gel. A plastic comb was inserted into the gel in order to create wells. Once the stacking gel had set, the gel was transferred to a Bio-Rad tank and submerged in 1x SDS-PAGE working buffer. Samples were mixed with 5x SDS-PAGE loading buffer, incubated at 95°C for 10 min and an appropriate volume was loaded into the wells. From 2-5 µl of protein ladder was loaded along with the samples. Proteins were separated by electrophoresis at 180 V until the blue dye front of the sample buffer reached the base of the gel plate.

2.8.4　Coomassie staining

After electrophoresis, SDS-PAGE gels were soaked in Coomassie Blue stain overnight and destained in Coomassie destain solution for 4 h or until the background was clear. Molecular sizes of proteins were estimated by comparison to the protein standards of known molecular weight.

2.8.5　Western blotting

Protein samples were separated in denaturing conditions in a 10% (w/v) SDS-PAGE gel. Following SDS-PAGE, the samples were transferred onto Hybond ECL Nitrocellulose Membrane (GE Healthcare) by electroblotting using a wet transfer at 100 V for 90 min. After the transfer, the membrane was blocked in blocking buffer (Section 2.2.7.3) at room temperature for 1 h with gentle shaking. The membrane was washed three times with 1x TBST for 10 min and incubated in blocking buffer containing primary antibodies at an appropriate dilution overnight at 4°C with gentle shaking. To remove unbound antibodies, the blot was washed three times with 1x TBST for 10 min. The membrane was then incubated in blocking buffer containing 1:10,000 peroxidase conjugated secondary antibodies for 1 h with gentle shaking. After three washes with 1x TBST for 10 min, the blot was drained and revealed using a SuperSignal West Pico Chemiluminescent Substrate (ThermoScientific) and imaged using ChemiDoc MP Imaging System (Bio-Rad).

2.8.6　Zymogram analysis

Proteins were separated in a 10% (w/v) SDSD-PAGE gel containing autoclaved *Micrococcus luteus* cells at an OD$_{600}$ of 2 as a substrate. The gel was incubated in dH$_2$O for 30 min to remove SDS. To renature proteins, the gel was incubated in renaturing buffer (pH 6.25 for AtlB or pH 7.4 for AtlA) at 37°C from 1 to 24 h.

2.9　Pull-down assay

2.9.1　Co-elution of potential partners interacting with LysM

300 µl of Ni-TA resin (Qiagen) was loaded onto a gravity flow column (G-Biosciences), washed with MilliQ H$_2$O and equilibrated twice with 3 ml of buffer A (Section 2.2.10.1). The resin was saturated with 2 mg of recombinant LysM domain containing 6 modules (provided by Stéphane Mesnage) in 50 mM phosphate buffer pH 7.5 supplemented with 100 mM NaCl. The resin with bound 'bait' was washed with 5

ml of buffer A. The soluble fraction of a whole cells lysate (Section 2.8.1) was loaded on the column. The resin was washed successively with 3 ml of buffer A and 5 ml of buffer A supplemented with 5 mM imidazole. The proteins were eluted with 1.5 ml of buffer B (Section 2.2.10.2) and fractions of around 0.5 ml were collected. The eluted proteins were analysed by SDS-PAGE.

2.9.2 Preparation of the samples for the mass spectrometry analysis

The eluted proteins (Section 2.9.1) were reduced by adding DTT to a final concentration of 1mM and incubation at 70°C for 10 minutes. Samples were cooled to room temperature and IAA was added to a final concentration of 2 mM. Samples were covered in aluminium foil and incubated for 30 minutes at room temperature. Proteins were loaded on a 4–15% (w/v) Mini-PROTEAN TGX Precast Protein Gel (Bio-Rad) and resolved as described above (Section 2.8.3). After SDS-PAGE, the gel was incubated in fixation solution for 30 minutes at room temperature and stained in a Colloidal Commassie solution until proteins could be detected. Next, the gel was destained in Colloidal Commassie destain for 2 h and washed in MilliQ water. Each gel line was cut out and further divided into three sections: below, above and at the bait size. Each fragment was cut into smaller fragments and transferred to a 2 ml eppendorf tube. The gel pieces were further destained by multiple 2 h incubations in 50% (v/v) acetonitrile in 50 mM ammonium bicarbonate pH 8.5 at room temperature. Destained gel fragments were soaked in 100% (v/v) acetonitrile for 15 minutes at room temperature. Trypsin was added to the samples to a final concentration of 0.1 mg ml^{-1}. Proteins were digested overnight at 25°C with gentle shaking. Peptides were extracted by subsequential incubations with 100% (v/v) acetonitrile and 0.5% (v/v) formic acid at 37°C for 15 minutes each time. The extracted peptides were vacuum dried and analysed on an Orbitrap Elite mass spectrometer (Thermo Fisher) by Dr Adelina Acosta Martin (University of Sheffield, biOMICS Facility).

2.10 DNA hybridisation techniques

2.10.1 Preparation of HRP labelled probe

DNA fragments obtained by PCR amplification were purified and labelled with HRP using an Amersham ECL Direct Nucleic Acid Labelling and Detection System (GE Healthcare).

2.10.2 Southern blotting

Chromosomal DNA was digested with restriction enzymes and DNA fragments were resolved in a 1% (w/v) agarose gel along with the a 1kb DNA ladder (New England Biolabs). After electrophoresis, the gel was incubated in a depurination solution for 10 min and washed 3 times 5 minutes in MilliQ H_2O. The gel was incubated in denaturation solution for 30 min and washed 3 times 5 minutes in MilliQ H_2O. The gel was neutralised by incubation in neutralisation solution for 30 min and washed 3 times 5 minutes in MilliQ H_2O. The gel was equilibrated in 20x SSC for 10 min. DNA was transferred from the gel to a Hybond-N+ Extra nylon membrane by capillary blotting overnight using 20x SSC as the transfer buffer.

2.10.3 Fixing DNA to the membrane

DNA was permanently fixed to the Amersham Hybond-N+ nylon membrane using a RPN 2500 UV crosslinker (Amersham) at 70 mJ cm^{-2} for 10 s. The membrane was rinsed with MilliQ H_2O and air-dried.

2.10.4 Hybridisation

The procedures were performed in a Techne Hybridiser HB-1D in a roller bottle. The membrane was prehybridised for 30 min at 42°C in pre-heated to 42°C ECL prehybridisation buffer (12.5 ml per 100 cm^2 of membrane). 30 µl of HRP labelled probe (Section 2.10.1) was added and the membrane was hybridised for 16 h at 42°C. The membrane was washed with 5x SSC wash solution at 55°C for 5 min. The membrane was then washed once for 20 min and twice for 10 min with 0.5x SSC wash solution at room temperature.

2.10.5 Detection of HRP labelled DNA

The membrane was drained from 0.5x SSC wash solution. The blot was covered with SuperSignal West Pico Chemiluminescent Substrate (Thermo Scientific) or Clarity ECL Western Blotting Substrate (Bio-Rad) and incubated for 2 min in dark. The membrane was drained from the excessive substrate, placed between two sheets of plastic and imaged using ChemiDoc MP Imaging System (Bio-Rad).

2.11 Transformation techniques

2.11.1 Transformation of *E. coli*

2.11.1.1 Preparation of *E. coli* electrocompetent cells

A single colony of *E. coli* TG1 $repA^+$ was used to inoculate 10 ml of SOB and incubated overnight at 37°C with agitation at 200 rpm. The overnight culture was used to inoculate 250 ml of fresh pre-warmed SOB in a 2l conical flask to an OD_{600} of 0.05 and grown at 37°C with shaking until log phase (OD_{600} 0.5-0.7). Cells were transferred on an ice bath and harvested by centrifugation (5,000 rcf, 20 min, 4°C) and washed twice by resuspension in 250 ml of ice-cold washing solution (Section 2.2.9.1) and centrifugation (5,000 rcf, 20 min, 4°C). Cells were resuspended in 1.25 ml of ice-cold washing solution. 75 µl aliquots were snap-frozen using liquid nitrogen and stored at -80°C.

2.11.1.2 Transformation of electrocompetent *E. coli* cells.

A 75 µl aliquot of *E. coli* TG1 $repA^+$ electrocompetent cells (Section 2.11.1.1) was thawed on ice. 5 ng of plasmid DNA or 4 µl of ligation reaction (Section 2.6.4) was added to the cells. The mixture was transferred into a pre-chilled 1 mm electroporation cuvette (Bio-Rad). Electroporation was carried out at 1.70 kV, 25 µF and 200 Ω using a GenePulser Xcell Electoporation system (Bio-Rad). Immediately 600 µl of SOC was added to the cuvette to recover cells. *E. coli* cells were incubated at 37°C with shaking at 250 rpm for 1 h. 100 µl aliquots were spread on selective BHI agar plates supplemented with an appropriate antibiotic. The plates were incubated at 37°C until colonies appeared.

2.11.2 Transformation of *E. faecalis*

2.11.2.1 Preparation of *E. faecalis* electrocompetent cells

A single colony of *E. faecalis* was used to inoculate 10 ml of M17-Glu and incubated overnight at 37°C without shaking. The overnight culture was used to inoculate 100 ml of fresh pre-warmed SGM17 in a 250 ml conical flask to an OD_{600} of 0.02 and grown at 37°C without shaking until log phase (OD_{600} 0.5-0.6). Cells were transferred on an ice bath and harvested by centrifugation (5,000 x g, 20 min, 4°C). Cells were washed three times by resuspension in 35 ml ice-cold Suc-Gly and centrifugation (5,000 x g, 20 min,

4°C). Cells were resuspended in 500 µl of Suc-Gly and 50 µl aliquots were snap-frozen in liquid nitrogen and stored at -80°C.

2.11.2.2 Transformation of electrocompetent *E. faecalis* cells

A 50 µl aliquot of electrocompetent *E .faecalis* cells (Section 2.11.2.1) was thawed on ice and 0.5-1 µg plasmid DNA was added. The mixture was transferred to a pre-chilled 1 mm electroporation cuvette (Bio-Rad). Electroporation was carried out at 2.4 kV, 25 µF and 200 Ω using a Gene Pulser Xcell Electoporation system (Bio-Rad). 1 ml ice cold SM17MC was added to the cuvette immediately after electroporation. Cells were incubated for 3 h at either 28°C (pGhost derivatives) or 37°C (non thermosensitive plasmids). 200 µl aliquots were spread on selective BHI agar plates and incubated at either 28°C or 37°C until colonies appeared.

2.12 Microscopy imaging

2.12.1 Fixing of cells for microscopy

Cell pellets were resuspended in 0.5 ml PBS. 0.5 ml of freshly prepared fixative (Section 2.2.5.3) was added and cells were incubated for 30 min at room temperature. Fixed cells were washed twice by resuspension in dH_2O and centrifugation (13,000 rcf for 1 min).

2.12.2 Immunostaining of cells for microscopy

Fixed cells (Section 2.12.1) were resuspended in blocking solution (Section 2.2.11.2) and incubated for 1 h at room temperature. Cells were washed in PBS and incubated with a primary antibody diluted at a 1:250 ratio in blocking solution overnight at 4°C. No primary antibody was added to a control sample. Cells were washed three times by resuspension in 0.5 ml of PBST (Section 2.2.11.1) and centrifugation (13,000 rcf for 1 min). Cells were incubated with a secondary antibody resuspended at a 1:400 ratio in blocking solution for 2 h at room temperature. After the incubation cells were washed twice by resuspension in 0.5 ml of PBST and centrifugation (13,000 rcf for 1 min) and additionally twice by resuspension in 0.5 ml of PBS and centrifugation (13,000 rcf for 1 min).

2.12.3 Labelling of peptidoglycan synthesis with HADA

A 1 ml aliquot of cells grown to early-exponential phase (OD_{600} ~0.1) was transferred to

a microcentrifuge tube. 5 µl of 100 mM HADA (hydroxycoumarin-carbonyl-amino-D-alanine; Department of Chemistry, University of Sheffield) was added to a final concentration of 500 µM and cells were incubated for 2 h at 37°C with shaking at 200 rpm. The cells were washed once with PBS and then fixed.

2.12.4 Labelling of membrane with FM4-64

Fixed cells were resuspended in 500 µlPBS. 1.5 µlof 1 mM FM4-64 dye (Invitrogen) was added to the sample. Cells were incubated with the dye for 30 min at room temperature. Stained cells were washed twice in MilliQ H_2O.

2.12.5 Preparation of samples for fluorescence microscopy

2.12.5.1 Preparation of cover slips

A high precision cover glass thickness no 1.5H was cleaned by sonicating in 1 M KOH for 15 min at room temperature. The coverslip was washed with MilliQ H_2O. The cover glass was submerged in 0.01% (w/v) poly-L-lysine solution (Sigma) and incubated for 30 min at room temperature. The coverslip was rinsed with dH_2O and dried with nitrogen.

2.12.5.2 Preparation of agarose pads

A gene frame (Life Technologies) was placed on a slide and filled with 100 µl of 2% (w/v) low melting point agarose in PBS. The agarose pad was covered with a coverslip and left to set.

2.12.5.3 Sample preparation for fluorescence microscopy

The samples were prepared by either:

- drying 5 µl of fixed cells onto a poly-L-lysine coated coverslip (Section 2.12.5.1). Cells attached to the cover slip were washed with MilliQ H_2O and dried with nitrogen. Cells were mounted on a glass slide with 5 µl PBS; or
- spotting 5 µl of fixed cells onto an agarose pad (Section 2.12.5.2). The agarose pad was sealed with a cover slip.

2.12.6 Conventional fluorescence microscopy

Fluorescence images were acquired using either a DeltaVision deconvolution microscope (Applied, precision, GE Healthcare) or a Nikon DualCam system (Elipse Ti

inverted research microscope). Images obtained by DeltaVision were denconvolved using SoftWoRx v.3.5.1 software. Appropriate filters and wavelengths used for visualisation of the fluorophores are listed in Table 2.5. Contrast and brightness adjustment and cell measurements were performed using ImageJ 1.49v.

Filter	Nikon DualCam	DeltaVision		Fluorophore
	Excitation wavelength (nm)	Excitation filter/bandpass (nm)	Emission filter/bandpass (nm)	
DAPI	395	360/40	457/50	HADA
FITC	470	492/20	528/38	GFP
RD-TR-PE/ TxRED	555	555/28	617/73	FM4-64
Cy5	640	640/20	685/40	AlexaFluor647

Table 2.5 Nikon DualCam light wavelengths and DeltaVision filter sets

2.12.7 SIM (Structured Illumination Microscopy)

3D-SIM was performed using the DeltaVision OMX (GE Healthcare) equipped with a Plan Apo 60x, 1.42 NA oil objective, using 1.514 immersion oil. Laser light was directed through a grating to generate a striped interference pattern on the sample plane. The pattern was shifted through five lateral phases and three angular rotations for each z-section (15 images per z-section). The z-sections were 0.125 μm in depth. Samples labelled with AlexaFluor647 were imaged using a 642 nm laser and a 683/40 emission filter. The raw data were reconstructed with SoftWoRx v.6.1.3 software. Data analysis was performed using a SIMcheck (Ball et al., 2015) plugin comprehensive with ImageJ. Contrast and brightness were adjusted using ImageJ 1.49v.

2.12.8 STORM (Stochastic Optical Reconstruction Microscopy)

Single molecule imaging of AlexaFluor647 was performed using an Olympus IX71 inverted optical microscope and a 60x, NA 1.4 oil immersion objective, a system described by Robert Turner (Turner et al., 2013). AlexaFluor647 imaging was performed using an OBIS 647 (120 mW) laser and a filter cube containing a 662 nm longpass dichroic filter and a 676/29 nm bandpass emission filter. A piezoelectric motor (Physik Instrumente) was used to adjust focus. An image expander comprising a 35 mm and 100 mm lens was used to project the image onto a Hamamatsu ImagEM camera set to acquire at 10-50 frames per second. Calibration data for 3D reconstructions was

obtained by recording images of TetraSpeck particles while stepping the objective piezo.

Image processing was conducted using methodology as previously described by others (Betzig et al., 2006; Huang et al., 2008). Data were processed by fitting Gaussian functions to individual molecule fluorescence, identified by very clear intrinsic blinks, using Matlab. Drift in the focal plane was corrected retrospectively by tracking a TetraSpeck beads throughout the acquisition sequence and offsetting localisations against its position.

2.13 Zebrafish model of infection

2.13.1 Ethics statement

Animal work was carried out according to guidelines and legislation set out in UK law in the Animals (Scientific Procedures) Act 1986 under Project License PPL 40/3574. Ethical approval was granted by the University of Sheffield Local Ethical Review Panel.

2.13.2 Zebrafish strains

London Wild Type (LWT) strain was used for all zebrafish experiments.

2.13.3 Zebrafish husbandry

Adult zebrafish were kept at $28^{\circ}C$ in a continuous re-circulating closed aquarium system with light day/night cycle of 14/10 hours, respectively. The embryos were kept in E3 1x (Section 2.13.4) at $28.5^{\circ}C$.

Zebrafish experiments were performed on embryos not protected under the Animals (Scientific Procedures) Act, as embryos used were younger than five days post fertilisation (dpf).

2.13.3.1 E3 10x

NaCl   50 mM

KCl   1.7 mM

$CaCl_2$ 3.3 mM

MgSO$_4$ 3.3 mM

To prevent fungal growth, E3 1x was supplemented with methylene blue at a final concentration of 0.00005% (w/v) (Nusslein-Volhard and Dahm, 2002).

2.13.4 Methylcellulose

3% (w/v) methylcellulose in prepared in E3 1x.

For full solubility of methylcellulose, the suspension was partially frozen, mixed and defrosted several times (Nusslein-Volhard and Dahm, 2002). The solution was aliquoted into 20 ml syringes and frozen for long-term storage. For use and short-term storage methylcellulose solution was kept at 28.5^{o}C.

2.13.5 Zebrafish anaesthesia

A stock solution of 0.4% (w/v) 3-amino benzoic acid ester (tricaine or MS322, Sigma) was prepared in 20 mM Tris-HCl (pH 7.0) and stored at -20°C. For use and short-term storage a working stock was kept at 4°C in the dark. Embryos were anaesthetized priory to bacterial injections in E3 1x supplemented with tricaine to a final concentration of 0.02% (w/v).

2.13.6 Microinjections of *E. faecalis* into zebrafish embryos

Exponentially growing *E. faecalis* cells were diluted in PBS prior to injection. Bacterial concentrations (CFU nl^{-1}) were determined by plating on BHI-agar 10 μl of a cell suspension diluted 250,000 times.

Zebrafish embryos (30 hpf) were manually dechorionated and anaesthetized by incubation in E3 1x supplemented with 0.02% (w/v) tricaine (Section 2.13.6). Embryos were immobilized in 3% (w/v) methylcellulose (Section 2.13.5). The electrode puller (World Precision Instruments, WPI) was used to make microinjection needles using the non-filament glass capillaries (Fisher Scientific Ltd). The bacterial sample was loaded to the microcapillary pipettes and the volume injected was calibrated using a graticule slide (approximately 1 nl). Individual embryos were injected to the circulation valley using a pneumatic micropump (World Precision Instruments PV820), a micromanipulator (World Precision Instruments) and a dissecting microscope (Olympus).

After the injections embryos were placed in fresh E3 1x in order to remove any remaining methylcellulose for 1 h. Washed embryos were transferred to a single well in a 96-well microtitre dish filled with E3 1x.

2.13.7 Determination of zebrafish embryo mortality following infection

For each experiment, at least 20 embryos were injected with *E. faecalis* (Section 2.13.7). Following infection, the survival of embryos was monitored up to 90 h post infection (hpi). The number of live and dead embryos was recorded at each time point (twice a day). Mortality was assumed by heart beat cessation.

2.13.8 Microscopy imaging of zebrafish embryos

2.13.8.1 Fixation of embryos

2.13.8.1.1 PFA solution

4% (w/v) paraformaldehyde in PBS

The solution was prepared by adding 4 g of paraformaldehyde to 80 ml of PBS. The solution was heated to 60°C while mixed vigorously. NaOH ($\geq$ 5 M) solution was added drop wise, with heating and vigorous mixing, until the solution cleared. The volume the solution was adjusted to 100 ml with PBS. The PFA solution was stored up to 3 months at 4°C.

2.13.8.1.2 Fixation

Anaesthetized embryos (Section 2.13.6) were transferred into ice-cold PFA solution (Section 2.13.9.1.1) for overnight incubation at 4°C.

2.13.8.2 Immunostaining of phagocytes

Fixed embryos (Section 2.13.9.1) were washed four times 20 minutes in PBS-TD (Section 2.2.2) and incubated in blocking solution (PBS-TD with 5% (v/v) sheep serum) for 1 hour at room temperature. Embryos were washed once in PBS for 20 minutes and incubated overnight at 4°C with rabbit anti-l-plastin antibodies (provided by S. Renshaw) suspended in blocking solution at a 1:400 dilution. The embryos were washed four times in blocking solution, 20 minutes each wash, and incubated with secondary anti-rabbit antibodies conjugated with AlexaFluor647 suspended in blocking solution for 2 hours at room temperature. After four 20 min washes in PBS, embryos

were fixed again in 4% (w/v) PFA (Section 2.13.9.1) overnight. Embryos were washed in PBS before microscopy visualisation.

2.13.8.3 Mounting samples for microscopy

Stained embryos were immersed in 1% (w/v) low melting point agarose (Sigma) solution in E3 1x (without methylene blue) and transferred to glass bottom petri dishes. Embryos were mounted flat on the glass bottom before the agarose solution solidified. PBS was used to cover embedded embryos.

2.13.8.4 Fluorescence microscopy of zebrafish embryos

Images of fluorescently labelled zebrafish embryos were collected using a spinning disc confocal Perkin Elmer Ultraview VoX inverted Olympus IX81 microscope equipped with an UplanSApo 20x (NA 0.8) objective and a Hammamatsu C9100-50 EM-CCD camera. Image acquisition was performed with the Volocity software and the images were processed with ImageJ 1.49v software.

2.13.9 PU.1 Morpholinos

The microcapillary pipet was loaded with a 1 mM solution of *pu.1* morpholino oligonucleotides (Table 2.6) and individual 1-2 cell stage embryo eggs were injected into the yolk sac using previously described equipment (Section 2.13.7).

MO against	Sequence (5'-3')	Quantity per embryo	Reference
pu.1	GATATACTGATACTCCATTGGTGGT	0.5 pmole	Rhodes et al., 2005

Table 2.6 List of morpholino oligonucleotides used in this study

2.14 Quantification of cells chain length

2.14.1 Flow cytometry analysis of cells chain length

Cells were grown over night without agitation at 37°C. Cells were diluted 1:100 in a fresh growth medium and grown in standing cultures to mid-exponential phase (OD$_{600}$~0.2-0.4). Bacterial cultures were diluted 1:100 in filtrated PBS and analysed by flow cytometry using Millipore Guava Easy Cyte system.

To measure the septum cleavage activity of recombinant proteins, the OG1RF Δ*atlA*

mutant was grown to exponential phase (OD_{600}~0.2) and collected by centrifugation. Cells were resuspended in filtered PBS containing various concentrations of recombinant proteins. Cell (chain) size distribution was determined by flow cytometry after 15 min of incubation at 37°C. Relative logarithmic values of forward scattered light (FSL log) were collected for 5,000 events and expressed as a percentage of the control strain incubated in the absence of enzyme.

2.14.2 Determination of the number of cells per chain

Cells from the expenentail phase of grow (OD_{600}~0.4) were harvested and fixed (Section 2.12.1). The microscopy samples were prepared as described in the sections 2.12.5.1 and 2.12.5.3. The samples were imaged using conventional light microscopy. Fiji software was used to optimise contrast of the bright-field images. The number of cells per chain was counted manually.

CHAPTER 3

The mechanisms controlling activity of *N*-acetylglucosaminidase, AtlA in *Enterococcus faecalis*

3.1   Comparative analysis of AtlA and AtlB production levels

Four PG hydrolases (EnpA, AtlA, AtlB and AtlC) were identified in *E. faecalis* by zymogram. An *N*-acetylglucosaminidase, AtlA plays predominant role in septum cleavage. Two *N*-acetylmuramidases, AtlB and AtlC can cleave the septum in the absence of AtlA with much lower efficiency (Mesnage et al., 2008). The biological specialisation of AtlA can dependent on the production level of this hydrolase

To compare AtlA and AtlB production levels, we constructed two strains producing AtlA or AtlB tagged to a polyhistidine tag and expressed under their promoters. An isogenic derivative of JH2-2 strain producing C-terminally tagged AtlA under the native *atlA* promoter (JH2-2 $P_{atlA}::atlA$-*his*) was present in the laboratory strain collection. To construct the strain producing a C-terminally tagged AtlB, a pGhost 9 derivative (pGBBH) was designed (Figure 3.1 A). First, two fragments (H1, 487 bp and H2, 467 bp) corresponding to the fragment encoding 3' end of *atlB* and the downstream region of *atlB* stop codon, were PCR amplified using two sets of primers BBH11/BBH12 and BBH21/BBH22 (Figure 3.1 B). The H1 and H2 fragments were fused by PCR using BBH11 and BBH22 primers (Figure 3.1 C), thereby introducing XhoI and EcoRI flanking restriction sites and a sequence encoding 6 histidine residues before *atlB* STOP codon. The amplification product was cut with XhoI and EcoRI and ligated to pGhost9. Following a transformation of *E. coli* TG1 *repA+* with the ligation product, transformants were screened by PCR using pGhost_up and pGhost_dn primers (Figure 3.1 D). The plasmid was extracted from a clone that gave the expected product size (1058bp). The final plasmid pGBBH was sent for sequencing to check the absence of mutations in the insert.
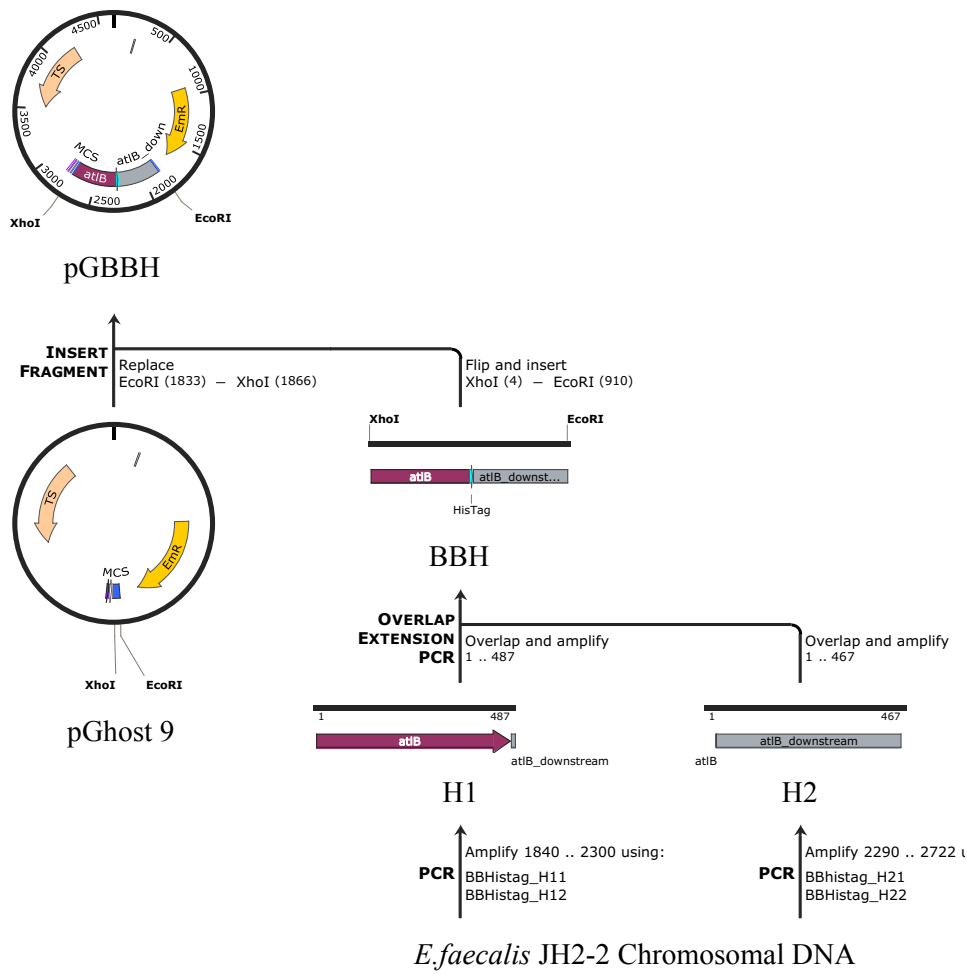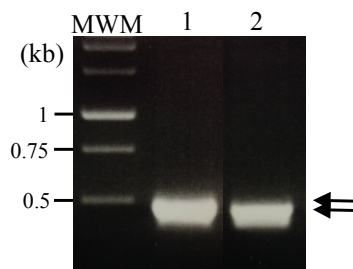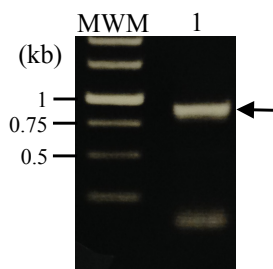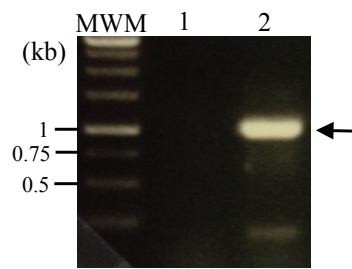
Figure 3.1 Construction of pGBBH

A.   A schematic representation of the cloning strategy. The homology fragments, H1 and H2 were amplified and fused by PCR to create an insert containing the fragment encoding 3'end of *atlB* (burgundy) fused to a 6 histidine tag (blue) and 430 nt downstream of *atlB* stop codon (grey). The insert was digested with XhoI and EcoRI and ligated into pGhost 9.

B. Amplification products corresponding to the fragment H1 (amplified with oligos BBH_H11 and BBH_H12, lane 1) and fragment H2 (amplified with oligos BBH_H21 and BBH_H22, lane 2). The expected DNA bands sizes of 487 bp and 467 bp are indicated with black arrows. The sizes of chosen molecular weight markers (MWM) are indicated on the left hand side of the gel.

C. Amplification product resulting from the fusion of the fragments H1 and H2 amplified with oligos BBH_H11 and BBH_H22 (lane 1). The expected DNA band size of 918 bp is indicated by a black arrow. The sizes of chosen molecular weight markers (MWM) are indicated on the left hand side of the gel.

D. Amplification products using primers pGhost_up and pGhost_dn for the negative (lane 1) and positive (lane 2) colonies. The expected DNA band size of 1058 bp for the positive colony is indicated by a black arrow. The sizes of chosen molecular weight markers (MWM) are indicated on the left hand side of the gel.
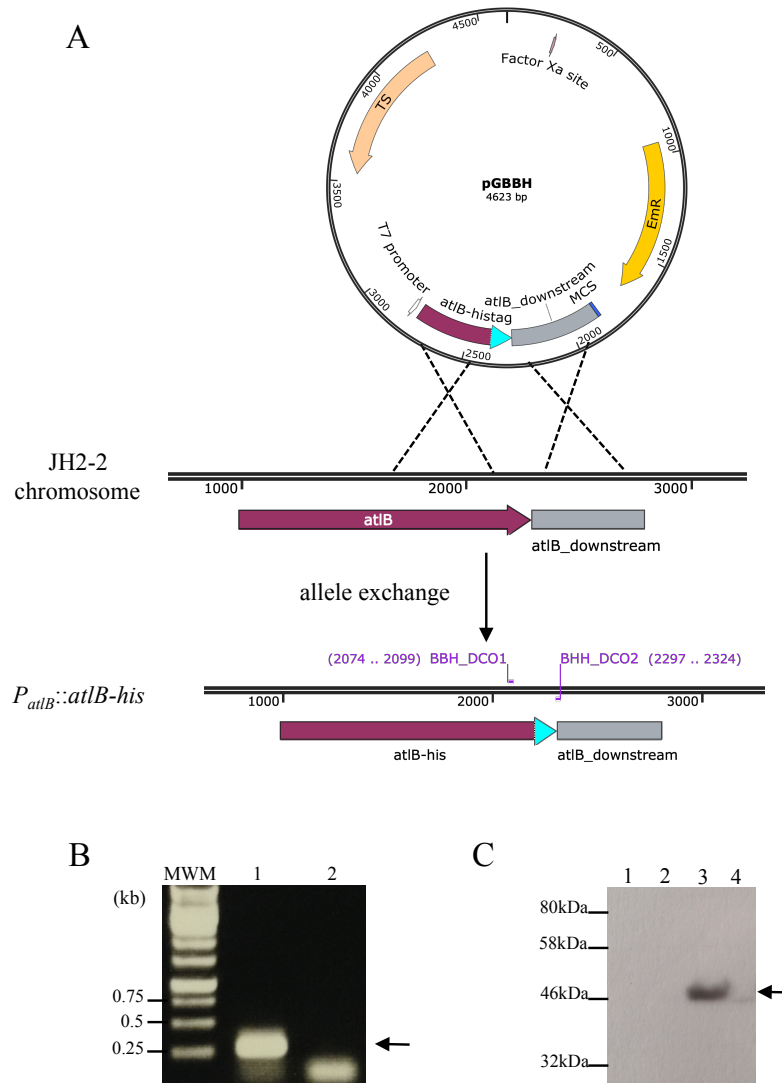
Figure 3.2 Construction of an *E. faecalis* JH2-2 derivative producing AtlB with a C-terminal polyhistidine tag

A. Construction of recombinant strain JH2-2 P_{atlB}::*atlB-his* by allele exchange using pGBBH.

B. Amplification products using primers BBH_DCO1 and BBH_DCO2 for positive (lane 1) and negative (lane 2) colonies. The expected DNA band size of 251 bp for the positive colony is indicated by a black arrow. The sizes of chosen molecular weight markers (MWM) are indicated on the left hand side of the gel.

C. Western blot detection of his-tagged proteins in *E. faecalis* JH2-2 (parental strain; WT) and the putative mutant P_{atlB}::*atlB-his*. Proteins precipitated from supernatants (lane 1, WT; lane 3, the mutant) and crude extract (lane 2, WT; lane 4, the mutant) were probed with anti-His polyclonal (rabbit) antibodies. The expected band size of 45.8 kDa for AtlB-HisTAG fusion is indicated with the black arrow. The sizes of chosen molecular weight markers are indicated on the left hand side of the blot.

pGBBH was transferred in *E. faecalis* JH2-2 by electroporation. The mutation was introduced on the chromosome by allele exchange to generate strain $P_{atlB}::atlB$-*his* (Figure 3.2 A). Erythromycin sensitive colonies were analysed by PCR using primers BBH_DCO1 and BBH_DCO2. The reverse primer, BBH_DCO2 has the 3' end homologous to the polyhistidine motif that only allows amplification in the mutants, giving a 251 bp PCR product (Figure 3.2 B).

A putative $P_{atlB}::atlB$-*his* mutant identified by PCR was analysed by Western Blot using anti-His antibodies to detect tagged AtlB (Figure 3.2 C). As expected, no signal was detected for the WT samples suggesting a high specificity of used antibodies in the conditions used. A band around 46kDa corresponding to expected size of AtlB-Histag (45.8kDa) was detected in supernatant and crud extract fractions (a faint band) for $P_{atlB}::atlB$-*his*.

The production level of AtlA and AtlB was compared by Dot blot using anti-his antibodies. The JH2-2 parental strain and isogenic derivatives ($P_{atlA}::atlA$-*his* and $P_{atlB}::atlB$-*his*) were grown in BHI broth in standing cultures. Cells and supernatant samples were harvested at early exponential phase ($OD_{600} \sim 0.3$), late exponential phase ($OD_{600} \sim 1$) and stationary phase ($OD_{600} \sim 1.8$) (Figure 3.3 A). Bacteria were centrifuged and resuspended in phosphate buffer contains an EDTA-free protease inhibitors cocktail. Cells were lysed in present of mutanolysin and DNAse from bovine serum. Lysates and supernatant fractions corresponding to the equivalents of 1000 µl, 500 µl, 250 µl, 125 µl, 62.5 µl, 31.2µl and 15.6 µl of culture were loaded on a membrane. His-tagged AtlA and AtlB were detected by dot blotting using an anti-His serum (Figure 3.3 B). The dot blot results for the lysed cell (Figure 3.3 B (i)) showed overall low signal detection. There was a weak signal in the early and late exponential phase for WT. No histidine motif was detected in the stationary phase sample for this strain. A similar pattern to WT was detected for the $P_{atlB}::atlB$-*his* samples, suggesting that very little (if any) AtlB-his protein was present in lysates. A small increase in signal intesity was observed for the $P_{atlA}::atlA$-*his* samples as compared to the parental strain. The his-tagged AtlA protein was present in each tested time points (Figure 3.3 B (ii)). A minor background was detected for the WT supernatant, whereas the analysis of the supernatant fractions of $P_{atlA}::atlA$-*his* showed strong signal (Figure 3.3 B (ii)).
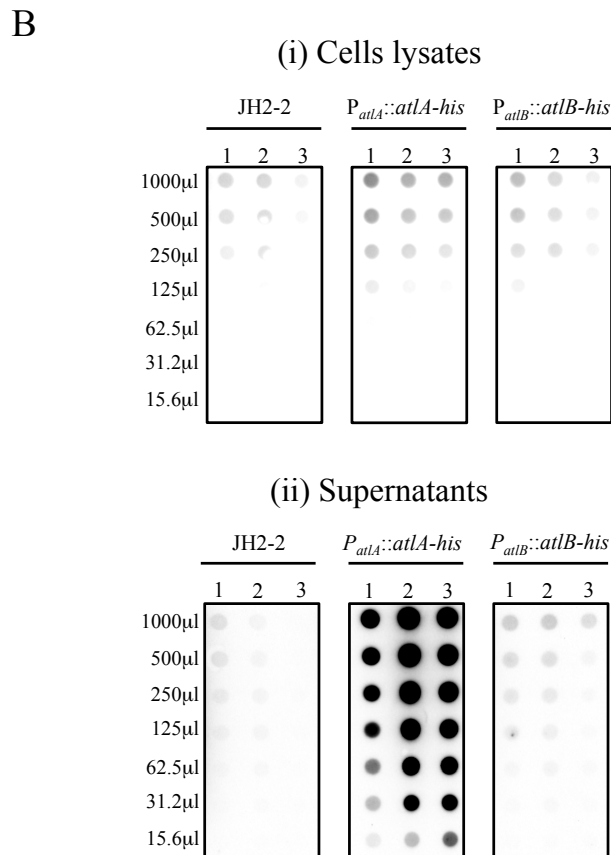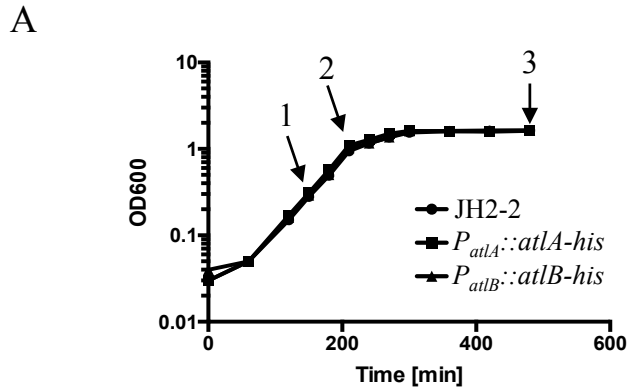
Figure 3.3 Comparative analysis of C-terminally tagged AtlA and AtlB production level in *E. faecalis* P_{atlA}::*atlA-his* and P_{atlB}::*atlB-his*, respectively

A. Grow curves of *E. faecalis* JH2-2, P_{atlA}::*atlA-his* and P_{atlB}::*atlB-his* derivatives. Cells were grown in BHI media in standing cultures at 37°C. Culture samples were harvested at early exponential phase (1), late exponential phase (2) and stationary phase (3) of bacterial growth (indicated with black arrows).

B. Dot blot detection of his-tagged proteins in *E. faecalis* JH2-2 (parental strain) and isogenic derivatives producing AtlA-Histag and AtlB-Histag (both expressed under the control of their own promoters). Proteins form cell lysates (i) and supernatants (ii) were probed with anti-His polyclonal antibodies

3.2   Impact of an increase AtlB production level on daughter cell separation

The fact that AtlB is less abundant than AtlA (Figure 3.3 (ii)) could account for the lower septum cleavage activity of this muramidase. If this hypothesis is correct, an increase of AtlB production level to a similar level as that of AtlA should increase the septum cleavage activity of this enzyme. To construct an *E. faecalis* JH2-2 strain producing AtlB under the *atlA* promoter ($P_{atlA}::atlB-his$) a pGhost-9 derivative (pGABH) was designed (Figure 3.4 A). A DNA fragment consists of (i) 530 bp upstream of the *atlA* start codon, (ii) 1323bp encoding C-terminally his tagged *atlB* ORF and (iii) 535 bp downstream of *atlA* stop codon was synthesised (IDT). The insert (2408 bp) was amplified by PCR using ABH_1 and ABH_2 primers, thereby introducing XhoI and EcoRI flanking restriction sites (Figure 3.4 B). The product of amplification was cut with XhoI and EcoRI and ligated to pGhost9 similarly digested. The product of ligation was used to transform competent *E. coli* TG1 $repA^+$ cells. Positive clones were verified by plasmid extraction and restriction analysis with EcoRI and XhoI (Figure 3.4 C). The plasmid was sent for sequencing to confirm the absence of mutations in the insert.

pGABH was introduced in *E. faecalis* JH2-2 by electroporation. The gene replacement was achieved by allele exchange (Figure 3.5 A). Erythromycin sensitive colonies were tested by PCR using AtlA_up and AtlA_dn primers (Figure 3.5 B).

A putative $P_{atlA}::atlB-his$ mutant identified by PCR was examined by zymogram assay using *E. faecalis* JH2-2 peptidoglycan as a substrate. Cells of JH2-2, $P_{atlA}::atlB-his$ and Δ*atlA* were grown to OD_{600} ~0.6 and 30 μl of the culture supernatants were analysed. Two autolytic bands corresponding to AtlA (higher band) and AtlB (lower band) hydrolytic activities were detected in the JH2-2 culture supernatant (Figure 3.5 C, lane 1). Analysis of $P_{atlA}::atlB-his$ and Δ*atlA* culture supernatants showed only presence of the lower band (Figure 3.5 C, lanes 2 and 3). The slight shift of the AtlB band for $P_{atlA}::atlB-his$ as compared to WT and Δ*atlA* extracts is caused by presence of the polyhistidine tag at the C-terminus.
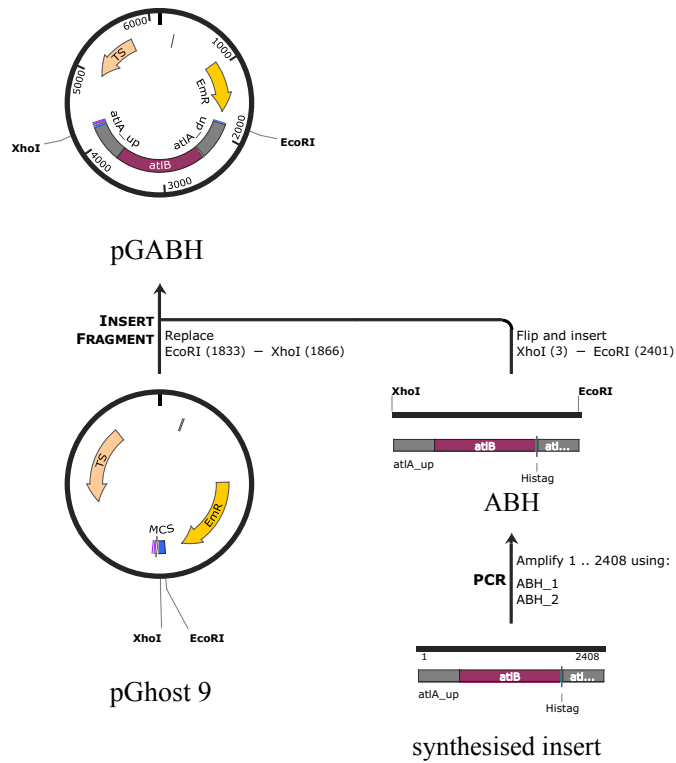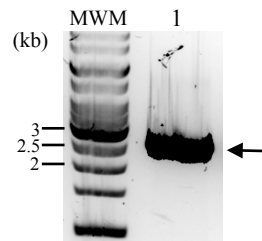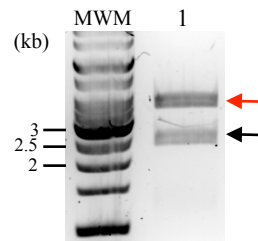
Figure 3.4 Construction of pGABH

A.   Schematic representation of the cloning strategy. The synthesised fragment was PCR amplified and digested with XhoI and EcoRI. The digestion product was cloned to pGhost 9.

B.   Amplification product of the synthesized DNA fragment using ABH_1, ABH_2 primers. The expected DNA band size of 2408 bp is indicated with a black arrow. The sizes of chosen molecular weight markers (MWM) are indicated on the left hand side of the gel.

C.   Restriction digest of pGABH using XhoI and EcoRI enzymes. The expected DNA bands size of 3750 bp for the pGhost vector is indicated with a red arrow and the 2402 bp band for the insert is indicated with a black arrow. The sizes of chosen molecular weight markers (MWM) are indicated on the left hand side of the gel.
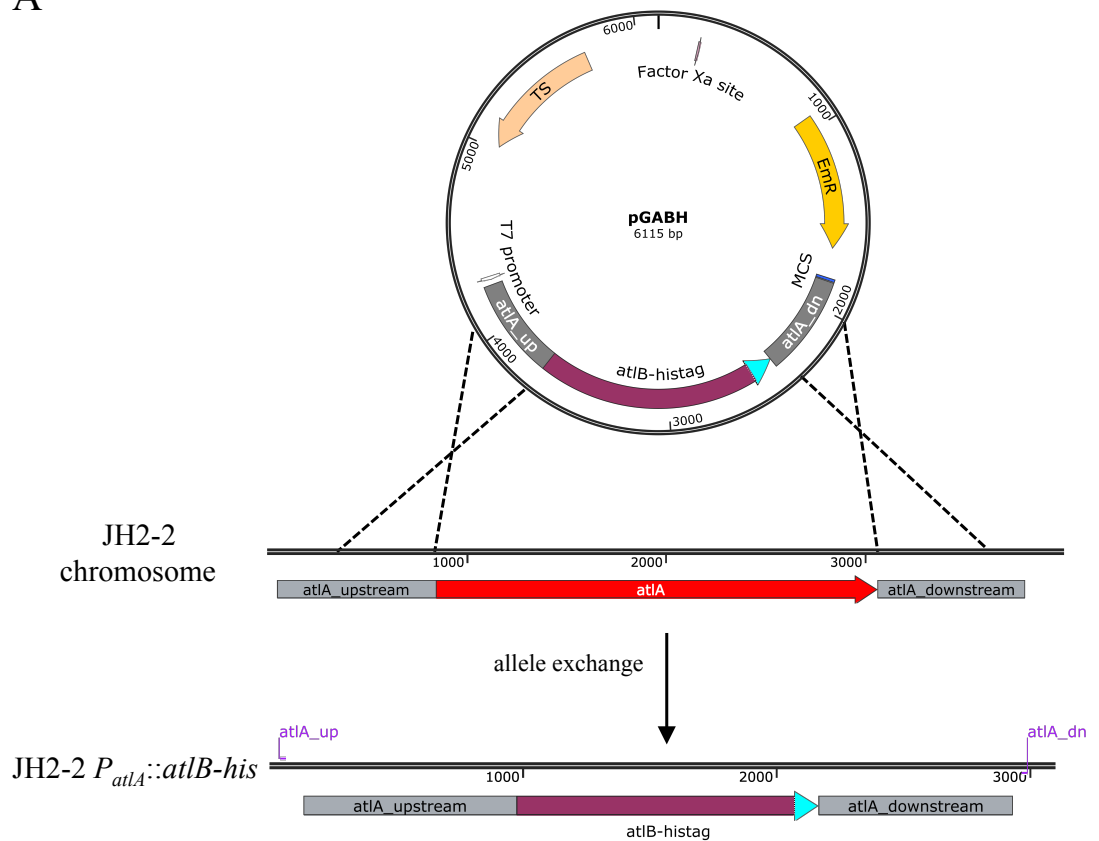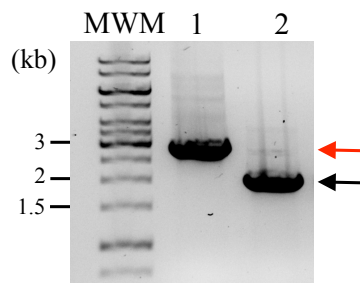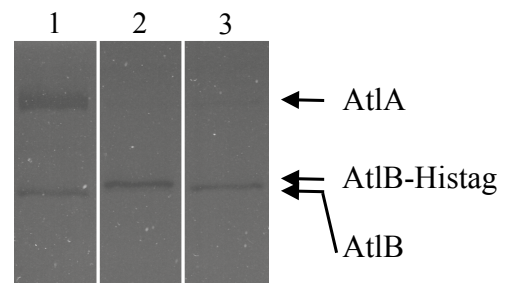
Figure 3.5 Construction of *E. faecalis* JH2-2 derivative producing a C-terminally His-tagged AtlB under the *atlA* promoter

A. Construction of recombinant strain JH2-2 P_{atlB}::*atlB-his* by allele exchange using pGBBH.

B. Amplification products using atlA_up and atlA_dn primers for negative (lane 1) and positive (lane 2) colonies. The expected DNA band sizes of: 2953 bp for the negative colony is indicated by a red arrow and 2062 bp for the positive colony is indicated by a black arrow. The sizes of chosen molecular weight markers (MWM) are indicated on the left hand side of the gel.

C. Zymogram analysis of PG hydrolases produced by *E. faecalis* JH2-2 (lane 1), the putative mutant *P$_{atlA}$::atlB-his* (lane 2) and Δ*atlA* (lane 3). *E. faecalis* JH2-2 peptidoglycan was used as a substrate. The expected band size of AtlA, AtlB and AtlB-Histag are indicated with black arrows.

The production level of C-terminally tagged AtlB produced under the *atlA* promoter was analysed by Western blot. Both strains producing tagged AtlA and AtlB under the *atlA* promoter ($P_{atlA}::atlA\text{-}his$ and $P_{atlA}::atlB\text{-}his$, respectively) were grown to late exponential phase ($OD_{600} \sim 1$) and samples corresponding to cells along with supernatant were disintegrated. The equivalents of 40 μl, 20 μl, 10 μl, and 5 μl of the cultures were analysed. Proteins were transferred on nitrocellulose membrane and probed with anti-His polyclonal antibodies. Bands with similar intensity were detected in the strains producing AtlA-Histag (Figure 3.6 A, lanes 2-5) and AtlB-Histag (Figure 3.6 A, lanes 6-9). In both samples the signal disappeared at the lowest volume analysed. The results indicate that production of AtlB under the *atlA* promoter increases amount of this muramidase to similar level as that of AtlA.

The impact of increased AtlB-His production level on a cell separation was analysed by flow cytometry. *E. faecalis* JH2-2 and isogenic derivatives ($P_{atlA}::atlB\text{-}his$ and $\Delta atlA$) were grown to early exponential phase ($OD_{600} \sim 0.3$) and diluted in PBS to the optimal cell density. The flow cytometry results showed there was no significant difference ($P=0.2466$; n=3) between forward scattered light medians of $P_{atlA}::atlB\text{-}his$ and $\Delta atlA$ mutants ($P_{atlA}::atlB\text{-}his = 465.78\pm7.40$; $\Delta atlA = 485.83\pm21.74$). A 10-fold increase ($P<0.0001$; n=3) in the median FCS value of $P_{atlA}::atlB\text{-}his$ compared to parental strain (WT=46.83 ± 0.36; $P_{atlA}::atlB\text{-}his = 465.78\pm7.40$;) was observed, suggesting formation of long cell chains by the mutant (Figure 3.6 B). This result indicated that the increased AtlB-His production is not sufficient for daughter cell separation as both mutants formed similar bacterial chains.

Altogether, results demonstrate that the functional specialisation of AtlA in cell separation during cell division relies on AtlA properties rather than on its relatively high production level.

A

B
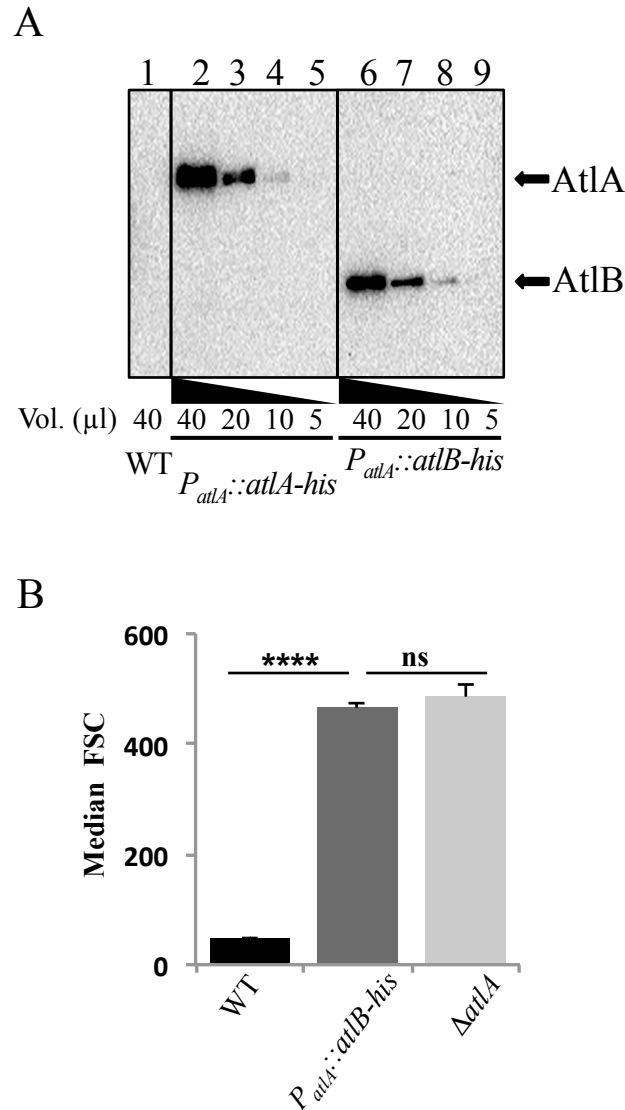
Figure 3.6 Increased level of AtlB production under the _atlA_ promoter leads to formation of long chains

A. Western blot detection of his-tagged proteins in _E. faecalis_ JH2-2 (WT) and isogenic derivatives P$_{atlA}$::_atlA-his_ and P$_{atlA}$::_atlB-his_. The samples of exponentially growing cultures were probed with anti-His polyclonal antibodies. The expected band sizes of 72 kDa for AtlA-His and 46 kDa for AtlB-His are indicated with black arrows.

B. Comparative analysis of median FSC values of _E. faecalis_ JH2-2 (WT) and isogenic derivatives P_atlA::atlB-his_ and Δ_atlA_ (****P<0.0001; n=3; ns, P>0.05; n=3).

3.3 Contribution of AtlA N-terminal proteolytic cleavage to enzymatic activity

Previous work in the lab showed that AtlA N-terminal domain was undergoing two post-translational modifications: a cleavage by proteases during cell growth (Eckert et al., 2006) and a glycosylation mediated by the *gtfAB* operon (Salamaga et al., 2017). The activities of recombinant proteins corresponding to the full length AtlA or AtlA truncated of the N-terminal domain were analysed *in vitro*; truncation of the N-terminal domain was associated with a limited decrease of activity using whole PG sacculi as a substrate (two-fold increase) and a more pronounced effect on septum cleavage activity using cell chains as a substrate (>10-fold) (Salamaga et al., 2017). My work followed up these observations. I measured the impact of AtlA N-terminal truncation on the formation of cell chains in live bacteria.

The contribution of AtlA N-terminal domain to daughter cells separation was investigated using flow cytometry. We compared the average cell chain lengths of *E. faecalis* JH2-2 strains to those of isogenic derivatives producing N-terminally truncated AtlA (AtlA$_{\Delta N}$). We studied the impact of the N-terminal truncation in two strains: (i) the wild-type JH2-2, forming diplococci and short chains (2-6 cells) and (ii) a JH2-2 derivative producing AtlA$_{1-4}$, a variant lacking two C-terminal LysM modules that forms longer chains (6-12 cells) (Figure 3.7 A). The *atlA*$_{\Delta N}$ allele was first introduced in the JH2-2 genetic background. The *atla*$_{1-4}$ allele, encoding a C-terminal truncation was then introduced in the *atlA*$_{\Delta N}$ background using the pGhost9 derivative pGAtlA$_{1-4}$ (Section 3.2.6) giving strain *atlA*$_{1-4\Delta N}$. A schematic representation of the AtlA proteins produced by the strains analysed is described in Fig. 3.7 A. The production of AtlA in supernatants was examined by Western-blot (Figure 3.7 B) using polyclonal antibodies raised against the catalytic domain of AtlA. A band with the expected molecular weight was detected in all strains indicating that AtlA was produced and secreted (full length AtlA, 72 kDa; AtlA$_{1-4}$, 58.2 kDa; AtlA$_{\Delta N}$, 61.2 kDa and AtlA$_{1-4\Delta N}$, 47.2 kDa).
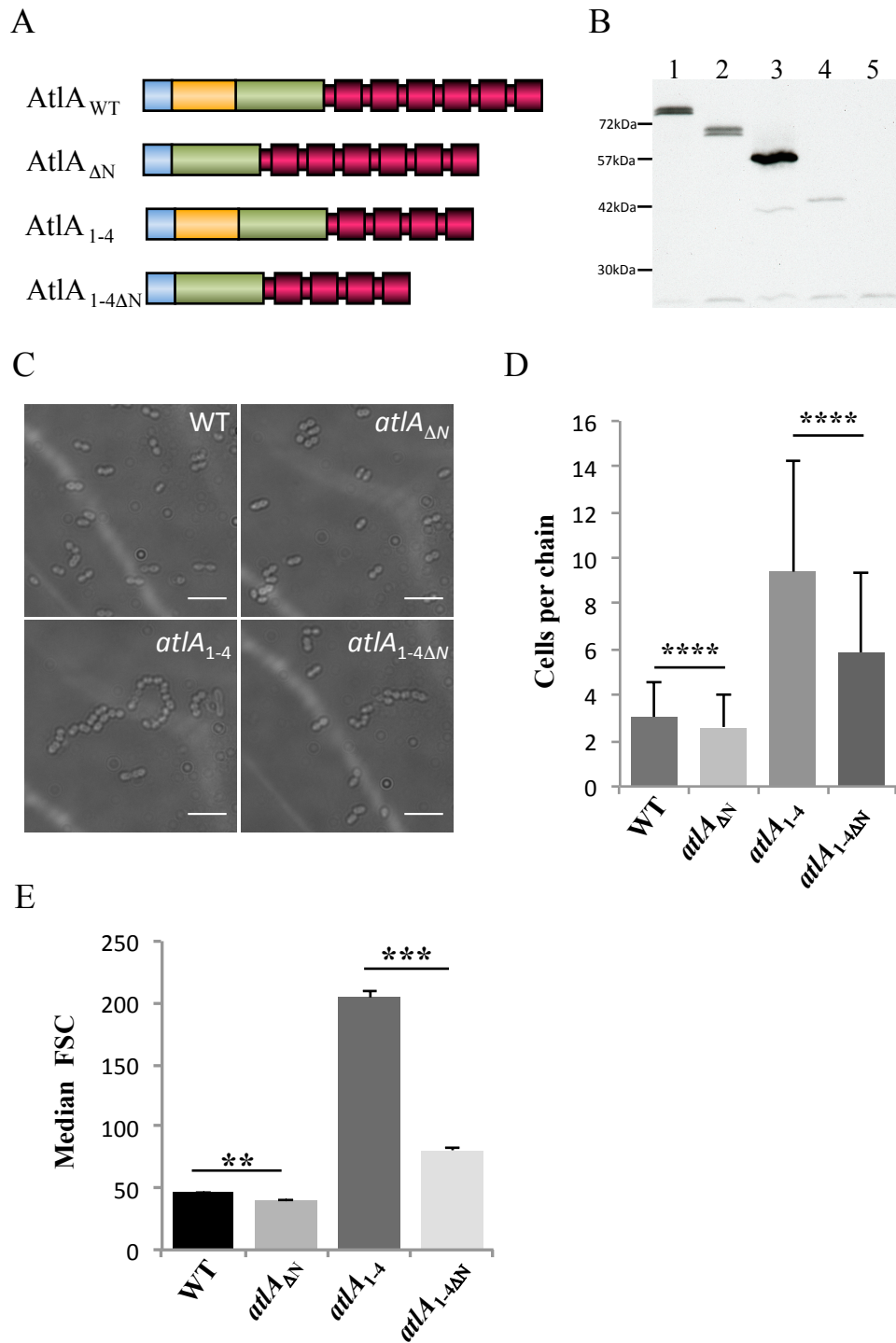
Figure 3.7 Truncation of the AtlA N-terminal domain leads to formation of shorter cell chains

A.   Schematic representation of AtlA variants produced by recombinant *E. faecalis* JH2-2 derivatives. WT, full-length AtlA; AtlA$_{\Delta N}$, AtlA variant lacking the N-terminal domain; AtlA$_{1-4}$, AtlA variant lacking the two C-terminal LysM modules; AtlA$_{1-4\Delta N}$, AtlA$_{\Delta N}$ variant

lacking the two C-terminal LysM modules. Blue, signal peptide; orange, N-terminal domain; green, catalytic domain; red, LysM domain.

B. Western blot detection of AtlA proteins in culture supernatants. Proteins precipitated from supernatants exponentially growing cells using 10% (w/v) TCA were recovered by centrifugation, washed with acetone and resuspended in PBS. Following SDS-PAGE and transfer on a nitrocellulose membrane, AtlA proteins were probed with anti-AtlA polyclonal serum against the catalytic domain of AtlA. Lane 1,WT-72 kDa; lane 2, AtlA$_{1-4}$ – 58.2 kDa; lane 3, AtlA$_{\Delta N}$-59 kDa; lane 4, AtlA$_{1-4\Delta N}$-46.2 kDa. A strain with an in-frame deletion of *atlA* (Δ*atlA*) was used as a negative control, lane 5. The sizes of chosen molecular weight markers are indicated on the left hand side of the blot.

C. Light microscopy images showing cell chain lengths of *E.faecalis* JH-2-2 and *atlA*$_{\Delta N}$ isogenic mutants.

D. Average numbers of cells per chain formed by WT (3.0 ± 1.6; n=427 cells); *atlA*$_{\Delta N}$ (2.6 ± 1.4; n=534 cells) ; *atlA*$_{1-4}$ (9.4 ± 4.8; n=442 cells) and *atlA*$_{1-4\Delta N}$ (5.9 ± 3.4; n=610 cells) strains (****P<0.0001).

E. Pairwise comparison of median FSC values (a) between WT and *atlA*$_{\Delta N}$ (**P=0.0015, n=3) and (b) between *atlA*$_{1-4}$ and *atlA*$_{1-4\Delta N}$ (***P=0.0001, n=3).

The cell chain lengths of strains: JH2-2, *atlA*ΔN , *atlA*1-4 and *atlA*1-4ΔN were first analysed using light microscopy (Figure 3.7 C). In both pairwise comparisons (JH2-2, 3.05 ± 1.56 cells per chain, n=140 versus *atlA*ΔN, 2.57 ± 1.43 cells per chain, n=208 and *atlA*1-4, 9.40 ± 4.83 cells per chain, n=47 versus *atlA*1-4ΔN 5.87 ± 3.45 cells per chain, n=104), derivatives producing N-terminally truncated AtlA formed significantly shorter chains (P<0.0001 for both comparison) (Figure 3.7 D).

Next, we analysed the impact of N-terminal domain truncation on daughter cell separation by flow cytometry (Figure 3.7 E). The results confirmed light microscopy analyses. Truncation of the N-terminal domain in a JH2-2 background significantly decreased the average cell chain length. Median FSC values of JH2-2 (47.07 ± 0.42) decreased to 40.68 ± 0.84 for *atlA*ΔN (**P=0.0015, n=3). A more pronounced decrease in cell chain length was observed when the FSC values of the *atlA*1-4 strain (206.10 ± 5.49) were compared to those of the *atlA*1-4ΔN (80.63 ± 2.15; ***P=0.0001, n=3).

Altogether, results showed that the presence of the N-terminal domain of AtlA inhibits the septum cleavage activity of this hydrolase.

3.4   Impact of AtlA N-terminal glycosylation on septum cleavage

The N-terminal domain of AtlA, consisting of 28% of threonine and 12% of serine residues (Figure 3.8 A) is *O*-glycosylated (Salamaga et al., 2017). Two glycosyl transferases named GtfA and GtfB are responsible for glycosylation of bacterial surface proteins in Gram-positive pathogens (Lee et al., 2014). Bioinformatics analysis of *Enterococcus faecalis* genome revealed two putative orthologs of *gtf*A and *gtf*B (*EF2891* and *EF2892*, respectively in V583). In-frame deletion of these genes in *E. faecalis* JH2-2 led to lack of AtlA glycosylation (Figure 3.8 B; Salamaga et al., 2017). To analyse an impact of AtlA glycosylation on septum cleavage, strains forming short (WT) and long (AtlA1-4) chains were compared with their isogenic counterparts harbouring in frame deletion in the *gtfAB* locus (Δ*gtfAB* and AtlA1-4Δ*gtfAB*, respectively).

The Δ*gtfAB* strain was available in the laboratory. An *atlA*$_{1-4}$Δ*gtfAB* was constructed by allele exchange using plasmid pGatlA$_{1-4}$ (Section 3.2.4.1) to introduce mutation leading to the truncation of the last 2 LysM modules in the Δ*gtfAB* background.

AtlA expression and secretion were analysed by Western-blot (Figure 3.8 C) using polyclonal antibodies raised against the catalytic domain of AtlA. Bands at the expected molecular weights were detected in all strains (*ca*. 72 kDa for full length AtlA and 61 kDa the the LysM truncated AtlA).

Mutants were first characterized using light microscopy (Figure 3.8 D) to count the average number of cells presence in individual chains. No significant difference was observed between the WT (3.05 ± 1.56 cells per chain, n=140) and the Δ*gtfAB* mutant (3.06±1.34 cells per chain, n=119). However, a significant decrease (***P=0.0005) in the average number of cells per chain was found between AtlA$_{1-4}$ (9.40 ± 4.83 cells per chain, n=47) and AtlA$_{1-4}$Δ*gtfAB* (6.21 ± 3.70 cells per chain, n=48) (Figure 3.8 E).

To confirm microscopy results, a pairwise comparison of cell chain length was measured by flow cytometry. The results showed a significant decrease in median FSC values of Δ*gtf*AB (42.04 ± 0.66; **P=0.0017) and *atlA*$_{1-4}$Δ*gtfAB* (101.66 ± 1.47; ***P=0.0002) strain as compared to their glycosylated parental strains (WT, 46.09 ± 0.43 and *atlA*$_{1-4}$, 200.87 ± 4.52) (Figure 3.8 F). These results suggested that posttranslational glycosylation of AtlA N-terminal domain impairs daughter cell separation.
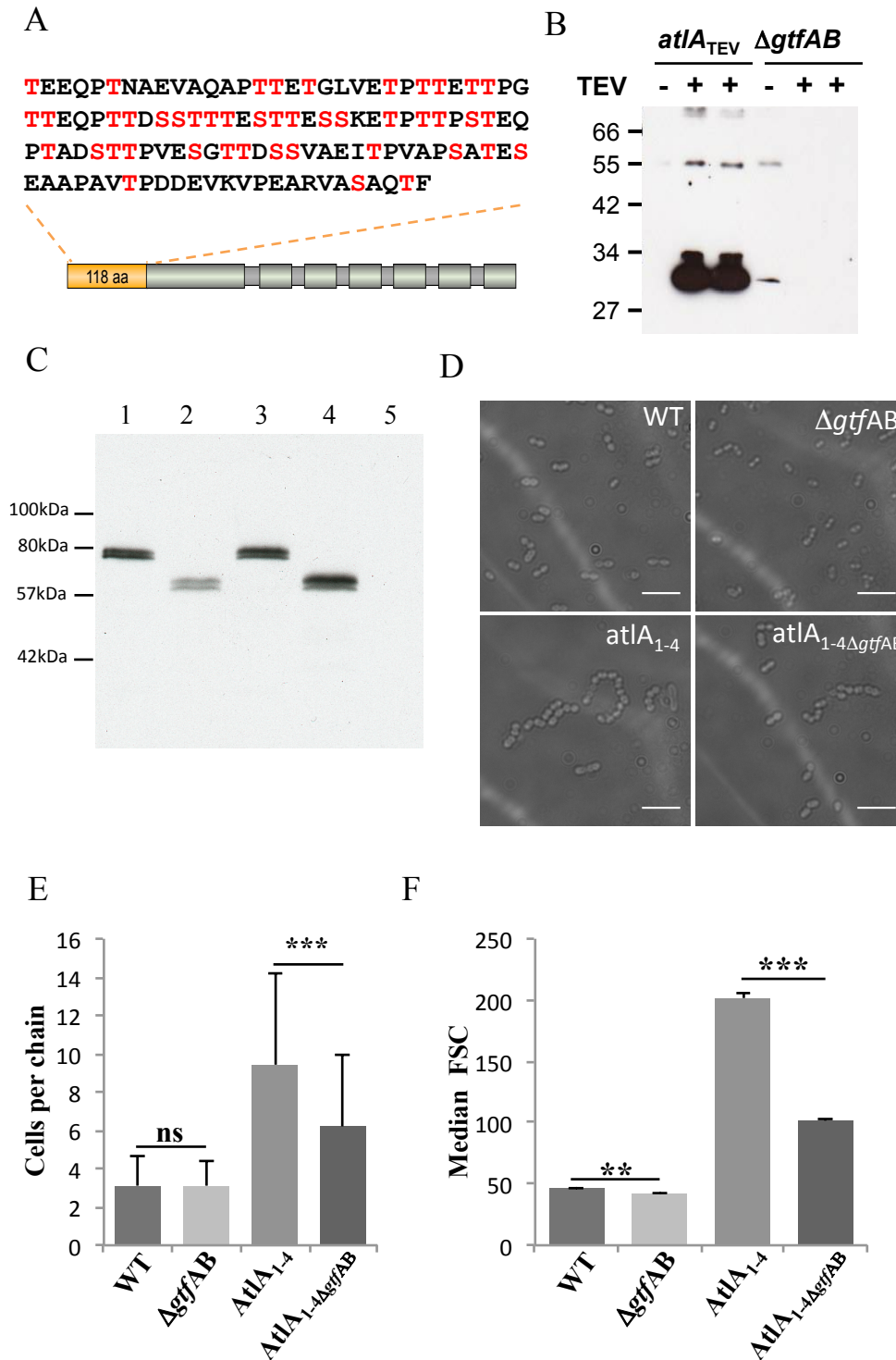
Figure 3.8 Lack of glycosylation of the AtlA N-terminal domain leads to higher septum cleavage activity

A. Amino acid composition of AtlA N-terminal domain. Threonine and serine residues are highlighted on red.

B. ECL detection of glycoproteins recovered after TEV treatment. Exponentially growing cells from a culture expressing AtlA_TEV (AtlA variant where TEV claveage side was

introduced between N-termianl and catalityc domains) were resuspended in buffer in the absence (-) or presence (+) of TEV protease to cleave the N-terminal domain of AtlA. Solubilized proteins were recovered by centrifugation, loaded on an SDS-PAGE and transferred on nitrocellulose to detect glycosylated proteins. Two independent cultures treated with the TEV protease were analysed in parallel. In both cases, a glycosylated polypeptide with the expected molecular weight for the N-terminal domain (~30kDa) was detected while no signal was observed in the negative control. When a similar experiment was repeated with protein extracts from a $\Delta gtfAB$ mutant, no glycosylated protein was detected, indicating that this operon is involved in the post translational modification of AtlA (Salamaga et al., 2017).

C.   Western blot detection of AtlA proteins in culture supernatants. Proteins precipitated from supernatants exponentially growing cells using 10% (w/v) TCA were recovered by centrifugation and washed with acetone and resuspended in PBS. Following SDS-PAGE and transfer on a nitrocellulose membrane, AtlA proteins were probed with anti-AtlA polyclonal serum against the catalytic domain of AtlA. Lane 1, WT – full-length AtlA; lane 2, $AtlA_{1-4}$ – AtlA variant lacking the two C-terminal LysM modules; lane 3, $\Delta gtfAB$ – derivative with an in frame deletion of the $gtfAB$ operon; lane 4, $AtlA_{1-4}\Delta gtfAB$ – $\Delta gtfAB$ derivative producing AtlA variant lacking the two C-terminal LysM modules. A strain with an in-frame deletion of atlA ($\Delta atlA$) was used as a negative control, lane 5. The sizes of chosen molecular weight markers are indicated on the left hand side of the blot.

D.   Light microscopy images showing cell chain lengths of *E. faecalis* JH2-2 the mutants.

E.   Average numbers of cells per chain formed by WT (3.0 ± 1.6; n=427 cells); $\Delta gtfAB$ (3.0 ± 1.3; n=364 cells); $atlA_{1-4}$ (9.4 ± 4.8; n=442 cells) and $atlA_{1-4}\Delta gtfAB$ (6.5 ± 3.7; n=298 cells) strains (ns, P>0.05; ***P=0.0005).

F.   Pairwise comparison of median FSC values (a) between WT and $\Delta gtfAB$ (**P=0.0017, n=3) and (b) between $atlA_{1-4}$ and $atlA_{1-4}\Delta gtfAB$ (***P=0.0002, n=3).

3.5 Impact of AtlA PG cleavage specificity on daughter cell separation

Hydrolases displaying distinct PG cleavage specificity dedicated to daughter cell separation have been reported in Gram-positive bacteria including the *N*-acetylglucosaminidase AtlA in *E. faecalis,* the D,L-endopeptidase Cse in *Streptococcus thermophilus* (Layec et al., 2009), the *N*-acetylmuramyl-L-Alanine amidase Atl in *Staphylococcus aureus* (Oshida et al., 1995) (Figure 3.9 A). This suggests that hydrolases might recognise specific PG structures in specific bacteria.

To investigate an impact of AtlA specificity on daughter cell separation isogenic derivatives were constructed. In these strains the catalytic domains of AtlA was replaced by catalytic domains of AtlB, Atl_{Ami} or Cse, thereby generating proteins with distinct peptidoglycan cleavage specificity (named $AtlA_{AtlB}$, $AtlA_{Ami}$, $AtlA_{Cse}$; Figure 3.9 B). I measured cell chain lengths of these strains by flow cytometry to measure septum cleavage activity of AtlA derivatives with distinct activities (Figure 3.9 C). Flow cytometry results revealed a significant decrease ($P<0.01$) of median FSC values of tested mutants as compared to the in-frame *atlA* deletion mutant ($\Delta atlA = 409.38 \pm 24.52$; $AtlA_{AtlB} = 117.35 \pm 6.32$, **$P = 0.0018$; $AtlA_{Ami} = 122.68 \pm 4.52$, **$P=0.0014$; $AtlA_{Cse}=219.57 \pm 2.66$, **$P=0.0051$) These results therefore indicated that *N*-acetylglucosaminidase specificity of AtlA is not essential for septum cleavage but it is optimal. Mutants were not able to separate the daughter cells as efficient as wild-type.
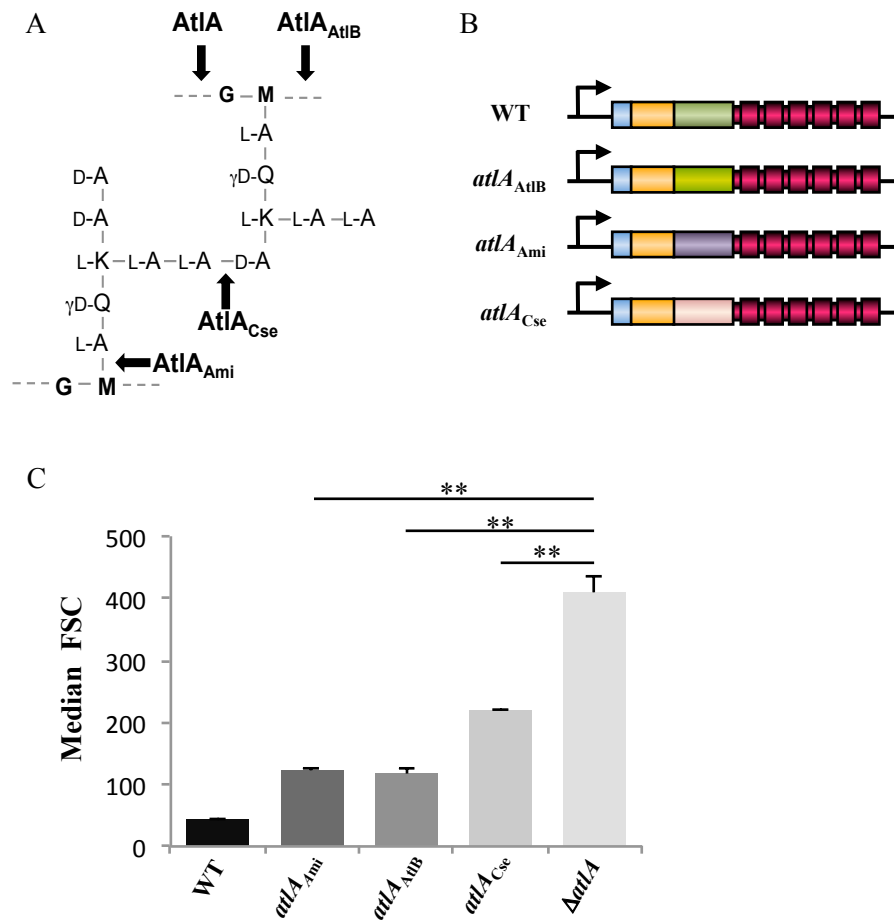
Figure 3.9 AtlA *N*-acetylglucosaminidase specificity is not essential for septum cleavage

A. Schematic representation of *E. faecalis* peptidoglycan structure. The cleavage sites of *E. faecalis* AtlA and AtlB, *S. aureus* Atl and *S. thermophilus* Cse are indicated with black arrows.

B. Schematic representation of AtlA variants produced by *E. faecalis* JH2-2 derivatives. To generate stains *atlA*_{AtlB}, *atlA*_{Ami} and *atlA*_{Cse}, a fragment encoding AtlA *N*-acetylglucosaminidase activity was replaced with fragments encoding the *N*-acetylmuramidase activity of *E. faecalis* AtlB, the amidase activity of *S. aureus* Atl or the endopeptidase activity of *S. thermophilus* Cse, respectively. Blue – fragment encoding signal peptide; orange – fragment encoding N-terminal domain; dark green – fragment encoding catalytic domain of AtlA; light green – fragment encoding catalytic domain of AtlB; purple – fragment encoding catalytic domain of Atl; pink – fragment encoding catalytic domain of Cse; burgundy – fragment encoding LysM domain.

C. Comparison of median FSC values of WT, *atlA*_{Ami}, *atlA*_{AtlB}, *atlA*_{Cse} and Δ*atlA*. All median FSC values were significantly different from the median FSC value of Δ*atlA* (**P<0.01; n=3).

3.6 Contribution of AtlA C-terminal LysM domain modularity to enzymatic activity

E. faecalis V583 encodes twelve surface proteins with LysM domains. AtlA LysM domain (LysM$_A$) is the most complex of all. It consists of six repeats separated by low complexity sequences mainly made of glycine, serine and asparagine residues (>90%). All AtlA LysM repeats have a very similar basic isoelectric point (pI ~10), giving an overall basic charge for the complete domain (pI=10.1). By contrast, the LysM domain of AtlB (LysM$_B$) is acidic (pI=5.5). It consists of two contiguous LysM modules: LysM$_{B1}$ (pI=4.65) and LysM$_{B2}$ (pI=8.3). We investigated the impact of both the binding domain modularity and LysM modules amino acid composition on the septum cleavage activity of AtlA.

To construct the strains expressing AtlA with LysM$_A$ domains consisting of 1 to 5 repeats, pGhost 9 derivatives pGAtlA$_1$, pGAtlA$_{1-2}$, pGAtlA$_{1-3}$, pGAtlA$_{1-4}$ and pGAtlA$_{1-5}$ were constructed as described in Figure 3.10 A. To construct pGAtlA$_{1-5}$, a fragment of DNA encoding AtlA catalytic domain (507 bp), 5 LysM$_A$ modules (1029 bp) and 253 bp downstream of *atlA* stop codon was cut out from pMQ-5LysM and cloned into pGhost9 using XhoI and KpnI. Plasmid pMQ-5LysM, available in the laboratory collection was purchased from Gene Art. The insert of pMQ-5LysM results from a gene synthesis and contains an NcoI restriction site at the end of catalytic domain and two BglII restriction sites flanking the 5th LysM modules. Following transformation, positive colonies were identified by PCR. After plasmid extraction restriction analyses with XhoI and KpnI confirmed the presence of an insert with the expected size (Figure 3.10 B).

To obtain pGAtlA$_{1-4}$, pGAtlA$_{1-5}$ was digested with BglII and self-ligated. Following transformation of the ligation product in *E. coli*, plasmids were extracted from candidate clones and analysed by digestion with XhoI and KpnI to confirm the presence of the insert (Figure 3.10 C).

To construct pGAtlA$_1$, pGAtlA$_{1-2}$ and pGAtlA$_{1-3}$, inserts were PCR amplified using three sets of primers: Cata_H11/AtlA1_H12; Cata_H11/AtlA1-2_H12 and Cata_H11/AtlA1-3_H12 (Figure 3.10 D). The amplification products were cloned into pGAtlA$_{1-4}$ using NcoI and BglII.

A

(i)

pGAtlA₁₋₅

pGhost 9

pMQ-5LysM

(ii)

pGAtlA₁₋₄

pGAtlA₁₋₅

(iv)

pGAtlA$_{1-2}$

pGAtlA$_{1-4}$

2 LysM
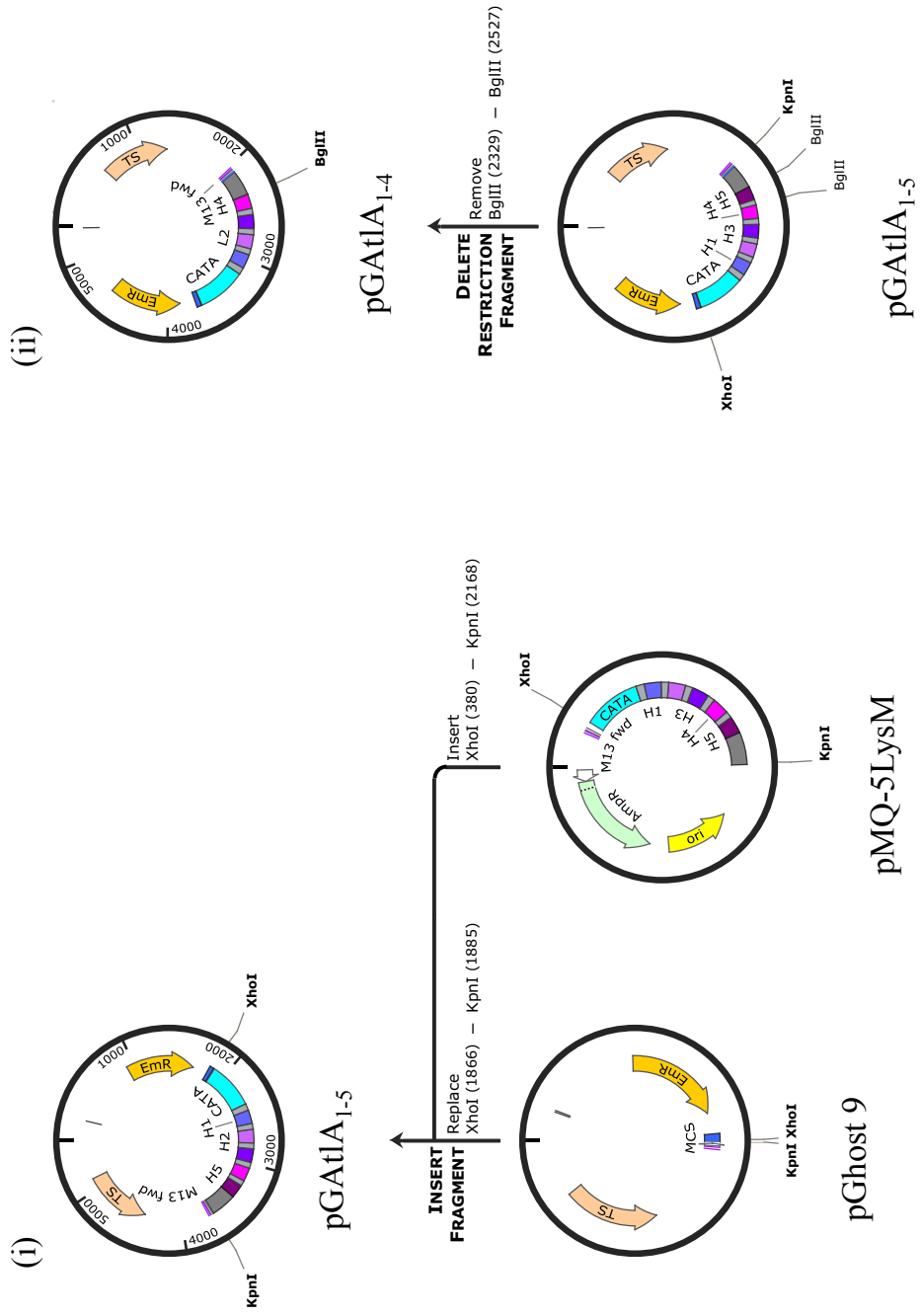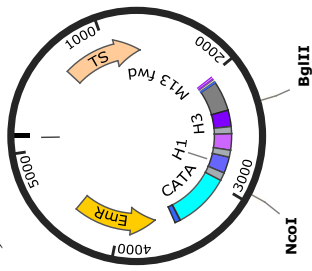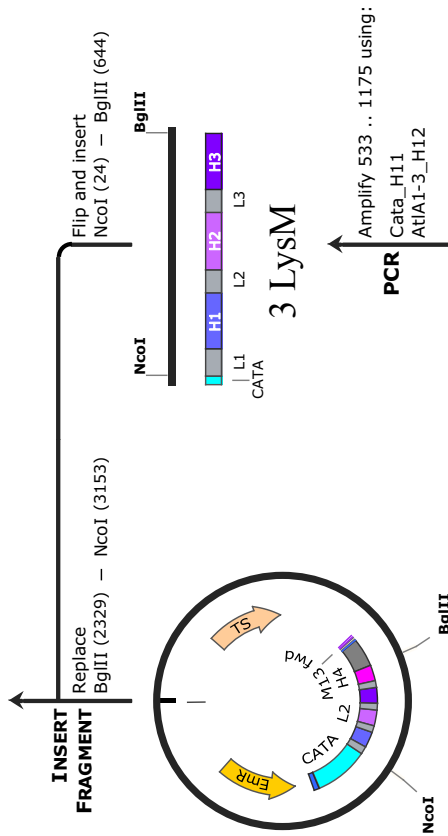
E.faecalis JH2-2
Chromosomal DNA

(iii)

pGAtlA$_{1-3}$

pGAtlA$_{1-4}$

3 LysM
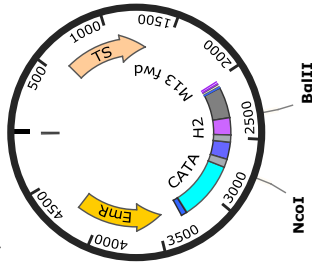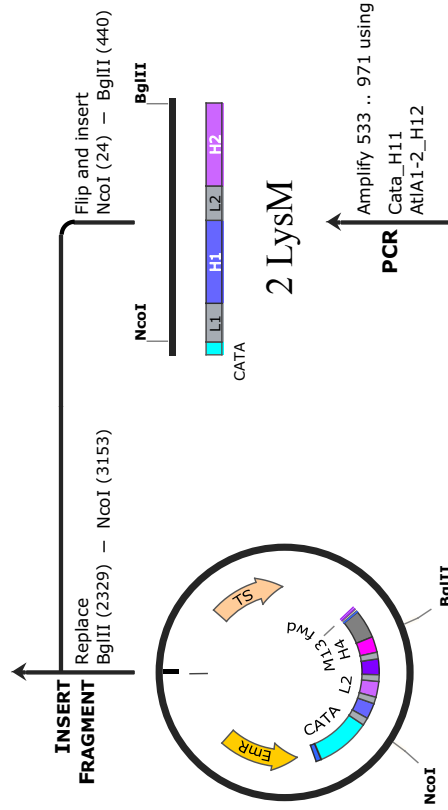
E.faecalis JH2-2
Chromosomal DNA
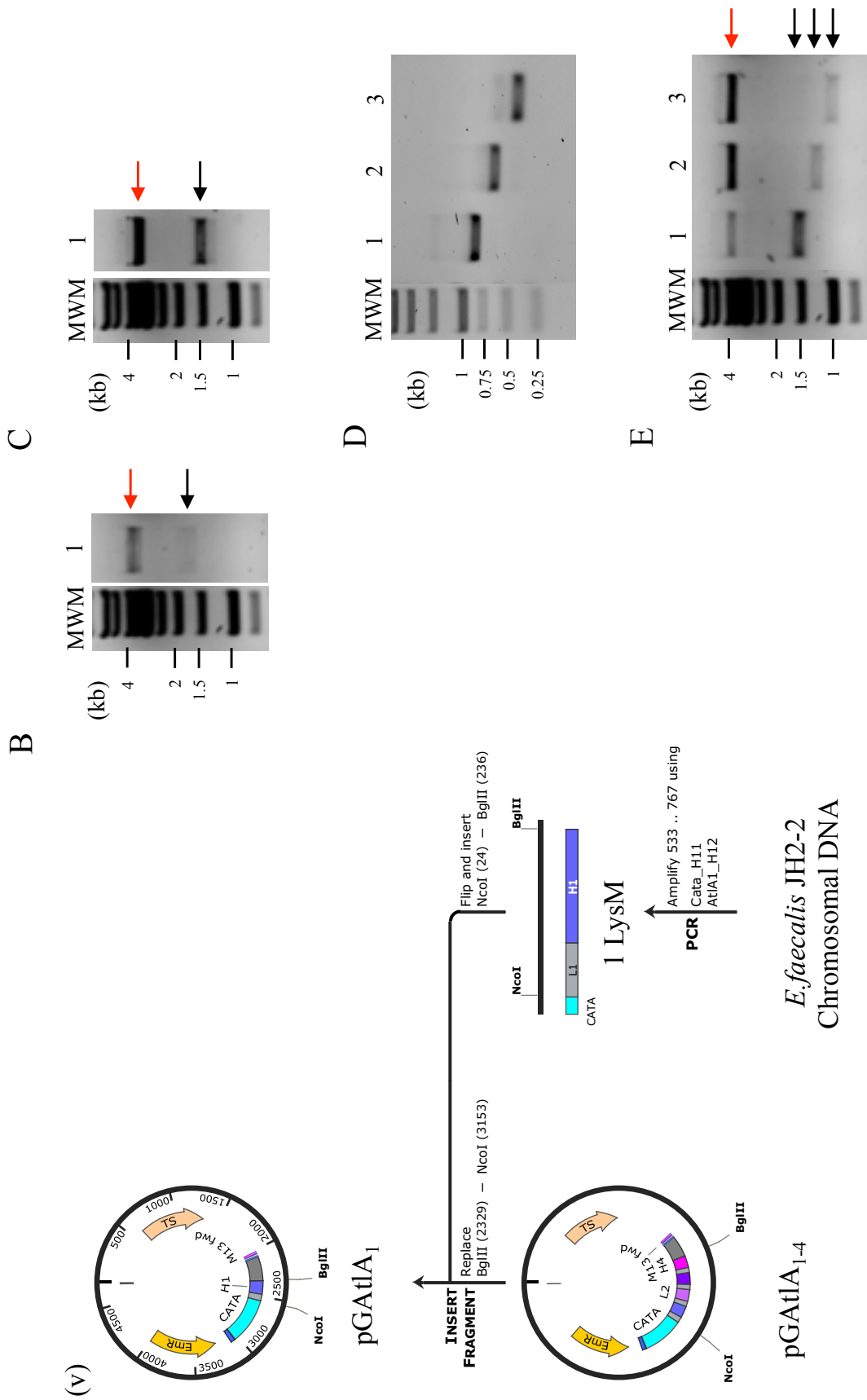
Figure 3.10 Construction of pGAtlA_{1-5}, pGAtlA_{1-4}, pGAtlA_{1-3}, pGAtlA_{1-2}, pGAtlA_1

A. Schematic representation of the cloning strategy of:

(i) pGAtlA$_{1-5}$; XhoI and KpnI fragment of pMQ-5LysM insert consisting of 507 bp of AtlA catalytic domain, 5 LysM modules (1029 bp) and 253 bp downstream of atlA stop codon was cloned in to pGhost 9 similarly digested.

(ii) pGAtlA$_{1-4}$; pGAtlA$_{1-5}$ was digested by BglII. Following the gel extraction, the high molecular weight DNA fragment was extracted and self-ligated.

(iii) pGAtlA$_{1-3}$; the amplification product using primers Cata_H11 and AtlA1-3_H12 was digested with NcoI and BglII and cloned to pGAtlA$_{1-4}$similarly cut.

(iv) pGAtlA$_{1-2}$; the amplification product using primers Cata_H11 and AtlA1-2_H12 was digested with NcoI and BglII and cloned to pGAtlA$_{1-4}$similarly cut.

(v) pGAtlA$_1$; the amplification product using primers Cata_H11 and AtlA1_H12 was digested with NcoI and BglII and cloned to pGAtlA$_{1-4}$ similarly cut.

B. Restriction digest of pGAtlA$_{1-5}$ using XhoI and KpnI. The expected DNA band of 3750 bp corresponding to the backbone is indicated with a red arrow and 1780 bp band corresponding to the insert is indicated with a black arrow. The sizes of chosen molecular weight markers (MWM) are indicated on the left hand side of the gel.

C. Restriction digest of pGAtlA$_{1-4}$ using XhoI and KpnI. The expected DNA band of 3750 bp corresponding to the backbone is indicated with a red arrow and 1582 bp band corresponding to the insert is indicated with a black arrow. The sizes of chosen molecular weight markers (MWM) are indicated on the left hand side of the gel.

D. Amplification products of 1 LysM (amplified with Cata_H11 and AtlA1_H12, lane 1), 2 LysM (amplified with Cata_H11 and AtlA1-2_H12, lane 2) and 3 LysM (amplified with Cata_H11 and AtlA1-3_H12, lane 3). The sizes of chosen molecular weight markers (MWM) are indicated on the left hand side of the gel.

E. Restriction digest of pGAtlA$_{1-3}$ (lane 1), pGAtlA$_{1-2}$ (lane2) and pGAtlA$_1$ (lane 3) using XhoI and KpnI. The expected DNA band size of 3750 bp (backbone; indicated with a red arrow), 1378 bp (pGAtlA$_{1-3}$), 1174 bp (pGAtlA$_{1-2}$) and 970 bp (pGAtlA$_1$). The sizes of chosen molecular weight markers (MWM) are indicated on the left hand side of the gel.

The restriction analysis of candidate plasmids with XhoI and KpnI is shown in Figure 3.10 E.

The inserts of plasmids pGAtlA$_1$, pGAtlA$_{1-2}$, pGAtlA$_{1-3}$, pGAtlA$_{1-4}$ and pGAtlA$_{1-5}$ were sequenced to confirm the absence of mutations.

The plasmids were used to transform electrocompetent *E.faecalis* JH2-2 cells. Deletions of the DNA encoding LysM$_A$ were introduced by allele exchange. Putative mutants sensitive to erythromycin were analysed by PCR using primers AtlA_5' and AtlA_dn showing PCR products of the expected sizes (Figure 3.11 A).

The truncation of LysM modules was verified by Southern Blot (Figure 3.11 B). Genomic DNAs of putative mutants (*atlA$_{1-5}$*, *atlA$_{1-4}$*, *atlA$_{1-3}$*, *atlA$_{1-2}$* and *atlA$_1$*), JH2-2 and Δ*atlA* were extracted and cut with BstXI and HindIII (Figure 3.11 B (i)), run on an agarose gel and transferred to a nitrocellulose membrane. The membrane was probed with a 506 bp fragment encoding the catalytic domain of AtlA. A signal of the expected size (2270 bp) was detected for the WT genomic DNA whilst no signal was detected for the Δ*atlA* mutant. An expected decrease in the molecular weight of the band detected (*ca*. 200bp) was observed for each of the putative mutants. (Figure 3.11 B (ii)).

Expression and secretion of AtlA by *E. faecalis* JH2-2 and *lysM* mutants were analysed by Western blot (Figure 3.11 C and D). The strain with in frame deletion of *atlA* was used as a negative control. Proteins precipitated from supernatants and crude extracts of exponentially growing cultures (OD$_{600}$ ~0.4) were probed with rabbit serum raised against the catalytic domain of AtlA. A single band with the expected molecular weight was detected in supernatatnats for all strains: 72 kDa for AtlA, 65 kDa for AtlA$_{1-5}$, 58 kDa for AtlA$_{1-4}$, 51 kDa for AtlA$_{1-3}$, 44 kDa for AtlA$_{1-2}$ and 38 kDa for AtlA$_1$. The analysis of the cell lysates reveled a presence of an additional band around 15kDa above the expected AtlA$_{1-4}$, AtlA$_{1-3}$, AtlA$_{1-2}$ and AtlA$_1$. The enzymatic activities of AtlA derivatives with truncated LysM domains were analysed by zymogram using *M. luteus* PG as a substrate (Figure 3.11 E). The full length AtlA showed the highest enzymatic activity. Sequential truncation of the LyM domain led to a progressive decrease of AtlA hydrolytic activity. No activity was detected in samples from *atlA$_1$* and Δ*atlA* strains (Figure 3.11 E, lanes 6 and 7).
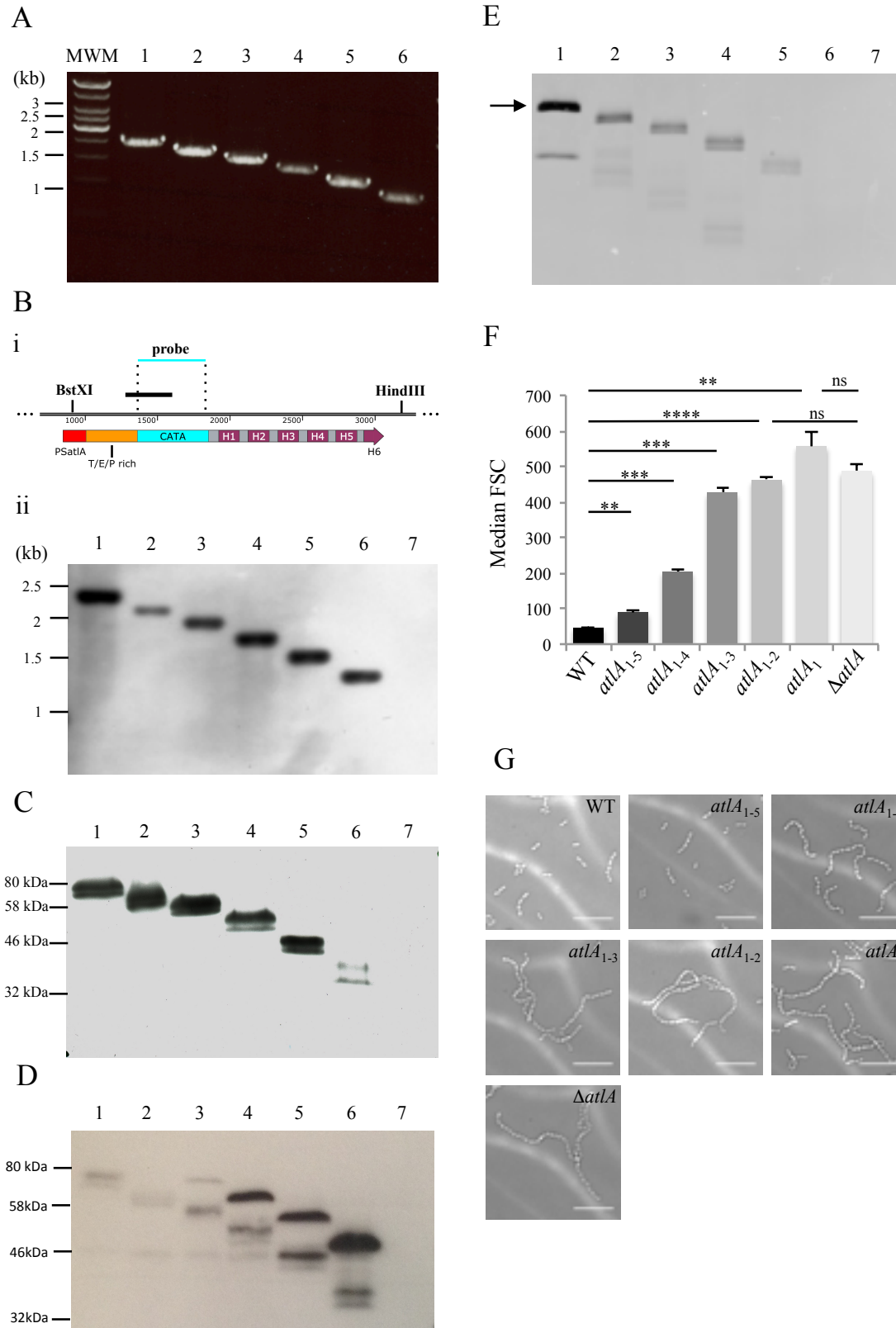
Figure 3.11 Characterisation of *lysM* mutants

A. Amplification products using atlA_up and atlA_dn primers for WT (lane 1), *atlA*₁₋₅ (lane 2), *atlA*₁₋₄ (lane 3), *atlA*₁₋₃ (lane 4), *atlA*₁₋₂ (lane 5) and *atlA*₁ (lane 6) colonies. The expected

DNA band sizes of 2479 bp for WT, 2293 bp for $atlA_{1-5}$, 095 bp for $atlA_{1-4}$, 1891 bp for $atlA_{1-3}$, 1687 bp for $atlA_{1-2}$ and 1483bp for $atlA_1$. The sizes of chosen molecular weight markers (MWM) are indicated on the left hand side of the gel.

B. Southern Blot analysis of the *E. faecalis* JH2-2 isogenic derivatives. (i) Schematic representation of the *atlA* allele with indicated restriction sites used for analysis and the site of the probe hybridisation. (ii) The genomes of WT (lane 1), $atlA_{1-5}$ (lane 2), $atlA_{1-4}$ (lane 3), $atlA_{1-3}$ (lane 4), $atlA_{1-2}$ (lane 5), $atlA_1$ (lane 6) and $\Delta atlA$ (lane 7) were digested with BstXI and HindIII and run on an agarose gel and transferred to a nitrocellulose membrane. The membrane was probed with a 506 bp fragment encoding the catalytic domain of AtlA. Bands of expected sizes were detected: 2270 bp for WT, 2084 bp for $atlA_{1-5}$, 1888 bp for $atlA_{1-4}$, 1684 bp for $atlA_{1-3}$, 1480 bp for $atlA_{1-2}$ and 1276 bp for $atlA_1$. No signal was detected for $\Delta atlA$. The sizes of chosen molecular weight markers (MWM) are indicated on the left hand side of the gel.

C. Western blot detection of AtlA proteins in culture supernatants. Proteins precipitated from supernatants exponentially growing cells were recovered by centrifugation and washed with acetone and resuspended in PBS. Following SDS-PAGE and transfer on a nitrocellulose membrane, AtlA proteins were probed with anti-AtlA polyclonal serum against the catalytic domain of AtlA. Lane 1, WT-72 kDa,; lane 2, $atlA_{1-5}$–65 kDa; lane 3, $atlA_{1-4}$– 58.2 kDa; lane 4, $atlA_{1-3}$– 51.3 kDa; lane 5, $atlA_{1-2}$– 44.4 kDa; lane 6, $atlA_1$– 37.5 kDa. A strain with an in-frame deletion of *atlA* ($\Delta atlA$) was used as a negative control, lane 7. The sizes of chosen molecular weight markers are indicated on the left hand side of the blot.

D. Western blot detection of AtlA proteins in crude extracts. Exponentially growing cells were harvested by centrifugation and resuspended in PBS. The cells were mechanically broken to extract proteins. Following SDS-PAGE and transfer on a nitrocellulose membrane, AtlA proteins were probed with anti-AtlA polyclonal serum against the catalytic domain of AtlA. Lane 1, WT-72 kDa,; lane 2, $atlA_{1-5}$–65 kDa; lane 3, $atlA_{1-4}$– 58.2 kDa; lane 4, $atlA_{1-3}$– 51.3 kDa; lane 5, $atlA_{1-2}$– 44.4 kDa; lane 6, $atlA_1$– 37.5 kDa. Additional band was detected in crude extracts from $atlA_{1-4}$, $atlA_{1-3}$, $atlA_{1-2}$ and $atlA_1$. The higher molecular waight band was detected around 15kDa above the expected AtlA forms. A strain with an in-frame deletion of *atlA* ($\Delta atlA$) was used as a negative control, lane 7. The sizes of chosen molecular weight markers are indicated on the left hand side of the blot.

E. Zymogram analysis of PG hydrolases produce by *E. faecalis* JH2-2 (lane 1), the *lysM* mutants: $atlA_{1-5}$ (lane 2), $atlA_{1-4}$ (lane 3), $atlA_{1-3}$ (lane 4), $atlA_{1-2}$ (lane 5), $atlA_1$ (lane 6) and $\Delta atlA$ (lane 7). *M. luteus* peptidoglycan was used as a substrate to detect AtlA activity. The high enzymatic activity lytic band of AtlA was detected for the wild-type strain (indicated

with a black arrow), whereas sequential truncation of the LyM domain led to a progressive decrease of hydrolytic activity of AtlA derivatives.

F. Comparison of median FSC values corresponding to an average cells chain length formed by WT, *atlA*$_{1-5}$, *atlA*$_{1-4}$, *atlA*$_{1-3}$, *atlA*$_{1-2}$, *atlA*$_1$ and Δ*atlA*. All median FSC values were significantly different from the median FSC value of WT (*atlA*$_{1-5}$ **P=0.0036; *atlA*$_{1-4}$, ***P=0.0004; *atlA*$_{1-3}$, ***P=0.0004; *atlA*$_{1-2}$, ****P<0.0001; *atlA*$_1$ **P=0.002). The average cell chain length of strains *atlA*$_{1-2,}$ *atlA*$_1$ was not significantly different from these formed by Δ*atlA* strain. All measurements were done in triplicates.

G. Light microscopy images showing cell chain lengths of the mutants.

The impact of LysM$_A$ truncations on daughter cell separation was investigated by measuring average cell chain length using flow cytometry (Figure 3.11 F). The results showed a significant cell chain length increase for all strains producing AtlA with a truncated LysM$_A$ as compared to the parental strain. The extent of LysM truncation was correlated with an increase in median FSC values: $atlA_{1-5}$; 88.45 ± 4.48, **P=0.0036; $atlA_{1-4}$=204.45 ± 5.71, ***P=0.0004; $atlA_{1-3}$=426.43 ± 12.45, ***P = 0.0004; $atlA_{1-2}$=461.78 ± 07.07, ****P<0.0001; $atlA_1$=556.79 ± 39.08, **P=0.002. No significant difference was observed between the average cell chain length of strains $atlA_{1-2,}$ $atlA_1$ and Δ$atlA$ (FSC=485.83 ± 21.74). The flow cytometry analyses of bacterial cell chain lengths were confirmed by light microscopy (Figure 3.11 G).

3.7 Impact of the LysM domain charge and amino acid composition on daughter cell separation

We explored the impact of LysM charge and composition on cell separation by replacing the basic LysM repeats from AtlA (pI=10) by the two LysM repeats of acidic AtlB (pI=5.5). The six LysM repeats of AtlA were replaced by 3 sets of LysM repeats from AtlB (Figure 3.12 A). To construct the strains producing AtlA with a binding domain made of LysM repeats from AtlB, the pGhost9 derivative pGAtlA$_{1-6HB}$ was constructed (Figure 3.12 B). The insert from pMK-RQ-6HB-GFP (obtained by gene synthesis) was cloned as a NsiI and BglII fragment into pGAtlA$_{1-4}$. The fragment cloned consists of 398 bp encoding AtlA catalytic domain followed by 1209 bp encoding 3 pairs of LysM$_{B1}$ and LysM$_{B2}$ separated by linkers from AtlA. After transformation of the ligation product in *E. coli* TG1 *repA*$^+$ cells, positive clones were identified after plasmid extraction and restriction analysis with XhoI and KpnI (Figure 3.12 C). The absence of mutation in the insert was verified by sequencing.

Plasmid pGAtlA$_{1-6HB}$ was used to transform *E. faecalis* $atlA_1$ cells and allele exchange was carried out. Erythromycin sensitive colonies were screened by PCR using primers AtlA_5' and AtlA_dn. A PCR product from a mutant with the expected DNA size is shown Figure 3.13 A.

The strain expressing a LysM domain with LysMB repeats ($atlA_{1-6HB}$) was analysed by Southern Blot. Genomic DNAs from the putative $atlA_{1-6HB}$, JH2-2 and $atlA_1$ strains were

extracted and digested with BstXI and BstXI and BamHI (Figure 3.13 B), run on an agarose gel and transferred to a nitrocellulose membrane. The DNA samples were probed with a 506 bp DNA fragment encoding the catalytic domain of AtlA. A single band with the expected size (2779 bp) was detected in both WT genomic digestions (Figure 3.13 C). A single band with the expected size (1791 bp) was detected for both $atlA_1$ digestions. Hybridisation with the $atlA_{1-6HB}$ digestion products gave a single band of the expected size for BstXI (2789 bp) and for the BstXI + BamHI digestion (1768 bp, Figure 3.13 C). The Southern blot analyses thus confirmed the allele replacement in strain $atlA_{1-6HB}$.

Production of the AtlA variants was analysed by Western blot using the parental JH2-2 and $\Delta atlA$ strains as controls (Figure 3.13 D). Proteins precipitated from supernatants were probed with rabbit polyclonal antibodies against the catalytic domain of AtlA. The result showed two bands of similar molecular weight below 75 kDa for WT and $AtlA_{1-6HB}$. The enzymatic activity of AtlA present at the cell surface of bacteria was analysed by spotting the cells on BHI-agar plates containing *M. luteus* autoclaved cells as a substrate (Figure 3.13 E). The $AtlA_{1-6HB}$ cells formed a lytic halo around the colonies smaller than that around WT cells. No enzymatic activity was detected around $\Delta atlA$ colonies. This shows that the replacement of basic LysM repeats on the acidic one in the binding domain decrease AtlA enzymatic activity.

The impact of the LysM charge and composition on daughter cell separation was investigated by measuring average cell chain length using flow cytometry (Figure 3.13 F). The FSC values measured showed significant increase in cell chain length in the $atlA_{1-6HB}$ strain as compared to the WT (WT=47.07 ± 0.42, $atlA_{1-6HB}$=173.18 ± 0.68; ***P=0.0003). These results indicated that amino acid composition / charge of LysM modules is important for optimal activity of AtlA.
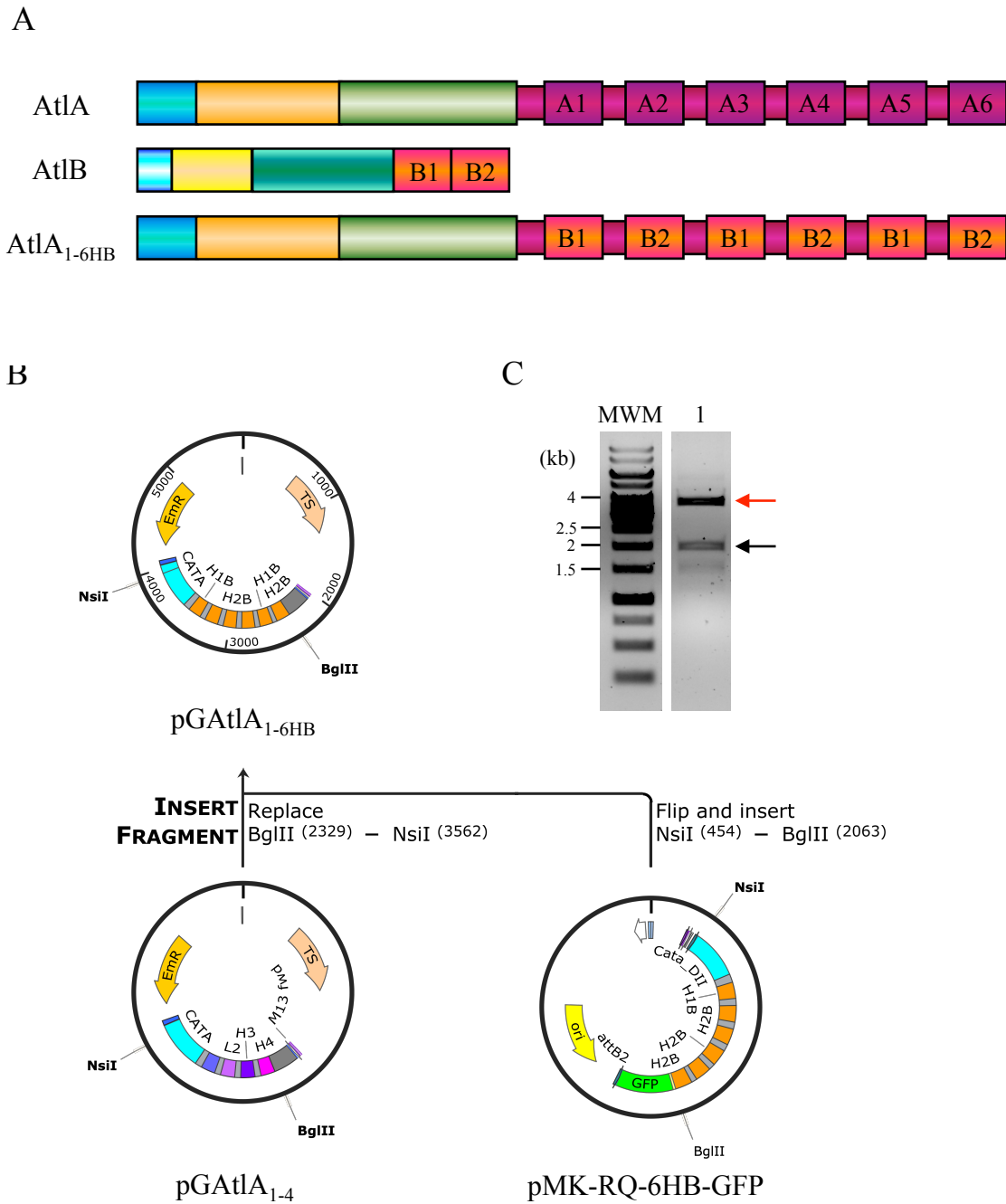
Figure 3.12 Construction of pGAtlA_{1-6HB}

A. Schematic representation of AtlA, AtlB and AtlA_{1-6HB} domain organization. The PG binding domain of AtlA_{1-6HB} consists of six AtlB LysM repeats (H1 and H2) preceded by low complexity sequences from AtlA LysM domain.

B. Schematic representation of the cloning strategy. The insert for the resulting plasmid, pGAtlA_{1-6HB} contains 398 bp encoding AtlA catalytic domain followed by a 6 LysM modules from AtlB and a 260 bp 3' homology region downstream of AtlA stop codon.

The 1609 bp NsiI-BglII fragment from pMK-RQ-6HB-GFP was cloned to pGAtlA$_{1-4}$ similarly digested.

C. Restriction digest of pGAtlA$_{1-6HB}$ using XhoI and KpnI. The expected DNA band of 3750 bp corresponding to the backbone is indicated with a red arrow and 1966 bp band corresponding to the insert is indicated with a black arrow. The sizes of chosen molecular weight markers (MWM) are indicated on the left hand side of the gel.
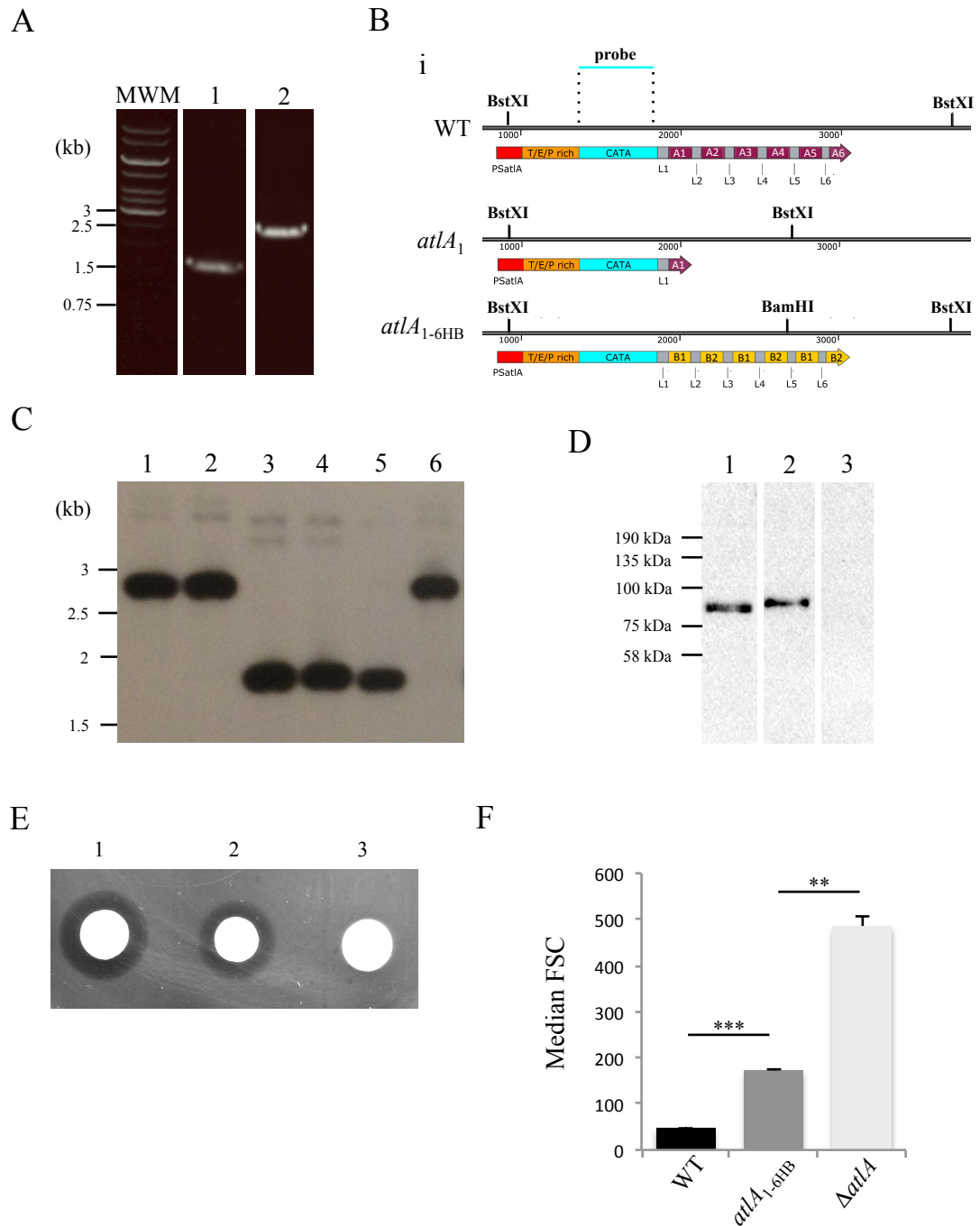
Figure 3.13 Characterisation of *E.faecalis* JH2-2 *atlA*₁₋₆ₕB mutant

A. Amplification products using atlA_up and atlA_dn primers for the parental strain *atlA*₁ (lane 1) and the *atlA*₁₋₆ₕB (lane 2). The expected DNA fragment of 1483bp for *atlA*₁ and 2485 bp for *atlA*₁₋₆ₕB were detected. The sizes of chosen molecular weight markers (MWM) are indicated on the left hand side of the gel.

B. Schematic representation of the wild-type *atlA, atlA*₁ *and atlA*₁₋₆ₕB alleles with selected restriction sites as well as the probe used for the Southern blot.

C. Southern Blot analysis of the *E. faecalis* JH2-2 $atlA_{1\text{-}6HB}$ strain. Chromosomal DNA of WT (lane 1, 2), $atlA_1$ (lane 3, 4), $atlA_{1\text{-}6HB}$ (lane 5, 6) were digested with BstXI and BamHI and run on an agarose gel and transferred on to a nitrocellulose membrane. The membrane was probed with a 506 bp fragment encoding the catalytic domain of AtlA. Bands of expected sizes were detected: 2779 bp (BstXI, lane 1) and 2779 bp (BstXI and BamHI, lane 2) for WT, 1791 bp (BstXI, lane 3) and 1791 bp (BstXI and BamH1, lane 4) for $atlA_1$, 2789 bp (BstXI, lane 5) and 1768 bp (BstXI and BamH1, lane 6) for $atlA_{1\text{-}6HB}$. The sizes of chosen molecular weight markers (MWM) are indicated on the left hand side of the gel.

D. Western blot detection of AtlA proteins in culture supernatants. Proteins precipitated from supernatants exponentially growing cells were recovered by centrifugation and washed with acetone and resuspended in PBS. Following SDS-PAGE and transfer on a nitrocellulose membrane, AtlA proteins were probed with anti-AtlA polyclonal serum against the catalytic domain of AtlA. Lane 1, WT-72 kDa; lane 2, $atlA_{1\text{-}6HB}$ −73 kDa; lane 3, Δ*atlA*. The sizes of chosen molecular weight markers are indicated on the left hand side of the blot.

E. Analysis of $AtlA_{1\text{-}6HB}$ enzymatic activity present at the cell surface of bacteria. Exponentially growing cells (OD_{600} ~1.0) of WT (1), $atlA_{1\text{-}6HB}$ (2) and Δ*atlA* (3) were spotted on BHI agar plates with *M. luteus* autoclaved cells as a substrate. The lytic halo formed by $atlA_{1\text{-}6HB}$ was smaller than that formed by WT. No enzymatic activity was detected for the Δ*atlA* strain.

F. Comparison of median FSC values corresponding to cell chains formed by *E. faecalis* WT, $atlA_{1\text{-}6HB}$ and Δ*atlA*. The median FSC value of $atlA_{1\text{-}6HB}$ was significantly higher than the median FSC value of WT (***P=0.0003) but lower from that of the Δ*atlA* strain (**P=0.0045). All measurements were done in triplicates.

3.8   Concluding remarks

Previous work indicated that AtlA plays a major role in cell separation. Another PG hydrolase (AtlB) was also shown to cleave the septum, but with a much weaker activity than AtlA.

In this chapter, we compared the abundance of AtlA and AtlB produced by *E. faecalis* JH2-2. We found that AtlA is at least 30-fold more abundant than AtlB. However, we showed that this difference does not account for the prominent role of AtlA in cell separation; the expression of *atlB* under the atlA promoter in the absence AtlA led to formation of long cell chains suggesting that the relatively high expression level of *atlA* is not sufficient to explain the functional specialization of this enzyme. We further investigated AtlA properties and found that both the N-terminal and LysM domain are important for the control of septum cleavage. The N-terminal domain of AtlA undergoes two post-translational modifications: *O*-glycosylation that inhibits the cells separation and a proteolytic cleavage that stimulates it. We established that the LysM domain, which consists of six basic LysM modules is also critical for cell separation. The sequential truncation of the LysM binding modules as well as the replacement of the basic modules by acidic ones from AtlB led to the formation of long cell chains, indicating that both the positive charge and multimodularity contribute to AtlA functional specialisation.

AtlA is the only *E. faecalis* PG hydrolase which can cause cell lysis (Qin et al., 1998). It was therefore expected that several mechanisms are in place to ensure a tight control of its activity. The results presented in this chapter indicate that the cleavage of the glycosylated N-terminal domain by extracellular proteases is required for AtlA to display its maximum cleavage activity. The metalloprotease GelE has been shown to be required for the formation of diplococci (Waters et al., 2003) and is therefore likely to contribute to AtlA cleavage during growth. No direct evidence supporting this hypothesis has been provided yet.

CHAPTER 4

Subcellular localisation of AtlA

4.1   Localisation of *E.faecalis* AtlA

Immunofluorescence microscopy was successfully used to study a subcellular distribution of AcmA, a major autolysin in *Lactococcus lactis* (Steen et al., 2005). The same approach was applied to study subcellular localisation of AtlA in *E. faecalis*. Rabbit polyclonal antibodies raised against the catalytic domain of AtlA, previously used in western blot (Section 3.2.3) were used to carry out the immunolabelling. To test the specificity of anti-catalytic domain of AtlA antibodies the Δ*atlA* cells were included as a negative control. Both strains were grown to early exponential phase, fixed with paraformaldehyde and probed with rabbit anti-AtlA and goat anti-rabbit IgG conjugated with AlexaFluor647 (AF647). Bacteria were immobilised on agarose pads and visualised immediately using conventional fluorescence microscopy.

A strong fluorescent signal associated with septa and poles was detected in WT cells. As expected, no fluorescent signal was detected for the Δ*atlA* mutant, indicating that antibodies were specifically detecting AtlA. To improve the resolution of the images, specific algorithms were applied to increase a signal-to-noise ratio. Deconvolved images showed the same defined pattern of AtlA localisation (Figure 4.1).

To further investigate AtlA subcellular localisation, images of 4 individual Z stacks were compressed to a Z-projection of maximum fluorescence intensity and used for analysis (Figure 4.2 A). The distribution of the immunolabelled AtlA was presented as a population demograph (Buss et al., 2017), showing a correlation between fluorescence signal intensity and the cell length. Cell length was determined by plotting intensity profiles along the longer cell axis of the cells (yellow line) imaged in bright-filed (Figure 4.2 A). The distribution of the fluorescent signal corresponding to labelled AtlA was measured by plotting a fluorescent intensity profile along the same axis (Figure 4.2 B). The fluorescent profiles of 50 randomly chosen cells were used to create a population demograph (Figure 4.2 C). The analyses of the population demograph

showed that AtlA was present both at the cell poles and in the septum of the diplococci. During the cell growth AtlA can also be detected in the next division sites also called equatorial rings (Figure 4.2 C).

Due to the light diffraction limit, AtlA localisation was also studied using two super resolution microscopy techniques: 3D SIM and STORM. 3D SIM reaches a resolution twice higher than standard light microscopy techniques (Schermelleh et al., 2010). *E. faecalis* JH2-2 cells were labelled as described above. Labelled cells were immobilised on a cover slip coated with poly-L-lysine and mounted in an antifade reagent, SlowFade Gold® to prevent signal lost during image acquisition. The AtlA distribution visualised by 3D SIM (microscopy performed in collaboration with Dr Christa Walther, University of Sheffield) was comparable to that determined by conventional fluorescence microscopy (Figure 4.3 A). The 3D SIM imaging showed more defined AtlA localisation. At the beginning of the division the hydrolase formed a ring-like structure at the division sites. Following the cell growth the AtlA 'ring' became smaller and formed two disc-like structures between adjacent cells. At the final stage of the division AtlA appears at the next division site (Figure 4.3 B). Those observations explain why AtlA appeared as a relatively wide 'ring' between daughter cells when visualized by conventional microscopy (Figure 4.3 B iii). Although the fluorescent profiles plotted for the same cells visualised by conventional and 3D SIM microscopy looked very similar (Figure 4.3 C).

Stochastic optical reconstruction microscopy (STORM) allows visualisation of two particles 20 nm apart (Betzig et al., 2006). *E. faecalis* JH2-2 cells labelled as described above, were immobilised on a cover slip coated with poly-L-lysine and mounted in GLOX MEA buffer. This buffer reduces oxygen (GLOX) and controls the excitation and emission of a fluorophore (MEA). Reconstruction of the STORM data was performed by Dr Robert Turner. The results showed the same distribution of AtlA as the one obtained by 3D SIM microscopy, that the hydrolase at the final stage of the division is associated with newly synthetized peptidoglycan. AtlA was detected at the septum and poles as well as in next division sites, equatorial rings (Figure 4.4).
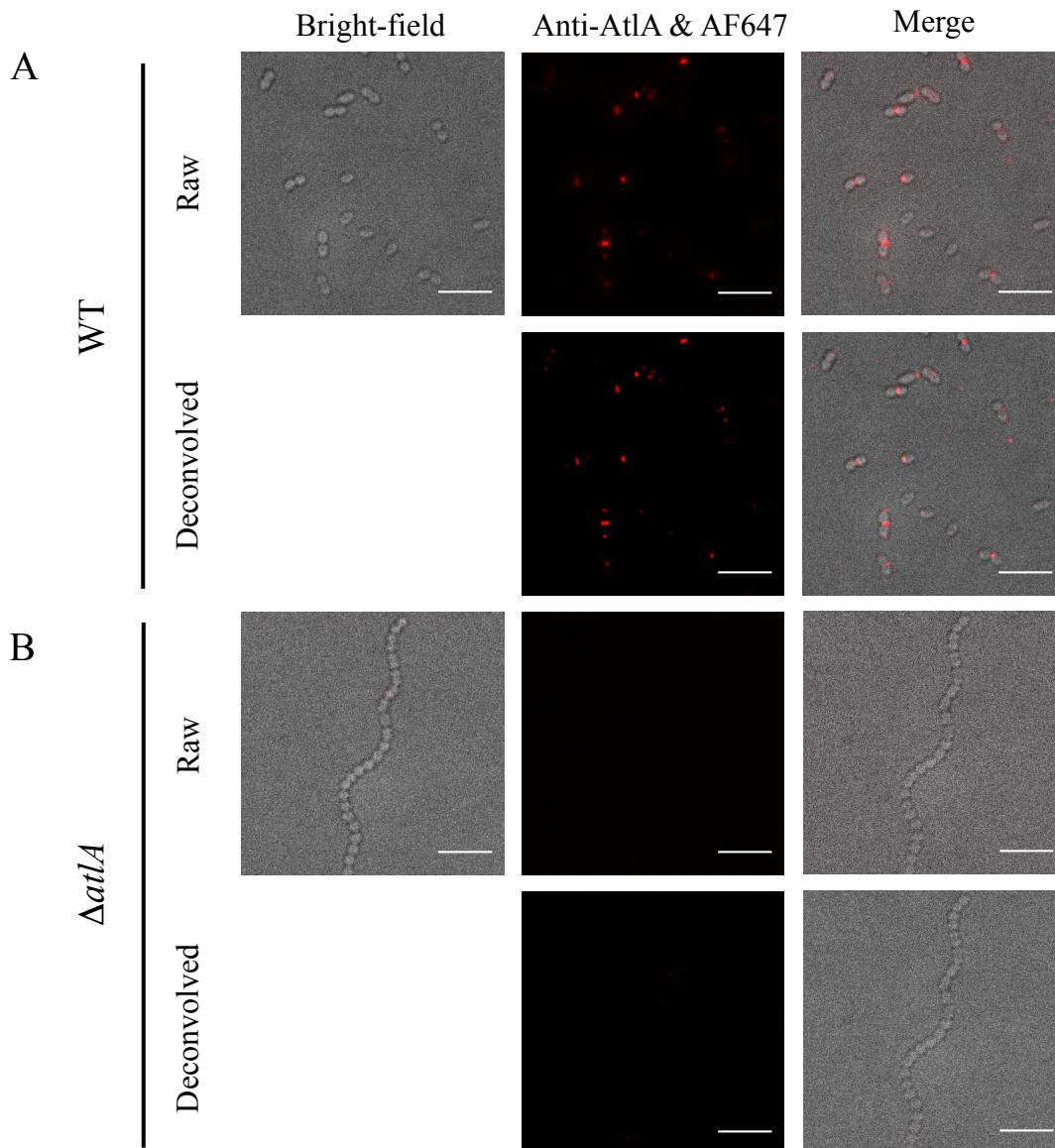
Figure 4.1 Immunolabelling of *E. faecalis* cells using anti-AtlA antibodies

Bright-field and fluorescent images of *E. faecalis* JH2-2 (A) and Δ*atlA* (B) probed with anti-AtlA serum at a 1:250 dilution and detected with anti-rabbit IgG antibodies conjugated with AlexaFluor647 (AF647). Scale bars are 5 μm.
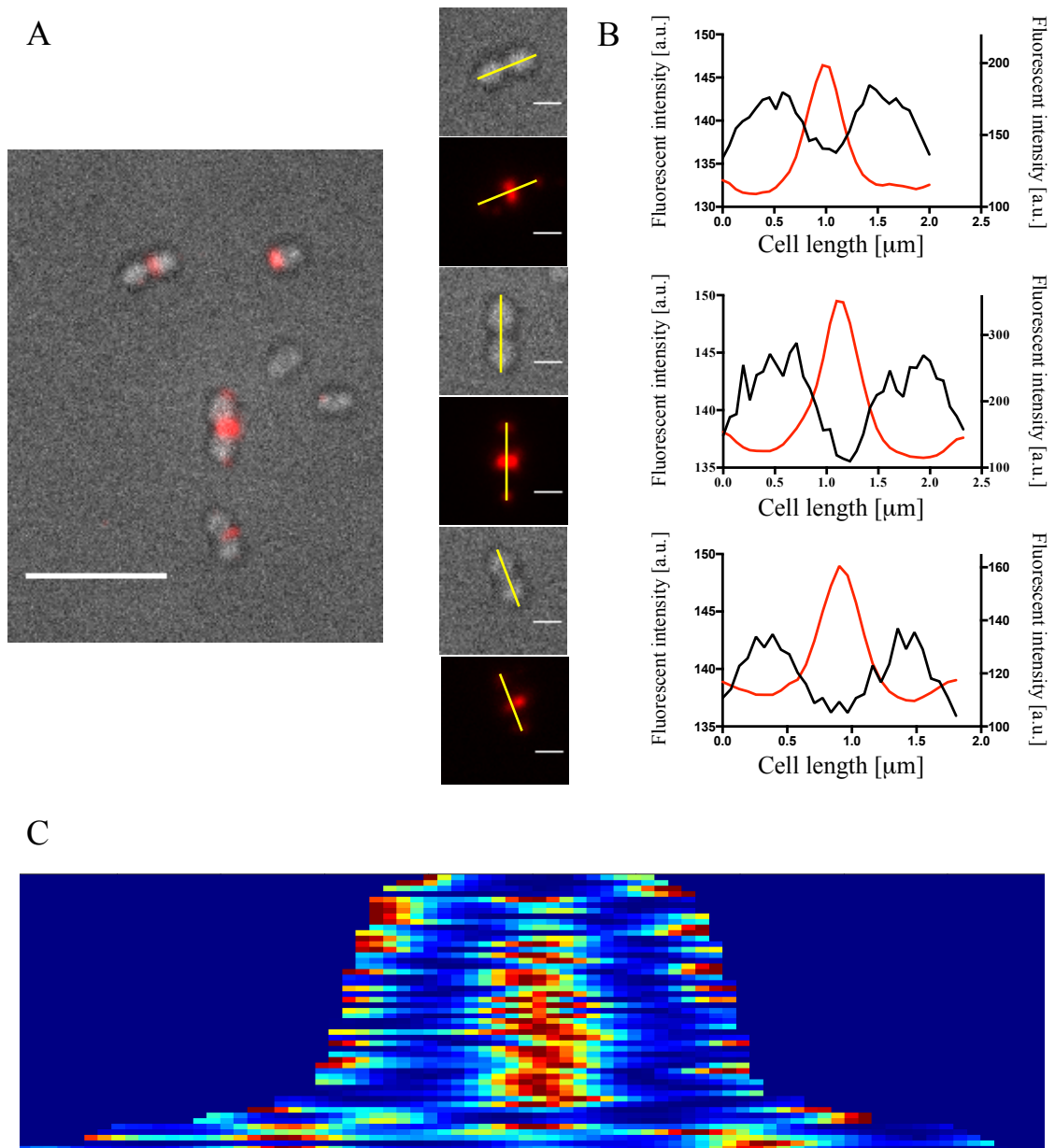
Figure 4.2. Subcellular localisation of AtlA

A. Z-projection of maximum fluorescent intensity of immunolabelled *E. faecalis* JH2-2 cells used to plot the intensity profiles. The intensity profiles were plotted along the longer cell axis indicated by yellow line. Scale bars, 5 μm (big image) and 1 μm (small images).

B. Cell length and the distribution of AtlA were determined by plotting intensity profiles of the cells imaged in bright-filed (black line) and fluorescent channel (red line), respectively.

C. Population demograph created by using the fluorescent profiles of 50 randomly chosen cells, showing a correlation between fluorescence signal intensity along the cell length.
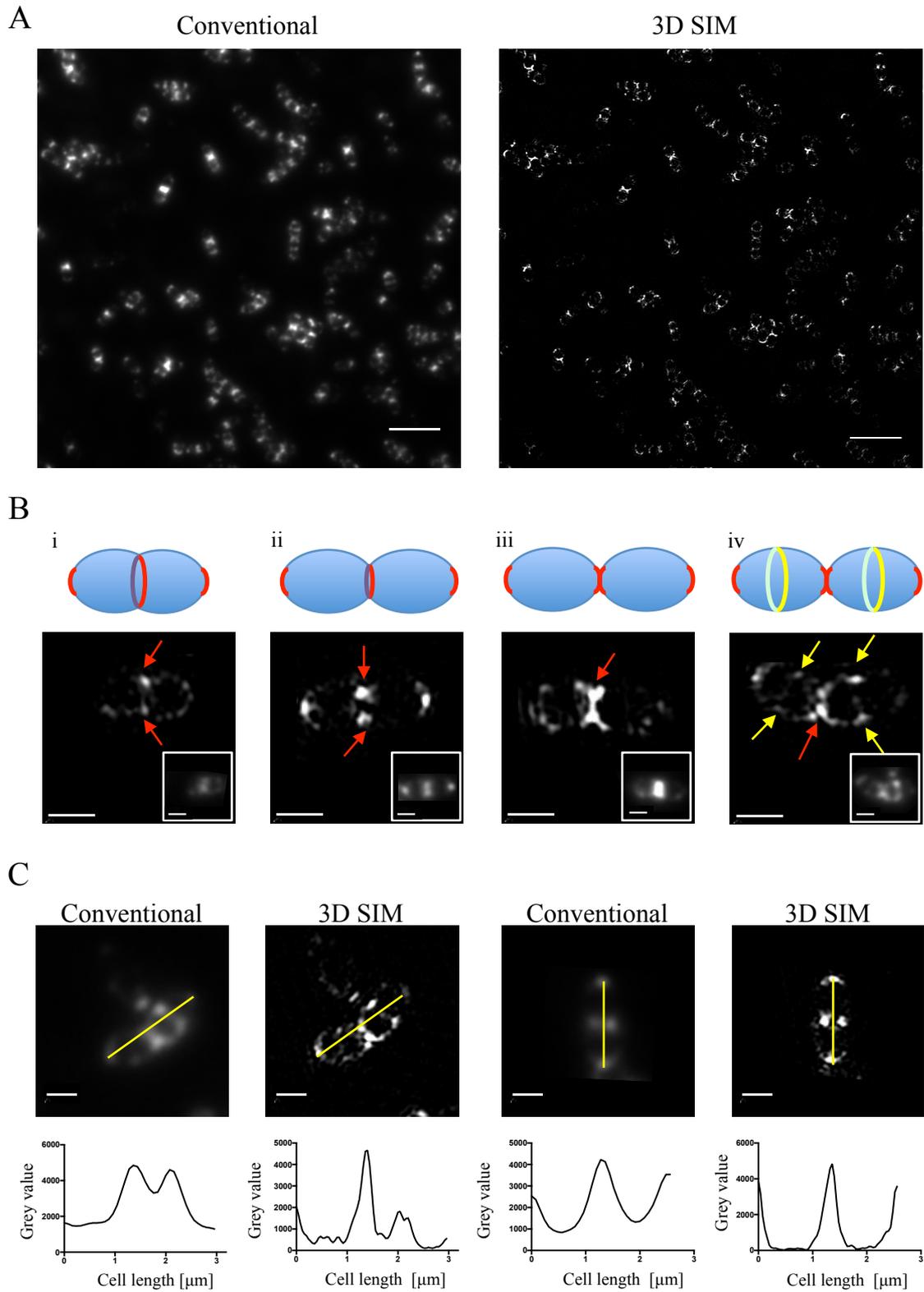
Figure 4.3 3D SIM localisation of immunolabelled AtlA in *E. faecalis* JH2-2

A. Conventional and 3D SIM visualisation of immunolabelled AtlA in *E. faecalis* JH2-2. Scale bars, 5 μm.

B. Schematic representation of AtlA localisation on the surface of dividing cells with example 3D SIM (large images) and conventional microscopy (small images, bottom left corner) images of individual cells at the particular stages of the cell growth. (i) At the first stage, AtlA localises at the septum (indicated with a red arrow). (ii and iii) Following the cell growth the AtlA 'ring' becomes smaller to the point where it forms an "X" shape between adjacent cells (indicated with a red arrows). (iv) At the final stage of the division AtlA localises at the old septum (indicated with a red arrow) and at the new division sites, forms a ring like structure (indicated with yellow arrows). Scale bars, 1μm.

C. Fluorescent profiles showing distribution of AtlA. AtlA distribution was measured along the indicated axis (yellow lines) for the same cells visualised by 3D SIM and conventional microscopy. Scale bars, 1 μm.
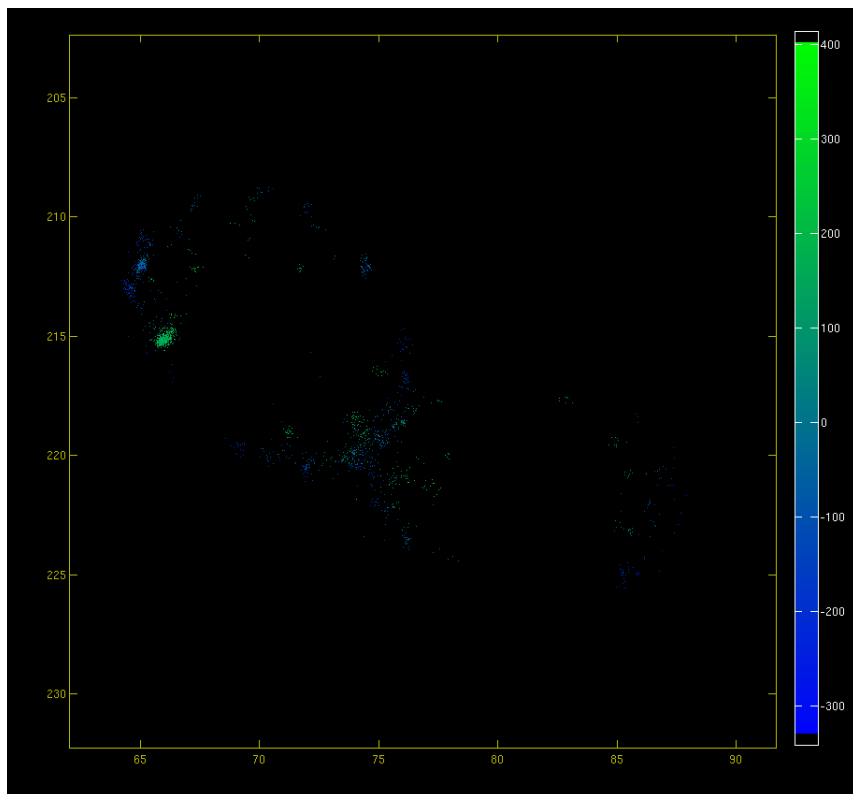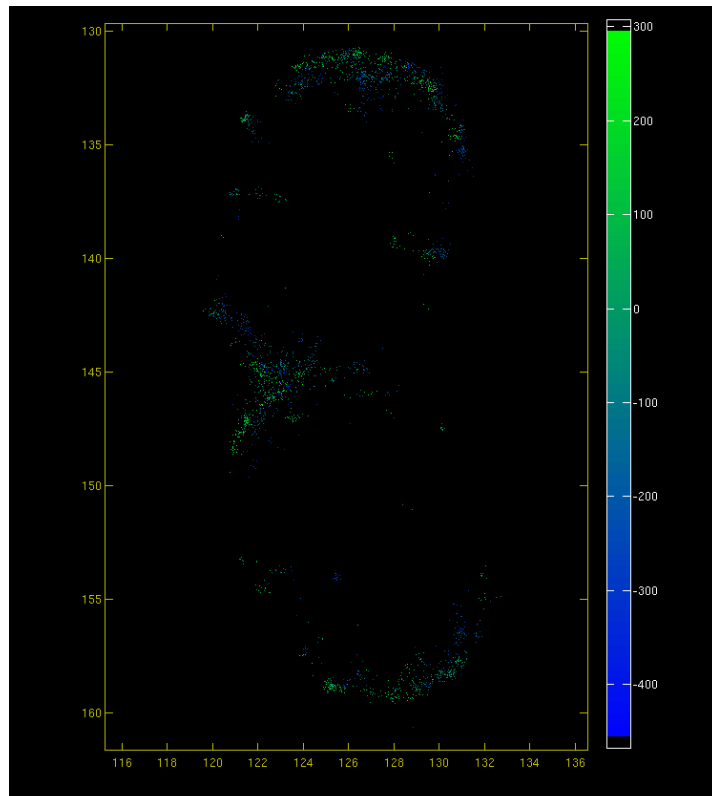
Figure 4.4 Localisation of immunolabelled AtlA in *E. faecalis* JH2-2 by 3D STORM

3D STORM reconstructions showing localisation of immunolabelled AtlA. Imaging performed in GLOX MEA. The colour scale represents the z-axis.

4.2   Localisation of AtlA-GFP fusions

To confirm the results of the immunolabelling experiments, a JH2-2 derivative producing AtlA fused to the GFP ($atlA_{1-6}$-gfp) was constructed. pGAtlA$_{1-6}$-GFP, a pGhost 9 derivative was constructed as presented in Figure 4.5 A. A fragment of DNA encoding a LysM biding domain of AtlA (LysM$_A$; 1218 bp) was PCR-amplified using primers AtlA1-6_H1 and AtlA1-6_H2 (Figure 4.5 B). The amplification product was cloned to pGAtlA$_1$-GFP (Section 5.2.2) using NcoI and BglII. Plasmid restriction analyses with XhoI and KpnI confirmed the presence of an insert of the expected size (Figure 4.5 C). The insert was sequenced to confirm the absence of mutations.

pGAtlA$_{1-6}$-GFP was transformed into electrocompetent *E. faecalis* JH2-2 cells. Following integration of the plasmid to the chromosome by homologous recombination and serial subcultures, the erythromycin sensitive colonies were screened by PCR using primers AtlA_5' and AtlA_dn. None of 31 putative mutants revealed the expected band (data not shown). We therefore used colony blotting to screen more colonies. DNA of lysed bacteria was probed with a DNA fragment encoding GFP. One out of 200 colonies screened gave a stronger signal than the rest (Figure 4.6 A). The allele replacement in the putatively positive clone was confirmed by PCR using primers AtlA_5' and AtlA_dn (Figure 4.6 B). Production and secretion of the AtlA$_{1-6}$-GFP fusion in *E. faecalis* JH2-2 $atlA_{1-6}$-gfp was further analysed by western blot. *E. faecalis* JH2-2 $atlA_{1-6}$-gfp was grown to early exponential phase. Proteins from supernatant were precipitated using 10% (w/v) TCA and analysed by western blot using anti-AtlA polyclonal serum. A single band slightly above 72 kDa was detected for the parental strain, *E. faecalis* JH2-2 (Figure 4.6. C). Two bands were observed for the putative mutant. The higher band was detected just above 100 kDa, the expected size for the AtlA$_{1-6}$-GFP fusion. The lower band was detected slightly above the wild-type AtlA band (Figure 4.6. C). These results indicated that the fusion was successfully produced and secreted by *E. faecalis* JH2-2 $atlA_{1-6}$-gfp. Detection of the lower band suggested a truncation of the fusion protein, albeit in relatively low abundance. The hydrolytic activity of the AtlA$_{1-6}$-GFP fusion was tested by zymogram assay using *M. luteus* PG as a substrate (Figure 4.6. D).
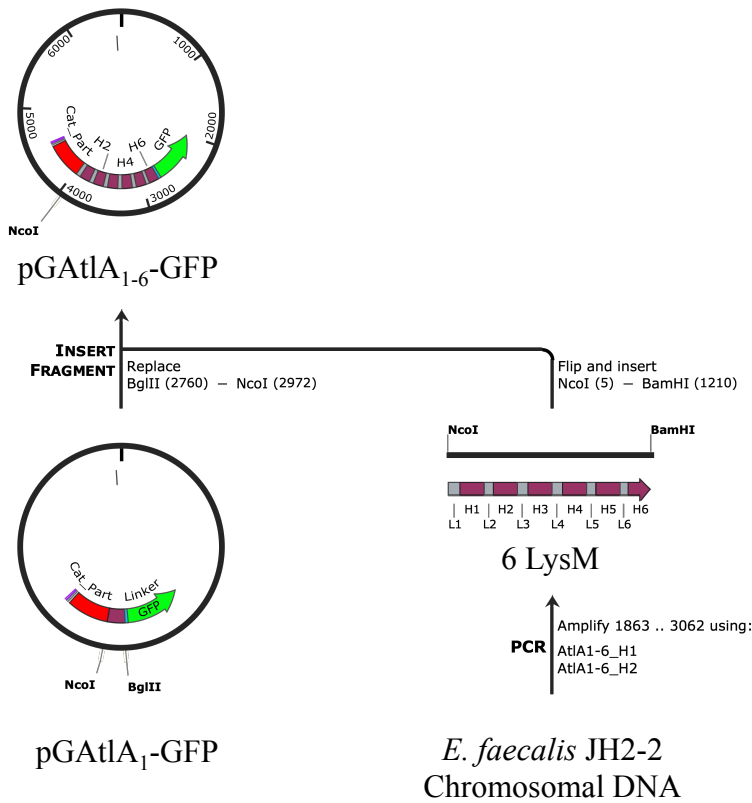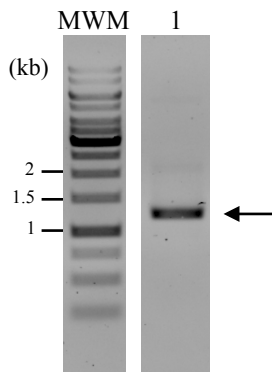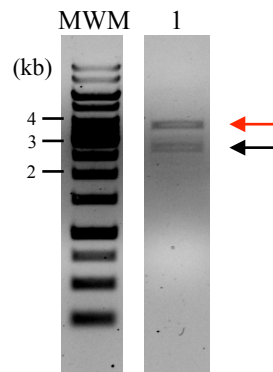
Figure 4.5 Construction of pGAtlA$_{1-6}$-GFP

A. Schematic representation of the cloning strategy of pGAtlA$_{1-6}$-GFP. A DNA fragment encoding LysM$_A$ was PCR-amplified using primers AtlA1-6_H1/AtlA1-6_H2 and cloned to pGAtlA$_1$-GFP using NcoI and BglII restriction enzymes.

B. Amplification product using primers AtlA1-6_H1 and AtlA1-6_H2. The expected DNA band size of 1218 bp is indicated by a black arrow. The sizes of selected molecular weight markers (MWM) are indicated on the left hand side of the gel.

C.   Restriction profile of pGAtlA$_{1-6}$-GFP digested with XhoI and KpnI. The expected DNA bands corresponding to the vector backbone (3750 bp) and the insert (2713 bp) are indicated by the red and black arrows, respectively. The sizes of selected molecular weight markers (MWM) are indicated on the left hand side of the gel.
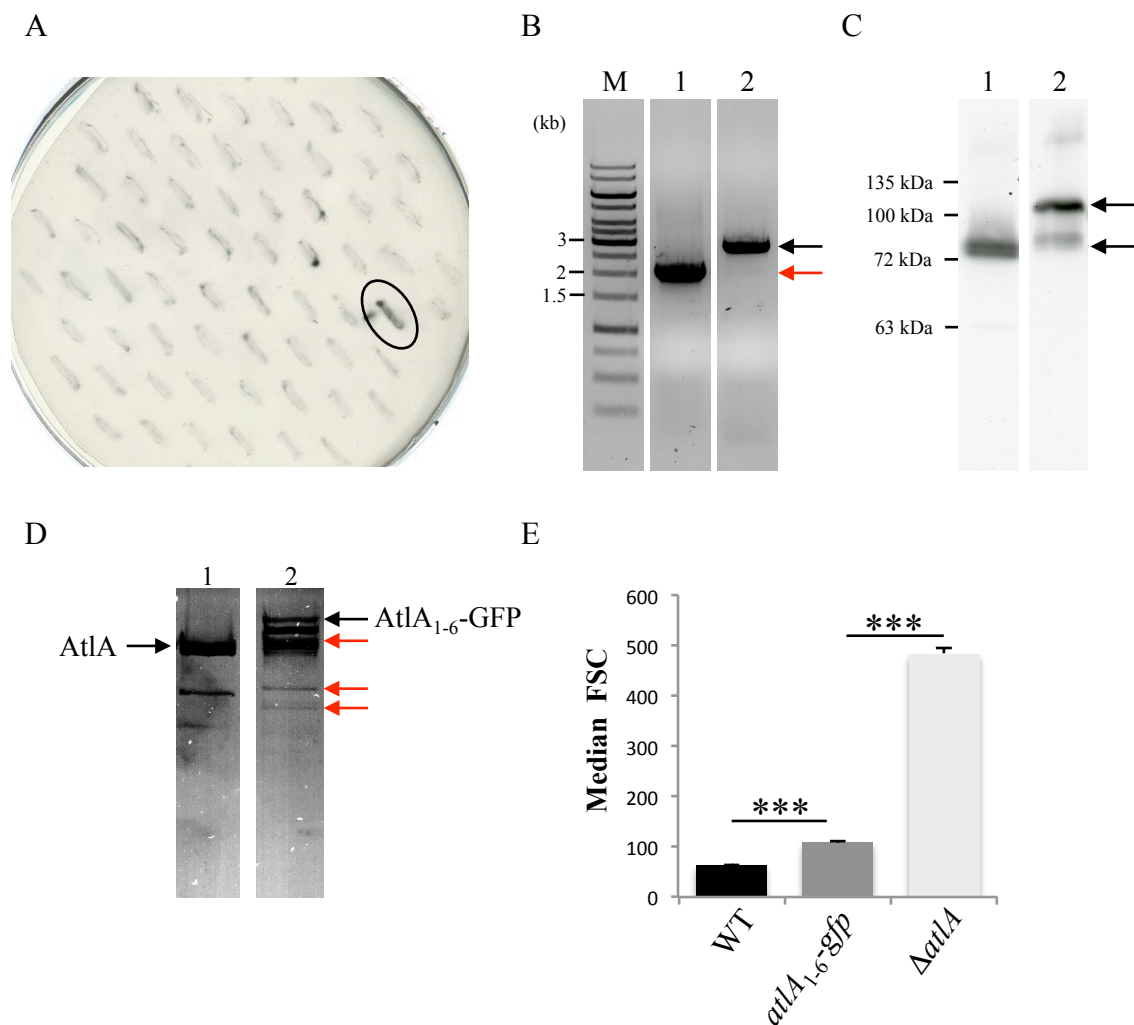
Figure 4.6 Characterization of *E. faecalis* JH2-2 *atlA₁₋₆-gfp*

A. Colony blotting of potential mutants expressing AtlA fused to the GFP. DNA of lysed bacteria was probed with a DNA fragment encoding GFP. The positive clone of *atlA₁₋₆-gfp* is circled.

B. PCR amplification products using AtlA_5' and AtlA_dn primers for the parental strain (lane 1) and the *atlA₁₋₆-gfp* putative mutant (lane2). The expected DNA band sizes of 2098 bp and 2851 bp of the parental strain and the putative mutant are indicated by a red and black arrow, respectively. The sizes of chosen molecular weight markers (MWM) are indicated on the left hand side of the gel.

C. Western blot detection of AtlA proteins in culture supernatants. Proteins precipitated from supernatants of exponentially grown cells using 10% (w/v) TCA were recovered by centrifugation and washed with acetone and resuspended in PBS. Following SDS-PAGE and transfer on a nitrocellulose membrane, proteins were probed with anti-AtlA polyclonal

serum raised against the catalytic domain of AtlA. Native AtlA in WT (lane 1) and AtlA$_{1-6}$-GFP in *atlA$_{1-6}$-gfp* (lane 2) are indicated with arrows.

D. Zymogram analysis of AtlA produced by *E. faecalis* JH2-2 (lane 1), the putative *atlA*1-6-*gfp* mutant (lane 2). *M. luteus* peptidoglycan was used as a substrate. The expected band sizes for AtlA and AtlA-GFP are indicated with the black arrows. The truncated versions of AtlA-GFP are indicated with the red arrows.

E. Comparison of median FSC values corresponding to an average cells chain length formed by WT, *atlA*1-6-*gfp* and Δ*atlA*. The median FSC value of *atlA*1-6-*gfp* was significantly different from the median FSC value of WT (***$P=0.0003$) and Δ*atlA* (***$P=0.0001$). All measurements were done in triplicates.

Proteins from supernatants of exponentially grown cells of JH2-2 and $atlA_{1-6}$-*gfp* were analysed. A main lytic band corresponding to wild-type AtlA was detected for the parental strain. Several lytic bands corresponding to the AtlA-GFP fusion and truncated forms of this fusion were detected for the $atlA_{1-6}$-*gfp* strain (Figure 4.6. D). This result revealed that the AtlA fusion to the GFP did not prevent activity. Next, cell chain length of the strain producing the AtlA-GFP fusion was measured by flow cytometry (Figure 4.6 E). The results showed a significant increase in cell chain length for the *atlA*1-6-*gfp* strain (FSC= 108±0.69) as compared to the parental strain (FSC= 62.22±1.05). However, the fluorescent mutant formed much shorter cell chains than the Δ*atlA* mutant (FSC=482.14±11.79). These results suggested that the GFP fusion had a minor effect on the daughter cell separation.

The subcellular distribution of the AtlA-GFP fusion in exponentially grown JH2-2 *atlA*1-6*gfp* was analysed by conventional fluorescence microscopy. Images before and after deconvolution showed that AtlA-GFP localised at the septum and poles of *E. faecalis* JH2-2 *atlA*1-6-*gfp* cells (Figure 4.7 A). The subcellular distribution of the AtlA fusion was analysed as previously described in paragraph 4.2.1. Cell length and the distribution of the AtlA-GFP were determined by plotting intensity profiles of the cells imaged in bright-filed (black line) and the fluorescent channel (green line) (Figure 4.7 B). The fluorescent profiles of 50 randomly chosen cells were used to crate a population demograph (Figure 4.7 C) and showed that the AtlA fusion was present both at the poles and in septum of the diplococci. Additionally, in short chains of four cells the fusion was detected at the equatorial rings (Figure 4.7 C).
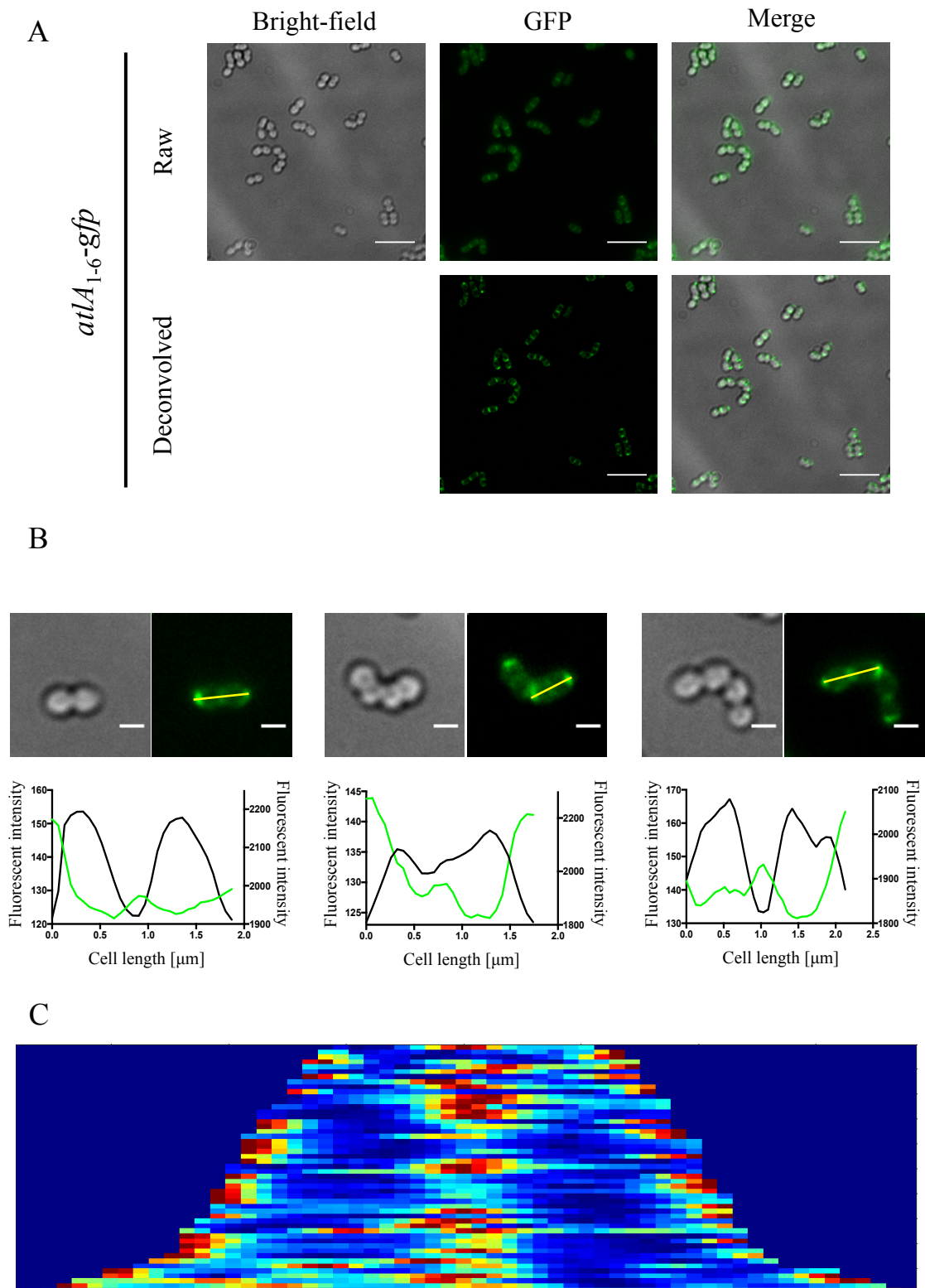
Figure 4.7 Subcellular localisation of AtlA$_{1-6}$-GFP fusion in *atlA$_{1-6}$-gfp* strain

A. Bright-field and fluorescent images of *E. faecalis* JH2-2 *atlA$_{1-6}$-gfp* before (raw) and after deconvolution. Scale bars, 5 μm.

B. Z-projection of maximum fluorescent intensity of *E. faecalis* JH2-2 *atlA*$_{1-6}$-*gfp* cells. Cell length and the distribution of AtlA-GFP were determined by plotting intensity profiles of the cells imaged in bright-filed (black line) and the fluorescent channel (green line), respectively; The profiles were plotted along the longer cell axis indicated by yellow line. Scale bars, 1 μm.

C. Population demograph created by using the fluorescent profiles of 50 randomly chosen cells, showing a correlation between fluorescence signal intensity along the cell length.

4.3 Concluding remarks

The prominent role of AtlA in septum cleavage suggested that this enzyme could be preferentially targeted to the septum. In this chapter, we confirmed that this hypothesis is correct and showed a restricted localisation of AtlA at the septum and cell poles. Interestingly, the polar localisation of AtlA was detected by both immuno- and GFP labelling, but the labelling was much more pronounced in the GFP strains. The most obvious explanation for this is that the presence of polymers could prevent access of the antibodies to AtlA. AtlA forms a ring-like structure on the cell surface where the division occurs. During growth/division the ring becomes smaller to the point where AtlA forms a two disc-like structures between adjacent cells, which appear as an 'X' shape (Figure 4.8). Along with the progress of cell division, AtlA appears at the next division sites, called the equatorial ring.

The septal localisation of enzymes involved in cell separation has been previously reported (De Las Rivas et al., 2002; Steen et al., 2003; Layec et al., 2009) but none of the experimental strategies used strains producing full length GFP translational fusions, hence introducing an experimental bias. As indicated above, potential issues can arise from a limited accessibility of antibodies during immunofluorescence experiments. This work indicates that GFP fusions can be used to study the subcellular localisation of surface proteins in *E. faecalis*. This was a key finding that enabled us to further study the mechanisms underpinning AtlA septal and polar localisation.

Figure 4.8 Model of AtlA cell surface display during cell growth/division

Shematic representation of the AtlA cell surface display during *E. faecalis* cell growth/division. The two disc-like structure formed by AtlA at the septum is highlited in a boxed area.

127
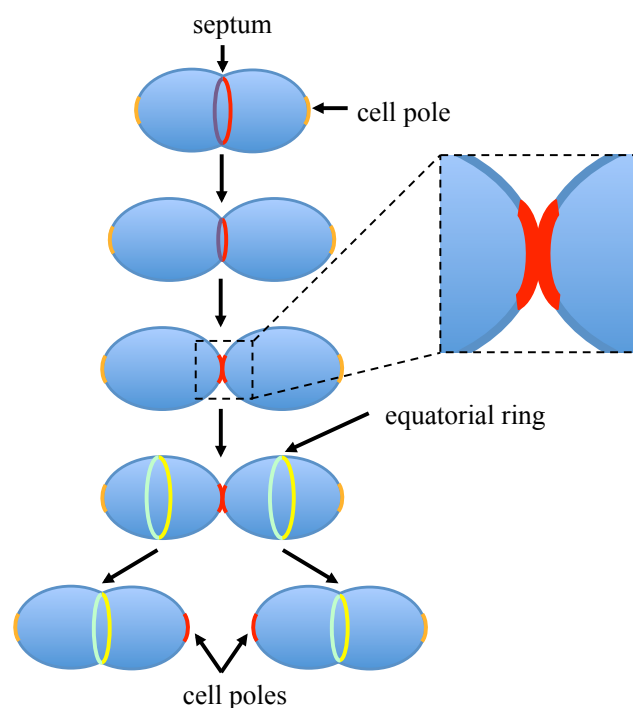
CHAPTER 5

Targeting of AtlA to the septum

5.1 Contribution of AtlA targeting signals (signal peptide and LysM domain) to its septal localisation

The signal peptide of AtlA is unusually long (53 residues) as compare to AtlB signal peptide (22 residues), suggesting that it could play a role in the targeting of AtlA to the septum. We used epifluorescence microscopy to compare the localisation of different GFP fusions containing either of these two signal peptides. Strains s_A-gfp-lysM$_A$, s_B-gfp-lysM$_B$, s_A-gfp-lysM$_B$, s_B-gfp-lysM$_A$, s_A-gfp and s_B-gfp, were available in the laboratory strain collection. All strains produce fluorescent fusions, expressed under the control of the *atlA* promoter. In strain s_A-gfp-lysM$_A$, the N-terminal and catalytic domains of AtlA were replaced by the GFP (Figure 5.1 A). As expected, this mutant formed long chains due to the lack of AtlA enzymatic activity. The fluorescent signal corresponding to the S_A-GFP-LysM$_A$ fusion was associated with septa and cell poles (Figure 5.1 B). This localisation was similar to the one observed for the full length AtlA-GFP fusion in the *atlA*$_{1-6}$-*gfp* strain (Chapter 4, Figure 4.7A). This result indicated that the N-terminal and catalytic domains of AtlA are not required for AtlA septal localisation. This result also indicated that we could use this strategy to study AtlA and AtlB targeting signals. Next, we studied the localisation of S_B-GFP-LysM$_B$, a fusion consisting of the signal peptide and LysM biding domain from AtlB (Figure 5.1 A). In the s_B-gfp-lysM$_B$ strain, S_B-GFP-LysM$_B$ was associated only with a half of a cell creating an 'X'-shaped pattern between adjacent cells. Moreover, the fusion was found at the next division site (equatorial rings), forming two foci at the end of 'X' arms (Figure 5.1 C). These results suggested that the targeting signals of AtlA confer a restricted localisation of the GFP, while the targeting signals of AtlB do not.

The differences observed in the localisation of the fusions could be due to differences between AtlA and AtlB binging domains. To investigate this possibility, we compared the subcellular localisation of S_A-GFP-LysM$_B$ and S_B-GFP-LysM$_A$. S_A-GFP-LysM$_B$ is a

fusion of the AtlA signal peptide with the GFP and the LysM domain of AtlB; S_B-GFP-LysM$_A$ is a fusion of the AtlB signal peptide with the GFP and the LysM domain of AtlA (Fig. 5.1 A). S_A-GFP-LysM$_B$ was found in the whole cell volume, suggesting that the fusion was sequestered in the cytoplasm (Figure 5.1 D). The strain producing S_B-GFP-LysM$_A$ fusion gave an 'X'-shaped pattern with foci in between every two or four adjacent cells (Figure 5.1 E). Overall this data suggest that AtlA requires the AtlA LysM domain for targeting to the septum. Furthermore, an accumulation of the S_A-GFP-LysM$_B$ but not S_B-GFP-LysM$_A$ suggested that the signal peptide from AtlA is not sufficient to ensure protein secretion and septal localisation.

To study AtlA and AtlB signal peptides, we compared strains s_A-*gfp* and s_B-*gfp*, producing fusions between the GFP and the signal peptide of AtlA or AtlB (Fig 5.1 A). The localisation of S_A-GFP was found in the cytoplasm, similar to what we observed for S_A-GFP-LysM$_B$ (Figure 5.1 F). By contrast, S_B-GFP gave a weak fluorescent signal suggesting an efficient secretion of the GFP in supernatants. The fluorescence was associated with only half of the cells, showing an 'X'-shaped distribution, similar to what we observed for S_B-GFP-LysM$_B$ (Figure 5.1 G).

Collectively, these results indicated that translocation of the GFP across the membrane and septal localisations require both AtlA signal peptide and LysM domain. The major autolysin of *E. faecalis* therefore seems to have a unique subcellular targeting mechanism It is intriguing that the C-terminal domain of AtlA can be involved in secretion of this hydrolase. We therefore decided to further explore the properties of AtlA LysM domain important for septal localisation.
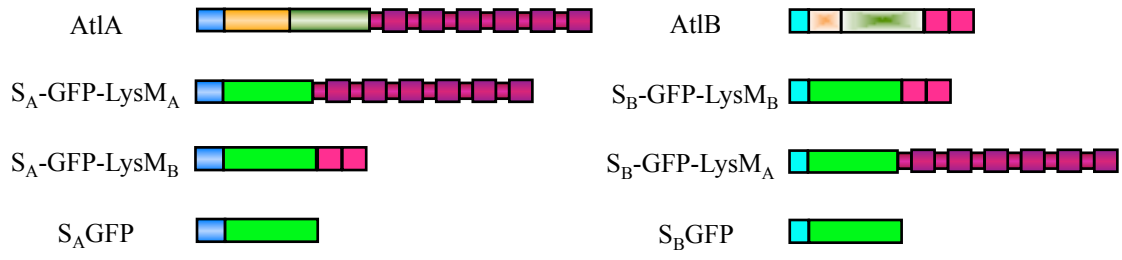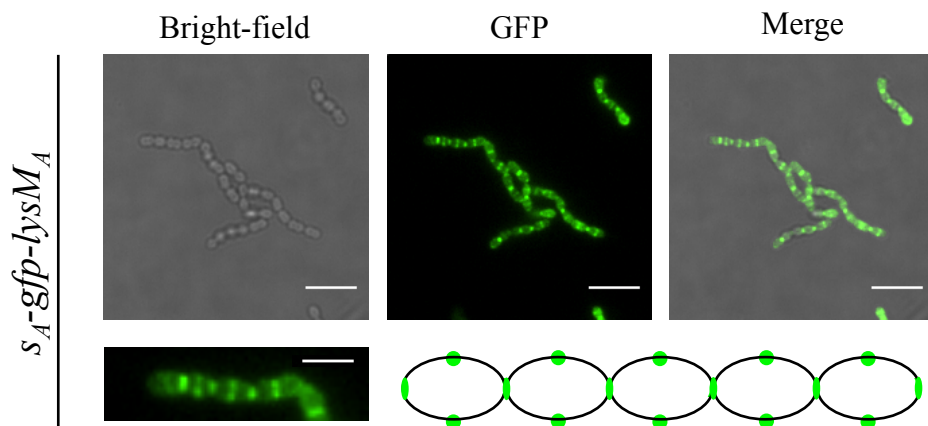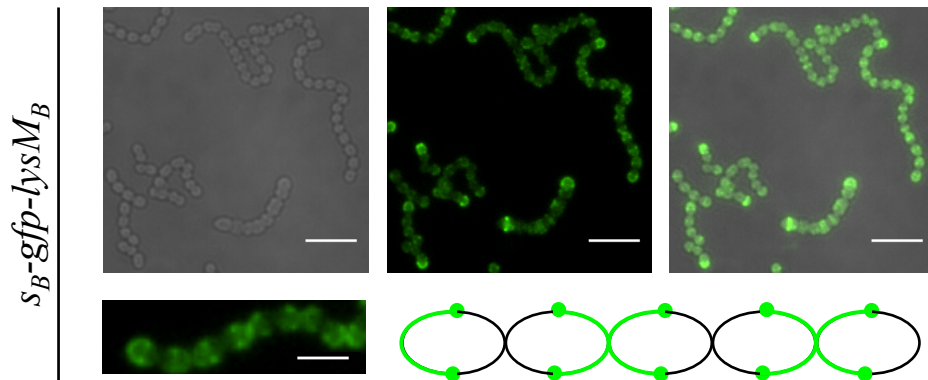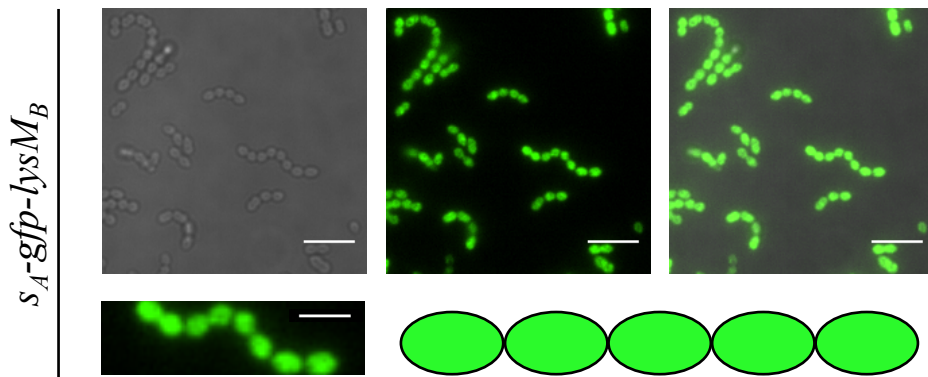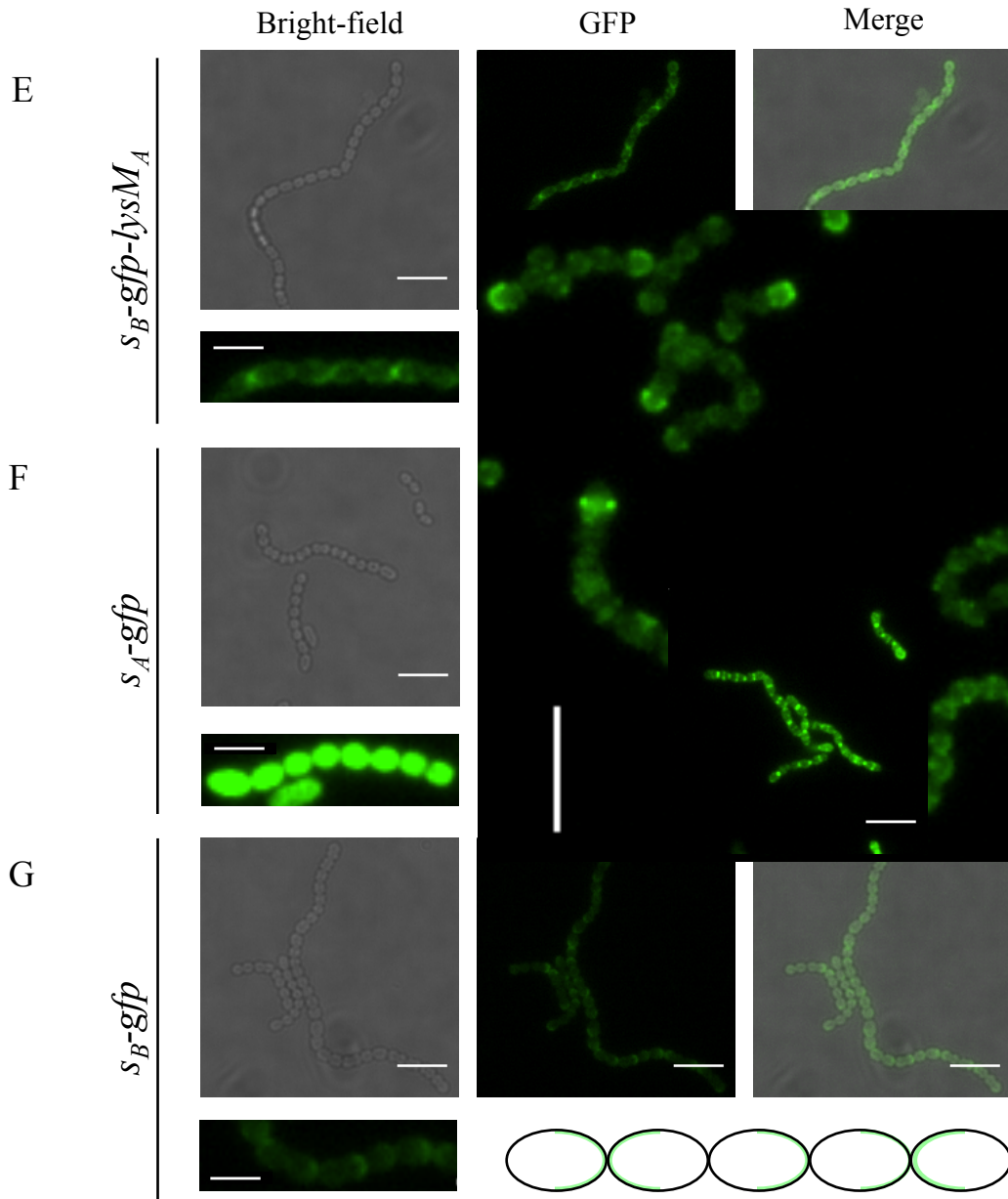
Figure 5.1 Localisation of GFP translational fusions produced by *E. faecalis*

A. Domain (Dom) organisation of AtlA, AtlB, S_A-GFP-LysM$_A$, S_B-GFP-LysM$_B$, S_A-GFP-LysM$_B$, S_B-GFP-LysM$_A$, S_A-GFP and S_B-GFP. S_A- AtlA signal peptide (blue); Dom II$_A$-AtlA N-terminal domain (orange); Cat$_A$- AtlA catalytic domain (green); LysM$_A$-AtlA LysM domain (magenta); S_B- AtlB signal peptide (cyan); Dom II$_B$- AtlA N-terminal domain (yellow); Cat$_B$- AtlB catalytic domain (white-green); LysM$_B$-AtlB LysM domain (pink); GFP (lime)

B-G. Bright-field and fluorescent images of *E. faecalis* JH2-2 derivatives *s$_A$-gfp-lysM$_A$* (B), *s$_B$-gfp-lysM$_B$* (C), *s$_A$-gfp-lysM$_B$* (D), *s$_B$-gfp-lysM$_A$* (E), *s$_A$-gfp* (F) and *s$_B$-gfp* (G) along with fluorescent image of individual cells and the schematic representation of fluorescent signal distribution. Scale bars, 5 μm big images; 2 μm small images.

131

5.2 Contribution of the AtlA LysM domain modularity to AtlA subcellular targeting

The work described in Chapter 3 (Section 3.2.4) showed that sequential truncation of the AtlA LysM modules leads to a chain forming phenotype. We investigated the impact of LysM truncations of AtlA subcellular localisation by immunofluorescence microscopy. *E. faecalis* JH2-2 and the mutants producing AtlA with truncated domains ($atlA_{1-5}$, $atlA_{1-4}$, $atlA_{1-3}$, $atlA_{1-2}$ and $atlA_1$) were grown to exponential phase and immunolabelled as previously described (Section 4.2.1). Immunolabelled bacteria were immobilised on agarose pads and visualised immediately using epifluorescence microscopy.

The fluorescent pattern observed with the WT, $atlA_{1-5}$ and $atlA_{1-4}$ strains was similar, with most of the signal localised at the septum and cells poles (Figure 5.2 A-C). As the number of LysM modules decreased, the signal became weaker. No signal associated with the cells was observed for mutants producing AtlA with 1 to 3 LysM modules or the *atlA* knockout mutant (Figure 5.2 D-G). To exclude a possible artefact due to the chain forming phenotype, we used mutant $atlA_{E212Q}$ as a control. The $atlA_{E212Q}$ strain carries a substitution of the catalytic Glu212 residue by a Gln residue. This mutant produces an inactive AtlA protein and thus forms long cell chains. A strong fluorescent signal associated with septa and cell poles was detected in the $atlA_{E212Q}$ strain (Figure 5.2 H), indicating that the formation of the long cell chains does not affect antibodies accessibility.

To sum up, the immunolabelling experiment showed that the number of the LysM modules is critical for cell surface display and binding to the substrate. As long as AtlA has at least four LysM modules, it is localised on the cell surface at the septum and cells poles.
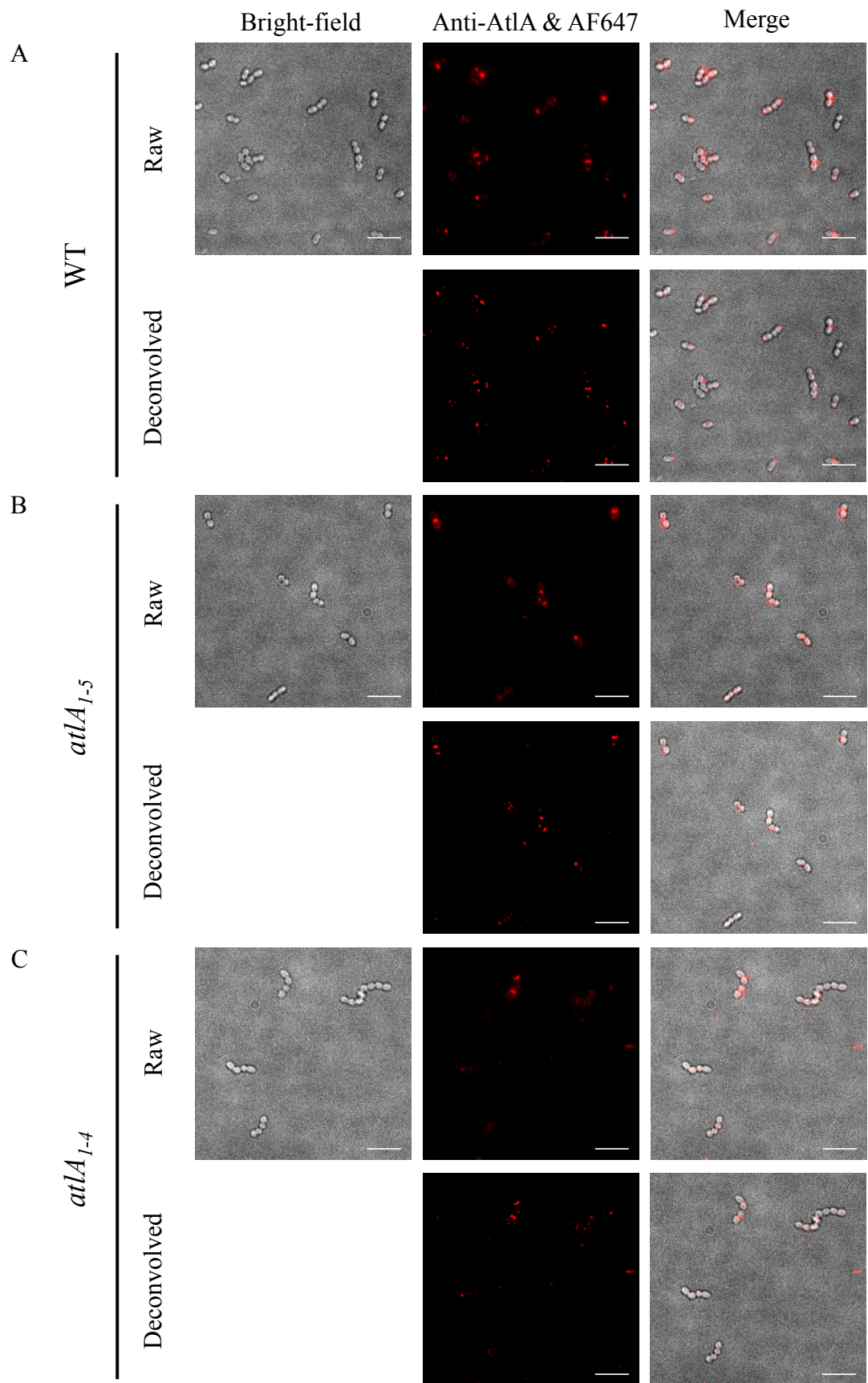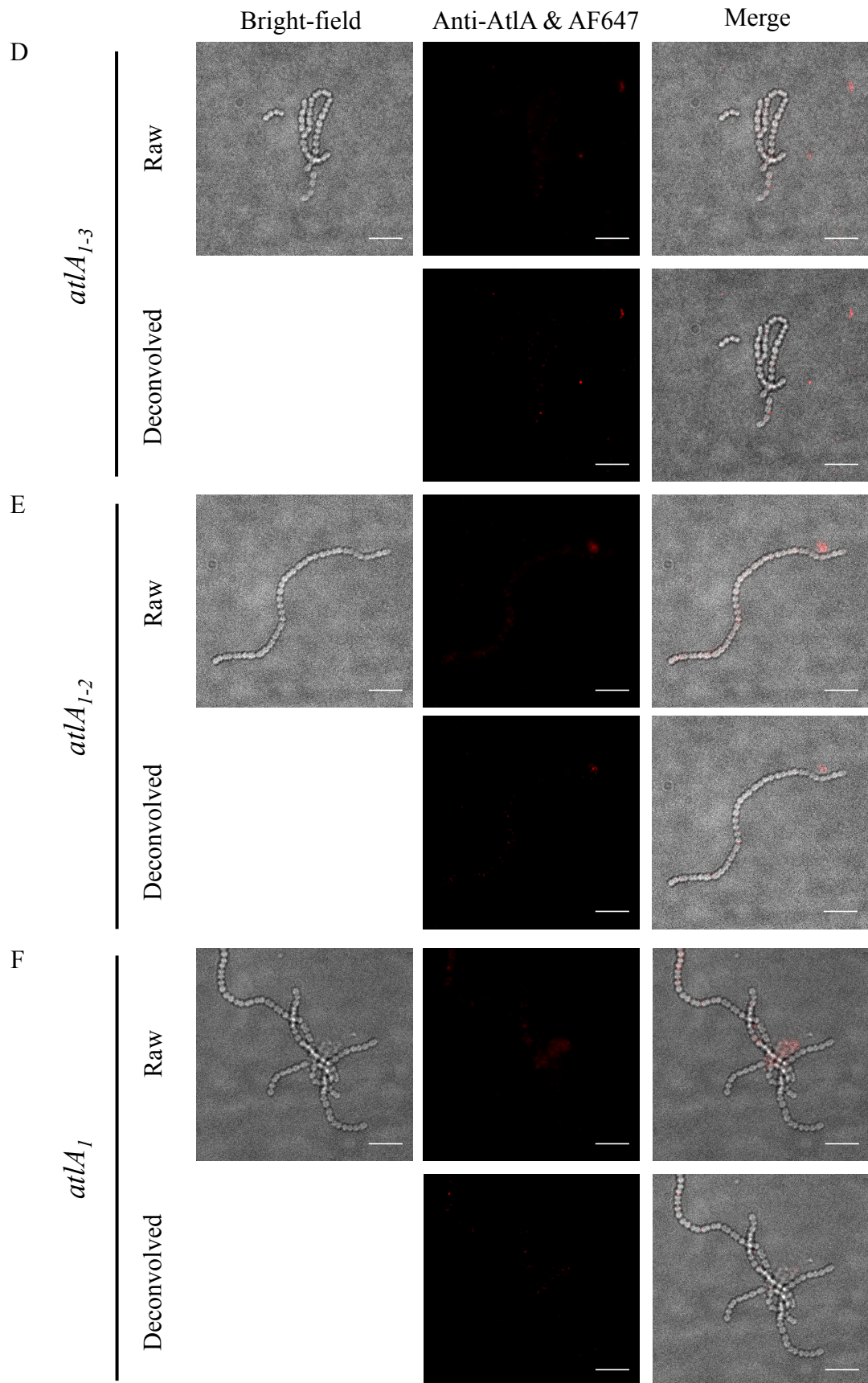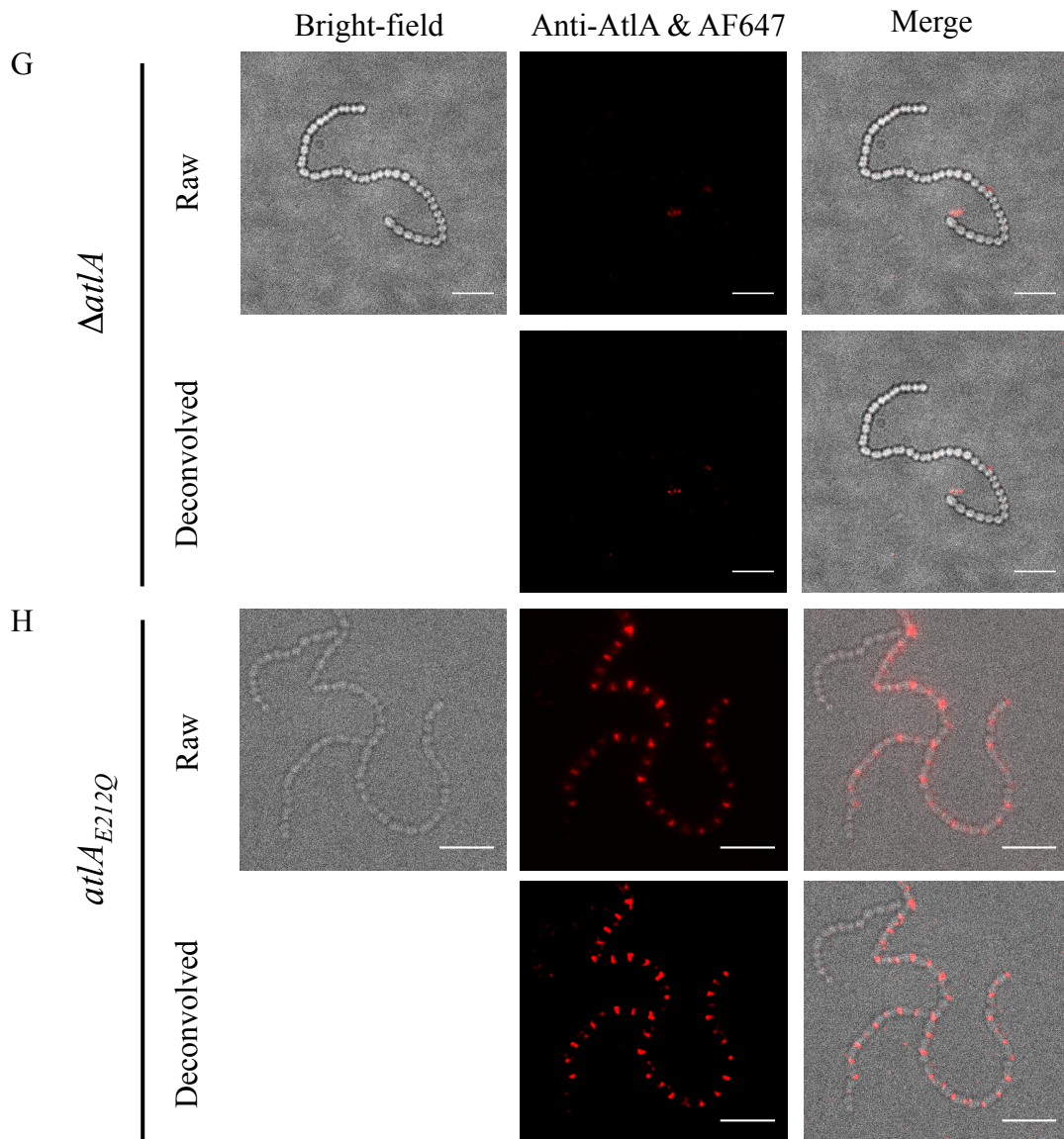
Figure 5.2 Cell surface immunodetection of AtlA variants containing truncated LysM domains

Bright-field and fluorescent images of *E. faecalis* JH2-2 (A), *atlA*₁₋₅ (B), *atlA*₁₋₄ (C), *atlA*₁₋₃ (D), *atlA*₁₋₂ (E), *atlA*₁ (F), Δ*atlA* (G) and *atlA*E212Q (H) probed with anti-AtlA serum at a 1:250 and detected with anti-rabbit IgG antibodies conjugated with AlexaFluor647 (AF647). Scale bars are 5 μm.

To confirm the immunofluorescence microscopy results, JH2-2 derivatives producing AtlA-GFP fusions with a variable number of LysM modules were constructed. First, the pGhost 9 derivatives pGAtlA$_{1-5}$-GFP, pGAtlA$_{1-4}$-GFP, pGAtlA$_{1-3}$-GFP, pGAtlA$_{1-2}$-GFP and pGAtlA$_{1}$-GFP were constructed as presented in Figure 5.3A. A DNA fragment encoding the AtlA catalytic domain (502 bp) and 1 LysM$_A$ module (213 bp) fused to *gfp* (717 bp) via a 12 amino acid linker, followed by a downstream region of *atlA* (255 bp down from the stop codon) was synthesised by GeneArt (5.3 C). The synthetic fragment contained NcoI and BglII sites flanking the DNA encoding the LysM module. The gene synthesis product was cloned into pGhost 9 using XhoI and KpnI (Figure 5.3 A (i)). Positive colonies were identified by restriction enzyme analysis with XhoI and KpnI and confirmed the presence of the insert of the expected size in pGAtlA$_{1}$-GFP (Figure 5.3 B, lane 1). To construct pGAtlA$_{1-5}$-GFP, pGAtlA$_{1-4}$-GFP, pGAtlA$_{1-3}$-GFP and pGAtlA$_{1-2}$-GFP, the NcoI –BglII fragments encoding truncated LysM domains from pGAtlA$_{1-5}$, pGAtlA$_{1-4}$, pGAtlA$_{1-3}$ and pGAtlA$_{1-2}$ were cloned into pGAtlA$_{1}$-GFP by replacing the DNA encoding 1LysM (Figure 5.3 A (ii-v)). Plasmids were extracted from presumptive positive clones and analysed by restriction enzyme digestion using XhoI and KpnI. The analysis confirmed the presence of the inserts of the expected sizes (Figure 5.3 B, lanes 2-5).

pGAtlA$_{1-5}$-GFP, pGAtlA$_{1-4}$-GFP, pGAtlA$_{1-3}$-GFP, pGAtlA$_{1-2}$-GFP and pGAtlA$_{1}$-GFP were transformed into electrocompetent *E. faecalis* JH2-2 cells. The *gfp* fusions were introduced at the *atlA* locus by allele exchange (Figure 5.4 A). Following homologous recombination, the erythromycin sensitive colonies were identified by PCR using primers AtlA_5' and AtlA_dn (Figure 5.4 B). Production and secretion of the fluorescent derivatives of AtlA in putative positive mutants was analysed by western blot. The GFP-tagged AtlA derivatives were precipitated from culture supernatants using 10% (w/v) TCA. Proteins were probed with anti-AtlA antibodies raised against the catalytic domain of AtlA. A single band around 75 kDa was detected for the parental strain, *E. faecalis* JH2-2 (Figure 5.4 C). All mutant samples revealed the bands of the expected sizes as the most abundant species, indicates that all GFP fusions were relatively stable (Figure 5.4 C). The hydrolytic activity of the fusion proteins was analysed by zymogram assay using *M. luteus* PG as a substrate (Figure 5.4D).

A (i)
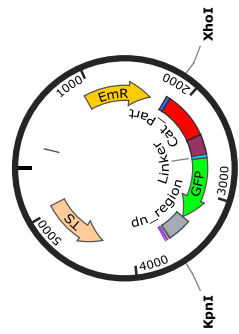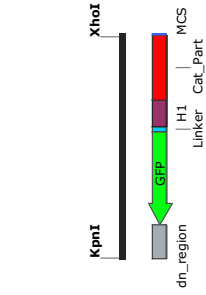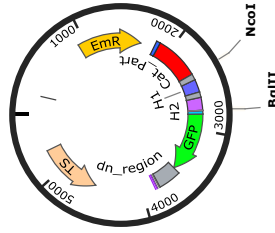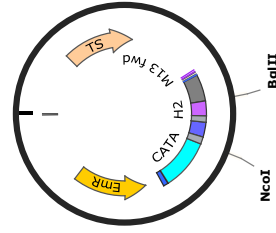
B (ii)

(iii)

(iv)

Figure 5.3 Construction of pGAtlA₁₋₅, pGAtlA₁₋₄, pGAtlA₁₋₃, pGAtlA₁₋₂ and pGAtlA₁
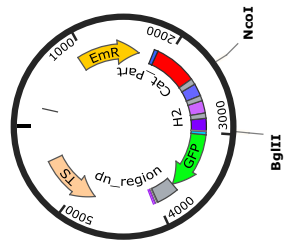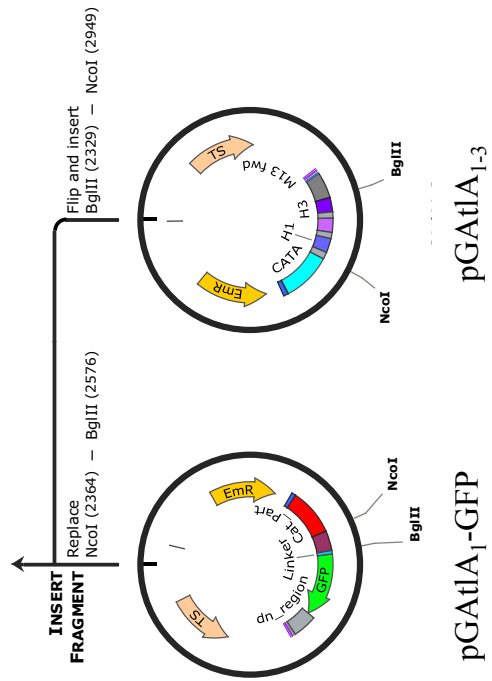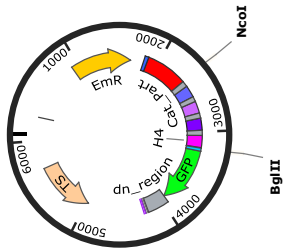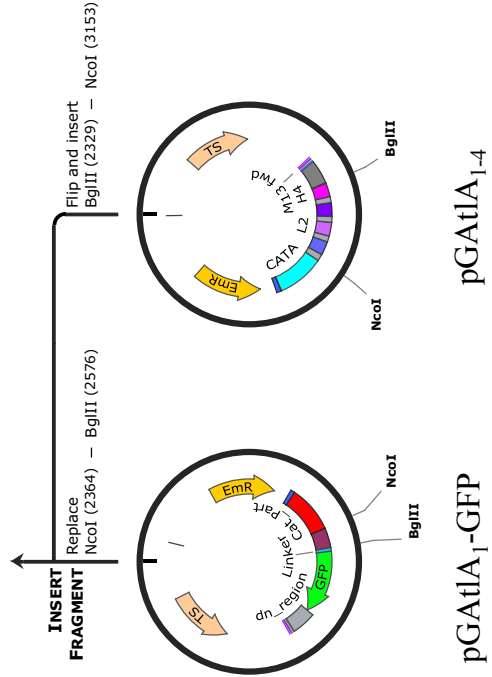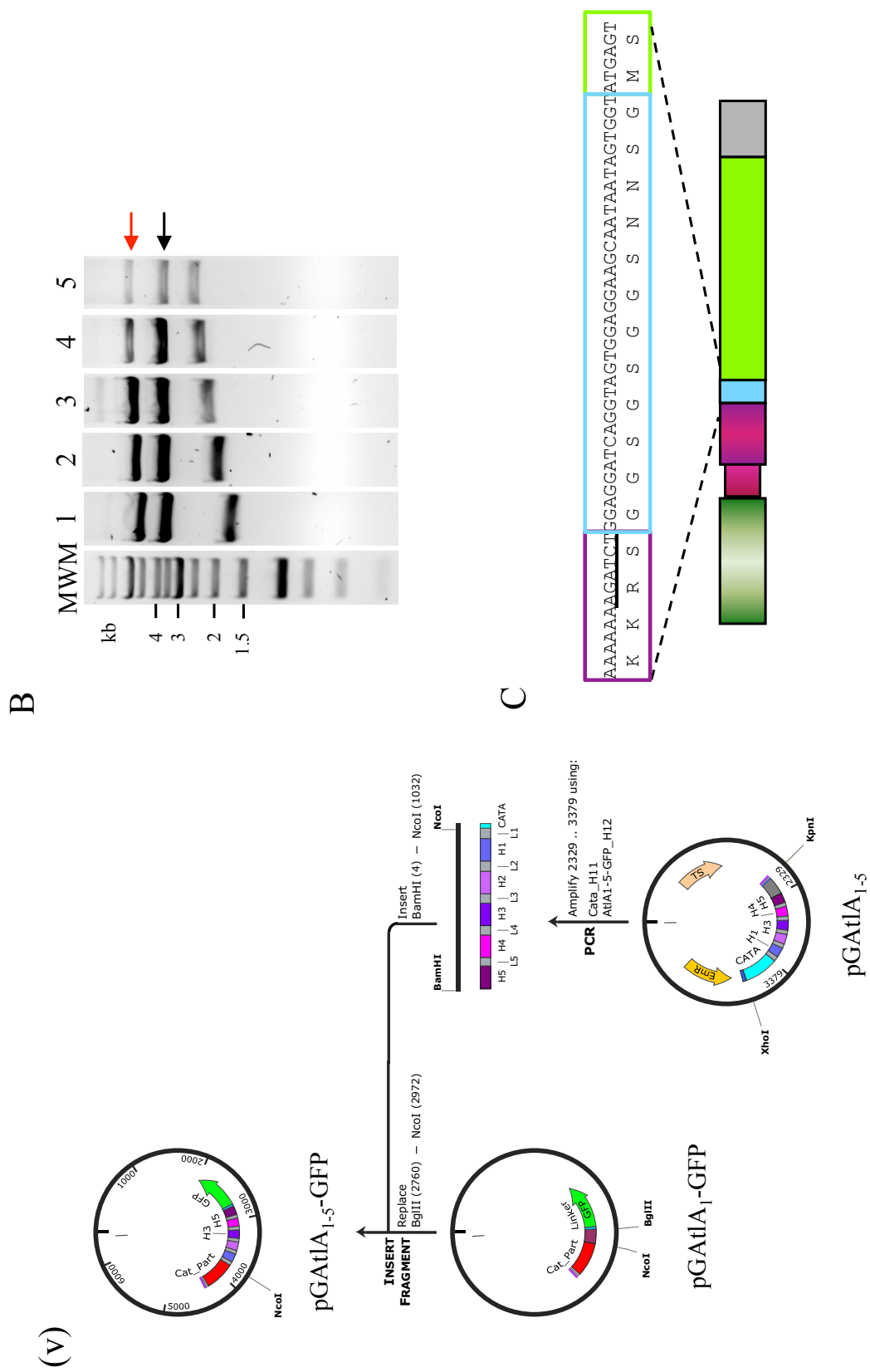
A.   Schematic representation of the cloning strategy of:

(i) pGAtlA$_1$-GFP; a synthesised gene encoding AtlA catalytic domain (502 bp), 1 LysM module (213 bp) fused to GFP (717 bp) and 255 bp downstream of *atlA* stop codon was cloned in to pGhost 9 using XhoI and KpnI. The cloned fragment has two additional restriction enzymes sides flanking the LysM module recognised by NcoI and BglII.

(ii) pGAtlA$_{1-2}$-GFP; a 416 bp NcoI and BglII fragment of pGAtlA$_{1-2}$ was cloned in to the pGAtlA$_1$-GFP similarly cut.

(iii) pGAtlA$_{1-3}$-GFP; a 620 bp NcoI and BglII fragment of pGAtlA$_{1-2}$ was cloned in to the pGAtlA$_1$-GFP similarly cut.

(iv) pGAtlA$_{1-4}$-GFP; a 824 bp NcoI and BglII fragment of pGAtlA$_{1-2}$ was cloned in to the pGAtlA$_1$-GFP similarly cut.

(v) pGAtlA$_{1-5}$-GFP; the 1026 bp NcoI and BglII fragment of pGAtlA$_{1-5}$ was cloned to the pGAtlA$_1$-GFP similarly cut.

B.   Restriction enzyme digestion of pGAtlA$_1$-GFP (lane 1), pGAtlA$_{1-2}$-GFP (lane 2), pGAtlA$_{1-3}$-GFP (lane 3), pGAtlA$_{1-4}$-GFP (lane 4) and pGAtlA$_{1-5}$-GFP (lane 5) using XhoI and KpnI. All digestions gave the expected DNA bands sizes. The 3750 bp fragment corresponding to the backbone is indicated with a black arrow. The undigested plasmids were indicated with a red arrow. The sizes of chosen molecular weight markers (MWM) are indicated on the left hand side of the gel.

C.   Nucleotide and amino acid composition of the linker (light blue frame) within flanking regions: LysM module (purple frame; BglII restriction site is underlined) and GFP (green frame).
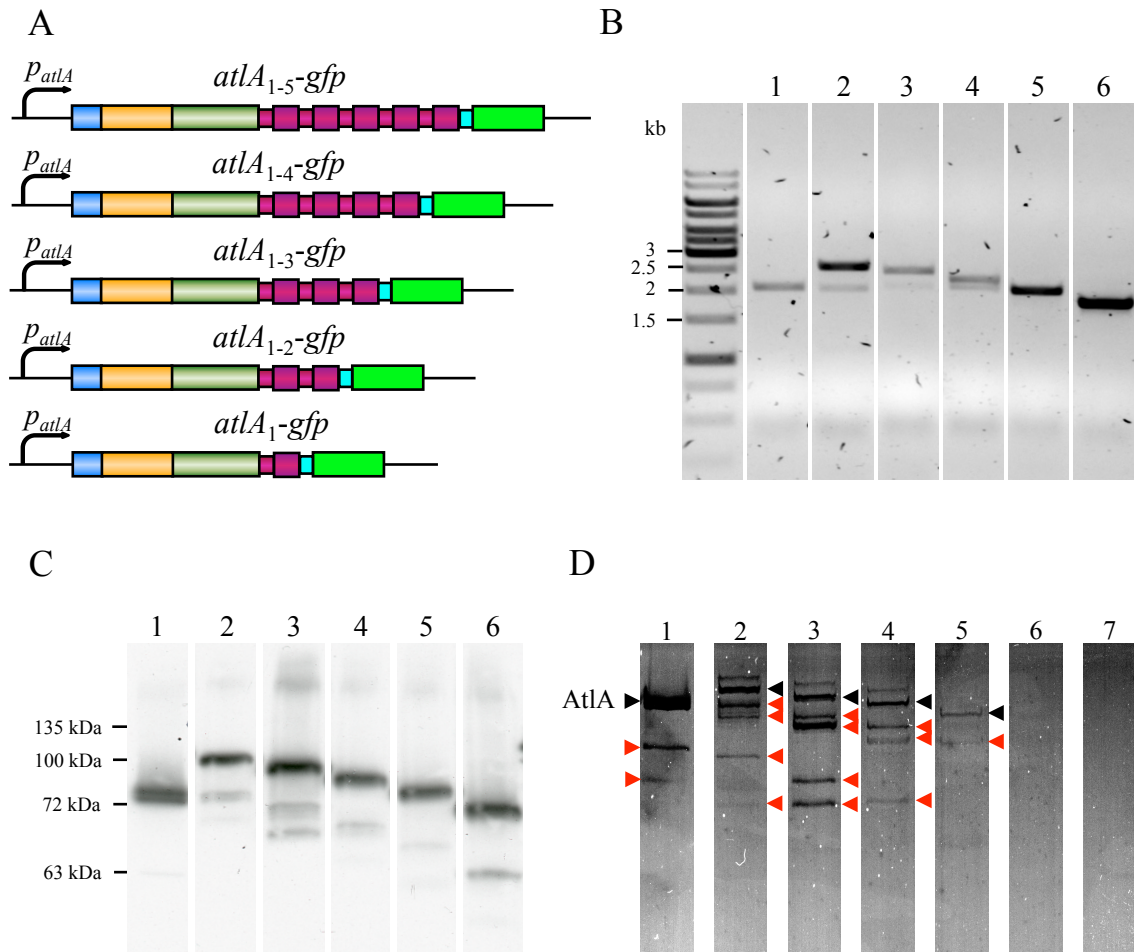
Figure 5.4 Characterisation of *lysM-gfp* mutants

A. Schematic representation of *atlA* locus in *E. faecalis* JH2-2 derivatives: *atlA*$_{1-5}$-*gfp*, *atlA*$_{1-4}$-*gfp*, *atlA*$_{1-3}$-*gfp*, *atlA*$_{1-2}$-*gfp* and *atlA*$_{1}$-*gfp*.

B. Amplification products using AtlA-5' and AtlA_dn primers for WT (lane 1), *atlA*$_{1-5}$-*gfp* (lane 2), *atlA*$_{1-4}$-*gfp* (lane 3), *atlA*$_{1-3}$-*gfp* (lane 4), *atlA*$_{1-2}$-*gfp* (lane 5) and *atlA*$_{1}$-*gfp* (lane 6) colonies. The expected DNA band sizes of 2125 bp for WT, 2660 bp for *atlA*$_{1-5}$-*gfp*, 2467 bp for *atlA*$_{1-4}$-*gfp*, 2258 bp for *atlA*$_{1-3}$-*gfp*, 2054 bp for *atlA*$_{1-2}$-*gfp* and 1850 bp for *atlA*$_{1}$-*gfp*. The sizes of chosen molecular weight markers (MWM) are indicated on the left hand side of the gel.

C. Western blot detection of AtlA fusions in culture supernatants. Proteins precipitated from supernatants exponentially growing cells were recovered by centrifugation, washed with acetone and resuspended in PBS. Following SDS-PAGE and transfer on a nitrocellulose membrane, AtlA fusions were probed with anti-AtlA polyclonal serum against the catalytic domain of AtlA. WT-72 kDa, lane 1; *atlA*$_{1-5}$-*gfp*–93 kDa, lane 2; *atlA*$_{1-4}$-*gfp*– 86.2 kDa, lane 3; *atlA*$_{1-3}$-*gfp* – 79.3 kDa, lane 4; *atlA*$_{1-2}$-*gfp* – 72.4 kDa, lane 5; *atlA*$_{1}$-*gfp*– 65.5

kDa, lane 6. The sizes of chosen molecular weight markers are indicated on the left hand side of the blot.

D. Zymogram analysis of PG hydrolases produce by *E. faecalis* JH2-2 (lane 1) and derivatives: *atlA*$_{1-5}$-*gfp* (lane 2), *atlA*$_{1-4}$-*gfp* (lane 3), *atlA*$_{1-3}$-*gfp* (lane 4), *atlA*$_{1-2}$-*gfp* (lane 5), *atlA*$_1$-*gfp* (lane 6) and Δ*atlA* (lane 7). *M. luteus* peptidoglycan was used as a substrate to detect AtlA activity. The high enzymatic activity lytic band of AtlA and AtlA fusions were detected (indicated with a black arrow) within degradation products (indicated with red arrows). No hydrolytic activity was detected for *atlA*$_1$-*gfp* and Δ*atlA* extracts.

All fusion proteins except AtlA$_1$-GFP showed enzymatic activity. As expected from the western blot analysis, several lytic bands were detected confirming truncation of AtlA$_{1-5}$-GFP, AtlA$_{1-4}$-GFP, AtlA$_{1-3}$-GFP and AtlA$_{1-2}$-GFP. The lytic bands corresponding to the full size fusions and degradation products are highlighted with black and red arrows, respectively (Figure 5.4 D).

The impact of AtlA LysM binding domain modularity on subcellular targeting of the enzyme was investigated using epifluorescence microscopy. *atlA$_{1-5}$-gfp, atlA$_{1-4}$- gfp, atlA$_{1-3}$-gfp, atlA$_{1-2}$- gfp* and *atlA$_1$- gfp* along with *E. faecalis* JH2-2 and *atlA$_{1-6}$-gfp* used as a negative and positive control, respectively, were visualised by diffraction limited microscopy and all fluorescent images were deconvolved (Figure 5.5 A-G). As expected, the negative control showed a very weak autofluorescence signal with no defined pattern (Figure 5.5A). Truncation of the last LysM domain led to changes in the AtlA distribution as compared to the positive control. Although in the *atlA$_{1-5}$-gfp* strain the fluorescent signal was detectable at the septa and cells poles, most of the signal corresponding to AtlA$_{1-5}$-GFP was associated with the cells outline (Figure 5.5 B and C). Truncation of 2 LysM modules led to a disappearance of both the septal and polar localisation of the fluorescent fusions, and to the sequestration of the fluorescent signal in the cells. The raw fluorescent images of the *atlA$_{1-4}$-gfp, atlA$_{1-3}$-gfp, atlA$_{1-2}$-gfp* and *atlA$_1$-gfp* strains showed the fluorescent signal was present in the whole cell volume and associated with the cell outline. This pattern became more pronounced after the deconvolution of the data (Figure 5.5 D-G).

Altogether, the immunofluorescence and epifluorescence microscopy results suggest that the modularity of the LysM domain is crucial for localisation and the binding of AtlA to peptidoglycan. The sequential truncation of LysM modules abolishes AtlA surface display and targeting to the septum and cell poles, resulting in accumulation of the enzyme in the cell.

	Bright-field	GFP	Merge

A — WT

Raw

Deconvolved

B — *atlA₁₋₆–gfp*

Raw

Deconvolved

C — *atlA₁₋₅–gfp*

Raw

Deconvolved

	Bright-field	GFP	Merge

D | *atlA_{1-4}-gfp* | Raw

Deconvolved

E | *atlA_{1-3}-gfp* | Raw

Deconvolved

F | *atlA_{1-2}-gfp* | Raw

Deconvolved

145
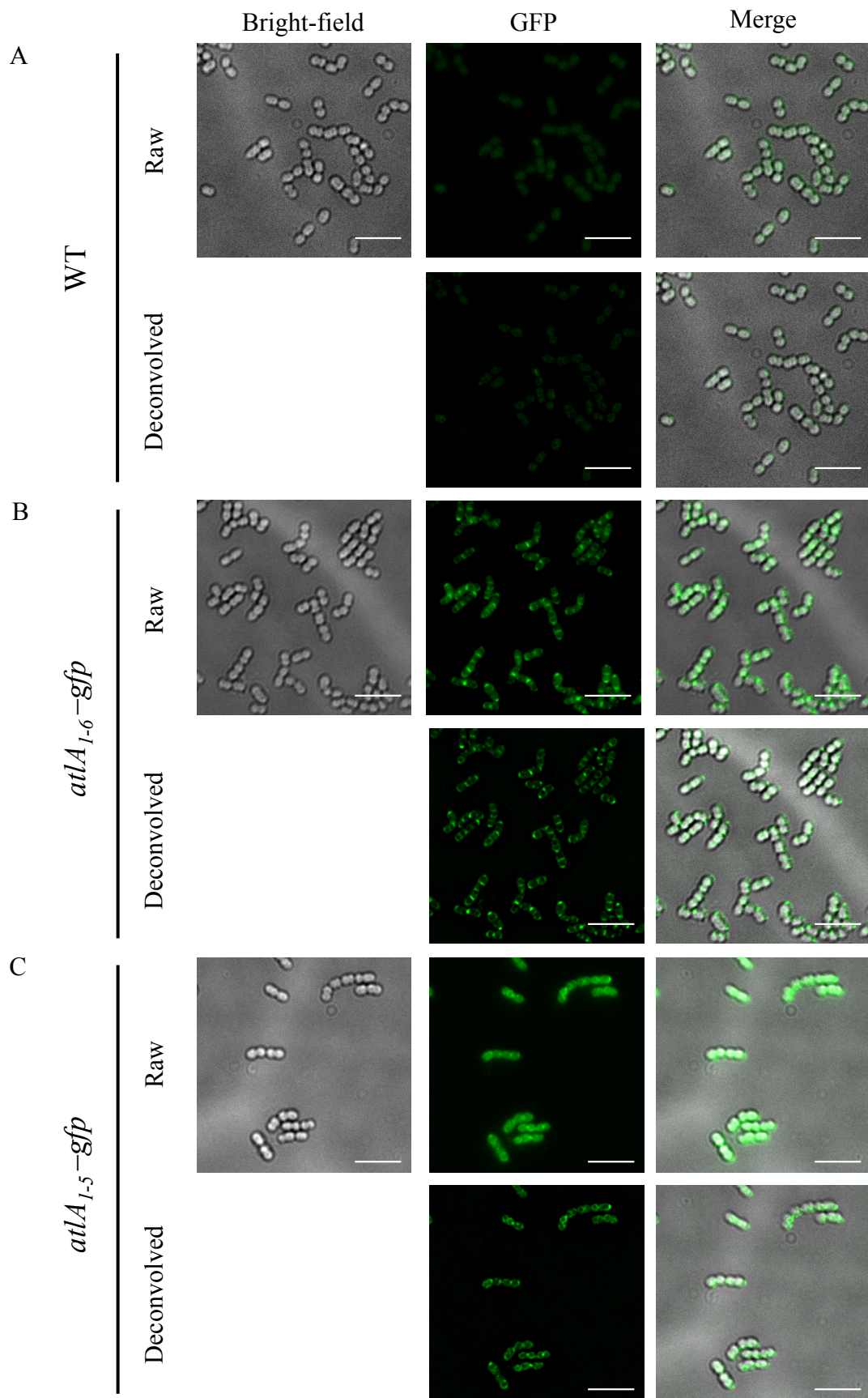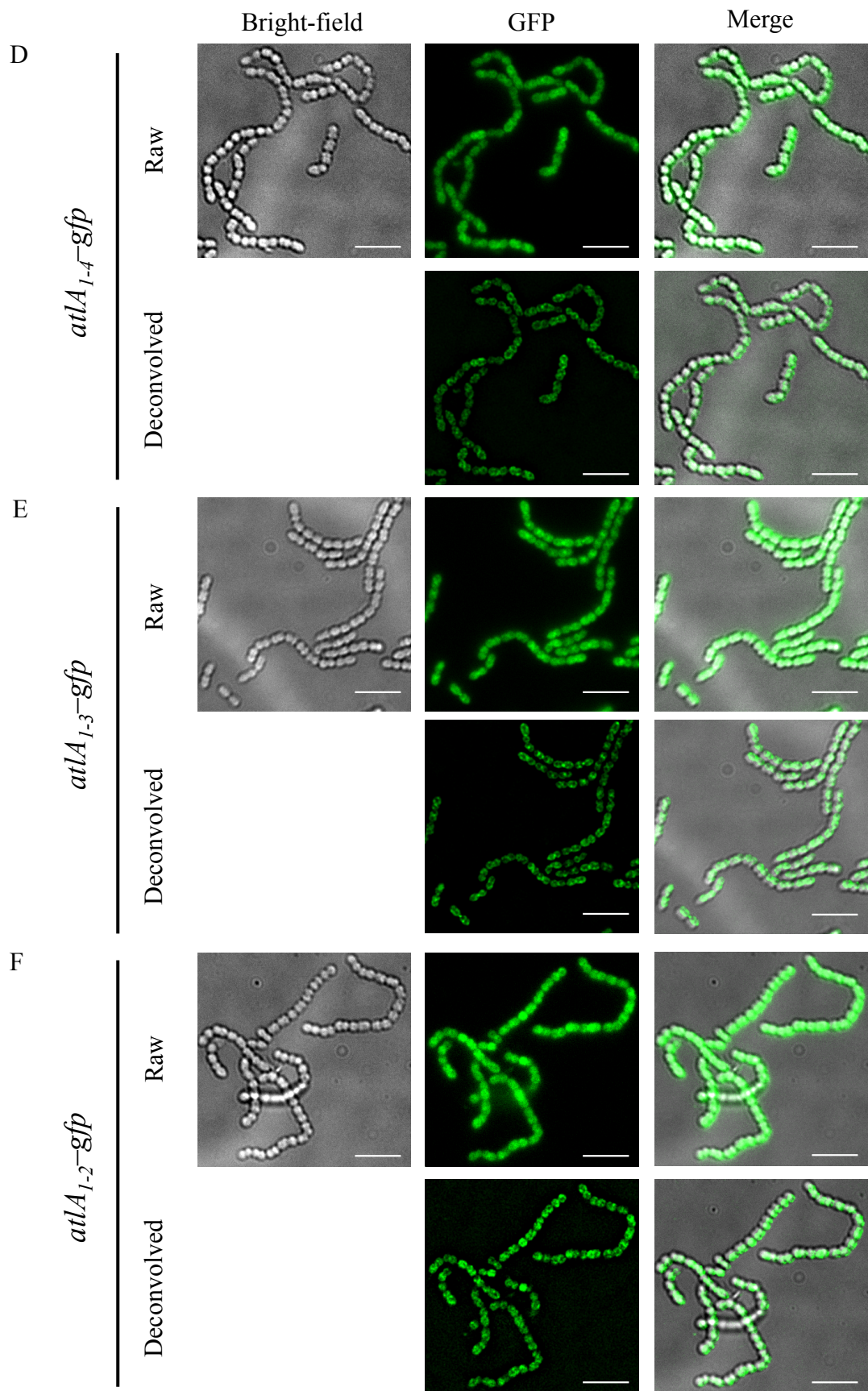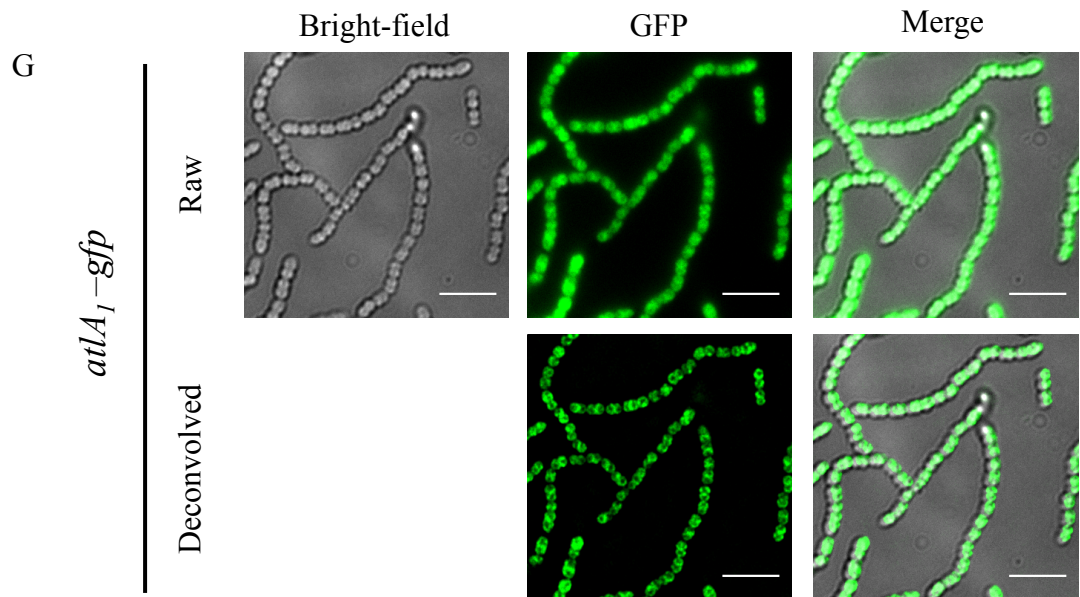
Figure 5.5 Subcellular localisation of AtlA-GFP fusions containing variable numbers of LysM modules

Bright-field and fluorescent images of *E. faecalis* JH2-2 (A), *atlA$_{1-6}$-gfp* (B), *atlA$_{1-5}$-gfp* (C), *atlA$_{1-4}$-gfp* (D), *atlA$_{1-3}$-gfp* (E), *atlA$_{1-2}$-gfp* (F), *atlA$_1$-gfp* (G) before (raw) and after deconvolution Scale bars, 5 μm

5.3 Impact of the LysM domain charge and amino acid composition on AtlA subcellular targeting

The $atlA_{1-6HB}$ mutant characterised in Section 3.2.5 showed an impaired daughter cells separation, suggesting that the amino acid composition/charge of the LysM modules plays an important role in the control of AtlA activity. The proton gradient across the cytoplasmic membrane implies that the distribution of charges across the bacterial cell wall is anisotropic. It has been proposed that LysM domain with different isoelectric points may bind to distinctive zones within the cell wall (Buist et al., 2008). To investigate the impact of the LysM modules amino acid composition/charge on protein cell surface display and localisation, immunofluorescence microscopy was carried out on *E. faecalis* JH2-2 and $atlA_{1-6HB}$ cells as previously described (Section 4.2.1). Bacterial cells were imaged using epifluorescence microscopy and images were deconvolved.

Although the fluorescent signal did not perfectly overlap with the bright-filed images due to the chromatic aberration of the optical system, a similar distribution of fluorescence was observed in both WT (Figure 5.6.A) and $atlA_{1-6HB}$ (Figure 5.6B). AtlA and AtlA$_{1-6HB}$ were localised at septum and cells poles, suggesting that different amino acid composition/charge has no impact on AtlA subcellular localisation.

To confirm the immunofluorescence microscopy results, we built strain $atlA_{1-6HB}$-*gfp* producing AtlA$_{1-6HB}$ fused to the GFP at its C-terminus. First, pGAtlA$_{1-6HB}$-GFP was constructed as showed in Figure 5.7 A. The insert from pMK-RQ-6HB-GFP (synthesized by GeneArt) consisting of a 398 bp fragment encoding the AtlA catalytic domain followed by a 1209 bp fragment of the 1-6HB LysM domain was cloned into pGAtlA$_1$-GFP cut by NsiI and BglII. Following transformation into competent *E. coli* cells, positive colonies were identified by restriction enzyme analysis with XhoI and KpnI to confirm the presence of the insert of the expected size (Figure 5.7 B).

A resulting pGAtlA$_{1-6HB}$-GFP plasmid was used to replace of the native *atlA* allele by a variant encoding AtlA with LysM$_B$ repeats fused to the GFP. Colonies sensitive to erythromycin were screened by PCR using primers AtlA_5' and AtlA_3' (Figure 5.7 C). Production and secretion of AtlA$_{1-6HB}$-GFP was analysed by probing proteins from

bacterial culture supernatants with the anti-AtlA antibodies (Figure 5.7 D). The result of the western blot showed two bands of 80 kDa and 110 kDa corresponding to the expected molecular weight mass of wild-type AtlA (72 kDa) and $AtlA_{1-6HB}$-GFP (102 kDa), respectively. No degradation products were observed, suggesting that the GFP fusion was stable. The intensity of the signal corresponding to $AtlA_{1-6HB}$-GFP was lower than that of AtlA, suggesting that $AtlA_{1-6HB}$-GFP secretion could be less efficient (Figure 5.7 D).

The impact of LysM amino acid composition/charge on subcellular targeting was investigated by comparing the localisation of the $AtlA_{1-6}$-GFP and $AtlA_{1-6HB}$-GFP fusions. Bacterial cells were visualised using epifluorescence microscopy and the images were deconvolved. The $AtlA_{1-6}$-GFP fusion had a characteristic septal and polar localisation (Figure 5.8 A). In the $atlA_{1-6HB}$-gfp strain, most of the fluorescence was associated with the whole cell volume (Figure 5.8B). A limited luorescence was associated with septa and poles. The fluorescence pattern of strain $atlA_{1-6HB}$-gfp was similar to that of strains $atlA_{1-5}$-gfp and $atlA_{1-4}$-gfp producing AtlA variants with 5 and 4 LysM modules, respectively.

Altogether, the composition of the AtlA binding domain is essential for the proper targeting the enzyme to the places where secretion of AtlA occurs. The control of the AtlA activity via the LysM binding domain probably occurs at two levels. First, the strong basic pI of the LysM domain allows for the proper targeting of AtlA to the secretion channels. The second control occurs via multi modularity of the LysM domain. The six LysM repeats act in synergy to potentiate and provide a strong binding to the peptidoglycan.
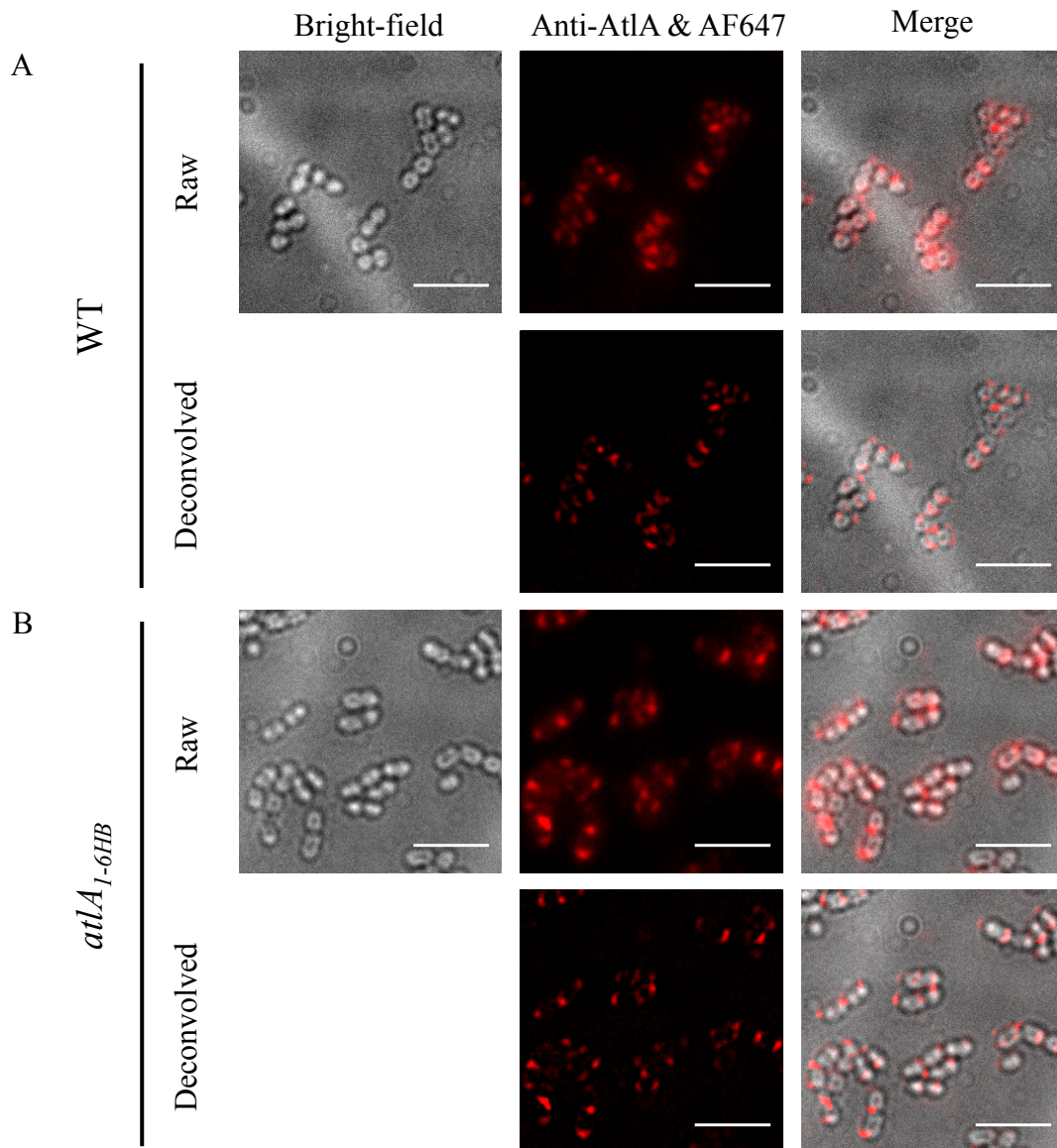
Figure 5.6. Immunolabelling of *atlA₁₋₆ₕᵦ* using anti-AtlA antibodies

Bright-field and fluorescent images of *E. faecalis* JH2-2 and *atlA*₁₋₆ₕᵦ probed with anti-AtlA serum at a 1:250 and detected with anti-rabbit IgG antibodies conjugated with AlexaFluor647 (AF647). Scale bars are 5 μm.
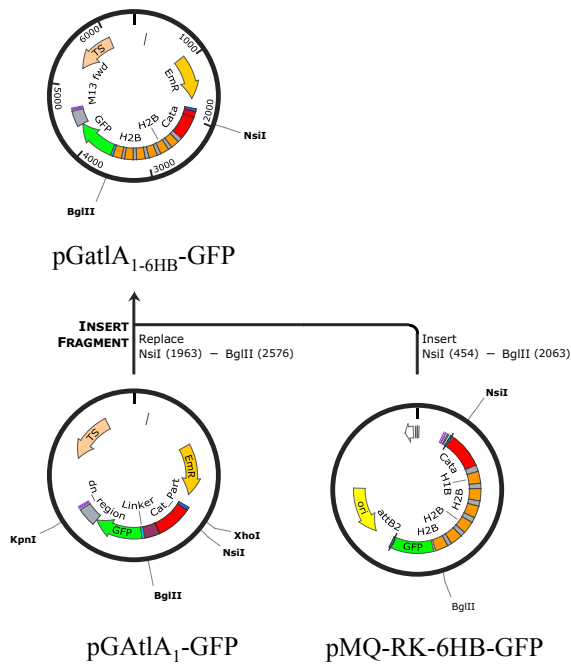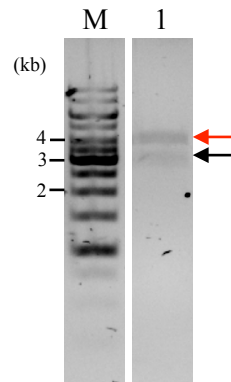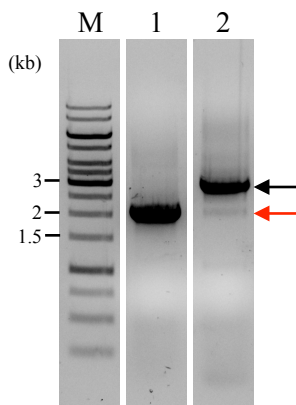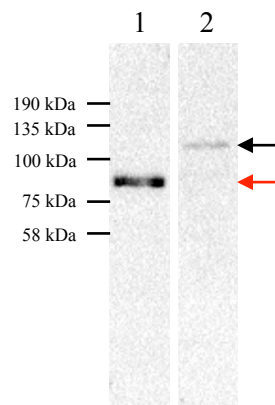
Figure 5.7 Construction of pGAtlA₁₋₆ₕB-GFP and *atlA₁₋₆ₕB-gfp* strain producing fluorescently labelled AtlA with binding domain consisting of six AtlB LysM modules

A.   Schematic representation of the cloning strategy. The 1609 bp NsiI and BglII fragment of pMK-RQ-6HB-GFP (gene synthesis) plasmid was cloned to pGAtlA₁-GFP similarly digested. The resulting plasmid pGAtlA₁₋₆ₕB-GFP consists of 496 bp of AtlA catalytic domain, 6 LysM modules from AtlB (three H1B and three H2B) preceded by linkers from AtlA (1209 bp), GFP fused via short 12 amino acid linker (719 bp)

B.   Restriction enzyme digest of pGAtlA₁₋₆ₕB-GFP using XhoI and KpnI. The expected DNA bands size of 3750 bp for the backbone is indicated with a red arrow and 2727 bp for the

insert is indicated with a black arrow. The sizes of chosen molecular weight markers (MWM) are indicated on the left hand side of the gel.

C. PCR amplification products using AtlA_5' and AtlA_dn primers for the parental strain (lane 1) and the $atlA_{1-6HB}$-*gfp* putative mutant (lane2). The expected DNA band sizes of: 2098 bp and 2871 bp of the parental strain and the putative mutant are indicated by a red and black arrow, respectively. The sizes of chosen molecular weight markers (MWM) are indicated on the left hand side of the gel.

D. Western blot detection of AtlA proteins in culture supernatants. Proteins precipitated from supernatants of exponentially grown cells using 10% (w/v) TCA were recovered by centrifugation and washed with acetone and resuspended in PBS. Following SDS-PAGE and transfer on a nitrocellulose membrane, proteins were probed with anti-AtlA polyclonal serum raised against the catalytic domain of AtlA. Native AtlA in WT (lane 1) and AtlA-GFP in $atlA_{1-6HB}$-*gfp* (lane 2) are indicated with red and black arrows, respectively.

Figure 5.8 Subcellular localisation of a fluorescently labelled AtlA derivative with a binding domain consisting of six AtlB LysM modules

Bright-field and fluorescent images of *atlA*$_{1-6}$-*gfp* and *atlA*$_{1-6HB}$-*gfp* before (raw) and after deconvolution Scale bars, 5 μm.

5.4 Co-localisation of AtlA with membrane and peptidoglycan.

Truncation or replacement of AtlA basic LysM modules by acidic ones led to a change of AtlA subcellular localisation. The localisation pattern associated with the cell outline in *atlA*$_{1-5}$*-gfp, atlA*$_{1-4}$*- gfp, atlA*$_{1-3}$*- gfp, atlA*$_{1-2}$*- gfp, atlA*$_{1}$*- gfp* and *atlA*$_{1-6HB}$*-gfp* mutants could result from accumulation of the protein in the membrane, which was unable to be directed to its secretion channel. To test this possibility, AtlA fluorescent fusions were co-localised with other cell compartments. The bacterial peptidoglycan was labelled using blue fluorescent D-amino acid (hydroxycoumarin-carbonyl-amino-D-alanine, HADA, Kuru et al., 2012), whilst membranes were stained with the lipophilic dye (FM4-64). The study was limited to two strains, *atlA*$_{1-6}$*-gfp* and *atlA*$_{1}$*-gfp*. Cells were grown in presence of HADA for 5 generation and once they reached exponential phase they were collected and fixed. The membrane of the fixed cells was stained by incubation with FM4-64. Bacterial cells were imaged using epifluorescence microscopy and the images were deconvolved.

To compare a localisation of AtlA with different numbers of LysM modules to other cell compartments, Z-stack images were used for the analysis. The fluorescent intensity profiles for PG (cyan), AtlA (magenta) and membrane (yellow) distribution were plotted along the long cell length axis indicated with the red line in the individual cell images (Figure 5.9 A and B). The fluorescent intensity values were normalized due to fact that chemical dyes were brighter than GFP. The analysis of the *atlA*$_{1-6}$*-gfp* fluorescent profiles showed a high overlap between PG, AtlA and membrane. The fluorescent intensity maxima of each fluorophore almost perfectly match, confirming localisation of full-length AtlA fusion at septum and cell poles (Figure 5.9 A). On the contrary, the maxima of AtlA$_{1}$-GFP fluorescent intensity were slightly sifted outside of the PG and membrane fluorescent intensity maxima. These results indicated that AtlA$_{1}$-GFP were not juxtaposed with other cell compartments (Figure 5.9 B). One representative profile of each strain is shown in Figure 5.9 C.

These results suggest that modifications of the AtlA LysM domain lead to sequestration of these proteins. However, due to diffraction limit of epifluorescence microscopy, it is hard to formally conclude that AtlA is or is not associated with the membrane.

A

atlA$_{1-6}$-*gfp*

BF	PG	AtlA	Membrane	Merge	Fluorescence profile

B

atlA₁-gfp

BF	PG	AtlA	Membrane	Merge	Fluorescence profile

C
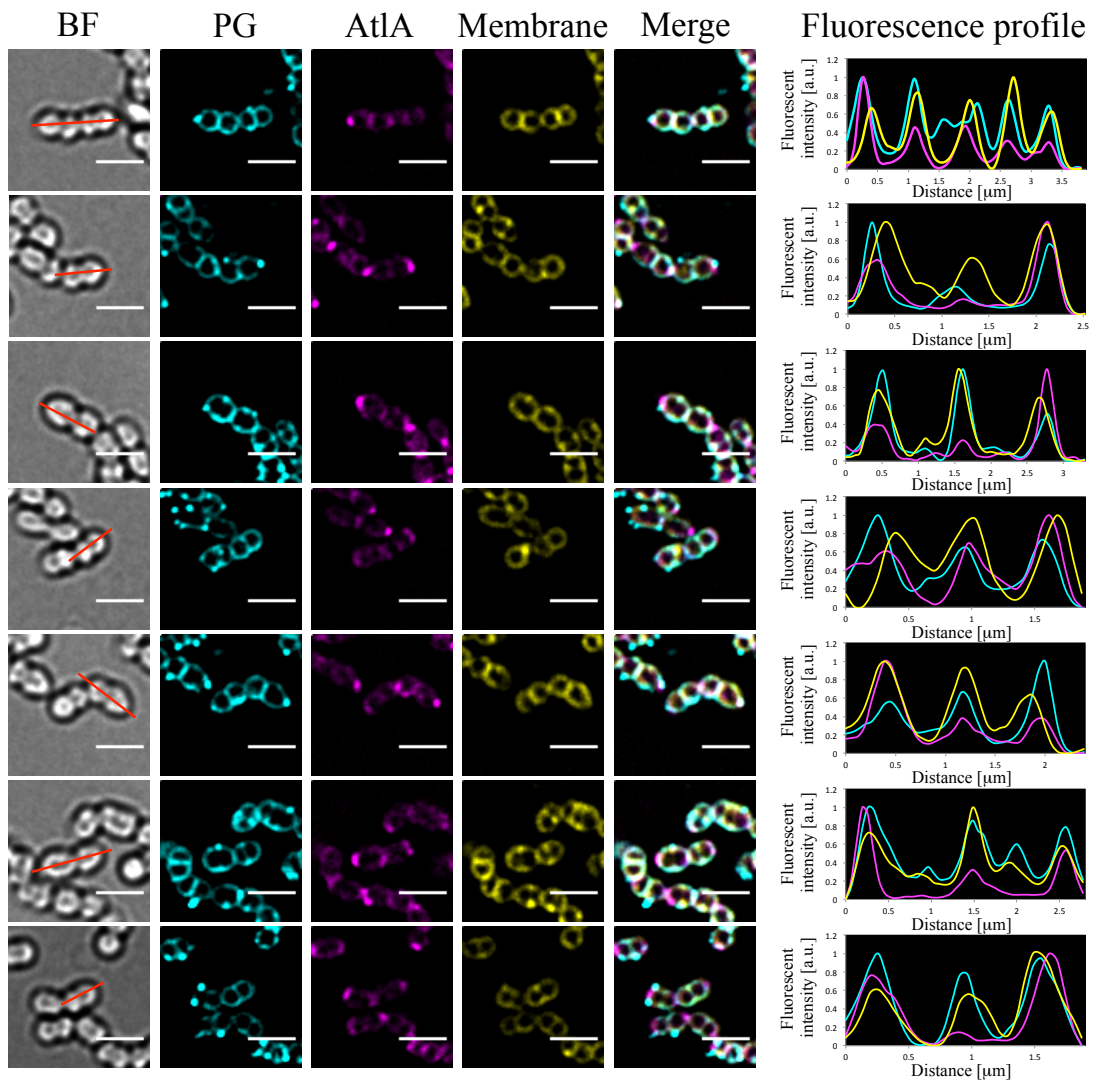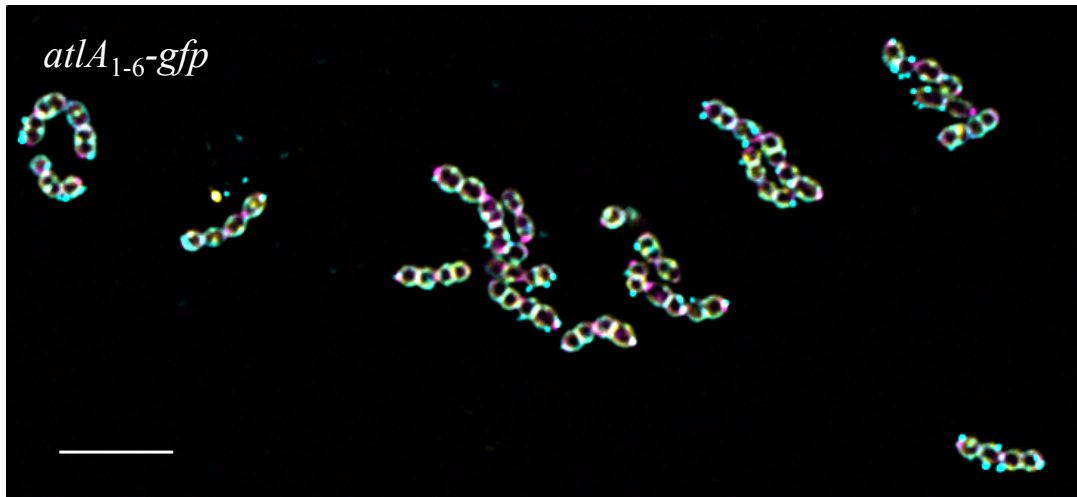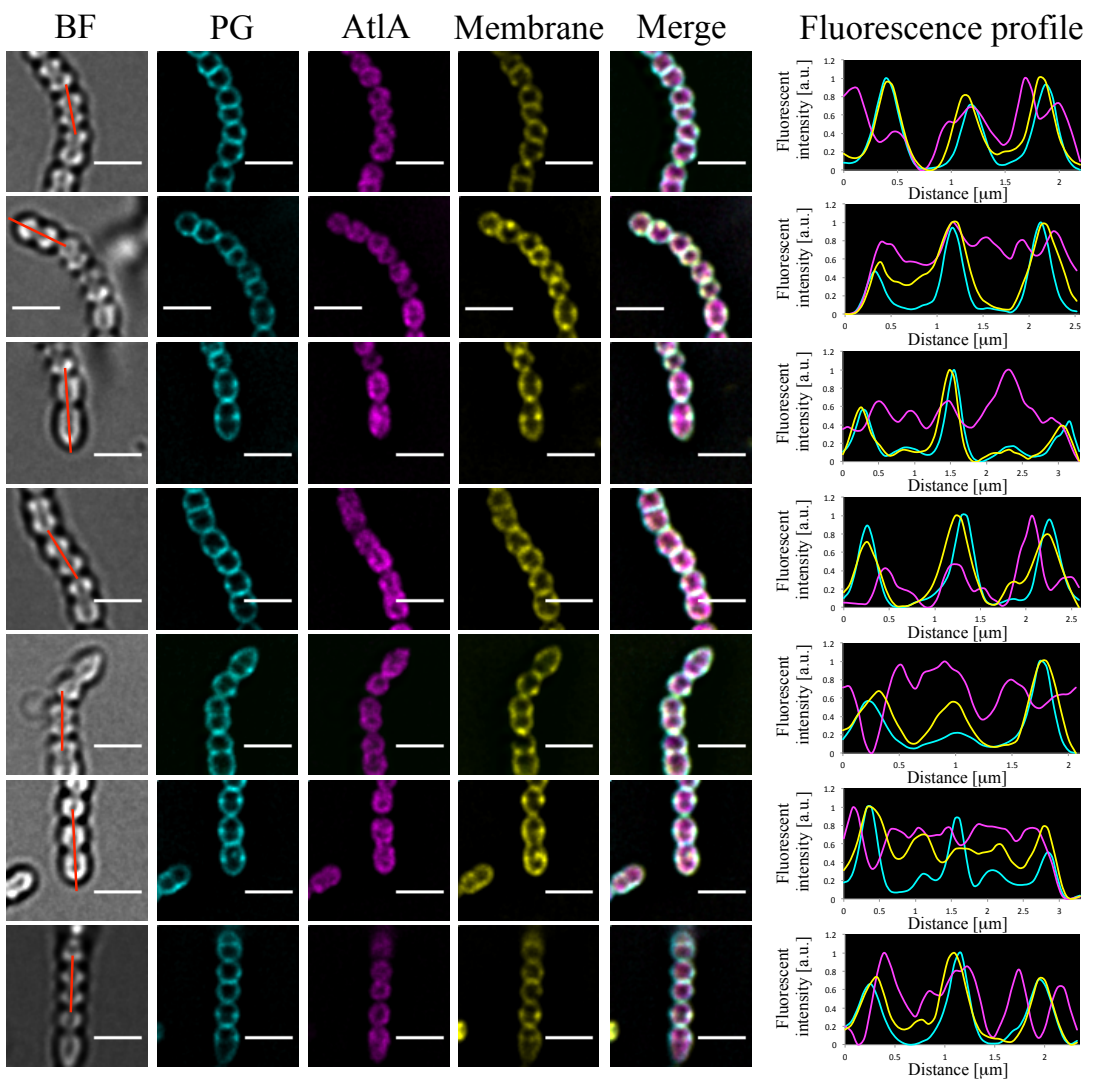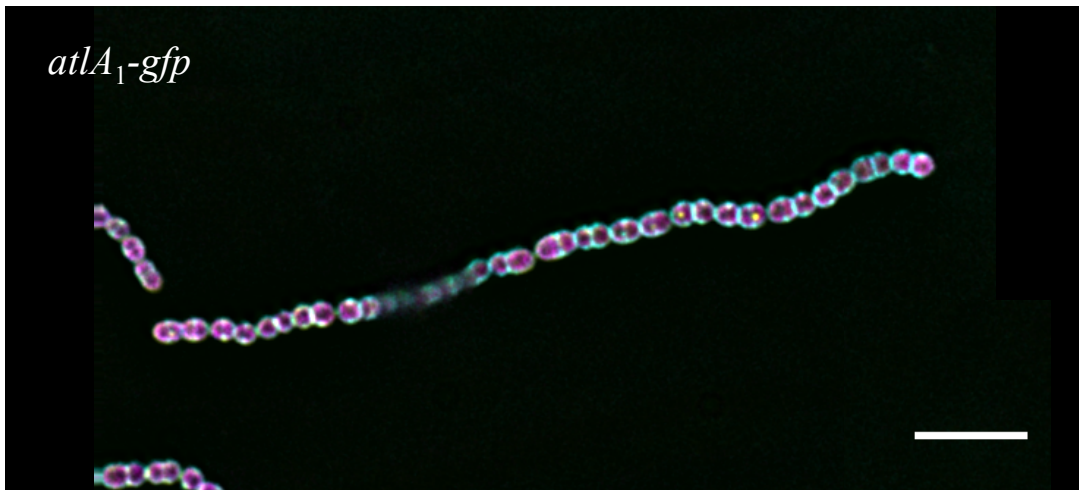
$atlA_{1-6}$-gfp
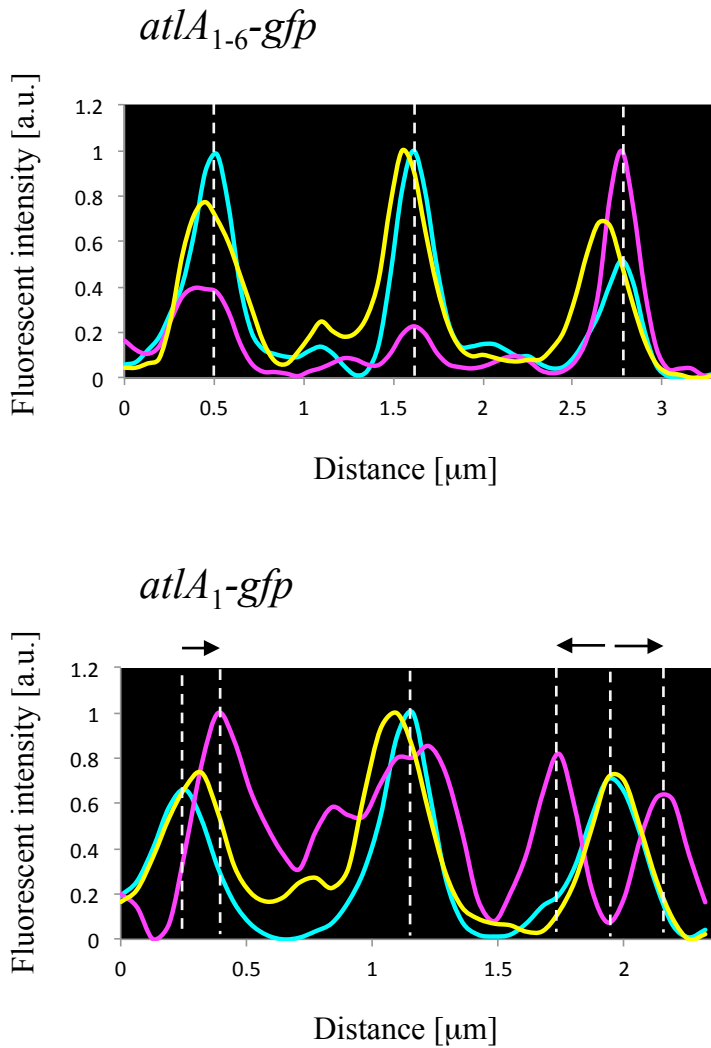
$atlA_1$-gfp

Figure 5.9 Co-localisation of fluorescently labelled AtlA derivatives with other cell compartments

A-B. Bright-field and fluorescent images of *E. faecalis* JH2-2 *atlA$_{1-6}$-gfp* (A) and *atlA$_1$-gfp* (B) cells. A co-localisation of peptidoglycan (cyan), AtlA (magenta) and membrane (yellow) was determined by plotting intensity profiles of each component for the individual cells along the longer cell axis indicated by red line. Scale bars, 5 μm (big images) and 2 μm (individual cells).

C. Representative fluorescent intensity profiles of each analysed strain: *atlA$_{1-6}$-gfp* and *atlA$_1$-gfp*. The maxima of florescent intensity are indicated with the white doted lines. The fluorescent intensity maxima of each fluorophore in *atlA$_{1-6}$-gfp* almost perfectly match, whereas the maxima of AtlA fluorescent intensity in *atlA$_1$-gfp* were slightly sifted outside of the PG and membrane fluorescent intensity maxima.

156

5.5   Pull-down assay using recombinant LysM domain

Collectively, the results revealed that the LysM domain is essential for the targeting of the enzyme to the poles and septum where it can be secreted. It is therefore possible that *E. faecalis* has a dedicated secretion pathway, which requires the partner/partners interacting with the AtlA binding domain. To test this hypothesis a pull-down assay using recombinant LysM domain produced in *E.coli* was obtained.

The N-terminally His tagged LysM domain was purified by Dr Stéphane Mesnage and used to saturate Ni-NTA-Agarose resin. The Δ*atlA* mutant cell lysate was loaded on to a column with saturated and no saturated resin as a negative control. The LysM domain and potential partners were eluted and analysed by SDS-PAGE (Figure 5.10 A). Three independent biological replicates of this experiment were done. The samples were resolved in gradient polyacrylamide gel and stained using colloidal coomassie. Each lane was divided on to three sections: above (I), below (III) and at the 'bait' (II) size (Figure 5.10 B). In-gel enzymatic digestion was used to degrade proteins with trypsin and resulting peptides analysed by mass spectrometry (by Dr Adelina Acosta-Martin). All datasets were subjected to a statistical analysis. 21 proteins were present only in samples co-purified with recombinant LysM domain. Among these proteins most of them (15 out of 21) were 50S and 30S ribosomal proteins. All proteins identified have known functions (Figure 5.10 C). Pull-down assay did not reveal any partners specifically interacting with LysM domain. Based on unpublished results in the laboratory (Elsarmane, 2016), we were expecting to find some candidate genes required for AtlA cell surface display. In particular, the characterisation of spontaneous and transposon mutants revealed that mutations in a gene downstream of *atlA* (*EF0773* in *E. faecalis* V583) led to formation of long cell chains. In the *EF0773* mutants, production of AtlA remains unchanged but the cell surface display of this autolysin is greatly reduced. The *EF0733* gene was named *admA* (AtlA display mutant A).
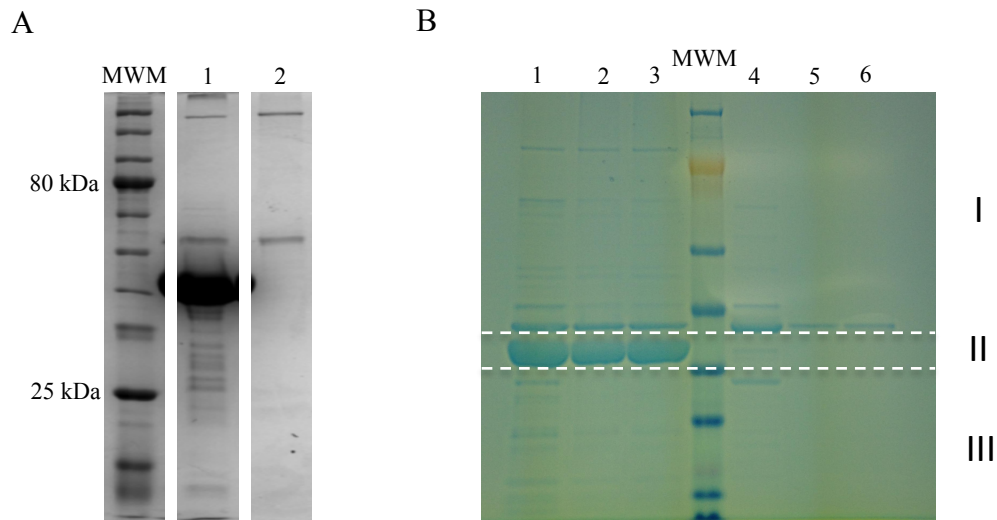
Fasta ID	Proteins	Gene ID
Q836X6	50S ribosomal protein	rplU
Q839G0	30S ribosomal protein	rpsS
Q839G2	50S ribosomal protein	rplW
Q839G1	50S ribosomal protein	rplB
Q839H0	30S ribosomal protein	rpsG
Q837W3	Trigger factor	Tig
Q830Q5	50S ribosomal protein	rplK
Q839F9	50S ribosomal protein	rplV
Q835U8	Translation initiation factor IF-2	infB
Q830Q6	50S ribosomal protein	rplA
P59754	30S ribosomal protein	rpsM
Q830Q7	50S ribosomal protein	rplJ
Q93EU6	60 kDa chaperonin	groL
Q82Z47	30S ribosomal protein	rpsI
Q839E0	30S ribosomal protein	rpsK
Q839G3	50S ribosomal protein	rplD
Q839G4	50S ribosomal protein	rplC
Q82ZI6	30S ribosomal protein	rpsD
Q837J2	DEAD-box ATP-dependent RNA helicase	cshA
Q839D9	DNA-directed RNA polymerase subunit alpha	rpoA
Q82Z41	DNA-directed RNA polymerase subunit beta	rpoC

Figure 5.10 Pull-down assay analysis

158

A. SDS-PAGE analysis of the proteins eluted from the resin with (1) or without (2) saturation with the recombinant LysM domain. The bait protein was indicated with a red arrow. The molecular weight marker (MWM) indicates sizes:

B. SDS-PAGE analysis of the proteins co-purified with recombinant LysM domain (1-3) and unspecific interacting with Ni-NTA resin (4-6). Samples were obtained in three independent biological replicates (1 and 4; 2 and 5; 3 and 6). The three areas above (I), below (III) and at the bait size (II) are separated with the horizontal lines. The molecular weight marker indicates sizes: 250 kDa, 150 kDa, 100 kDa, 80 kDa (indicated), 60 kDa, 50 kDa, 40 kDa, 30 kDa, 25 kDa (indicated), 20 kDa, 15 kDa and 10 kDa.

C. Table showing all identified proteins specifically co-purified with recombinant LysM domain.

5.6   Role of AdmA in daughter cells separation.

AdmA was identified by Dr Fathe Elsarmane as a protein required for the cell surface display of AtlA (Elsarmane, 2016). A transposon insertion in the OG1RF *admA* gene led to a chain forming phenotype and a reduced activity on agar plates containing *M. luteus* cells. To confirm the role of AdmA, an in-frame deletion of this gene was constructed (Δ*admA*) along with a complementation of this mutation using a plasmid allowing inducible expression of *admA* (pTetH-*admA*). To obtain the deletion of *admA*, a pGhost 9 derivative, pGAdmA was constructed as described in Figure 5.11 A. Two fragments corresponding to the upstream (H1) and downstream (H2) regions of *admA* (695 nt and 546 nt, respectively) were PCR amplified from the *E. faecalis* genomic DNA using two sets of primers, AdmA_H11/AdmA_H12 and AdmA_H21/AdmA_H22, respectively (Figure 5.11 B). The H1 and H2 fragments were joined by overlap PCR using AdmA_H11 and AdmA_H22 primers, generating a fragment flanked by XhoI and EcoRI restriction sites (Figure 5.11 C). The PCR amplification product, (H1H2) was cloned in pGhost 9 using XhoI and EcoRI. Restriction enzyme digestion of the resulting plasmid pGAdmA confirmed the presence of the insert of the expected size (Figure 5.11 D). The insert was sequenced to confirm the absence of mutations.

pGAdmA was transformed into electrocompetent *E. faecalis* JH2-2 cells. Following integration of the plasmid to the chromosome by homologous recombination and serial subcultures, bacteria were plated on BHI supplemented with autoclaved *M. luteus* cells, in order to screen for colonies with reduced AltA enzymatic activity. Colonies surrounded by a smaller halo (indicated with the red arrows in Figure 5.11 E) were screened by PCR using primers AdmA_up and AdmA_dn (Figure 5.11 F).

The complementation vector, pTetH-*admA* was constructed by Lauren Brown, a 3rd year undergraduate student. In this vector, the *admA* ORF is placed under the control of the anhydrotetracycline (ATc) inducible promoter (P$_{tetH}$). pTetH-*admA* was transformed into electrocompetent *E. faecalis* JH2-2 Δ*admA* cells. and The Δ*admA* knockout and complemented derivative (Δ*admA*/pTetH-*admA*) were analysed by flow cytometry to investigate the impact of AdmA production on cell separation in *E. faecalis* (Figure

5.12). Deletion of *admA* lead to a significant increase in the median FSC value (FSC=162.19±3.89, ***P=0.0003) as compared to the parental strain (FSC=45.59±0.54;), indicating the formation of longer cell chains. In the absence of inducer, no significant difference (P=0.0767; n=3) in median FSC values was observed between Δ*admA*/pTetH-*admA* strain (FSC=195.95±17.96) and the Δ*admA* mutant. Addition of ATc to the Δ*admA*/pTetH-*admA* complementation strain led to a significant decrease (**P=0.0081; n=3) in the median FSC value (FSC=83.59±1.31), indicating that the production of AdmA restored the short chain phenotype of the parental Δ*admA* strain. The Δ*admA* mutant formed significantly (**P=0.0020; n=3) shorter cell chains than the Δ*atlA* mutant (FSC=501.77±28.40). Altogether, these results confirmed that AdmA plays an important role in the daughter cell separation.
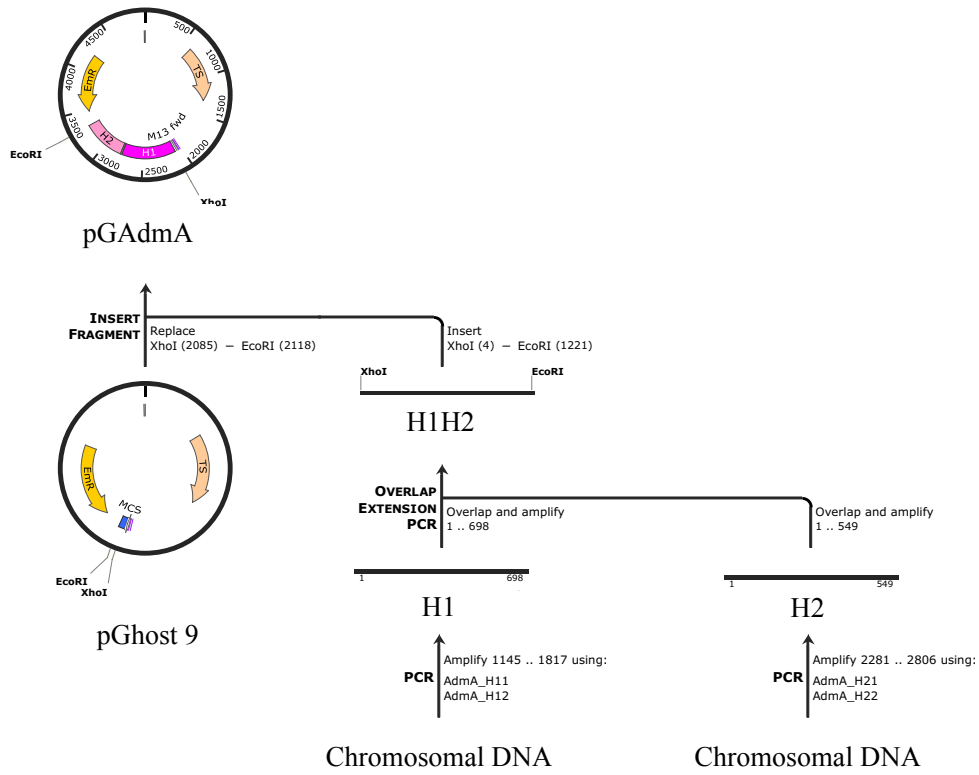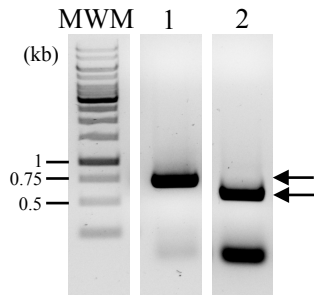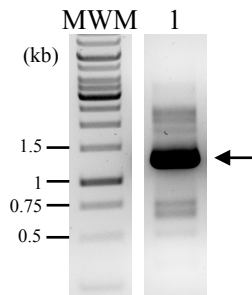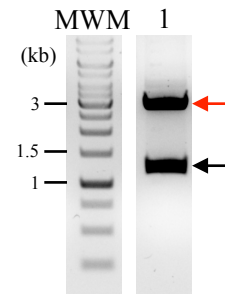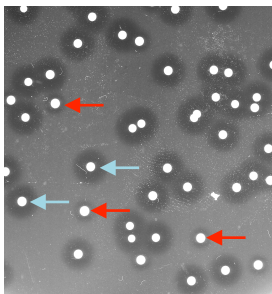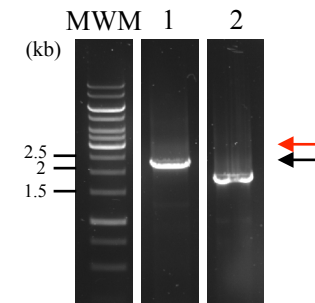
Figure 5.11 Construction of pGAdmA and Δ*admA* strain, an *E.faecalis* JH2-2 derivative with in-frame deletion of *admA*

A. A schematic representation of the cloning strategy followed to build pGAdmA. Two homology fragments, H1 and H2 were amplified from *E. faecalis* genomic DNA and fused by PCR to create a 1227 bp insert (H1H2) containing 695 bp upstream of the *admA* start codon, a 516bp *admA* ORF and 546 bp downstream of the *admA* stop codon. H1H2 was cloned to pGhost9 using XhoI and EcoRI restriction sites.

B. PCR amplification products corresponding to the H1 fragment (amplified with oligos AdmA_H11 and AdmA_H12, lane 1) and H2 fragment (amplified with oligos AdmA_H21 and AdmA_H22, lane 2). The expected DNA bands of 695 bp and 546 bp are indicated with black arrows. The sizes of chosen molecular weight markers (MWM) are indicated on the left hand side of the gel.

C. Overlap extension PCR product resulting from the fusion of fragments H1 and H2 (amplified with oligos AdmA_H11 and AdmA_H22, lane 1). The expected DNA band size of 1223 bp is indicated by a black arrow. The sizes of chosen molecular weight markers (MWM) are indicated on the left hand side of the gel.

D. Restriction profile of pGAdmA digested with XhoI and EcoRI. The expected DNA bands corresponding to the vector backbone (3717 bp) and the insert (1217 bp) are indicated by the red and black arrows, respectively. The sizes of selected molecular weight markers (MWM) are indicated on the left hand side of the gel.

E. AtlA enzymatic activity of *E. faecalis* JH2-2 cells, after double crossover event, plated on BHI supplemented with autoclaved *M. luteus* cells. Putative mutants forming smaller halo around colonies (lower AtlA enzymatic activity) are indicated with red arrows. The single-crossover mutants or revertants with bigger halo (normal AtlA enzymatic activity) are indicated with light blue arrows.

F. PCR screen of Δ*admA* mutants using AdmA_up and AdmA_dn primers. The expected DNA bands sizes of 2243 bp for WT (lane 1) and 1793 bp for Δ*admA* (lane 2) are indicated with red and black arrows, respectively.
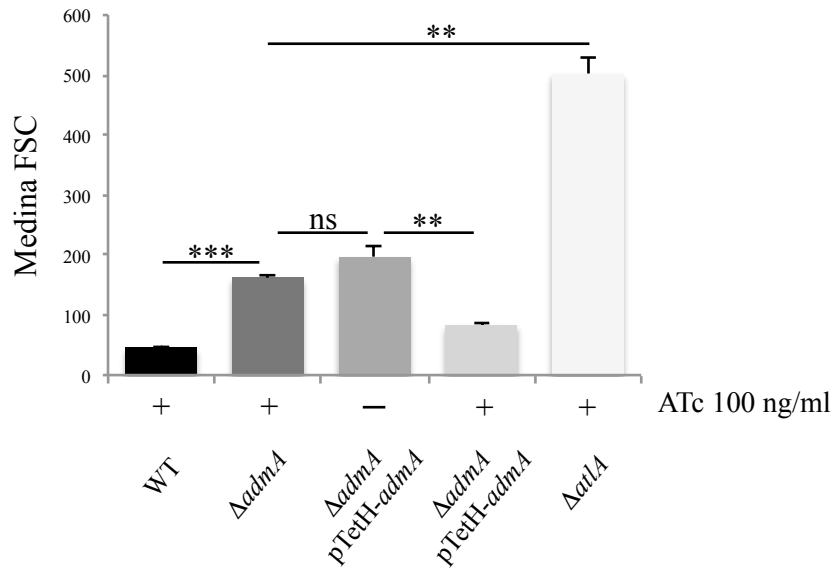
Figure 5.12 AdmA controls septum cleavage in *E. faecalis* JH2-2 cells

Comparison of median FSC values corresponding to an average cells chain length formed by *E. faecalis* JH2-2 (WT), *ΔadmA*, *ΔadmA/*pTetH-*admA* and Δ*atlA* in the absence (-) or presence (+) of anhydrotetracycline (ATc). The Δ*admA* median FSC value was significantly different from these for WT (***P=0.0003) and Δ*atlA* (**P=0.002). There was no significant difference (P=0.0767) between the median FSC values of Δ*admA* and not induced Δ*admA*/pTetH-*admA*. The median FSC values of Δ*admA*/pTetH-*admA* cells grown in presence (+) or absence (-) of ATc were significantly different (**P=0.0081). All measurements were done in triplicate.

The impact of the *admA* deletion on AtlA subcellular localisation was investigated by epifluorescence microscopy. The *admA* deletion and the pTetH-*admA* plasmid were introduced into the *atlA*$_{1-6}$-*gfp* background as previously described. *atlA*$_{1-6}$-*gfp*, *atlA*$_{1-6}$-*gfp* *ΔadmA* and *atlA*$_{1-6}$-*gfp* *ΔadmA* pTetH-*admA,* grown in the presence and absence of ATc were imaged (Figure 5.13). Microscopy visualisation was performed using fixed cells harvested in exponential phase. As previously described, the AtlA$_{1-6}$-GFP fusion was localised at the septum and poles (Figure 5.13 A). The in-frame deletion of *admA* caused the delocalisation of AtlA$_{1-6}$-GFP. The fluorescent signal was observed in the whole cell volume (Figure 5.13 B). Deconvolution of the *ΔadmA* images revealed that the fluorescent fusion of AtlA was not uniformly distributed across the cells and it was mostly associated with the outline of cells. The same fluorescence distribution was observed with the uninduced *ΔadmA* pTetH-*admA* strain (Figure 5.13 C). Images of *atlA*$_{1-6}$-*gfp* *ΔadmA* pTetH-*admA* grown in the presence of the inducer showed that AtlA$_{1-6}$-GFP restored the septal and polar localisation, and the short cell chains phenotype (Figure 5.13 D).

The changes in subcellular distribution of the AtlA$_{1-6}$-GFP fusion in the cells of *atlA*$_{1-6}$-*gfp* *ΔadmA* pTetH-*admA* grown in the absence or presence of anhydrotetracycline were analysed in details. The cell length and the distribution of the AtlA$_{1-6}$-GFP fluorescence were determined by plotting intensity profiles of the cells imaged in the bright-filed (black line) and fluorescent channel (green line) (Figure 5.14 A). The fluorescent profiles of 30 randomly chosen cells were used to create population demographs (Figure 5.14 B). In the absence of AdmA, the signal corresponding to the AtlA$_{1-6}$-GFP fusion was distributed across the cell. Inducing the production of AdmA led to changes in the subcellular distribution of AtlA. The polar and septal distribution of AtlA$_{1-6}$-GFP was observed.

	Bright-field	GFP	Merge

A *atlA*$_{1-6}$-*gfp*

Raw

Deconvolved

B *atlA*$_{1-6}$-*gfp* Δ*admA*

Raw

Deconvolved

C *atlA*$_{1-6}$-*gfp* Δ*admA* pTetH-*admA* ATc 0 ng/ml

Raw

Deconvolved
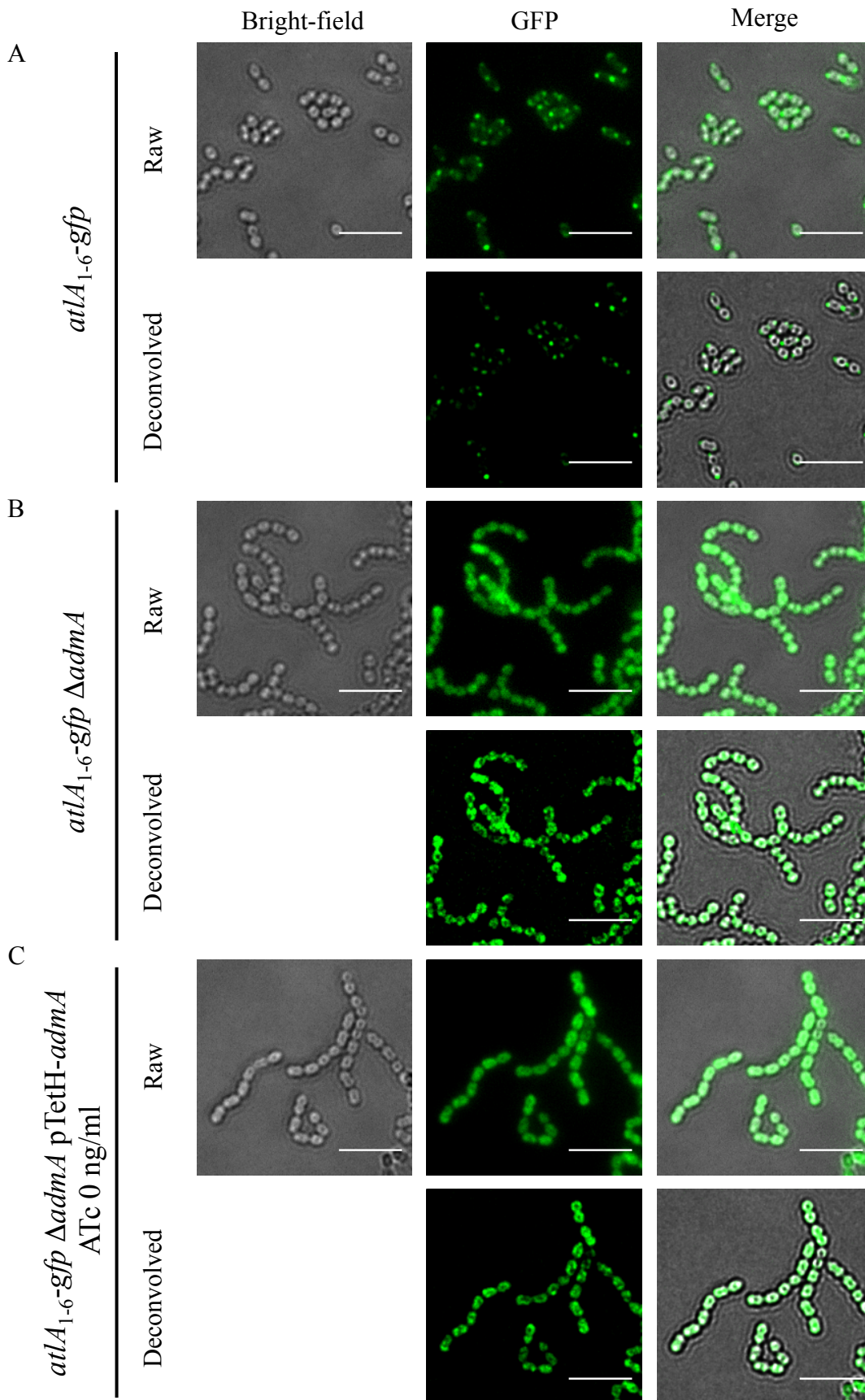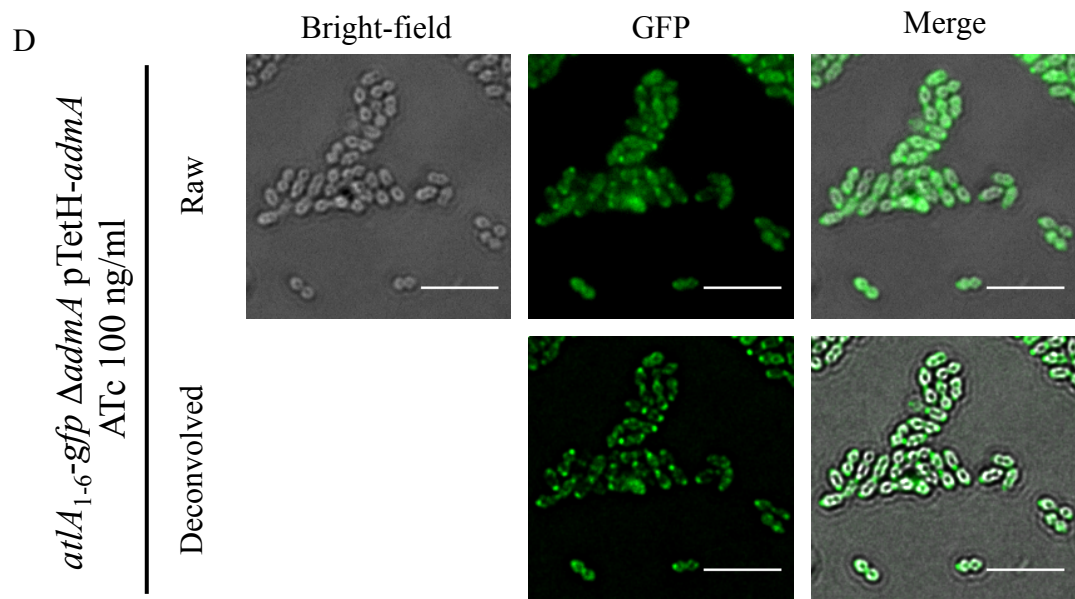
Figure 5.13 Localisation of the AtlA$_{1-6}$-GFP fusion in *E. faecalis* derivatives carrying an in-frame deletion of *admA*

Bright-field and fluorescent images of *atlA$_{1-6}$-gfp* (A)*, atlA$_{1-6}$-gfp ΔadmA* (B) and *atlA$_{1-6}$-gfp ΔadmA pTetH-admA* grown either in the absence (C) or presence (D) of ATc (100 ng/ml). Scale bars, 5 μm.
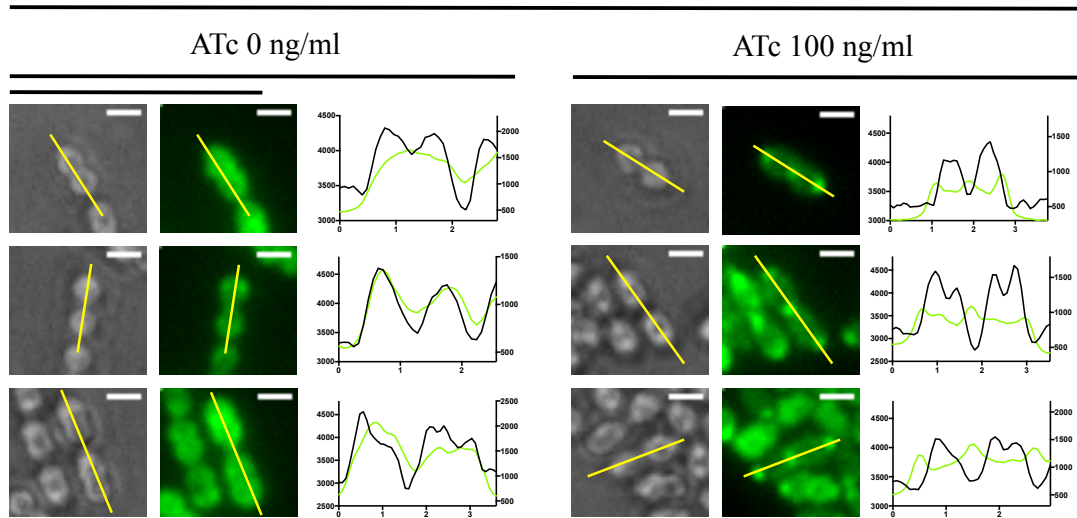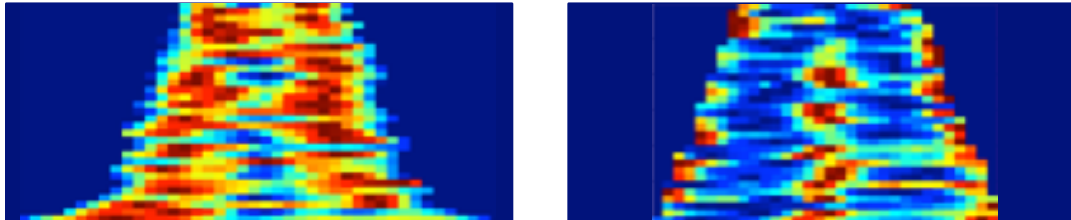
Figure 5.14 Production of AdmA is essential for the proper subcellular targeting of AtlA

A. Z-projections of maximum fluorescent intensity of *E. faecalis* JH2-2 *atlA*$_{1-6}$*-gfp/Δ admA*/pTetH-*admA* grown in the absence or presence of anhydrotetracycline. Intensities profiles corresponding to cell length (black) and fluorescence (green) across the long axis of the cells (yellow line) were plotted; Scale bars, 1 μm

B. Population demographs created by using the fluorescent profiles of 30 randomly chosen cells showing a correlation between the fluorescence signal intensity distribution along the cell length.

To further explore AdmA function, a strain producing an AdmA-GFP fusion was constructed to study the subcellular localisation of AdmA. A pGhost9 derivative, pGAdmA-GFP was constructed as presented in Figure 5.15 A. Fragments H1, H2 and H3 corresponding to the *admA* ORF (684 nt), the *gfp* ORF preceded by an linker (761 nt) and a 536 nt fragment downstream of the *admA* stop codon were PCR amplified from genomic DNA and pGAltA$_{1-6}$GFP using three sets of primers: AdmA-GFP_H11/AdmA-GFP_H12, AdmA-GFP_H21/AdmA-GFP_H22 and AdmA-GFP_H31/AdmA-GFP_H32, respectively (Figure 5.15 B). Fragments H1 and H2 were fused by overlap extension PCR using primers AdmA-GFP_H11 and AdmA-GFP_H22. Next, the H3 fragment was fused to H1H2 by overlap extension PCR using primers AdmA-GFP_H11 and AdmA-GFP_H32 (Figure 5.15 C). The amplification product was cloned to pGhost9 using XhoI and EcoRI sites. Plasmid restriction analysis using XhoI and EcoRI confirmed the presence of an insert of the expected size (Figure 5.14 D). The insert was sequenced to confirm the absence of mutations.

Due to the time constrains I was not able to construct *E. faecalis* JH2-2 *admA-gfp* using the pGAdmA-GFP vector.
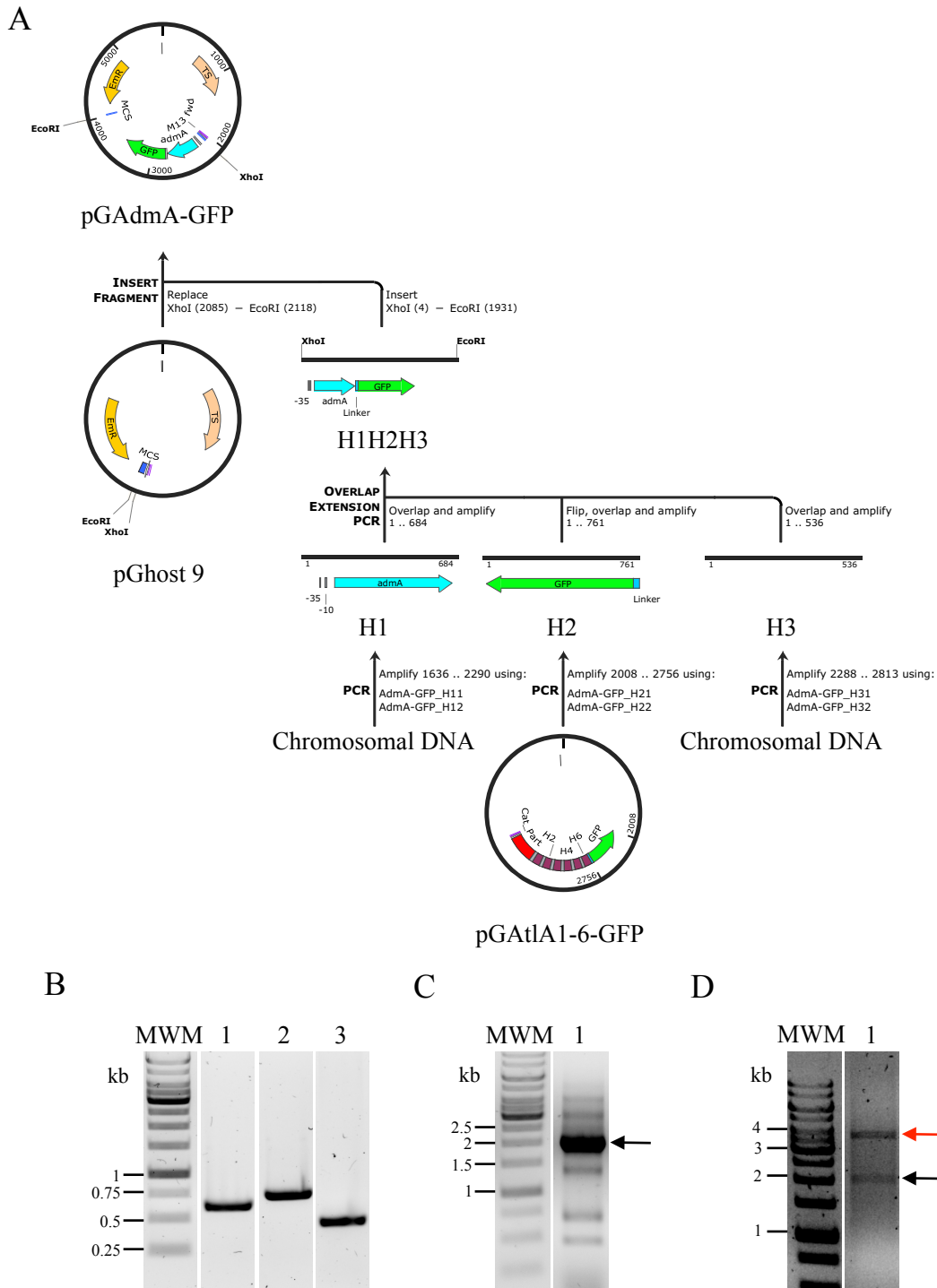
Figure 5.15 Construction of pGAdmA-GFP

A. A schematic representation of the cloning strategy. H1 and H2 fragments were amplified from genomic DNA; and H3 was amplified from pGAltA1-6GFP; H1, H2 and H3 were fused by PCR to create an insert consisting of the *admA* ORF fused to the *gfp* via a 36 nt linker followed by a 536 nt downstream region of the *admA* stop codon. The H1H3H3 amplification product (1937 bp) was cloned to pGhost9 using XhoI and EcoRI.

B. Amplification products corresponding to fragments H1 (684 bp, amplified with oligos AdmA-GFP_H11/AdmA-GFP_H12, lane 1), H2 (761 bp, amplified with oligos AdmA-GFP_H21/AdmA-GFP_H22, lane 2) and H3 (536 bp, amplified with oligos AdmA-GFP_H31/AdmA-GFP_32, lane 3). The sizes of chosen molecular weight markers (MWM) are indicated on the left hand side of the gel.

C. Amplification product resulting from the fusion of H1, H2 and H3 fragments (lane 1). The expected DNA band size of 1937 bp is indicated by a black arrow. The sizes of chosen molecular weight markers (MWM) are indicated on the left hand side of the gel.

D. Restriction profile of pGAdmA-GFP digested with XhoI and EcoRI. The expected DNA bands corresponding to the vector backbone (3717 bp) and the insert (1937 bp) are indicated by the red and black arrows, respectively. The sizes of selected molecular weight markers (MWM) are indicated on the left hand side of the gel.

5.7 Concluding remarks

In this chapter, it was shown that the two targeting sequences in AtlA (the signal peptide and LysM binding domain) are required for septal localisation of this enzyme. The deletion or replacement of AtlA LysM domain by AtlB LysM domain led to the sequestration of the protein inside the cells. This indicated that the signal peptide of AtlA is not sufficient to target the preprotein to the secretion channels. We also showed that the composition of the LysM moules and their number is critical for the subcellular localisation of AtlA. The sequential truncation of LysM domains led to a progressive disappearance of AtlA on the cell surface detected by immunolabelling. The analysis of strains producing GFP fusions revealed that LysM truncation caused an accumulation of the fluorescent signal inside the cells. Collectively, the microscopy results indicated that the simultaneous presence of the full length LysM domain and the signal peptide is essential for the septal and polar targeting of AtlA. This result is unexpected and entirely new as the LysM domain is expected to be exclusively involved in the non-covalent binding to peptidoglycan. This conclusion made us hypothesize that the LysM domain or the signal peptide could interact with a specific partner(s) that would recruit AtlA to the septum. A pull-down assay attempt using recombinant LysM protein to find the partner(s) interacting directly with the LysM domain of AtlA was unsuccessful. Similar experiments could be carried out using an *E. faecalis* strain expressing a tagged AtlA and *in vivo* cross-linking experiments. The pull-down assays could also be carried out using the tagged signal peptide as a bait.

Recent work in the lab identified a membrane protein with a C-terminal cytoplasmic extension (AdmA) required for the surface display of AtlA (F. Elsarmane and S. Mesnage, unpublished). The contribution of AdmA to AtlA subcellular localisation was explored. The in-frame deletion of *admA* recapitules the atlA phenotype and led to the sequestration of AtlA inside the cells and the formation of long cell chains. The wild-type phenotype and localisation of AtlA is restored when the *admA* knockout is complemented. These experiments suggest that AdmA is a candidate that could recruit AtlA at the septum. Further experiments are required to confirm this hypothesis to show if there is any direct or indirect interaction between AtlA LysM domain or signal peptide and AdmA. If this hypothesis is correct, we will also have to figure out AdmA itself is targeted to the septum.

.

172

CHAPTER 6

Formation of diplococci is crusial for *E. faecalis* pathogenesis

6.1   Impact of a long cell chains formation on *E. faecalis* virulence in the zebrafish model of infection

Previous studies revealed that the virulence of the JH2-2 strain is severely attenuated in the zebrafish model of infection (Prajsnar et al., 2013). We therefore used *E. faecalis* OG1RF and derivative strains in this study. An OG1RF Δ*atlA* mutant available in the laboratory strain collection was used to investigate the impact of long cell chains formation on *E. faecalis* virulence in the zebrafish model of infection. The lethality induced by the OG1RF Δ*atlA* mutant which has a cell separation defect was compared to the OG1RF parental strain that forms diplococci and/or short cell chains. Due to the fact that one long chain of the Δ*atlA* mutant consists of a higher number of viable cells, we injected the same number of viable cells rather than the same number of colony forming units (CFUs). To estimate the number of Δ*atlA* viable cells to inject into fish, long cells chains were dispersed into single cells using mild sonication, a treatment which does not alter cell viability (Dubée et al., 2011).

Zebrafish embryos 30 hours post-fertilisation (hpf) were injected intravenously into the yolk sac circulation valley with 1000 cells of *E. faecalis* OG1RF wild-type and Δ*atlA*. A group of fish injected with PBS was used as a negative control. The zebrafish larvae were observed up to 90 hours post-infection (hpi). The survival graphs for two independent biological replicates showed a significant reduction in virulence for the Δ*atlA* mutant as compared to OG1RF (**$P<0.01$; Figure 6.1). Following injection of OG1RF cells, 50 to 54% of larvae died whilst the same number of Δ*atlA* cells induced mortality of only 8 to 16% of the larvae. 100% of the zebrafish injected with PBS survived (Figure 6.1). These results showed that the Δ*atlA* mutant is severely attenuated in the zebrafish model of infection.

The reduction of virulence in the Δ*atlA* mutant could result from factors other than the chain-forming phenotype, like a defect in biofilm formation (Kristich et al., 2008; Paganelli *et.al,* 2013) or alterations in cell surface properties as observed for *Streptococcus mutans atlA* mutant (Ahn and Burne, 2006). To rule out these possibilities, we decided to compare the virulence of the Δ*atlA* mutant before and after sonication. As a preliminary experiment, we tested the impact of sonication on *E. faecalis* OG1RF virulence. OG1RF cells before (WT) and after (WT[S]) treatment with ultrasounds were injected at low doses (975-1200 viable cells). In both cases, 40% to 65% of infected zebrafish larvae died and the sonication did not lead to any significant differences in survival (Figure 6.2). Next, we wanted to confirm that sonication did not affect the growth rate of the *E. faecalis*. An overnight culture of the Δ*atlA* mutant was divided in half and one sample was sonicated. Sonicated (Δ*atlA*[S]) and non-sonicated (Δ*atlA*) cell were used to inoculate fresh media and growth was monitored for 8 h. No significant difference in growth rate was observed between Δ*atlA* and Δ*atlA*[S] (P=0.188). Δ*atlA* and Δ*atlA*[S] doubling times were 36.99±0.29 minutes and 36.45±0.10 minutes, respectively (Figure 6.3). Our preliminary experiments thus indicated that sonication did not affect the *E. faecalis* virulence or growth rate. Based on these results, we therefore decided to proceed and compared the virulence of the Δ*atlA* mutant before and after mild sonication to disperse long cell chains. Low dose injections (1000-1300 viable cells) of non-sonicated Δ*atlA* caused a limited zebrafish mortality (4% to 20%) 90 hpi, confirming the previous results (Figure 6.4). A similar number of cells of the Δ*atlA* mutant after sonication (Δ*atlA*[S]) were able to kill significantly more zebrafish larvae (between 46% and 60%; Figure 6.4). No significant differences in lethality were detected between OG1RF WT and Δ*atlA*[S] in two out of three biological replicates of zebrafish survival tests, suggesting that mild sonication of Δ*atlA* was able to restore its virulence similar to the wild-type strain (killing between 60% and 77% of larvae; Figure 6.4). These results showed a clear increase in OG1RF Δ*atlA* virulence caused by dispersion of long cell chains by ultrasounds.
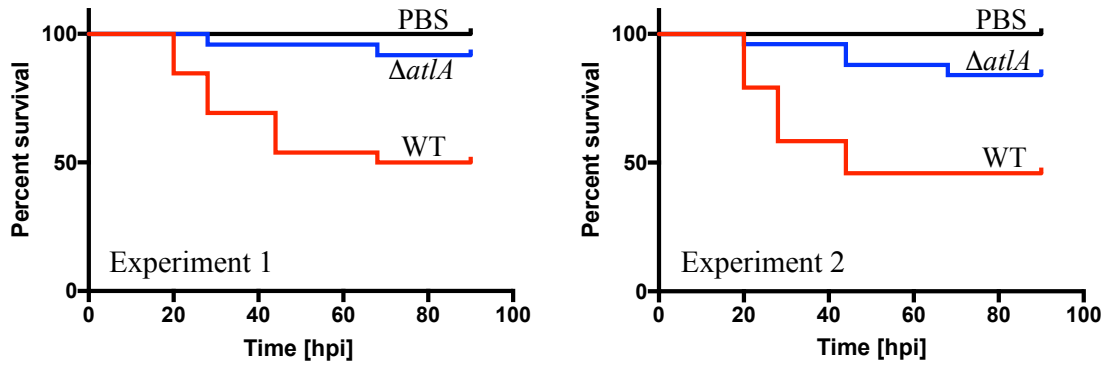
Experiment	Injected strain	Cells	Number of larvae infected	Number of larvae surviving	Percent survival
	WT	1000	26	13	50
1	ΔatlA	1000	24	22	92
	PBS	-	28	28	100
	WT	1100	24	11	46
2	ΔatlA	1050	25	21	84
	PBS	-	23	23	100

	P values	
	Experiment 1	Experiment 2
WT vs ΔatlA	0.0012 (**)	0.0032 (**)

Figure 6.1 Analysis of the virulence of *E. faecalis* Δ*atlA* mutant forming long cell chains

Survival of London wild-type (LWT) zebrafish embryos injected with *E. faecalis* OG1RF (WT) and Δ*atlA*. Results from two independent biological replicates are shown. For each experiment, the number of viable cells injected, the number of infected embryos, the number and percentage of surviving larvae are indicated. *P* values resulting from pairwise comparisons using the Log Rank Test are shown. The PBS injected group was used as a control.
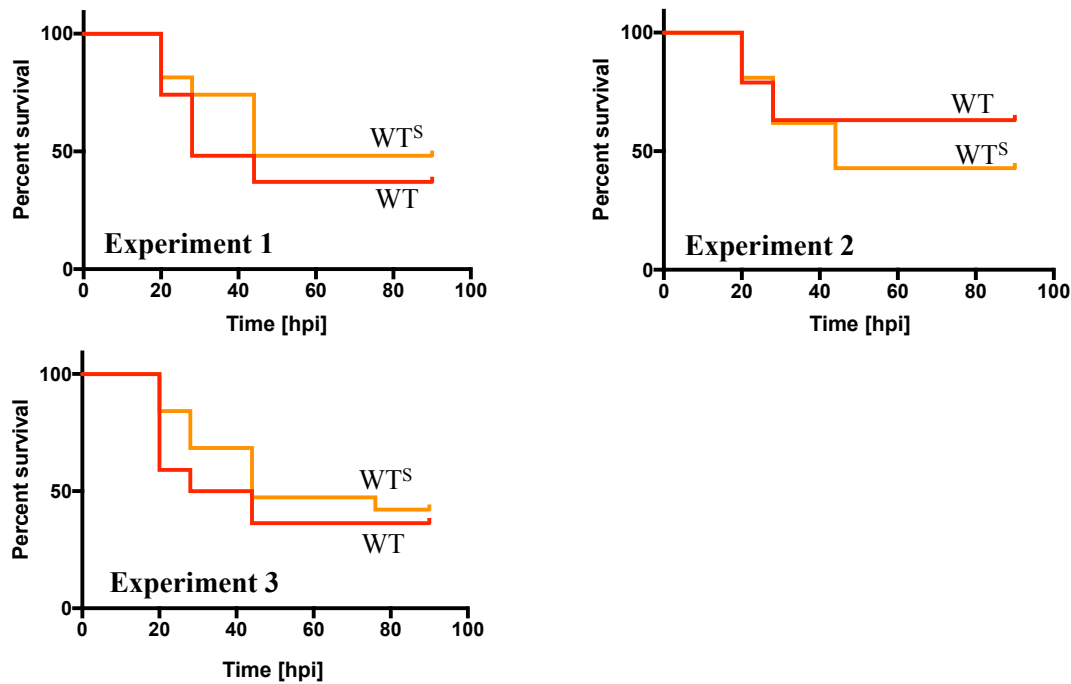
Experiment	Injected strain	Cells	Number of larvae infected	Number of larvae surviving	Percent survival
1	WT	1200	27	10	37
	WT^S	1050	27	13	48
2	WT	975	19	12	63
	WT^S	1200	21	9	43
3	WT	1050	22	8	36
	WT^S	1150	19	8	42

	P values		
	Experiment 1	Experiment 2	Experiment 3
WT vs WT^S	0.253 (NS)	0.312 (NS)	0.452 (NS)

Figure 6.2 Analysis of the virulence of *E. faecalis* OG1RF wild-type after sonication

Survival of LWT zebrafish embryos injected with *E. faecalis* OG1RF WT non-sonicated (WT) and sonicated (WT^S). Results corresponding to three independent biological replicates are shown. For each experiment, the number of viable cells injected, the number of infected embryos, the number and percentage of survival are indicated. *P* values resulting from pairwise comparisons using the Log Rank Test are shown.
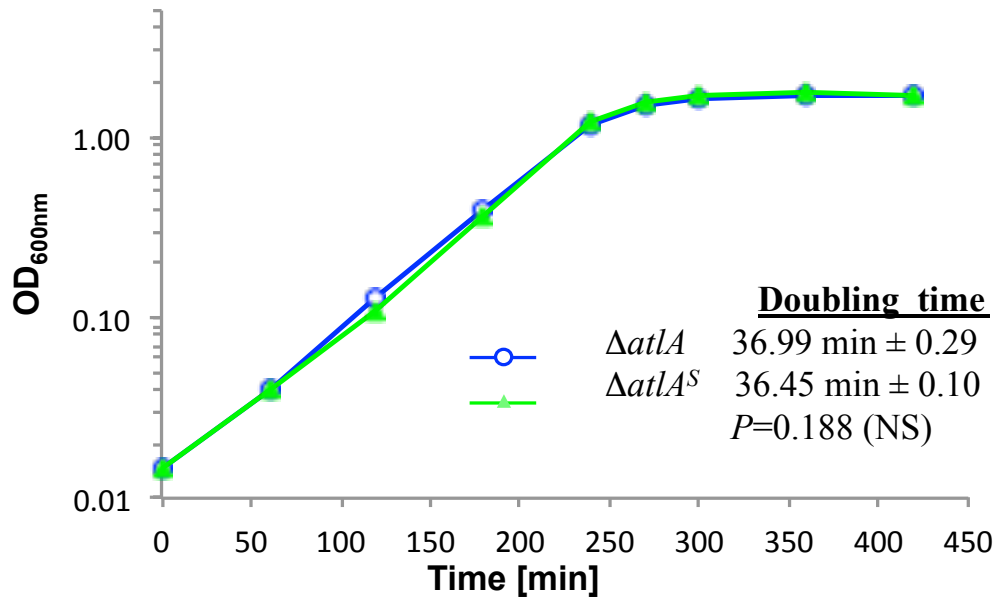
Figure 6.3 Analysis of growth rate of the *atlA* mutant sonicated ($\Delta atlA^S$) and non-sonicated ($\Delta atlA$)

Cell cultures were grown from an OD600 ~0.02 and the optical density was measured every 60 or 30 minutes. Three independent bacterial cultures were prepared and the growth curve was plotted using mean values. No significant difference (P=0.188) was found between the doubling time of $\Delta atlA$ (36.99±0.29 minute) and $\Delta atlA^S$ (36.45±0.10 minute).
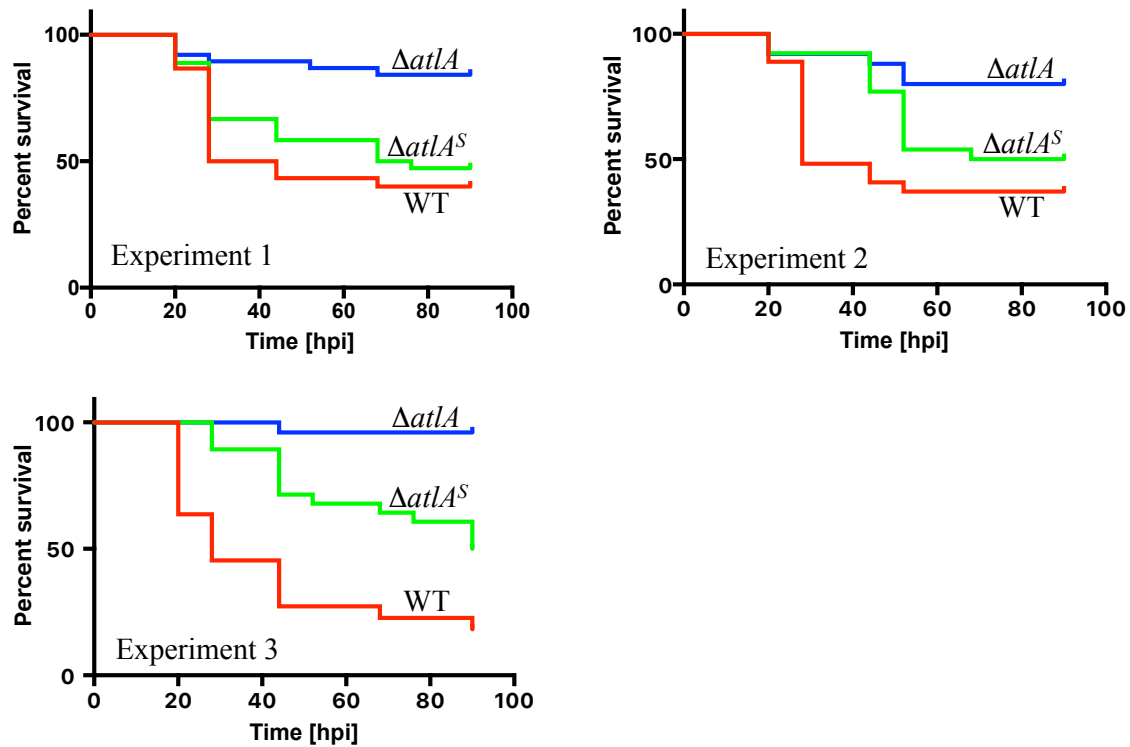
Experiment	Injected strain	Cells	Number of larvae infected	Number of larvae surviving	Percent survival
	WT	1000	30	12	40
1	$\Delta atlA$	1200	38	32	84
	$\Delta atlA^S$	1100	36	15	41
	WT	1000	27	10	37
2	$\Delta atlA$	1250	25	20	80
	$\Delta atlA^S$	1015	26	13	50
	WT	1300	22	5	23
3	$\Delta atlA$	1020	25	24	96
	$\Delta atlA^S$	1030	28	15	54

	P values		
	Experiment 1	Experiment 2	Experiment 3
WT vs $\Delta atlA$	0.0002 (***)	0.0017 (**)	<0.0001 (****)
WT vs $\Delta atlA^S$	0.455 (NS)	0.108 (NS)	0.0012 (**)
$\Delta atlA$ vs $\Delta atlA^S$	0.0011 (**)	0.0358 (*)	0.0003 (***)

Figure 6.4 Analysis of the virulence of the *E. faecalis* $\Delta atlA$ mutant after sonication

Survival of LWT zebrafish embryos injected with *E. faecalis* OG1RF (WT) and $\Delta atlA$ mutant before ($\Delta atlA$) and after sonication ($\Delta atlA^S$). Results corresponding to three independent

biological replicates are shown. For each experiment, the number of viable cells injected, the number of infected embryos, the number and percentage of survived larvae are indicated. *P* values resulting from pairwise comparisons using the Log Rank Test are shown.

6.2 Impact of cell chain formation on *E. faecalis* interaction with phagocytes

Fluorescently labelled bacteria and phagocytes were used to follow host-pathogen interactions in zebrafish embryos. *E. faecalis* OG1RF and isogenic Δ*atlA* derivative were transformed with plasmid pMV158-gfp allowing constitutive production of the GFP (Nieto and Espinosa, 2003). Zebrafish embryos were infected 30hpf with 1100 to 1300 cells of OG1RF (pMV158-*gfp*), Δ*atlA* (pMV158-gfp) and Δ*atlA*^{S} (pMV158-*gfp*) and fixed 1.5 hpi. The phagocytes were immunolabelled using anti-l-plastin antibodies and detected with secondary antibodies conjugated with AlexaFluor647. Stained embryos were immersed in low malting point agarose in E3 medium to image bacteria and phagocytes using a Leica DMi8 SPE-TSC confocal microscope.

Microscopy analysis revealed that diplococci and short chains formed by the OG1RF and Δ*atlA*^{S} strains were mostly found outside phagocytes, suggesting that they were able to evade the phagocytosis. By contrast, long cell chains formed by the Δ*atlA* mutant were nearly always found inside phagocytes (Figure 6.5 A). The bacterial uptake was measured as a ratio of green fluorescent area associated with phagocytes to the area of free bacteria. The uptake of Δ*atlA* was significantly higher than that of the sonicated *atlA* mutant cells (**P=0.0098; Figure 6.5 B). No significant difference in uptake was found between Δ*atlA*^{S} and OG1RF cells. These results revealed that diplococci and short chains are able to evade the phagocytosis, whilst long cell chains are not. This suggests that the formation of long cell chains is responsible for the reduction of Δ*atlA* virulence in the zebrafish model of infection.

To test this hypothesis, we compared the lethality of OG1RF and Δ*atlA* cells in immunocompromised zebrafish embryos. Phagocytes were depleted following injection of morpholino against *pu.1*, a transcription factor essential for development of myeloid cells (Klemsz et al., 1990). The *pu.1* morphants were infected with OG1RF, Δ*atlA* and a control group was injected with PBS. As expected, 100% survival was observed for the immunocompromised larvae injected with PBS. Approximately 1200 OG1RF or Δ*atlA* cells killed over 95% of phagocytes-depleted embryos in the first 20 h following infection (Figure 6.6). No significant difference was observed in each biological

180

replicates. These results suggested that in absence of phagocytes, the ΔatlA mutant is as virulent as the wild-type OG1RF strain.

Collectively, our data indicate that the reduced virulence of the *E. faecalis* ΔatlA mutant results from its inability to evade phagocytosis at the early stage of infection, showing an important biological role of AtlA in *E. faecalis*.

A

OG1RF

ΔatlA

ΔatlA^S

182
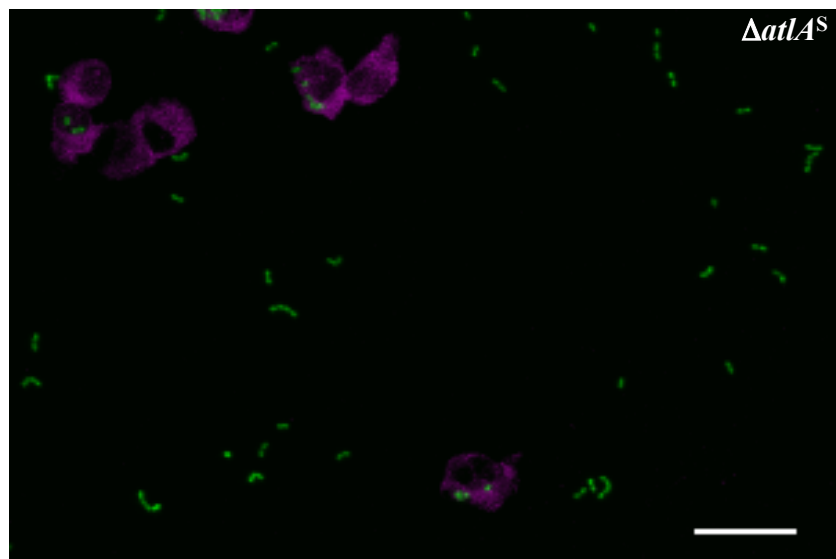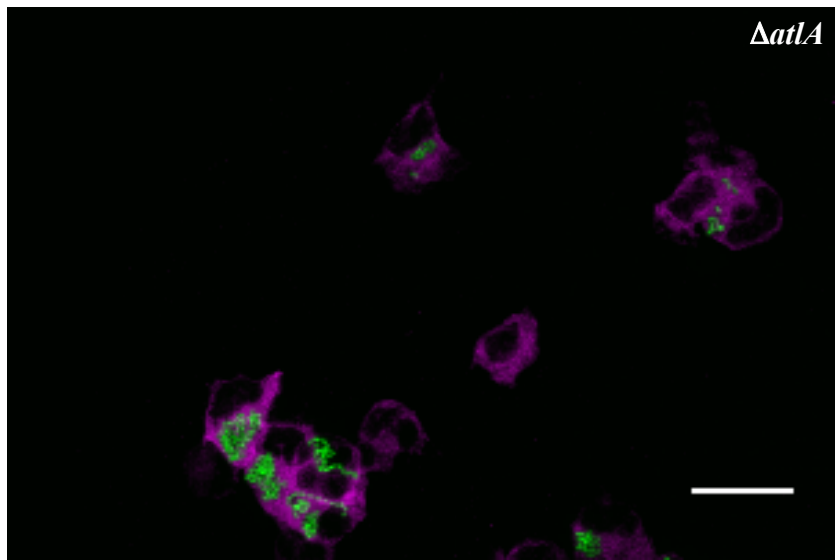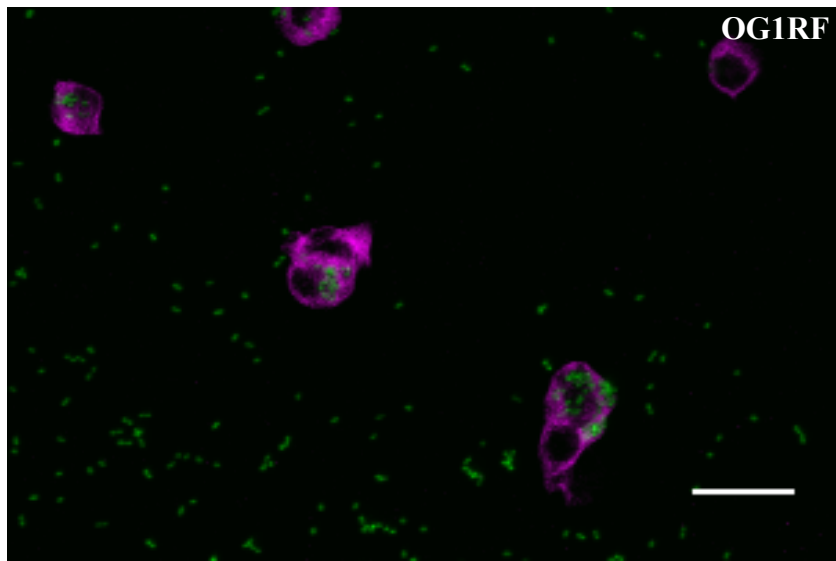
B
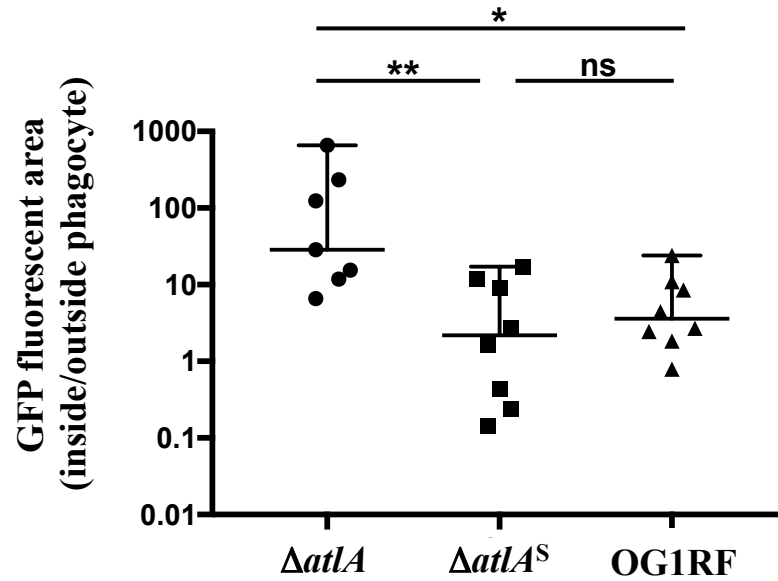
Figure 6.5 Quantification of *E. faecalis* uptake by zebrafish phagocytes

A. Embryos infected with low dose of *E. faecalis* cells producing GFP were fixed in 4% paraformaldehyde 1.5 h post infection. Phagocytes were immunolabelled using anti-l-plastin antibodies raised in rabbit and detected with goat anti-rabbit IgG conjugated to AlexaFluor647. Fluorescent bacteria and phagocytes were imaged by scanning confocal microscopy. Representative images of phagocytes (magenta) following infection with OG1RF carrying pMV158-*gfp* (OG1RF), *atlA* mutant carrying pMV158-*gfp* (Δ*atlA*) and sonicated Δ*atlA* carrying pMV158-*gfp* (Δ*atlA*^S) cells (green) are shown. Scale bars, 20μm.

B. Comparison of fluorescently labelled OG1RF wild-type, Δ*atlA* and sonicated Δ*atlA* (Δ*atlA*^S) phagocytosis. The confocal microscopy images were used to measure the area of GFP fluorescent signal in- and outside of phagocytes using a dedicated Fiji plugin. The uptake of the Δ*atlA* long cell chains was significantly higher as compared to Δ*atlA*^S (**P=0.0098) and WT (*P=0.0438). No difference in phagocytosis was found between short chains of wild-type and Δ*atlA*^S (NS, *P*>0.05).
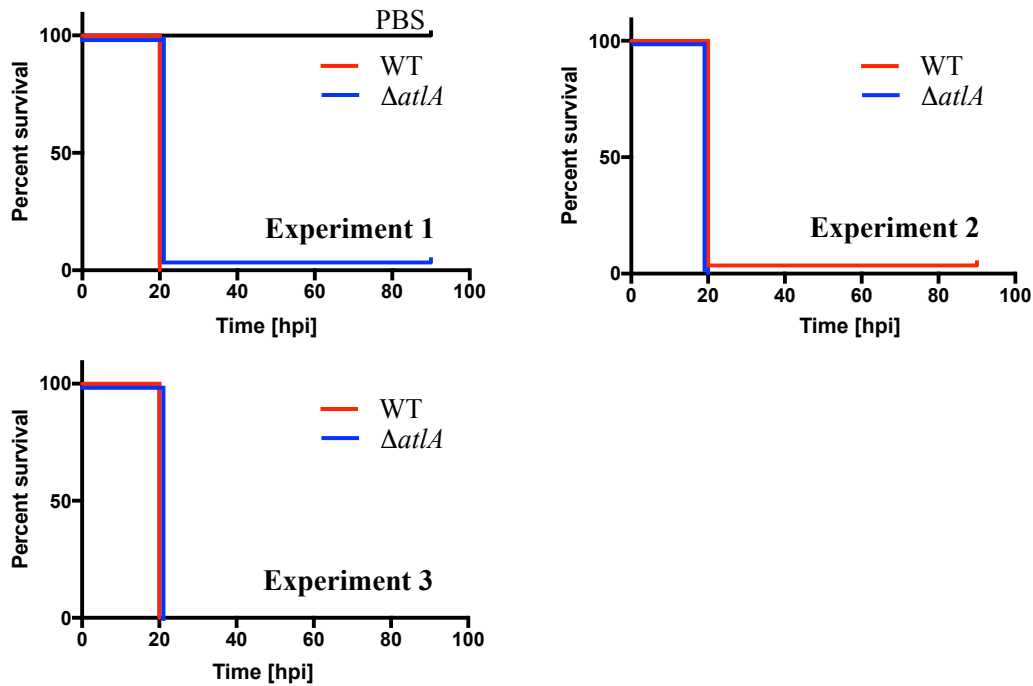
Experiment	Injected strain	Cells	Number of larvae infected	Number of larvae surviving	Percent survival
1	WT	1100	34	0	0
	ΔatlA	1200	30	1	4
	PBS	-	25	25	100
2	WT	1250	27	0	0
	ΔatlA	1250	28	1	4
3	WT	1150	29	0	0
	ΔatlA	1250	26	0	0

	P values		
	Experiment 1	Experiment 2	Experiment 3
WT vs ΔatlA	0.287 (NS)	0.326 (NS)	>0.999 (NS)

Figure 6.6 Analysis of the virulence of *E. faecalis* OG1RF Δ*atlA* in immunocompromised zebrafish embryos

Survival of *pu.1* morphants injected with low doses of *E. faecalis* OG1RF WT and Δ*atlA*. Results corresponding to three independent biological replicates are shown. For each experiment, the number of viable cells injected, the number of infected embryos, the number and percentage of survived larvae are indicated. *P* values resulting from pairwise comparisons using the log rank test are shown. The PBS injected group was used as a control

6.3   Concluding remarks

In the final chapter of results, it was shown that the Δ*atlA* mutant with impaired septum cleavage, was severely attenuated in the zebrafish model of infections as compared to wild-type. To eliminate a bias caused by the comparison of two different genetic backgrounds, the virulence of the Δ*atlA* mutant was compared before and after sonication. The mild sonication mechanically breaks the cell chains without affecting cell virulence, viability or growth rate. This treatment revealed that sonication of the Δ*atlA* cells restored virulence. Further investigation revealed that an increased uptake of long cell chains by phagocytes, suggesting that Δ*atlA* is unable to evade phagocytosis. To confirm the role of phagocytes in the clearance of the infection the virulence of Δ*atlA* was tested in phagocyte-depleted zebrafish. Δ*atlA* induced mortality of more that 95% of embryos with phagocytes depletion in the first 20 hpi, showing similar virulence as the wild-type strain. Collectively, these results showed that formation of diplococci is an important factor contributing to *E. faecalis* virulence in the zebrafish model of infection.

Pathogens have evolved strategies to overcome the host innate immune system. Increasing the bacterial cell size as a strategy to evade phagocytosis has been reported for uropathogenic *E. coli* which form filaments (Justice et al., 2004) and *Mycobacteria* which form serpentine cords (Bernut et al., 2014). Some fungi also use this strategy: *Cryptococcus neoformans* forms titan cells (up to 100μm in diameter), whilst pathogenic *Aspergillus* species form hyphae that can grow up to tens of μm in length (Erwig and Gow, 2016). Minimization of the bacterial cell size appears to be a less common strategy. In *S. pneumoniae,* it has been shown to reduce complement deposition and complement-dependent opsonophagocytosis (Dalia and Weiser, 2011). In the case of *E. faecalis*, the basis for resistance to phagocytosis is different since increased phagocytosis of long cell chains still occurs in the absence of complement. We proposed that the minimization of cell size in *E. faecalis* allows cells to disseminate within the host and produce tissue damage before being neutralized by the immune system.

CHAPTER 7

General discussion

Enterococcus faecalis is a Gram-positive commensal bacterium that occurs as diplococci and short chains. It dwells in the gastrointestinal tract of animals including humans. Following an antibiotic treatment or in an immunocompromised host, *E. faecalis* can cause infections, including life-threatening bacteremia, infective endocarditis and peritonitis, and urinary tract infections. The mechanism behind the change from a commensal to opportunistic pathogen remains unknown.

Our research group investigates the contribution of cell wall homeostasis to host innate immunity. One of the studied aspects is a control of hydrolytic enzymes involved in peptidoglycan metabolism. A bioinformatics analysis showed that *E. faecalis* might encode 21 PG hydrolase. So far, only four enzymes were studied: AtlA, AtlB, AtlC and EnpA (Mesnage et al., 2008). AtlA is a major PG hydrolase responsible for daughter cell separation after cell division. An in-frame deletion of an *atlA* gene leads to formation of long cell chains. AtlB plays a minor role in this process and requires 24 hours to reduce long cell chains to diplococci. Only AtlA has been shown to cause cell lysis (Qin et al., 1998).

AtlA activity can be lethal therefore it has to be tightly controlled. In this study, we investigated the contribution of different AtlA properties to its septum cleavage activity and we sought to characterise mechanisms involved. Moreover, using a zebrafish model of infection we showed that an impaired daughter cells separation affects virulence of *E. faecalis*.

7.1 AtlA has unusual subcellular targeting signals

A bioinformatics analysis of an AtlA amino acid sequence predicts a presence of an unusually long signal peptide at the protein N-terminus and a cleavage side between alanine 53 and threonine 54 (a standard Sec signal peptide consists of around 23 amino acids) (Fletcher and Braunstein, 2012). The AtlA signal peptide was assigned as a

canonical Sec system signal peptide. In this study the functional analyses of the AtlA signal peptide showed that this peptide is not able to efficiently translocate the protein across the membrane on its own and the AtlA LysM binding domain is required for that. This indicates that AtlA is secreted post-translationally since the full length of preprotein is essential to be targeted to the right cell compartments: septum and cell poles. The generic Sec system signal peptide is recognised by SecB or other chaperones to prevent protein folding and further is bound by the SecA ATPase, which delivers to and pushes the protein throughout the SecYEG channel (Fletcher and Braunstein, 2012). It seems that AtlA has a more complex secretion pathway than the one described above. In AtlA the LysM domain is responsible for AtlA targeting to the secretion channels location area. This process is probably based on a charge of the LysM modules rather than a specific targeting motif as it was described for some eukaryotic proteins (Izeta et al., 2003). In the neutral cytoplasmic pH the AtlA LysM modules (pI=10.0) are positively charged. The sequential truncation of the AtlA LysM modules or their replacement for the AtlB LysM modules (pI=6) leads to a reduction of the positive charge of the C-terminus. This results in fluorescent signal distributed across the entire cell.

Differences in the subcellular localization of AtlA and AtlB suggest that AtlA has a unique secretion pathway. The localisation of the generic Sec secretion system in *E. faecalis* is poorly studied and a presence of 'ExPortal' was proposed (Kline et al., 2009). In this model secretion occurs via a single pore frequently localised in the division side. Since the ExPortal model has been controversial it will not be further discussed here. In *S. pneumoniae* both major components of the Sec system SecA and SecY have localisation associated with only half of a cell, resulting in an 'X'-shaped distribution (Tsui et al., 2011), similar to what was observed for the GFP fusions with the AtlB signal peptide. This suggests that AtlB could be translocated via the generic Sec system, whereas AtlA could be secreted via a defined subset of channels localised at the septum and cell poles.

We showed that the presence of one protein AdmA, is essential for the proper cellular targeting of the full length AtlA. This small membrane protein is probably involved in an assembly of a protein complex that attracts the LysM domain as a direct AtlA-AdmA interaction was not found when the pull-down assay was performed. We hypothesise that when the AtlA preprotein is in the right cell compartment, the signal peptide is recognised by SecA and translocated across the membrane via the SecYEG channel

(Fletcher and Braunstein, 2012). The role of the unusual long signal peptide may be to slow down the protein secretion to allow for a proper folding of the LysM domain and binding to the glycan strands through a similar mechanism was described for an autotransporter, EspP in *E. coli* (Szabady et al., 2005). In EspP the elongated signal peptide slows down its Sec-dependent secretion across the inner membrane to allow for the proper folding of a C-terminal β-barrel and its interaction with the outer membrane (Szabady et al., 2005).

7.2   Control of AtlA activity

In this study we showed that the sequential truncation and changes in the amino acid composition of the LysM modules impaired the septum cleavage mediated by the AtlA derivatives. From a previous study it is known that the LysM binding domain is important for the AtlA activity and the deletion of the C-terminal domain led to a 270-fold reduction in a hydrolytic activity of the recombinant protein as compared to full length AtlA (Eckert et al., 2006). A similar result was observed when the AcmA binding domain modularity was studied. It was shown that this hydrolase requires exactly 3 LysM modules for optimal enzymatic activity (Steen et al., 2005). Moreover, recently it has been shown that the LysM modules can fold independently of one another and do not interact, thus they do not form a quaternary structure. They more likely behave as "beads on a string" where each module binds separately to the substrate (Mesnage et al., 2014). Bearing in mind the role of the LysM domain in AtlA targeting to the secretion channels (Chapter 7, section 7.1) we propose a mechanism in which the AtlA septum cleavage activity is controlled by a complexity of the LysM domain. Although the bioinformatics analysis of *E. faecalis* genome revealed that there are 12 genes encoding proteins with the LysM binding domain however only AtlA has a binding domain consisting of six LysM modules. There is a fine balance between the number of the LysM modules and their overall charge which controls the amount of the secreted protein as well as the protein binding strength.

The N-terminal domain of AtlA undergoes two post-translational modifications: *O*-glycosylation and proteolytic cleavage. *O*-glycosylation (Salamaga et al., 2017) has an inhibitory impact on the AtlA septum cleavage, whereas the degradation (Eckert et al., 2006) of this domain promotes the AtlA activity. Although AtlA is not the first

hydrolase for which glycosylation of the N-terminal region was described, the mechanism of the protein activity inhibition remains unknown. Rolain *et al.* proposed a model in which glycosylation of *Lactococcus plantarum* AcmA2 leads to a formation of a 'pin' as a result of interaction between an SH3b binding domain and substituted GlcNAc residues (Rolain et al., 2013). A bioinformatics prediction (http://prdos.hgc.jp) showed that the AtlA N-terminal domain is disordered, therefore we hypothesise that *O*-glycosylation leads to a steric hindrance inhibiting the catalytic activity. The degradation of the N-terminal domain by extracellular proteases is to ensure that AtlA is full active only when it has reached the substrate. In some *E. faecalis* strains like OG1RF, deletion of an extracellular gelatinase, GelE was associated with impaired septum cleavage (Waters et al., 2003). Moreover, production of the GelE is controlled by the quorum-sensing *fsr* system. The OG1RG cells form shorter chains in higher optical density as compared to the cells in early exponential phase (Salamaga, unpublished). For the above reasons, we propose the post-translation modification as a temporal and special control of the AtlA septum cleavage activity.

The PG structural diversity promotes an idea that the activity of PG hydrolases can be controlled by their enzymatic specificity. This was proposed as a control mechanism for streptococcal LytB and pneumococcal LytA. It was shown that the *N*-acetylglucosaminidase LytB requires fully acetylated GlcNAc moieties for cleavage. To underpin this requirement the C2-acetamido group of the GlcNAc moiety plays a role of an anchimeric assistant involved in a substrate-assisted catalytic mechanism (Rico-Lastres, 2015). In LytA several amino acids were proposed to be responsible for positioning of the substrate in the catalytic cleft providing the optimal distance between the scissile bonds and catalytic residue (Sandalova et al., 2016). However, in our studies we showed that the substitution of the *N*-acetylglucosaminidase activity of AtlA for activities of the other hydrolases, Atl, AtlB and Cse results in minor changes in daughter cells separation. This indicates that no special PG structures are required for AtlA septum cleavage activity.

AtlA specifically localises to the septum and cell poles, however the mechanism underpinning such localisation remains unknown. Several mechanisms to be responsible for specific targeting of PG hydrolases in other Gram-positive bacteria were proposed. *S. aureus* Atl amidase is targeted to the septum by a lack of wall teichoic acids (WTA)

in the cross-wall (Schlag et al., 2010). The immuno-labelling of Atl in a *ΔtagO* mutant, which does not produce WTA, showed that a fluorescent signal corresponding to Atl localisation is dispersed across the whole cell surface rather than being associated only with septa as it was shown for the parental strain (Schlag et al., 2010). The PG hydrolases form *S. pneumoniae* LytA and LytB have a choline binding domain (ChBD) that binds choline present in the teichoic acids. Moreover, it was proposed that both hydrolases require additional surface receptors for the proper localisation on the cell surface (Fernández -Tornero et al., 2001; De Las Rivas et al., 2002). In our studies we did not explore the contribution of WTAs to the special control of AtlA activity. However, previous studies showed that HF treatment contributes to AtlB activity increasing it over 30 times in OG1RF, whereas a two-fold increase was observed for AtlA (Emirian et al., 2009). Therefor, we hypothesise that the AtlA PG binding occurs in the same place where its secretion occurs, contributing to the special control of AtlA activity.

7.3   Formation of short chains contributes to *E. faecalis* virulence

In this study we showed the impact of the long cell chains formation by the Δ*atlA* mutant on its virulence in the zebrafish model of infection. The *E. faecalis* OG1RF derivative harbouring an in frame deletion of *atlA* was severely attenuated. The reduced virulence could however result from other factors than the formation of long cell chains. In *Steptococcus mutans*, a deletion of the major autolysin, AtlA leads to alterations in the cell surface properties (Ahn and Burne, 2006). Moreover, the AtlA depletion impairs the biofilm formation in *E. faecalis* which is important for enterococcal pathogenesis (Paganelli et al*.,* 2013). Therefore, we compared the virulence of the sonicated and non-sonicated Δ*atlA* cells. Mild treatment with ultrasound was shown to disperse the long cell chains without affecting the cells viability (Dubée et al., 2011). Furthermore, we showed that sonication does not affect a virulence of *E. faecalis* OG1RF neither its growth ability. Short chains of Δ*atlA* (sonicated) were significantly more virulent than their non treated counterpart, showing that dispersion of the long cell chains restores the virulence of the Δ*atlA* mutant. A comparison of the uptake by phagocytes revealed that the long cell chains are significantly more phagocytosed than the wild type and sonicated Δ*atlA* cells. This indicates that minimisation of the *E.*

faecalis size is important to evade the phagocytosis. What is more, long cell chains were able to induce more than 90% mortality of immunocompromised embryos (PU.1 morphants) in the first 20 hours post-infection confirming a predominate role of phagocytes in the clearance of *E. faecalis* at the early stages of infection. A smilar mechanism of minimisation as a strategy to evade the opnophagocytosis was described for *Streptococcus pneumoniae* (Dalia and Weiser, 2011). Although, in both *E. faecalis* and *S. pneumoniae* minimisation led to evade the uptake by phagocytes, a filamentation was proposed to be responsible for survival of other pathogens. *Mycobacterium tuberculosis* developed a defence mechanism in which the FtsZ polymerisation into the Z-ring is altered after phagocytosis. This leads to cell division inhibition and formation of filamentous cells that can persist killing by phagocytes (Chauhan *et al.*, 2006). Another example is uropathogenic *E. coli* (UPEC). UPEC can inhibit cell division in a small subset of bacteria which results in a mixed population of filamentous and wild-type-like (bacillary) cells. During the innate immune response the bacillary cells are phagocytosed by neutrophils, enriching the population of filamentous ones (Justice et al., 2004). The mechanism how the filamentous cells evade the phagocytosis remains unknown. Champion and colleagues showed that *in vitro* the geometry of polystyrene particles is important during the contact with macrophages that may or may not induced phagocytosis (Champin and Mitragotri, 2006). Furthermore, it was proposed that elongation in filamentous bacteria is responsible for lowering a probability of a contact between a phagocyte and cell poles, thus hence the formation of a phagocytic cup essential for the uptake is halted (Möller et al., 2012). In contrast to the rigid UPEC filamentous cells, the enterococcal long cells chains are quite flexible and not able to withstand the mechanical pressure of the phagocyte, thus not affecting the generation of the phagocyte-cell poles contact point.

7.4   Future work

In this work we showed several mechanisms temporally and specialty controlling the AtlA septum cleavage activity in *E. faecalis* as well as the contribution of formation of short chains during pathogenesis in zebrafish model of infection. However, there are still a few questions that due to the time constrains we were not answered. How AtlA is targeted to the cell poles and septum via the LysM domain and AdmA remains unknown. In this work, we constructed a vector allowing us to obtain a strain expressing

the translational fusion of AdmA with GFP. Studies on localisation od AdmA and its co-localisation with AtlA are important part of better understanding the role of AdmA in the AtlA targeting process. Additionally, the studies using ITC could be performed to check if AdmA and AtlA interact with each other. Collectively, these experiments could provide information on how AtlA is targeted to the cell poles and septum.

Several mutations in SecA and SecY discovered in our laboratory were associated with formation of shorter chains in the JH2-2 $atlA_{E212Q}$ background (Elsarmane, 2016) There are two hypotheses explaining such an observation. (i) The point mutations in SacA and SecY alter specifically secretion of AtlA leaving a space in septum for other hydrolases to separate daughter cells or (ii) promote secretion of other hydrolases that leads to over all increase peptidoglycan metabolism including septum cleavage. The quantification of AtlA secreted in parental strain and mutants could give the answer which hypothesis is true. Moreover, studies investigated the interaction between SecA, SecY and the AtlA signal peptide could provide information how these mutations affect AtlA secretion if any. Additionally, the role of unusually long signal peptide could be determined by testing how mutations $e.g.$ truncation or extension in this peptide influence an AtlA translocation pace. The inducible expression of AtlA with an altered signal peptide in $\Delta atlA$ mutant followed by flow cytometry measurement of cell chains dynamic could tackle such question.

Based on the microscopic observation we proposed a model of AtlA display at the cell surface during the cell division. To investigate this further, a co localisation with a nascent PG or proteins involved in cell division like FtsZ or PBPs is good option to show the correlation between AtlA presence at the cell surface and cell growth/devising.

References

Adams, D.W., and Errington, J. (2009). Bacterial cell division: assembly, maintenance and disassembly of the Z ring. Nat. Rev. Microbiol. *7*, 642–653.

Adlerberth, I., and Wold, A.E. (2009). Establishment of the gut microbiota in Western infants. Acta Paediatr. *98*, 229–238.

Ahn, S.-J., and Burne, R.A. (2006). The *atlA* operon of *Streptococcus mutans*: role in autolysin maturation and cell surface biogenesis. J. Bacteriol. *188*, 6877–6888.

Alborn, W.E., Allen, N.E., and Preston, D.A. (1991). Daptomycin disrupts membrane potential in growing *Staphylococcus aureus*. Antimicrob. Agents Chemother. *35*, 2282–2287.

Ali, L., Goraya, M.U., Arafat, Y., Ajmal, M., Chen, J.-L., and Yu, D. (2017). Molecular Mechanism of Quorum-Sensing in *Enterococcus faecalis*: Its Role in Virulence and Therapeutic Approaches. International Journal of Molecular Sciences *18*, 960.

Anderson, D.J., Murdoch, D.R., Sexton, D.J., Reller, L.B., Stout, J.E., Cabell, C.H., and Corey, G.R. (2004). Risk factors for infective endocarditis in patients with enterococcal bacteremia: a case-control study. Infection *32*, 72–77.

Andrewes, F.W., and Horder, T.J. (1906). A study of the streptococci pathogenic for man. The Lancet *168*, 708–713.

Andrews, J., Ashby, J., Jevons, G., Marshall, T., Lines, N., and Wise, R. (2000). A comparison of antimicrobial resistance rates in Gram-positive pathogens isolated in the UK from October 1996 to January 1997 and October 1997 to January 1998. J. Antimicrob. Chemother. *45*, 285–293.

Arbeloa, A., Segal, H., Hugonnet, J.-E., Josseaume, N., Dubost, L., Brouard, J.-P., Gutmann, L., Mengin-Lecreulx, D., and Arthur, M. (2004). Role of class A penicillin-binding proteins in PBP5-mediated beta-lactam resistance in *Enterococcus faecalis*. J. Bacteriol. *186*, 1221–1228.

Arias, C.A., and Murray, B.E. (2008). Emergence and management of drug-resistant enterococcal infections. Expert Rev Anti Infect Ther *6*, 637–655.

Arias, C.A., Panesso, D., McGrath, D.M., Qin, X., Mojica, M.F., Miller, C., Diaz, L., Tran, T.T., Rincon, S., Barbu, E.M., et al. (2011). Genetic basis for *in vivo* daptomycin resistance in enterococci. N. Engl. J. Med. *365*, 892–900.

Aslangul, E., Massias, L., Meulemans, A., Chau, F., Andremont, A., Courvalin, P., Fantin, B., and Ruimy, R. (2006). Acquired gentamicin resistance by permeability impairment in *Enterococcus faecalis*. Antimicrob. Agents Chemother. *50*, 3615–3621.

Atrih, A., Bacher, G., Allmaier, G., Williamson, M.P., and Foster, S.J. (1999). Analysis of peptidoglycan structure from vegetative cells of *Bacillus subtilis* 168 and role of PBP 5 in peptidoglycan maturation. J. Bacteriol. *181*, 3956–3966.

Baba, T., and Schneewind, O. (1996). Target cell specificity of a bacteriocin molecule: a C-terminal signal directs lysostaphin to the cell wall of *Staphylococcus aureus*. EMBO J. *15*, 4789–4797.

Ball, G., Demmerle, J., Kaufmann, R., Davis, I., Dobbie, I.M., and Schermelleh, L. (2015). SIMcheck: a Toolbox for Successful Super-resolution Structured Illumination Microscopy. Scientific Reports *5*, srep15915.

Barthe, P., Mukamolova, G.V., Roumestand, C., and Cohen-Gonsaud, M. (2010). The structure of PknB extracellular PASTA domain from *Mycobacterium tuberculosis* suggests a ligand-dependent kinase activation. Structure *18*, 606–615.

Bartual, S.G., Straume, D., Stamsås, G.A., Muñoz, I.G., Alfonso, C., Martínez-Ripoll, M., Håvarstein, L.S., and Hermoso, J.A. (2014). Structural basis of PcsB-mediated cell separation in *Streptococcus pneumoniae*. Nat Commun *5*, 3842.

Bera, A., Herbert, S., Jakob, A., Vollmer, W., and Götz, F. (2005). Why are pathogenic staphylococci so lysozyme resistant? The peptidoglycan *O*-acetyltransferase OatA is the major determinant for lysozyme resistance of *Staphylococcus aureus*. Mol. Microbiol. *55*, 778–787.

Bern, M., Beniston, R., and Mesnage, S. (2017). Towards an automated analysis of bacterial peptidoglycan structure. Anal Bioanal Chem *409*, 551–560.

Bernhardt, T.G., and de Boer, P.A.J. (2005). SlmA, a nucleoid-associated, FtsZ binding protein required for blocking septal ring assembly over chromosomes in *E. coli.* Mol. Cell *18*, 555–564.

Bernut, A., Herrmann, J.-L., Kissa, K., Dubremetz, J.-F., Gaillard, J.-L., Lutfalla, G., and Kremer, L. (2014). Mycobacterium abscessus cording prevents phagocytosis and promotes abscess formation. Proc. Natl. Acad. Sci. U.S.A. *111*, E943-952.

Betzig, E., Patterson, G.H., Sougrat, R., Lindwasser, O.W., Olenych, S., Bonifacino, J.S., Davidson, M.W., Lippincott-Schwartz, J., and Hess, H.F. (2006). Imaging intracellular

194

fluorescent proteins at nanometer resolution. Science *313*, 1642–1645.

de Boer, P.A., Crossley, R.E., and Rothfield, L.I. (1989). A division inhibitor and a topological specificity factor coded for by the minicell locus determine proper placement of the division septum in *E. coli*. Cell *56*, 641–649.

de Boer, P.A., Crossley, R.E., and Rothfield, L.I. (1992). Roles of MinC and MinD in the site-specific septation block mediated by the MinCDE system of *Escherichia coli*. J. Bacteriol. *174*, 63–70.

Boneca, I.G., and Chiosis, G. (2003). Vancomycin resistance: occurrence, mechanisms and strategies to combat it. Expert Opin. Ther. Targets *7*, 311–328.

Booth, M.C., Bogie, C.P., Sahl, H.G., Siezen, R.J., Hatter, K.L., and Gilmore, M.S. (1996). Structural analysis and proteolytic activation of *Enterococcus faecalis* cytolysin, a novel lantibiotic. Mol. Microbiol. *21*, 1175–1184.

Bouhss, A., Josseaume, N., Severin, A., Tabei, K., Hugonnet, J.-E., Shlaes, D., Mengin-Lecreulx, D., Van Heijenoort, J., and Arthur, M. (2002). Synthesis of the L-alanyl-L-alanine cross-bridge of *Enterococcus faecalis* peptidoglycan. J. Biol. Chem. *277*, 45935–45941.

Bradley, C.R., and Fraise, A.P. (1996). Heat and chemical resistance of enterococci. J. Hosp. Infect. *34*, 191–196.

Bravetti, A.-L., Mesnage, S., Lefort, A., Chau, F., Eckert, C., Garry, L., Arthur, M., and Fantin, B. (2009). Contribution of the Autolysin AtlA to the Bactericidal Activity of Amoxicillin against *Enterococcus faecalis* JH2-2. Antimicrob Agents Chemother *53*, 1667–1669.

Brinster, S., Posteraro, B., Bierne, H., Alberti, A., Makhzami, S., Sanguinetti, M., and Serror, P. (2007a). Enterococcal leucine-rich repeat-containing protein involved in virulence and host inflammatory response. Infect. Immun. *75*, 4463–4471.

Brinster, S., Furlan, S., and Serror, P. (2007b). C-terminal WxL domain mediates cell wall binding in *Enterococcus faecalis* and other gram-positive bacteria. J Bacteriol *189*, 1244–1253.

Brock, T.D., Peacher, B., and Pierson, D. (1963). Survey of the bacteriocines of enterococci. J. Bacteriol. *86*, 702–707.

Bublitz, M., Polle, L., Holland, C., Heinz, D.W., Nimtz, M., and Schubert, W.-D. (2009). Structural basis for autoinhibition and activation of Auto, a virulence-associated peptidoglycan hydrolase of *Listeria monocytogenes*. Molecular Microbiology *71*, 1509–1522.

Buist, G., Steen, A., Kok, J., and Kuipers, O.P. (2008). LysM, a widely distributed protein motif for binding to (peptido)glycans. Mol. Microbiol. *68*, 838–847.

Buss, J.A., Peters, N.T., Xiao, J., and Bernhardt, T.G. (2017). ZapA and ZapB form an FtsZ-independent structure at midcell. Molecular Microbiology *104*, 652–663.

Candela, T., and Fouet, A. (2006). Poly-gamma-glutamate in bacteria. Molecular Microbiology *60*, 1091–1098.

Carabetta, V.J., Greco, T.M., Tanner, A.W., Cristea, I.M., and Dubnau, D. (2016). Temporal regulation of the *Bacillus subtilis* acetylome and evidence for a role of MreB acetylation in cell wall growth. mSystems *1*.

Carballido-López, R., Formstone, A., Li, Y., Ehrlich, S.D., Noirot, P., and Errington, J. (2006). Actin homolog MreBH governs cell morphogenesis by localization of the cell wall hydrolase LytE. Dev. Cell *11*, 399–409.

Champion, J.A., and Mitragotri, S. (2006). Role of target geometry in phagocytosis. Proc. Natl. Acad. Sci. U.S.A. *103*, 4930–4934.

Chauhan, A., Lofton, H., Maloney, E., Moore, J., Fol, M., Madiraju, M.V.V.S., and Rajagopalan, M. (2006). Interference of *Mycobacterium tuberculosis* cell division by Rv2719c, a cell wall hydrolase. Mol. Microbiol. *62*, 132–147.

Chow, J.W., Thal, L.A., Perri, M.B., Vazquez, J.A., Donabedian, S.M., Clewell, D.B., and Zervos, M.J. (1993). Plasmid-associated hemolysin and aggregation substance production contribute to virulence in experimental enterococcal endocarditis. Antimicrob. Agents Chemother. *37*, 2474–2477.

Chuang, O.N., Schlievert, P.M., Wells, C.L., Manias, D.A., Tripp, T.J., and Dunny, G.M. (2009). Multiple functional domains of *Enterococcus faecalis* aggregation substance Asc10 contribute to endocarditis virulence. Infect. Immun. *77*, 539–548.

Coburn, P.S., and Gilmore, M.S. (2003). The *Enterococcus faecalis* cytolysin: a novel toxin active against eukaryotic and prokaryotic cells. Cell. Microbiol. *5*, 661–669.

Coque, T.M., Patterson, J.E., Steckelberg, J.M., and Murray, B.E. (1995). Incidence of hemolysin, gelatinase, and aggregation substance among enterococci isolated from patients with endocarditis and other infections and from feces of hospitalized and community-based persons. J. Infect. Dis. *171*, 1223–1229.

196

Costa, Y., Galimand, M., Leclercq, R., Duval, J., and Courvalin, P. (1993). Characterization of the chromosomal *aac(6')-Ii* gene specific for *Enterococcus faecium*. Antimicrob. Agents Chemother. *37*, 1896–1903.

Courvalin, P., Carlier, C., and Collatz, E. (1980). Plasmid-mediated resistance to aminocyclitol antibiotics in group D streptococci. J. Bacteriol. *143*, 541–551.

Cox, C.R., Coburn, P.S., and Gilmore, M.S. (2005). Enterococcal cytolysin: a novel two component peptide system that serves as a bacterial defense against eukaryotic and prokaryotic cells. Curr. Protein Pept. Sci. *6*, 77–84.

Dalia, A.B., and Weiser, J.N. (2011). Minimization of bacterial size allows for complement evasion and is overcome by the agglutinating effect of antibody. Cell Host Microbe *10*, 486–496.

Davis, J.M., Clay, H., Lewis, J.L., Ghori, N., Herbomel, P., and Ramakrishnan, L. (2002). Real-time visualization of mycobacterium-macrophage interactions leading to initiation of granuloma formation in zebrafish embryos. Immunity *17*, 693–702.

De Las Rivas, B., García, J.L., López, R., and García, P. (2002). Purification and polar localization of pneumococcal LytB, a putative endo-beta-N-acetylglucosaminidase: the chain-dispersing murein hydrolase. J. Bacteriol. *184*, 4988–5000.

D'Elia, M.A., Millar, K.E., Beveridge, T.J., and Brown, E.D. (2006). Wall teichoic acid polymers are dispensable for cell viability in *Bacillus subtilis*. J. Bacteriol. *188*, 8313–8316.

Den Blaauwen, T., De Pedro, M.A., Nguyen-Distèche, M., and Ayala, J.A. (2008). Morphogenesis of rod-shaped sacculi. FEMS Microbiology Reviews *32*, 321–344.

Donachie, W.D. (1968). Relationship between cell size and time of initiation of DNA replication. Nature *219*, 1077–1079.

Donachie, W.D., and Begg, K.J. (1989). Cell length, nucleoid separation, and cell division of rod-shaped and spherical cells of *Escherichia coli*. J Bacteriol *171*, 4633–4639.

Dubée, V., Chau, F., Arthur, M., Garry, L., Benadda, S., Mesnage, S., Lefort, A., and Fantin, B. (2011). The *in vitro* contribution of autolysins to bacterial killing elicited by amoxicillin increases with inoculum size in *Enterococcus faecalis*. Antimicrob. Agents Chemother. *55*, 910–912.

Dunny, G.M., Brown, B.L., and Clewell, D.B. (1978). Induced cell aggregation and mating in

Streptococcus faecalis: evidence for a bacterial sex pheromone. Proc. Natl. Acad. Sci. U.S.A. *75*, 3479–3483.

Dupont, H., Montravers, P., Mohler, J., and Carbon, C. (1998). Disparate findings on the role of virulence factors of *Enterococcus faecalis* in mouse and rat models of peritonitis. Infect. Immun. *66*, 2570–2575.

Eaton, T.J., and Gasson, M.J. (2001). Molecular screening of *Enterococcus* virulence determinants and potential for genetic exchange between food and medical isolates. Appl. Environ. Microbiol. *67*, 1628–1635.

Eckert, C., Lecerf, M., Dubost, L., Arthur, M., and Mesnage, S. (2006). Functional Analysis of AtlA, the Major N-Acetylglucosaminidase of *Enterococcus faecalis*. J. Bacteriol. *188*, 8513–8519.

Elsarmane, F. (2016). Analysis of Enterococcus faecalis mutants affected in septum cleavage during cell division. phd. University of Sheffield.

Emirian, A., Fromentin, S., Eckert, C., Chau, F., Dubost, L., Delepierre, M., Gutmann, L., Arthur, M., and Mesnage, S. (2009). Impact of peptidoglycan O-acetylation on autolytic activities of the *Enterococcus faecalis N*-acetylglucosaminidase AtlA and *N*-acetylmuramidase AtlB. FEBS Lett. *583*, 3033–3038.

Errington, J., Daniel, R.A., and Scheffers, D.-J. (2003). Cytokinesis in bacteria. Microbiol Mol Biol Rev *67*, 52–65.

Erwig, L.P., and Gow, N.A.R. (2016). Interactions of fungal pathogens with phagocytes. Nat. Rev. Microbiol. *14*, 163–176.

Facklam, R.R., Carvalho, M. da G.S., and Teixeira, L.M. (2002). History, Taxonomy, Biochemical Characteristics, and Antibiotic Susceptibility Testing of Enterococci. 1–54.

Feltcher, M.E., and Braunstein, M. (2012). Emerging themes in SecA2-mediated protein export. Nat. Rev. Microbiol. *10*, 779–789.

Fernández-Tornero, C., López, R., García, E., Giménez-Gallego, G., and Romero, A. (2001). A novel solenoid fold in the cell wall anchoring domain of the pneumococcal virulence factor LytA. Nat. Struct. Biol. *8*, 1020–1024.

Fleurie, A., Lesterlin, C., Manuse, S., Zhao, C., Cluzel, C., Lavergne, J.-P., Franz-Wachtel, M., Macek, B., Combet, C., Kuru, E., et al. (2014). MapZ marks the division sites and positions

FtsZ rings in *Streptococcus pneumoniae*. Nature *516*, 259–262.

Ferretti, J.J., Gilmore, K.S., and Courvalin, P. (1986). Nucleotide sequence analysis of the gene specifying the bifunctional 6'-aminoglycoside acetyltransferase 2"-aminoglycoside phosphotransferase enzyme in *Streptococcus faecalis* and identification and cloning of gene regions specifying the two activities. J. Bacteriol. *167*, 631–638.

Galimand, M., Schmitt, E., Panvert, M., Desmolaize, B., Douthwaite, S., Mechulam, Y., and Courvalin, P. (2011). Intrinsic resistance to aminoglycosides in *Enterococcus faecium* is conferred by the 16S rRNA m5C1404-specific methyltransferase EfmM. RNA *17*, 251–262.

Galli, D., Lottspeich, F., and Wirth, R. (1990). Sequence analysis of *Enterococcus faecalis* aggregation substance encoded by the sex pheromone plasmid pAD1. Molecular Microbiology *4*, 895–904.

Galli, D., Friesenegger, A., and Wirth, R. (1992). Transcriptional control of sex-pheromone-inducible genes on plasmid pAD1 of *Enterococcus faecalis* and sequence analysis of a third structural gene for (pPD1 -encoded) aggregation substance. Molecular Microbiology *6*, 1297–1308.

Gibson, C.W., Daneo-Moore, L., and Higgins, M.L. (1983). Cell wall assembly during inhibition of DNA synthesis in *Streptococcus faecium*. J Bacteriol *155*, 351–356.

Gordon, E., Mouz, N., Duée, E., and Dideberg, O. (2000). The crystal structure of the penicillin-binding protein 2x from *Streptococcus pneumoniae* and its acyl-enzyme form: implication in drug resistance. J. Mol. Biol. *299*, 477–485.

Graninger, W., and Ragette, R. (1992). Nosocomial bacteremia due to *Enterococcus faecalis* without endocarditis. Clin. Infect. Dis. *15*, 49–57.

Green, E.R., and Mecsas, J. (2016). Bacterial secretion systems – an overview. Microbiol Spectr *4*.

Guiton, P.S., Hung, C.S., Hancock, L.E., Caparon, M.G., and Hultgren, S.J. (2010). Enterococcal biofilm formation and virulence in an optimized murine model of foreign body-associated urinary tract infections. Infect. Immun. *78*, 4166–4175.

Gutierrez, J., Smith, R., and Pogliano, K. (2010). SpoIID-mediated peptidoglycan degradation is required throughout engulfment during *Bacillus subtilis* sporulation. J. Bacteriol. *192*, 3174–3186.

Hancock, L.E., and Gilmore, M.S. (2002). The capsular polysaccharide of *Enterococcus faecalis* and its relationship to other polysaccharides in the cell wall. Proc. Natl. Acad. Sci. U.S.A. *99*, 1574–1579.

Hancock, L.E., Murray, B.E., and Sillanpää, J. (2014). Enterococcal cell wall components and structures. in enterococci: from commensals to leading causes of drug resistant infection, M.S. Gilmore, D.B. Clewell, Y. Ike, and N. Shankar, eds. (Boston: Massachusetts Eye and Ear Infirmary), p.

Harz, H., Burgdorf, K., and Höltje, J.V. (1990). Isolation and separation of the glycan strands from murein of *Escherichia coli* by reversed-phase high-performance liquid chromatography. Anal. Biochem. *190*, 120–128.

Hayhurst, E.J., Kailas, L., Hobbs, J.K., and Foster, S.J. (2008). Cell wall peptidoglycan architecture in *Bacillus subtilis*. Proc. Natl. Acad. Sci. U.S.A. *105*, 14603–14608.

Hébert, L., Courtin, P., Torelli, R., Sanguinetti, M., Chapot-Chartier, M.-P., Auffray, Y., and Benachour, A. (2007). *Enterococcus faecalis* constitutes an unusual bacterial model in lysozyme resistance. Infect. Immun. *75*, 5390–5398.

van Heijenoort, J. (1998). Assembly of the monomer unit of bacterial peptidoglycan. Cell. Mol. Life Sci. *54*, 300–304.

van Heijenoort, J. (2001). Formation of the glycan chains in the synthesis of bacterial peptidoglycan. Glycobiology *11*, 25R–36R.

van Heijenoort, J. (2007). Lipid Intermediates in the Biosynthesis of Bacterial Peptidoglycan. Microbiol Mol Biol Rev *71*, 620–635.

Heilmann, C., Hussain, M., Peters, G., and Götz, F. (1997). Evidence for autolysin-mediated primary attachment of *Staphylococcus epidermidis* to a polystyrene surface. Mol. Microbiol. *24*, 1013–1024.

Hendrickx, A.P.A., Willems, R.J.L., Bonten, M.J.M., and van Schaik, W. (2009). LPxTG surface proteins of enterococci. Trends Microbiol. *17*, 423–430.

Herbomel, P., Thisse, B., and Thisse, C. (1999). Ontogeny and behaviour of early macrophages in the zebrafish embryo. Development *126*, 3735–3745.

Hidron, A.I., Edwards, J.R., Patel, J., Horan, T.C., Sievert, D.M., Pollock, D.A., Fridkin, S.K., National Healthcare Safety Network Team, and Participating National Healthcare Safety

Network Facilities (2008). NHSN annual update: antimicrobial-resistant pathogens associated with healthcare-associated infections: annual summary of data reported to the National Healthcare Safety Network at the Centers for Disease Control and Prevention, 2006-2007. Infect Control Hosp Epidemiol *29*, 996–1011.

Holečková, N., Doubravová, L., Massidda, O., Molle, V., Buriánková, K., Benada, O., Kofroňová, O., Ulrych, A., and Branny, P. (2015). LocZ Is a new cell division protein involved in proper septum placement in *Streptococcus pneumoniae*. mBio *6*, e01700-14.

Hollenbeck, B.L., and Rice, L.B. (2012). Intrinsic and acquired resistance mechanisms in enterococcus. Virulence *3*, 421–433.

Huang, B., Wang, W., Bates, M., and Zhuang, X. (2008). Three-Dimensional Super-Resolution Imaging by Stochastic Optical Reconstruction Microscopy. Science *319*, 810–813.

Huebner, J., Wang, Y., Krueger, W.A., Madoff, L.C., Martirosian, G., Boisot, S., Goldmann, D.A., Kasper, D.L., Tzianabos, A.O., and Pier, G.B. (1999). Isolation and chemical characterization of a capsular polysaccharide antigen shared by clinical isolates of *Enterococcus faecalis* and vancomycin-resistant *Enterococcus faecium*. Infect. Immun. *67*, 1213–1219.

Huebner, J., Quaas, A., Krueger, W.A., Goldmann, D.A., and Pier, G.B. (2000). Prophylactic and Therapeutic Efficacy of Antibodies to a Capsular Polysaccharide Shared among Vancomycin-Sensitive and -Resistant Enterococci. Infect. Immun. *68*, 4631–4636.

Hufnagel, M., Hancock, L.E., Koch, S., Theilacker, C., Gilmore, M.S., and Huebner, J. (2004). Serological and genetic diversity of capsular polysaccharides in *Enterococcus faecalis*. J. Clin. Microbiol. *42*, 2548–2557.

Humphries, R.M., Kelesidis, T., Tewhey, R., Rose, W.E., Schork, N., Nizet, V., and Sakoulas, G. (2012). Genotypic and phenotypic evaluation of the evolution of high-level daptomycin nonsusceptibility in vancomycin-resistant *Enterococcus faecium*. Antimicrob Agents Chemother *56*, 6051–6053.

Huycke, M.M., Sahm, D.F., and Gilmore, M.S. (1998). Multiple-drug resistant enterococci: the nature of the problem and an agenda for the future. Emerging Infect. Dis. *4*, 239–249.

Ike, Y., Clewell, D.B., Segarra, R.A., and Gilmore, M.S. (1990). Genetic analysis of the pAD1 hemolysin/bacteriocin determinant in *Enterococcus faecalis*: Tn917 insertional mutagenesis and cloning. J Bacteriol *172*, 155–163.

Izeta, A., Malcomber, S., O'Rourke, D., Hodgkin, J., and O'Hare, P. (2003). A C-terminal targeting signal controls differential compartmentalisation of *Caenorhabditis elegans* host cell factor (HCF) to the nucleus or mitochondria. Eur. J. Cell Biol. *82*, 495–504.

Jacob, A.E., and Hobbs, S.J. (1974). Conjugal transfer of plasmid-borne multiple antibiotic resistance in *Streptococcus faecalis* var. *zymogenes*. J. Bacteriol. *117*, 360–372.

Jett, B.D., Jensen, H.G., Nordquist, R.E., and Gilmore, M.S. (1992). Contribution of the pAD1-encoded cytolysin to the severity of experimental *Enterococcus faecalis* endophthalmitis. Infect. Immun. *60*, 2445–2452.

Justice, S.S., Hung, C., Theriot, J.A., Fletcher, D.A., Anderson, G.G., Footer, M.J., and Hultgren, S.J. (2004). Differentiation and developmental pathways of uropathogenic *Escherichia coli* in urinary tract pathogenesis. Proc. Natl. Acad. Sci. U.S.A. *101*, 1333–1338.

Kalina, A.P. (1970). The position of enterococci in the system of microorganisms. Zh. Mikrobiol. Epidemiol. Immunobiol. *47*, 20–21.

Kao, S.M., Olmsted, S.B., Viksnins, A.S., Gallo, J.C., and Dunny, G.M. (1991). Molecular and genetic analysis of a region of plasmid pCF10 containing positive control genes and structural genes encoding surface proteins involved in pheromone-inducible conjugation in *Enterococcus faecalis*. J Bacteriol *173*, 7650–7664.

Kemp, K.D., Singh, K.V., Nallapareddy, S.R., and Murray, B.E. (2007). Relative contributions of *Enterococcus faecalis* OG1RF sortase-encoding genes, *srtA* and *bps* (*srtC*), to biofilm formation and a murine model of urinary tract infection. Infect. Immun. *75*, 5399–5404.

Kihlberg, B.M., Collin, M., Olsén, A., and Björck, L. (1999). Protein H, an antiphagocytic surface protein in *Streptococcus pyogenes*. Infect. Immun. *67*, 1708–1714.

Klemsz, M.J., McKercher, S.R., Celada, A., Van Beveren, C., and Maki, R.A. (1990). The macrophage and B cell-specific transcription factor PU.1 is related to the ets oncogene. Cell *61*, 113–124.

Kline, K.A., Kau, A.L., Chen, S.L., Lim, A., Pinkner, J.S., Rosch, J., Nallapareddy, S.R., Murray, B.E., Henriques-Normark, B., Beatty, W., et al. (2009). Mechanism for sortase localization and the role of sortase localization in efficient pilus assembly in *Enterococcus faecalis*. J. Bacteriol. *191*, 3237–3247.

Kobayashi, R. Studies concerning hemolytic streptococci: typing of human hemolytic

streptococci and their relation to diseases and their distribution on mucous membranes. The Kitasato Archives of Experimental Medicine *17*, 218–241.

Kristich, C.J., Nguyen, V.T., Le, T., Barnes, A.M.T., Grindle, S., and Dunny, G.M. (2008). Development and use of an efficient system for random mariner transposon mutagenesis to identify novel genetic determinants of biofilm formation in the core *Enterococcus faecalis* genome. Appl. Environ. Microbiol. *74*, 3377–3386.

Kuroda, A., and Sekiguchi, J. (1993). High-level transcription of the major *Bacillus subtilis* autolysin operon depends on expression of the sigma D gene and is affected by a *sin* (*flaD*) mutation. J. Bacteriol. *175*, 795–801.

Kuru, E., Hughes, H.V., Brown, P.J., Hall, E., Tekkam, S., Cava, F., de Pedro, M.A., Brun, Y.V., and VanNieuwenhze, M.S. (2012). *In situ* probing of newly synthesized peptidoglycan in live bacteria with fluorescent d-amino acids. Angew. Chem. Int. Ed. *51*, 12519–12523.

Lancefield, R.C. (1933). A serological differentiation of human and other groups of hemolytic streptococci. J Exp Med *57*, 571–595.

Larson, T.R., and Yother, J. (2017). *Streptococcus pneumoniae* capsular polysaccharide is linked to peptidoglycan via a direct glycosidic bond to β-D-N-acetylglucosamine. Proc. Natl. Acad. Sci. U.S.A. *114*, 5695–5700.

Layec, S., Gérard, J., Legué, V., Chapot-Chartier, M.-P., Courtin, P., Borges, F., Decaris, B., and Leblond-Bourget, N. (2009). The CHAP domain of Cse functions as an endopeptidase that acts at mature septa to promote *Streptococcus thermophilus* cell separation. Mol. Microbiol. *71*, 1205–1217.

Leavis, H., Top, J., Shankar, N., Borgen, K., Bonten, M., van Embden, J., and Willems, R.J.L. (2004). A novel putative enterococcal pathogenicity island linked to the *esp* virulence gene of *Enterococcus faecium* and associated with epidemicity. J. Bacteriol. *186*, 672–682.

Lebreton, F., Riboulet-Bisson, E., Serror, P., Sanguinetti, M., Posteraro, B., Torelli, R., Hartke, A., Auffray, Y., and Giard, J.-C. (2009). *ace*, which encodes an adhesin in *Enterococcus faecalis*, is regulated by Ers and is involved in virulence. Infect. Immun. *77*, 2832–2839.

Leclerc, V., and Reichhart, J.-M. (2004). The immune response of *Drosophila melanogaster*. Immunol. Rev. *198*, 59–71.

Lee, I.-C., Swam, I.I. van, Tomita, S., Morsomme, P., Rolain, T., Hols, P., Kleerebezem, M.,

and Bron, P.A. (2014). GtfA and GtfB are both required for protein *O*-glycosylation in *Lactobacillus plantarum*. J. Bacteriol. *196*, 1671–1682.

Leendertse, M., Willems, R.J.L., Giebelen, I.A.J., van den Pangaart, P.S., Wiersinga, W.J., de Vos, A.F., Florquin, S., Bonten, M.J.M., and van der Poll, T. (2008). TLR2-dependent MyD88 signaling contributes to early host defense in murine *Enterococcus faecium* peritonitis. J. Immunol. *180*, 4865–4874.

Liu, Q., Ponnuraj, K., Xu, Y., Ganesh, V.K., Sillanpää, J., Murray, B.E., Narayana, S.V.L., and Höök, M. (2007). The *Enterococcus faecalis* MSCRAMM ACE binds its ligand by the Collagen Hug model. J. Biol. Chem. *282*, 19629–19637.

Liu, T., Liu, Z., Song, C., Hu, Y., Han, Z., She, J., Fan, F., Wang, J., Jin, C., Chang, J., et al. (2012). Chitin-induced dimerization activates a plant immune receptor. Science *336*, 1160–1164.

Lopez, N., Kobayashi, L., and Coimbra, R. (2011). A comprehensive review of abdominal infections. World Journal of Emergency Surgery *6*, 7.

Low, Y.L., Jakubovics, N.S., Flatman, J.C., Jenkinson, H.F., and Smith, A.W. (2003). Manganese-dependent regulation of the endocarditis-associated virulence factor EfaA of *Enterococcus faecalis*. J. Med. Microbiol. *52*, 113–119.

Lu, J.Z., Fujiwara, T., Komatsuzawa, H., Sugai, M., and Sakon, J. (2006). Cell wall-targeting domain of glycylglycine endopeptidase distinguishes among peptidoglycan cross-bridges. J. Biol. Chem. *281*, 549–558.

MacCallum, W.G., and Hastings, T.W. (1899). A case of acute endocarditis caused by *Micrococcus zymogenes* (nov. spec.), with a description of the microorganism. J. Exp. Med. *4*, 521–534.

Maestro, B., Novaková, L., Hesek, D., Lee, M., Leyva, E., Mobashery, S., Sanz, J.M., and Branny, P. (2011). Recognition of peptidoglycan and β-lactam antibiotics by the extracellular domain of the Ser/Thr protein kinase StkP from *Streptococcus pneumoniae*. FEBS Lett. *585*, 357–363.

Maguin, E., Duwat, P., Hege, T., Ehrlich, D., and Gruss, A. (1992). New thermosensitive plasmid for gram-positive bacteria. J. Bacteriol. *174*, 5633–5638.

Margot, P., Mauël, C., and Karamata, D. (1994). The gene of the *N*-acetylglucosaminidase, a

Bacillus subtilis 168 cell wall hydrolase not involved in vegetative cell autolysis. Mol. Microbiol. *12*, 535–545.

Marshall, J.C., and Innes, M. (2003). Intensive care unit management of intra-abdominal infection. Crit. Care Med. *31*, 2228–2237.

Martin, J.D., and Mundt, J.O. (1972). Enterococci in insects. Appl Microbiol *24*, 575–580.

Matias, V.R.F., and Beveridge, T.J. (2005). Cryo-electron microscopy reveals native polymeric cell wall structure in *Bacillus subtilis* 168 and the existence of a periplasmic space. Molecular Microbiology *56*, 240–251.

McDonald, J.R., Olaison, L., Anderson, D.J., Hoen, B., Miro, J.M., Eykyn, S., Abrutyn, E., Fowler, V.G., Habib, G., Selton-Suty, C., et al. (2005). *Enterococcal endocarditis*: 107 cases from the international collaboration on endocarditis merged database. Am. J. Med. *118*, 759–766.

Mederski-Samoraj, B.D., and Murray, B.E. (1983). High-level resistance to gentamicin in clinical isolates of enterococci. J. Infect. Dis. *147*, 751–757.

Meeske, A.J., Sham, L.-T., Kimsey, H., Koo, B.-M., Gross, C.A., Bernhardt, T.G., and Rudner, D.Z. (2015). MurJ and a novel lipid II flippase are required for cell wall biogenesis in *Bacillus subtilis*. Proc. Natl. Acad. Sci. U.S.A. *112*, 6437–6442.

Mercier, C., Durrieu, C., Briandet, R., Domakova, E., Tremblay, J., Buist, G., and Kulakauskas, S. (2002). Positive role of peptidoglycan breaks in lactococcal biofilm formation. Mol. Microbiol. *46*, 235–243.

Mesnage, S., Fontaine, T., Mignot, T., Delepierre, M., Mock, M., and Fouet, A. (2000). Bacterial SLH domain proteins are non-covalently anchored to the cell surface via a conserved mechanism involving wall polysaccharide pyruvylation. EMBO J *19*, 4473–4484.

Mesnage, S., Chau, F., Dubost, L., and Arthur, M. (2008). Role of N-acetylglucosaminidase and *N*-acetylmuramidase activities in *Enterococcus faecalis* peptidoglycan metabolism. J. Biol. Chem. *283*, 19845–19853.

Mesnage, S., Dellarole, M., Baxter, N.J., Rouget, J.-B., Dimitrov, J.D., Wang, N., Fujimoto, Y., Hounslow, A.M., Lacroix-Desmazes, S., Fukase, K., et al. (2014). Molecular basis for bacterial peptidoglycan recognition by LysM domains. Nature Communications *5*, ncomms5269.

Miller, W.R., Munita, J.M., and Arias, C.A. (2014). Mechanisms of antibiotic resistance in

enterococci. Expert Rev Anti Infect Ther *12*, 1221–1236.

Migocki, M.D., Freeman, M.K., Wake, R.G., and Harry, E.J. (2002). The Min system is not required for precise placement of the midcell Z ring in *Bacillus subtilis*. EMBO Rep *3*, 1163–1167.

Mingeot-Leclercq, M.P., Glupczynski, Y., and Tulkens, P.M. (1999). Aminoglycosides: activity and resistance. Antimicrob. Agents Chemother. *43*, 727–737.

Mir, M., Asong, J., Li, X., Cardot, J., Boons, G.-J., and Husson, R.N. (2011). The extracytoplasmic domain of the *Mycobacterium tuberculosis* Ser/Thr kinase PknB binds specific muropeptides and is required for PknB localization. PLoS Pathog. *7*, e1002182.

Mistou, M.-Y., Sutcliffe, I.C., and van Sorge, N.M. (2016). Bacterial glycobiology: rhamnose-containing cell wall polysaccharides in Gram-positive bacteria. FEMS Microbiol. Rev. *40*, 464–479.

Miyazaki, S., Ohno, A., Kobayashi, I., Uji, T., Yamaguchi, K., and Goto, S. (1993). Cytotoxic effect of hemolytic culture supernatant from *Enterococcus faecalis* on mouse polymorphonuclear neutrophils and macrophages. Microbiol. Immunol. *37*, 265–270.

Mohamed, J.A., Huang, W., Nallapareddy, S.R., Teng, F., and Murray, B.E. (2004). Influence of origin of isolates, especially endocarditis isolates, and various genes on biofilm formation by *Enterococcus faecalis*. Infect. Immun. *72*, 3658–3663.

Mohammadi, T., van Dam, V., Sijbrandi, R., Vernet, T., Zapun, A., Bouhss, A., Diepeveen-de Bruin, M., Nguyen-Distèche, M., de Kruijff, B., and Breukink, E. (2011). Identification of FtsW as a transporter of lipid-linked cell wall precursors across the membrane. EMBO J. *30*, 1425–1432.

Moir, A. (2006). How do spores germinate? Journal of Applied Microbiology *101*, 526–530.

Möller, J., Luehmann, T., Hall, H., and Vogel, V. (2012). The race to the pole: how high-aspect ratio shape and heterogeneous environments limit phagocytosis of filamentous *Escherichia coli* bacteria by macrophages. Nano Lett. *12*, 2901–2905.

Morlot, C., Noirclerc-Savoye, M., Zapun, A., Dideberg, O., and Vernet, T. (2004). The D,D-carboxypeptidase PBP3 organizes the division process of *Streptococcus pneumoniae*. Mol. Microbiol. *51*, 1641–1648.

Mundt, J.O. (1963). Occurrence of enterococci in animals in a wild environment. Appl

Microbiol *11*, 136–140.

Murdoch, D.R., Corey, G.R., Hoen, B., Miró, J.M., Fowler, V.G., Bayer, A.S., Karchmer, A.W., Olaison, L., Pappas, P.A., Moreillon, P., et al. (2009). Clinical presentation, etiology, and outcome of infective endocarditis in the 21st century: the International Collaboration on Endocarditis-Prospective Cohort Study. Arch. Intern. Med. *169*, 463–473.

Murphy, C.K., Stewart, E.J., and Beckwith, J. (1995). A double counter-selection system for the study of null alleles of essential genes in *Escherichia coli*. Gene *155*, 1–7.

Murray, B.E. (1990). The life and times of the *Enterococcus*. Clin. Microbiol. Rev. *3*, 46–65.

Murray, B.E. (1992). Beta-lactamase-producing enterococci. Antimicrob. Agents Chemother. *36*, 2355–2359.

Murray, B.E., and Mederski-Samaroj, B. (1983). Transferable beta-lactamase. A new mechanism for *in vitro* penicillin resistance in *Streptococcus faecalis*. J. Clin. Invest. *72*, 1168–1171.

Nallapareddy, S.R., and Murray, B.E. (2006). Ligand-signaled upregulation of *Enterococcus faecalis ace* transcription, a mechanism for modulating host-*E. faecalis* interaction. Infect Immun *74*, 4982–4989.

Nallapareddy, S.R., Singh, K.V., Duh, R.-W., Weinstock, G.M., and Murray, B.E. (2000). Diversity of *ace*, a gene encoding a microbial surface component recognizing adhesive matrix molecules, from different strains of *Enterococcus faecalis* and evidence for production of *ace* during human infections. Infect. Immun. *68*, 5210–5217.

Nallapareddy, S.R., Singh, K.V., Sillanpää, J., Garsin, D.A., Höök, M., Erlandsen, S.L., and Murray, B.E. (2006). Endocarditis and biofilm-associated pili of *Enterococcus faecalis*. J. Clin. Invest. *116*, 2799–2807.

Nallapareddy, S.R., Singh, K.V., Sillanpää, J., Zhao, M., and Murray, B.E. (2011). Relative contributions of Ebp Pili and the collagen adhesin ace to host extracellular matrix protein adherence and experimental urinary tract infection by *Enterococcus faecalis* OG1RF. Infect. Immun. *79*, 2901–2910.

Natale, P., Brüser, T., and Driessen, A.J.M. (2008). Sec- and Tat-mediated protein secretion across the bacterial cytoplasmic membrane--distinct translocases and mechanisms. Biochim. Biophys. Acta *1778*, 1735–1756.

Neuhaus, F.C., and Baddiley, J. (2003). A continuum of anionic charge: structures and functions of D-alanyl-teichoic acids in gram-positive bacteria. Microbiol. Mol. Biol. Rev. *67*, 686–723.

Nieto, C., and Espinosa, M. (2003). Construction of the mobilizable plasmid pMV158GFP, a derivative of pMV158 that carries the gene encoding the green fluorescent protein. Plasmid *49*, 281–285.

Noskin, G.A., Cooper, I., and Peterson, L.R. (1995). Vancomycin-resistant *Enterococcus faecium* sepsis following persistent colonization. Arch. Intern. Med. *155*, 1445–1447.

Nothaft, H., and Szymanski, C.M. (2010). Protein glycosylation in bacteria: sweeter than ever. Nat. Rev. Microbiol. *8*, 765–778.

Nusslein-Volhard, C., and Dahm, R. (2002). Zebrafish (Oxford, New York: Oxford University Press).

Ohnuma, T., Onaga, S., Murata, K., Taira, T., and Katoh, E. (2008). LysM domains from *Pteris ryukyuensis* chitinase-A: a stability study and characterization of the chitin-binding site. J. Biol. Chem. *283*, 5178–5187.

Ono, S., Muratani, T., and Matsumoto, T. (2005). Mechanisms of resistance to imipenem and ampicillin in *Enterococcus faecalis*. Antimicrob. Agents Chemother. *49*, 2954–2958.

Orla-Jensen S. (1919). The lactic acid bacteria. Memoirs of the Academy of the Royal Society of Denmark. Section of Sciences Series. *85*, 81–197.

Oshida, T., Sugai, M., Komatsuzawa, H., Hong, Y.M., Suginaka, H., and Tomasz, A. (1995). A *Staphylococcus aureus* autolysin that has an *N*-acetylmuramoyl-L-alanine amidase domain and an endo-beta-*N*-acetylglucosaminidase domain: cloning, sequence analysis, and characterization. Proc. Natl. Acad. Sci. U.S.A. *92*, 285–289.

Paganelli, F.L., Willems, R.J.L., Jansen, P., Hendrickx, A., Zhang, X., Bonten, M.J.M., and Leavis, H.L. (2013). *Enterococcus faecium* biofilm formation: identification of major autolysin AtlAEfm, associated Acm surface localization, and AtlAEfm-independent extracellular DNA Release. MBio *4*, e00154.

Pawson, T. (1995). Protein modules and signalling networks. Nature *373*, 573–580.

Peltier, J., Courtin, P., El Meouche, I., Lemée, L., Chapot-Chartier, M.-P., and Pons, J.-L. (2011). *Clostridium difficile* has an original peptidoglycan structure with a high level of N-acetylglucosamine deacetylation and mainly 3-3 cross-links. J. Biol. Chem. *286*, 29053–29062.

Poyart, C., Quesne, G., and Trieu-Cuot, P. (2002). Taxonomic dissection of the *Streptococcus bovis* group by analysis of manganese-dependent superoxide dismutase gene (*sodA*) sequences: reclassification of "*Streptococcus infantarius subsp. coli*" as *Streptococcus lutetiensis* sp. nov. and of *Streptococcus bovis* biotype 11.2 as *Streptococcus pasteurianus* sp. nov. Int. J. Syst. Evol. Microbiol. *52*, 1247–1255.

Prajsnar, T.K., Renshaw, S.A., Ogryzko, N.V., Foster, S.J., Serror, P., and Mesnage, S. (2013). Zebrafish as a novel vertebrate model to dissect enterococcal pathogenesis. Infect. Immun. *81*, 4271–4279.

Qin, X., Singh, K.V., Xu, Y., Weinstock, G.M., and Murray, B.E. (1998). Effect of disruption of a gene encoding an autolysin of *Enterococcus faecalis* OG1RF. Antimicrob. Agents Chemother. *42*, 2883–2888.

Qin, X., Singh, K.V., Weinstock, G.M., and Murray, B.E. (2000). Effects of *Enterococcus faecalis fsr* genes on production of gelatinase and a serine protease and virulence. Infect. Immun. *68*, 2579–2586.

Qin, X., Singh, K.V., Weinstock, G.M., and Murray, B.E. (2001). Characterization of *fsr*, a regulator controlling expression of gelatinase and serine protease in *Enterococcus faecalis* OG1RF. J. Bacteriol. *183*, 3372–3382.

Rakita, R.M., Quan, V.C., Jacques-Palaz, K., Singh, K.V., Arduino, R.C., Mee, M., and Murray, B.E. (2000). Specific antibody promotes opsonization and PMN-mediated killing of phagocytosis-resistant *Enterococcus faecium*. FEMS Immunol. Med. Microbiol. *28*, 291–299.

Raymond, J.B., Mahapatra, S., Crick, D.C., and Pavelka, M.S. (2005). Identification of the namH gene, encoding the hydroxylase responsible for the *N*-glycolylation of the mycobacterial peptidoglycan. J. Biol. Chem. *280*, 326–333.

Reste de Roca, F.R., Duché, C., Dong, S., Rincé, A., Dubost, L., Pritchard, D.G., Baker, J.R., Arthur, M., and Mesnage, S. (2010). Cleavage specificity of *Enterococcus faecalis* EnpA (EF1473), a peptidoglycan endopeptidase related to the LytM/lysostaphin family of metallopeptidases. J. Mol. Biol. *398*, 507–517.

Rhodes, J., Hagen, A., Hsu, K., Deng, M., Liu, T.X., Look, A.T., and Kanki, J.P. (2005). Interplay of *pu.1* and *gata1* determines myelo-erythroid progenitor cell fate in zebrafish. Dev. Cell *8*, 97–108.

Rice, L.B., Calderwood, S.B., Eliopoulos, G.M., Farber, B.F., and Karchmer, A.W. (1991).

Enterococcal endocarditis: a comparison of prosthetic and native valve disease. Rev. Infect. Dis. *13*, 1–7.

Rich, R.L., Kreikemeyer, B., Owens, R.T., LaBrenz, S., Narayana, S.V., Weinstock, G.M., Murray, B.E., and Höök, M. (1999). Ace is a collagen-binding MSCRAMM from *Enterococcus faecalis*. J. Biol. Chem. *274*, 26939–26945.

Rico-Lastres, P., Díez-Martínez, R., Iglesias-Bexiga, M., Bustamante, N., Aldridge, C., Hesek, D., Lee, M., Mobashery, S., Gray, J., Vollmer, W., et al. (2015). Substrate recognition and catalysis by LytB, a pneumococcal peptidoglycan hydrolase involved in virulence. Scientific Reports *5*, srep16198.

Rigel, N.W., Gibbons, H.S., McCann, J.R., McDonough, J.A., Kurtz, S., and Braunstein, M. (2009). The accessory SecA2 system of mycobacteria requires ATP binding and the canonical SecA1. J. Biol. Chem. *284*, 9927–9936.

Righino, B., Galisson, F., Pirolli, D., Vitale, S., Réty, S., Gouet, P., and De Rosa, M.C. (2017). Structural model of the full-length Ser/Thr protein kinase StkP from *S. pneumoniae* and its recognition of peptidoglycan fragments. J. Biomol. Struct. Dyn. 1–14.

Rigottier-Gois, L., Alberti, A., Houel, A., Taly, J.-F., Palcy, P., Manson, J., Pinto, D., Matos, R.C., Carrilero, L., Montero, N., et al. (2011). Large-Scale Screening of a Targeted *Enterococcus faecalis* Mutant Library Identifies Envelope Fitness Factors. PLoS One *6*.

Rigottier-Gois, L., Madec, C., Navickas, A., Matos, R.C., Akary-Lepage, E., Mistou, M.-Y., and Serror, P. (2015). The surface rhamnopolysaccharide Epa of *Enterococcus faecalis* is a key determinant of intestinal colonization. J Infect Dis *211*, 62–71.

Rince, A., Flahaut, S., and Auffray, Y. (2000). Identification of general stress genes in *Enterococcus faecalis*. Int. J. Food Microbiol. *55*, 87–91.

Robert, L., Hoffmann, M., Krell, N., Aymerich, S., Robert, J., and Doumic, M. (2014). Division in *Escherichia coli* is triggered by a size-sensing rather than a timing mechanism. BMC Biol. *12*, 17.

Rolain, T., Bernard, E., Beaussart, A., Degand, H., Courtin, P., Egge-Jacobsen, W., Bron, P.A., Morsomme, P., Kleerebezem, M., Chapot-Chartier, M.-P., et al. (2013). *O*-glycosylation as a novel control mechanism of peptidoglycan hydrolase activity. J. Biol. Chem. *288*, 22233–22247.

Rozdzinski, E., Marre, R., Susa, M., Wirth, R., and Muscholl-Silberhorn, A. (2001). Aggregation substance-mediated adherence of *Enterococcus faecalis* to immobilized extracellular matrix proteins. Microb. Pathog. *30*, 211–220.

Salamaga, B., Prajsnar, T.K., Jareño-Martinez, A., Willemse, J., Bewley, M.A., Chau, F., Belkacem, T.B., Meijer, A.H., Dockrell, D.H., Renshaw, S.A. and Mesnage, S. (2017). Bacterial size matters: Multiple mechanisms controlling septum cleavage and diplococcus formation are critical for the virulence of the opportunistic pathogen *Enterococcus faecalis*. PLoS Pathog. *13*, e1006526.

Sandalova, T., Lee, M., Henriques-Normark, B., Hesek, D., Mobashery, S., Mellroth, P., and Achour, A. (2016). The crystal structure of the major pneumococcal autolysin LytA in complex with a large peptidoglycan fragment reveals the pivotal role of glycans for lytic activity. Mol. Microbiol. *101*, 954–967.

van der Sar, A.M., Musters, R.J.P., van Eeden, F.J.M., Appelmelk, B.J., Vandenbroucke-Grauls, C.M.J.E., and Bitter, W. (2003). Zebrafish embryos as a model host for the real time analysis of *Salmonella typhimurium* infections. Cell. Microbiol. *5*, 601–611.

Sardis, M.F., and Economou, A. (2010). SecA: a tale of two protomers. Molecular Microbiology *76*, 1070–1081.

Scheffers, D.-J., and Pinho, M.G. (2005). Bacterial cell wall synthesis: new insights from localization studies. Microbiol. Mol. Biol. Rev. *69*, 585–607.

Schermelleh, L., Heintzmann, R., and Leonhardt, H. (2010). A guide to super-resolution fluorescence microscopy. J. Cell Biol. *190*, 165–175.

Schindler, M., Mirelman, D., and Schwarz, U. (1976). Quantitative determination of *N*-acetylglucosamine residues at the non-reducing ends of peptidoglycan chains by enzymic attachment of [14C]-D-galactose. European Journal of Biochemistry *71*, 131–134.

Schlag, M., Biswas, R., Krismer, B., Kohler, T., Zoll, S., Yu, W., Schwarz, H., Peschel, A., and Götz, F. (2010). Role of staphylococcal wall teichoic acid in targeting the major autolysin Atl. Mol. Microbiol. *75*, 864–873.

Schleifer, K.H. (1975). Chemical structure of the peptidoglycan, its modifiability and relation to the biological activity. Z Immunitatsforsch Exp Klin Immunol *149*, 104–117.

Schleifer, K.H., and Kilpper-Bälz, R. (1984). Transfer of *Streptococcus faecalis* and

Streptococcus faecium to the Genus *Enterococcus* nom. rev. as *Enterococcus faecalis* comb. nov. and *Enterococcus faecium* comb. nov. International Journal of Systematic and Evolutionary Microbiology *34*, 31–34.

Schlievert, P.M., Chuang-Smith, O.N., Peterson, M.L., Cook, L.C.C., and Dunny, G.M. (2010). *Enterococcus faecalis* endocarditis severity in rabbits is reduced by IgG Fabs interfering with aggregation substance. PLOS ONE *5*, e13194.

Schneewind, O., Model, P., and Fischetti, V.A. (1992). Sorting of protein A to the staphylococcal cell wall. Cell *70*, 267–281.

Schulenburg, H., Kurz, C.L., and Ewbank, J.J. (2004). Evolution of the innate immune system: the worm perspective. Immunol. Rev. *198*, 36–58.

Schuster, B., and Sleytr, U.B. (2015). Relevance of glycosylation of S-layer proteins for cell surface properties. Acta Biomater *19*, 149–157.

Scott, J.R., and Barnett, T.C. (2006). Surface proteins of gram-positive bacteria and how they get there. Annu. Rev. Microbiol. *60*, 397–423.

Sghir, A., Gramet, G., Suau, A., Rochet, V., Pochart, P., and Dore, J. (2000). Quantification of Bacterial Groups within Human Fecal Flora by Oligonucleotide Probe Hybridization. Appl Environ Microbiol *66*, 2263–2266.

Shah, I.M., Laaberki, M.-H., Popham, D.L., and Dworkin, J. (2008). A eukaryotic-like Ser/Thr kinase signals bacteria to exit dormancy in response to peptidoglycan fragments. Cell *135*, 486–496.

Sham, L.-T., Butler, E.K., Lebar, M.D., Kahne, D., Bernhardt, T.G., and Ruiz, N. (2014). Bacterial cell wall. MurJ is the flippase of lipid-linked precursors for peptidoglycan biogenesis. Science *345*, 220–222.

Shankar, N., Lockatell, C.V., Baghdayan, A.S., Drachenberg, C., Gilmore, M.S., and Johnson, D.E. (2001). Role of *Enterococcus faecalis* surface protein Esp in the pathogenesis of ascending urinary tract infection. Infect. Immun. *69*, 4366–4372.

Shankar, N., Baghdayan, A.S., and Gilmore, M.S. (2002). Modulation of virulence within a pathogenicity island in vancomycin-resistant *Enterococcus faecalis*. Nature *417*, 746–750.

Shankar, V., Baghdayan, A.S., Huycke, M.M., Lindahl, G., and Gilmore, M.S. (1999). Infection-derived *Enterococcus faecalis* strains are enriched in *esp*, a gene encoding a novel

surface protein. Infect. Immun. *67*, 193–200.

Sharpe, M.E., Hauser, P.M., Sharpe, R.G., and Errington, J. (1998). Bacillus subtilis cell cycle as studied by fluorescence microscopy: constancy of cell length at initiation of DNA replication and evidence for active nucleoid partitioning. J. Bacteriol. *180*, 547–555.

Sherman, J.M. (1937). The streptococci. Bacteriol Rev *1*, 3–97.

Sherman J. M, and Wing H. U. (1935). An unnoted hemolytic *Streptococcus* associated with milk products. Journal of Dairy Science *18*, 657–660.

Shi, L., Pigeonneau, N., Ventroux, M., Derouiche, A., Bidnenko, V., Mijakovic, I., and Noirot-Gros, M.-F. (2014). Protein-tyrosine phosphorylation interaction network in *Bacillus subtilis* reveals new substrates, kinase activators and kinase cross-talk. Front Microbiol *5*, 538.

Shlaes, D.M., Levy, J., and Wolinsky, E. (1981). Enterococcal bacteremia without endocarditis. Arch. Intern. Med. *141*, 578–581.

Sievert, D.M., Ricks, P., Edwards, J.R., Schneider, A., Patel, J., Srinivasan, A., Kallen, A., Limbago, B., Fridkin, S., and National Healthcare Safety Network (NHSN) Team and Participating NHSN Facilities (2013). Antimicrobial-resistant pathogens associated with healthcare-associated infections: summary of data reported to the National Healthcare Safety Network at the Centers for Disease Control and Prevention, 2009-2010. Infect Control Hosp Epidemiol *34*, 1–14.

Silhavy, T.J., Kahne, D., and Walker, S. (2010). The bacterial cell envelope. Cold Spring Harb Perspect Biol *2*, a000414.

Sillanpää, J., Xu, Y., Nallapareddy, S.R., Murray, B.E., and Höök, M. (2004). A family of putative MSCRAMMs from *Enterococcus faecalis*. Microbiology (Reading, Engl.) *150*, 2069–2078.

Singh, K.V., Qin, X., Weinstock, G.M., and Murray, B.E. (1998). Generation and testing of mutants of *Enterococcus faecalis* in a mouse peritonitis model. J. Infect. Dis. *178*, 1416–1420.

Singh, K.V., Nallapareddy, S.R., and Murray, B.E. (2007). Importance of the *ebp* (endocarditis- and biofilm-associated pilus) locus in the pathogenesis of *Enterococcus faecalis* ascending urinary tract infection. J. Infect. Dis. *195*, 1671–1677.

Singh, K.V., Nallapareddy, S.R., Sillanpää, J., and Murray, B.E. (2010). Importance of the collagen adhesin *ace* in pathogenesis and protection against *Enterococcus faecalis* experimental

endocarditis. PLoS Pathog. *6*, e1000716.

Smith, R., Salamaga, B., Hajdomawicz, N., Bulmer, G., Szkuta, P., Herry, J., Kołodziejczyk, J., Prajsnar, T., Serror, P., and Mesnage, S. (submitted). The charge of the enterococcal rhamnopolysaccharide Epa is critical for virulence and resistance to antimicrobial peptides.

Solà, R., and Soriano, G. (2002). Why do bacteria reach ascitic fluid? Eur J Gastroenterol Hepatol *14*, 351–354.

Soldo, B., Lazarevic, V., and Karamata, D. (2002). *tagO* is involved in the synthesis of all anionic cell-wall polymers in *Bacillus subtilis* 168. Microbiology (Reading, Engl.) *148*, 2079–2087.

Squeglia, F., Marchetti, R., Ruggiero, A., Lanzetta, R., Marasco, D., Dworkin, J., Petoukhov, M., Molinaro, A., Berisio, R., and Silipo, A. (2011). Chemical basis of peptidoglycan discrimination by PrkC, a key kinase involved in bacterial resuscitation from dormancy. J. Am. Chem. Soc. *133*, 20676–20679.

Steen, A., Buist, G., Leenhouts, K.J., El Khattabi, M., Grijpstra, F., Zomer, A.L., Venema, G., Kuipers, O.P., and Kok, J. (2003). Cell wall attachment of a widely distributed peptidoglycan binding domain is hindered by cell wall constituents. J. Biol. Chem. *278*, 23874–23881.

Steen, A., Buist, G., Horsburgh, G.J., Venema, G., Kuipers, O.P., Foster, S.J., and Kok, J. (2005). AcmA of *Lactococcus lactis* is an *N*-acetylglucosaminidase with an optimal number of LysM domains for proper functioning. FEBS J. *272*, 2854–2868.

Swoboda, J.G., Meredith, T.C., Campbell, J., Brown, S., Suzuki, T., Bollenbach, T., Malhowski, A.J., Kishony, R., Gilmore, M.S., and Walker, S. (2009). Discovery of a small molecule that blocks wall teichoic acid biosynthesis in *Staphylococcus aureus*. ACS Chem. Biol. *4*, 875–883.

Szabady, R.L., Peterson, J.H., Skillman, K.M., and Bernstein, H.D. (2005). An unusual signal peptide facilitates late steps in the biogenesis of a bacterial autotransporter. Proc. Natl. Acad. Sci. U.S.A. *102*, 221–226.

Teng, F., Jacques-Palaz, K.D., Weinstock, G.M., and Murray, B.E. (2002). Evidence that the enterococcal polysaccharide antigen gene (*epa*) cluster is widespread in *Enterococcus faecalis* and influences resistance to phagocytic killing of *E. faecalis*. Infect. Immun. *70*, 2010–2015.

Teng, F., Singh, K.V., Bourgogne, A., Zeng, J., and Murray, B.E. (2009). Further

characterization of the *epa* gene cluster and Epa polysaccharides of *Enterococcus faecalis*. Infect. Immun. *77*, 3759–3767.

Theilacker, C., Kaczyński, Z., Kropec, A., Sava, I., Ye, L., Bychowska, A., Holst, O., and Huebner, J. (2011). Serodiversity of opsonic antibodies against *Enterococcus faecalis* glycans of the cell wall revisited. PLOS ONE *6*, e17839.

Theilacker, C., Holst, O., Lindner, B., Huebner, J., and Kaczyński, Z. (2012). The structure of the wall teichoic acid isolated from *Enterococcus faecalis* strain 12030. Carbohydr. Res. *354*, 106–109.

Thiercelin M. E. (1899). Morphologie et modes de reproduction de l'enterocoque. Comptes Rendus Des Seances de La Societe de Biologie et Des Ses Filiales *11*, 551–553.

Thomas, V.C., Hiromasa, Y., Harms, N., Thurlow, L., Tomich, J., and Hancock, L.E. (2009). A fratricidal mechanism is responsible for eDNA release and contributes to biofilm development of *Enterococcus faecalis*. Mol. Microbiol. *72*, 1022–1036.

Thumm, G., and Götz, F. (1997). Studies on prolysostaphin processing and characterization of the lysostaphin immunity factor (Lif) of *Staphylococcus simulans* biovar staphylolyticus. Mol. Microbiol. *23*, 1251–1265.

Thurlow, L.R., Thomas, V.C., and Hancock, L.E. (2009). Capsular polysaccharide production in *Enterococcus faecalis* and contribution of CpsF to capsule serospecificity. J. Bacteriol. *191*, 6203–6210.

Thurlow, L.R., Thomas, V.C., Narayanan, S., Olson, S., Fleming, S.D., and Hancock, L.E. (2010). Gelatinase contributes to the pathogenesis of endocarditis caused by *Enterococcus faecalis*. Infect. Immun. *78*, 4936–4943.

Tipper, D.J., and Strominger, J.L. (1965). Mechanism of action of penicillins: a proposal based on their structural similarity to acyl-D-alanyl-D-alanine. Proc. Natl. Acad. Sci. U.S.A. *54*, 1133–1141.

Todd E. W. (1934). A comparative serological study of streptolysins derived from human and from animal infections, with notes on pneumococcal haemolysin, tetanolysin and staphylococcus toxin. The Journal of Pathology and Bacteriology *39*.

Toledo-Arana, A., Valle, J., Solano, C., Arrizubieta, M.J., Cucarella, C., Lamata, M., Amorena, B., Leiva, J., Penadés, J.R., and Lasa, I. (2001). The enterococcal surface protein, Esp, is

involved in *Enterococcus faecalis* biofilm formation. Appl Environ Microbiol *67*, 4538–4545.

Ton-That, H., Marraffini, L.A., and Schneewind, O. (2004). Sortases and pilin elements involved in pilus assembly of *Corynebacterium diphtheriae*. Mol. Microbiol. *53*, 251–261.

Tran, T.T., Jaijakul, S., Lewis, C.T., Diaz, L., Panesso, D., Kaplan, H.B., Murray, B.E., Wanger, A., and Arias, C.A. (2012). Native valve endocarditis caused by *Corynebacterium striatum* with heterogeneous high-level daptomycin resistance: collateral damage from daptomycin therapy? Antimicrob. Agents Chemother. *56*, 3461–3464.

Trueba, F.J. (1982). On the precision and accuracy achieved by *Escherichia coli* cells at fission about their middle. Arch. Microbiol. *131*, 55–59.

Tsui, H.-C.T., Keen, S.K., Sham, L.-T., Wayne, K.J., and Winkler, M.E. (2011). Dynamic distribution of the SecA and SecY translocase subunits and septal localization of the HtrA surface chaperone/protease during *Streptococcus pneumoniae* D39 Cell Division. mBio *2*, e00202-11.

Turner, R.D., Hurd, A.F., Cadby, A., Hobbs, J.K., and Foster, S.J. (2013). Cell wall elongation mode in Gram-negative bacteria is determined by peptidoglycan architecture. Nature Communications *4*, ncomms2503.

Uttley, A.H., George, R.C., Naidoo, J., Woodford, N., Johnson, A.P., Collins, C.H., Morrison, D., Gilfillan, A.J., Fitch, L.E., and Heptonstall, J. (1989). High-level vancomycin-resistant enterococci causing hospital infections. Epidemiol. Infect. *103*, 173–181.

Van Tyne, D., Martin, M.J., and Gilmore, M.S. (2013). Structure, Function, and Biology of the *Enterococcus faecalis* Cytolysin. Toxins (Basel) *5*, 895–911.

Vincent, J.-L. (2003). Nosocomial infections in adult intensive-care units. Lancet *361*, 2068–2077.

Vollmer, W. (2008). Structural variation in the glycan strands of bacterial peptidoglycan. FEMS Microbiol. Rev. *32*, 287–306.

Vollmer, W., and Bertsche, U. (2008). Murein (peptidoglycan) structure, architecture and biosynthesis in *Escherichia coli*. Biochim. Biophys. Acta *1778*, 1714–1734.

Vollmer, W., and Seligman, S.J. (2010). Architecture of peptidoglycan: more data and more models. Trends Microbiol. *18*, 59–66.

Vollmer, W., Joris, B., Charlier, P., and Foster, S. (2008a). Bacterial peptidoglycan (murein) hydrolases. FEMS Microbiol. Rev. *32*, 259–286.

Vollmer, W., Blanot, D., and De Pedro, M.A. (2008b). Peptidoglycan structure and architecture. FEMS Microbiology Reviews *32*, 149–167.

Wang, Y., Huebner, J., Tzianabos, A.O., Martirosian, G., Kasper, D.L., and Pier, G.B. (1999). Structure of an antigenic teichoic acid shared by clinical isolates of *Enterococcus faecalis* and vancomycin-resistant *Enterococcus faecium*. Carbohydr. Res. *316*, 155–160.

Waters, C.M., Antiporta, M.H., Murray, B.E., and Dunny, G.M. (2003). Role of the *Enterococcus faecalis* GelE protease in determination of cellular chain length, supernatant pheromone levels, and degradation of fibrin and misfolded surface proteins. J. Bacteriol. *185*, 3613–3623.

Weart, R.B., Lee, A.H., Chien, A.-C., Haeusser, D.P., Hill, N.S., and Levin, P.A. (2007). A metabolic sensor governing cell size in bacteria. Cell *130*, 335–347.

Wehrli, W., Knüsel, F., Schmid, K., and Staehelin, M. (1968). Interaction of rifamycin with bacterial RNA polymerase. Proc Natl Acad Sci U S A *61*, 667–673.

Weidenmaier, C., Kokai-Kun, J.F., Kristian, S.A., Chanturiya, T., Kalbacher, H., Gross, M., Nicholson, G., Neumeister, B., Mond, J.J., and Peschel, A. (2004). Role of teichoic acids in *Staphylococcus aureus* nasal colonization, a major risk factor in nosocomial infections. Nat. Med. *10*, 243–245.

Weigel, L.M., Clewell, D.B., Gill, S.R., Clark, N.C., McDougal, L.K., Flannagan, S.E., Kolonay, J.F., Shetty, J., Killgore, G.E., and Tenover, F.C. (2003). Genetic analysis of a high-level vancomycin-resistant isolate of *Staphylococcus aureus*. Science *302*, 1569–1571.

Wheeler, R., Mesnage, S., Boneca, I.G., Hobbs, J.K., and Foster, S.J. (2011). Super-resolution microscopy reveals cell wall dynamics and peptidoglycan architecture in ovococcal bacteria. Mol. Microbiol. *82*, 1096–1109.

Willett, C.E., Cortes, A., Zuasti, A., and Zapata, A.G. (1999). Early hematopoiesis and developing lymphoid organs in the zebrafish. Dev. Dyn. *214*, 323–336.

Woodford, N., Morrison, D., Cookson, B., and George, R.C. (1993). Comparison of high-level gentamicin-resistant *Enterococcus faecium* isolates from different continents. Antimicrob. Agents Chemother. *37*, 681–684.

Wu, L.J., and Errington, J. (2004). Coordination of cell division and chromosome segregation by a nucleoid occlusion protein in *Bacillus subtilis*. Cell *117*, 915–925.

Xu, Y., Jiang, L., Murray, B.E., and Weinstock, G.M. (1997). *Enterococcus faecalis* antigens in human infections. Infect. Immun. *65*, 4207–4215.

Xu, Y., Singh, K.V., Qin, X., Murray, B.E., and Weinstock, G.M. (2000). Analysis of a gene cluster of *Enterococcus faecalis* involved in polysaccharide biosynthesis. Infect. Immun. *68*, 815–823.

Yamada, S., Sugai, M., Komatsuzawa, H., Nakashima, S., Oshida, T., Matsumoto, A., and Suginaka, H. (1996). An autolysin ring associated with cell separation of *Staphylococcus aureus*. J. Bacteriol. *178*, 1565–1571.

Yeats, C., Finn, R.D., and Bateman, A. (2002). The PASTA domain: a beta-lactam-binding domain. Trends Biochem. Sci. *27*, 438.

Yu, X.C., and Margolin, W. (1999). FtsZ ring clusters in min and partition mutants: role of both the Min system and the nucleoid in regulating FtsZ ring localization. Mol. Microbiol. *32*, 315–326.

Zeng, J., Teng, F., Weinstock, G.M., and Murray, B.E. (2004). Translocation of *Enterococcus faecalis* strains across a monolayer of polarized human enterocyte-like T84 cells. J. Clin. Microbiol. *42*, 1149–1154.

Appendix

As a part of my PhD thesis I am including my published paper "Bacterial size matters: Multiple mechanisms controlling septum cleavage and diplococcus formation are critical for the virulence of the opportunistic pathogen *Enterococcus faecalis*", which was originally published in PLOS Pathogens.

This work is under a creative commons attribution licence (https://creativecommons.org/licenses/by/4.0/) and therefor I have permission to use this article in my thesis.

Bacterial size matters: Multiple mechanisms controlling septum cleavage and diplococcus formation are critical for the virulence of the opportunistic pathogen *Enterococcus faecalis*

Bartłomiej Salamaga[1,2], **Tomasz K. Prajsnar**[1,3,4], **Ana Jareño-Martinez**[1,2], **Joost Willemse**[5], **Martin A. Bewley**[1,3], **Françoise Chau**[6], **Tassadit Ben Belkacem**[1,2], **Annemarie H. Meijer**[5], **David H. Dockrell**[1,3¤], **Stephen A. Renshaw**[1,3,4], **Stéphane Mesnage**[1,2]*

1 Krebs Institute, University of Sheffield, Sheffield, United Kingdom, 2 Department of Molecular Biology and Biotechnology, University of Sheffield, Sheffield, United Kingdom, 3 Department of Infection and Immunity and Cardiovascular Disease, University of Sheffield, Sheffield, United Kingdom, 4 The Bateson Centre, University of Sheffield, Sheffield, United Kingdom, 5 Institute of Biology, Leiden University, Leiden, The Netherlands, 6 INSERM, UMR 1137, Infection, Antimicrobiens Modelisation, Evolution (IAME), Université Paris Diderot, Sorbonne Paris cité, Paris, France

¤ Current address: Centre for Inflammation Research, University of Edinburgh, Edinburgh, United Kingdom
* s.mesnage@sheffield.ac.uk

OPEN ACCESS

Abstract

Enterococcus faecalis is an opportunistic pathogen frequently isolated in clinical settings. This organism is intrinsically resistant to several clinically relevant antibiotics and can transfer resistance to other pathogens. Although *E. faecalis* has emerged as a major nosocomial pathogen, the mechanisms underlying the virulence of this organism remain elusive. We studied the regulation of daughter cell separation during growth and explored the impact of this process on pathogenesis. We demonstrate that the activity of the AtlA peptidoglycan hydrolase, an enzyme dedicated to septum cleavage, is controlled by several mechanisms, including glycosylation and recognition of the peptidoglycan substrate. We show that the long cell chains of *E. faecalis* mutants are more susceptible to phagocytosis and are no longer able to cause lethality in the zebrafish model of infection. Altogether, this work indicates that control of cell separation during division underpins the pathogenesis of *E. faecalis* infections and represents a novel enterococcal virulence factor. We propose that inhibition of septum cleavage during division represents an attractive therapeutic strategy to control infections.

Author summary

Enterococcus faecalis is a commensal bacterium that colonizes the gastrointestinal tract of humans. This organism is an opportunistic pathogen that can cause a wide range of life-threatening infections in hospital settings. Despite the identification of several virulence factors, the mechanisms by which *E. faecalis* evades host immunity and causes infections remains poorly understood. Here, we explore how the formation of diplococci and short

cell chains, a distinctive property of *E. faecalis*, contributes to pathogenesis. We describe several mechanisms that control the activity of AtlA, the enzyme dedicated to septum cleavage during division. Using a combination of *in vitro* assays and flow cytometry analyses of *E. faecalis* mutants, we show that AtlA activity is regulated by several mechanisms. We reveal that during pathogenesis, AtlA activity is critical for overcoming the host immune response. In the absence of AtlA, the long cell chains of *E. faecalis* mutants are more susceptible to phagocytosis and can no longer cause lethality in the zebrafish model of infection, thus indicating that control of cell chain length is a novel virulence factor in *E. faecalis*. This work highlights a link between cell division and pathogenesis and suggests that cell separation represents a step that can be targeted to control bacterial infections.

Introduction

Enterococci are Gram-positive commensal bacteria colonizing the gastrointestinal tract of humans. They are opportunistic nosocomial pathogens that can cause a wide range of life-threatening infections in immunocompromised patients or following antibiotic-induced dysbiosis [1]. The emergence of enterococci as nosocomial pathogens relies on the capacity of these bacteria to colonize the host and to grow in a wide range of harsh conditions (*e.g.*, in the presence of bile salts or in iron-depleted environments) [2]. Enterococci are intrinsically resistant to multiple antibiotics, such as cephalosporins and several aminoglycosides, and can also acquire resistance to glycopeptides. Vancomycin-Resistant Enterococci (VRE) represent a major problem in clinical settings as they can potentially transfer resistance genes to other pathogens such as *Staphylococcus aureus* [3, 4].

Two enterococcus species, *Enterococcus faecium* and *Enterococcus faecalis* are the most clinically relevant [5]. *E. faecium* infections are caused by a particular subset of clones specifically found in hospital settings that share several acquired mobile genetic elements [6]. In contrast, the *E. faecalis* strains responsible for hospital-acquired infections are also found in healthy individuals and genes associated with virulence are not only exclusively present in clinical isolates [7]. How this organism can cause infections therefore remains poorly understood.

In the present work, we study the regulation of daughter cell separation during cell division and explore the impact of this process on pathogenesis. We previously revealed that in *E. faecalis*, one peptidoglycan (PG) hydrolase with *N*-acetylglucosaminidase activity (named AtlA) is dedicated to septum cleavage to allow separation of daughter cells at the end of division [8]. Using a combination of *in vitro* experiments and sets of isogenic strains, we describe multiple mechanisms controlling the activity of AtlA. We show that control of septum cleavage during growth underpins the formation of diplococci and short chains, a property critical to cause lethality in the zebrafish model of infection.

Results

High expression levels of septum hydrolytic enzymes are not sufficient for cell separation

In vitro enzymatic assays using recombinant *E. faecalis* PG hydrolases indicated that AtlA specific activity is 20- to 30-fold lower than the activity of the *N*-acetylmuramidase AtlB [9]. We hypothesized that a high level of AtlA expression could explain the predominant role of this enzyme in septum cleavage. To test this hypothesis, we compared the amount of AtlA and AtlB produced during growth. We generated two strains producing His-tagged AtlA and AtlB
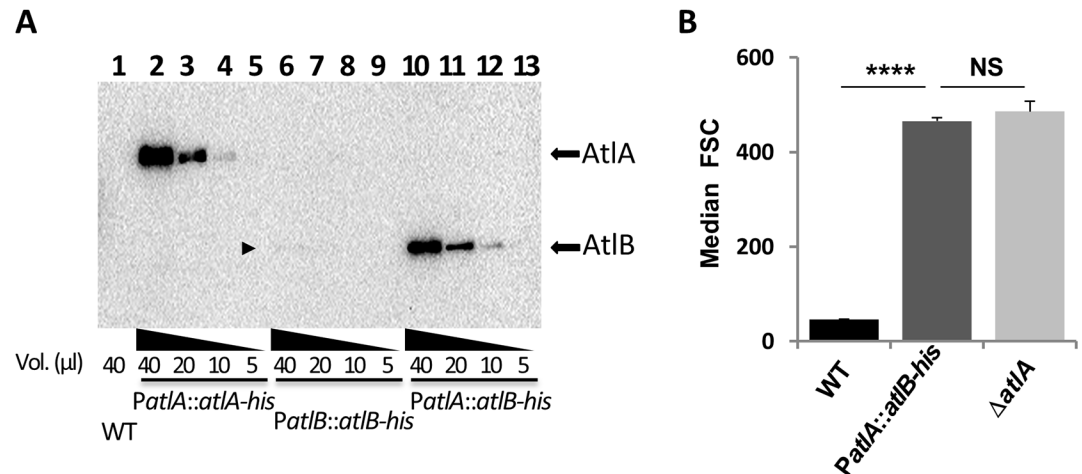
Fig 1. *E. faecalis* **expressing** *atlB* **under the P***atlA* **promoter forms cell chains. A**. Western blot detection of His-tagged AtlA and AtlB proteins expressed under the control of the *atlA* (P*atlA*) or *atlB* (P*atlB*) promoters. Various amounts of exponentially growing cultures were harvested and total extracts corresponding to mixtures of broken cells and supernatants were analyzed by Western blot using anti-His antibodies. The faint band corresponding to AtlB-His is indicated by an arrowhead. **B**. Comparison of median forward scattered (FSC) light values corresponding to the cell chain lengths of WT, Δ*atlA* and P*atlB*::*atlB-his* strains; ****$P<0.0001$; n = 3; NS, $P>0.05$; n = 3.

proteins expressed under their own promoters (P*atlA*::*atlA-his* and P*atlB*::*atlB-his*). Culture samples were harvested at the end of exponential growth (OD$_{600}$ = 1) and His-tagged AtlA and AtlB were detected by western blotting using an anti-histidine serum (Fig 1A). Unlike His-tagged AtlA, AtlB was barely detectable (Fig 1A, lanes 2–5 and lanes 6–9; see arrowhead on Fig 1A). Next, we tested whether increasing the level of expression of AtlB could enable this peptidoglycan hydrolase to cleave the septum efficiently. We built a strain producing an AtlB-His tagged protein expressed under the *atlA* promoter (P*atlA*::*atlB-his*), thereby replacing the AtlA open reading frame by AtlB. As expected, expression of *atlB-his* under the control of the *atlA* promoter increased the production of AtlB-His to levels similar to AtlA-His (Fig 1A, compare lanes 2–5 with lanes 10–13). The impact of AtlB production on septum cleavage was analyzed by flow cytometry to measure bacterial chain lengths, as previously described [8]. Increasing the production of AtlB to levels similar to those of AtlA was not sufficient to shorten bacterial cell chains (Fig 1B). The cell chain length of the P*atlA*::*atlB-his* strain was not significantly different from that of the Δ*atlA* strains ($P>0.05$; n = 3). This result indicated that the relatively low production level of AtlB does not account for the low septum cleavage activity of this enzyme. This prompted us to explore the enzymatic properties of AtlA and their impact on cell separation.

N-terminal proteolytic cleavage of recombinant AtlA stimulates septum cleavage

Previous studies indicated that truncation of the AtlA N-terminal domain (residues 54 to 172) only had a marginal impact on the activity of the recombinant enzyme tested *in vitro* against whole PG molecules (sacculi) as a substrate [10]. We sought to re-investigate the contribution of the N-terminal domain to AtlA activity using an *in vitro* assay (as described in [8]) to specifically measure septum cleavage. A recombinant AtlA protein (residues 54 to 737) harboring an N-terminal 6-Histidine tag and a Tobacco Etch Virus (TEV) protease site at the end of the N-terminal domain was expressed in *Escherichia coli* and purified (Fig 2A, lane 1). Following
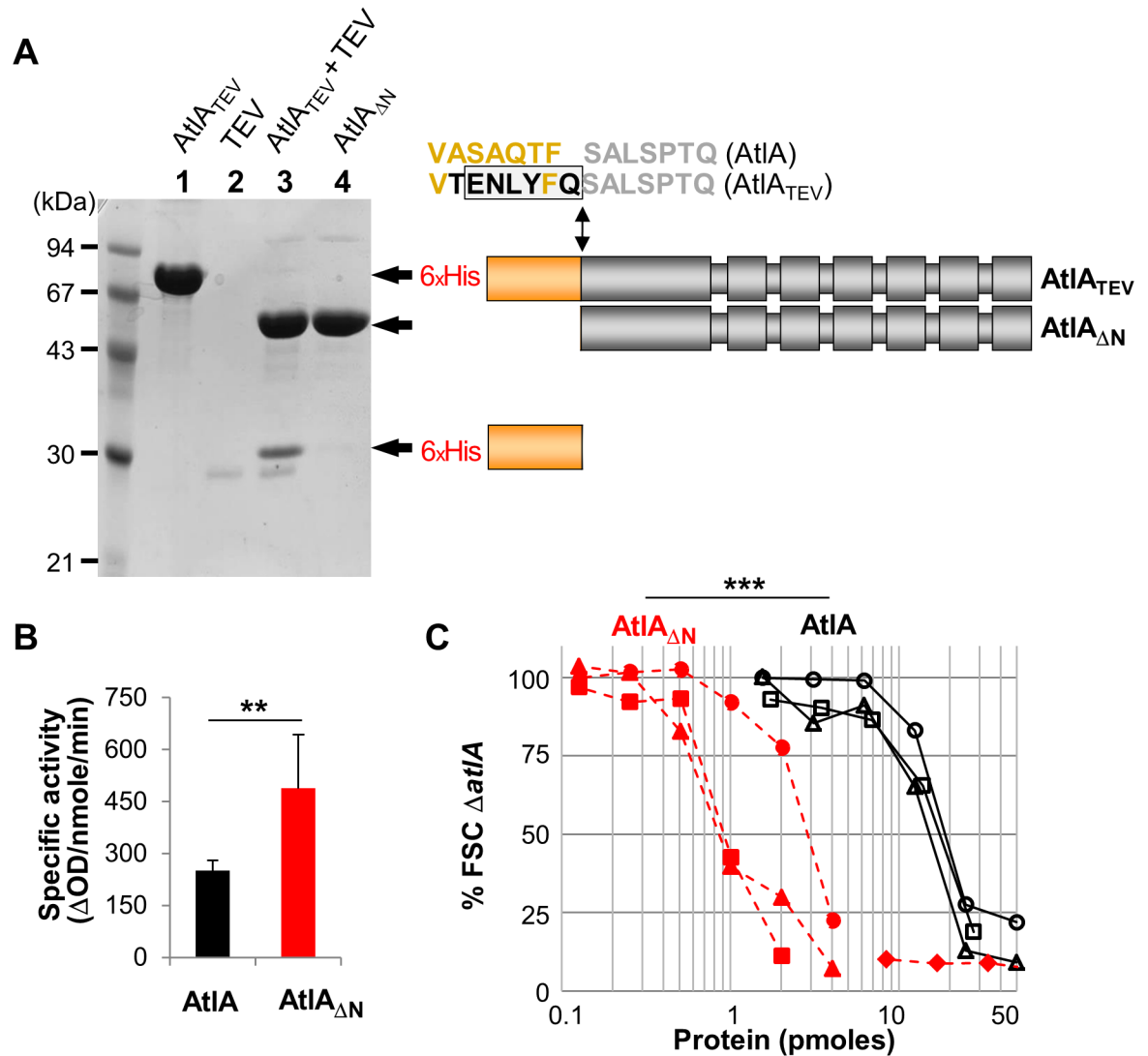
Fig 2. Truncation of AtlA N-terminal domain enhances septum cleavage activity *in vitro*. A. SDS-PAGE analysis of purified recombinant proteins: lane 1, full-length AtlA$_{TEV}$ (residues 53–737) corresponding to the mature protein (without the signal peptide), with a TEV site between domains 1 and 2; lane 2, TEV protease (TEV); lane 3, TEV digestion product of AtlA$_{TEV}$ (AtlA$_{TEV}$+TEV); lane 4, AtlA truncated of its N-terminal domain (AtlA$_{\Delta N}$). The amino acid sequences between N-terminal (orange) and catalytic (grey) domains in AtlA and AtlA$_{TEV}$ are described. The TEV cleavage site is boxed. **B**. Comparison of specific enzymatic activities of AtlA and AtlA$_{\Delta N}$ *in vitro* using whole PG sacculi as a substrate; **$P = 0.0018$; n = 9. **C**. Flow cytometry analysis of septum cleavage activity of recombinant full-length AtlA and the N-terminally truncated variant (AtlA$_{\Delta N}$). Activity is expressed as a percentage of the median forward scattered (FSC) light value corresponding to cell chains formed by the *atlA* mutant (Δ*atlA*) used as a substrate; ***$P = 0.0008$; n = 3.

cleavage with TEV protease, truncated AtlA was recovered by metal affinity chromatography (Fig 2A, lanes 2 to 4). In agreement with previous results, the specific activity of the truncated AtlA (AtlA$_{\Delta N}$; 488.2 ± 155.6 ΔOD$_{600}$/nmole/min) was slightly higher than that of AtlA (252.5 ± 27.4 ΔOD$_{600}$/nmole/min) when assayed against whole sacculi (**$P = 0.0018$; n = 9; Fig 2B). However, using the specific septum cleavage assay, AtlA$_{\Delta N}$ was more than 10-fold active than the full-length AtlA enzyme. Whilst 1.6 ± 1.2 pmoles of AtlA$_{\Delta N}$ were sufficient to disperse 50% of the cell chains, 18.2 ± 2.0 pmoles of AtlA were required for a similar septum cleavage activity (***$P = 0.0008$; n = 3; Fig 2C).
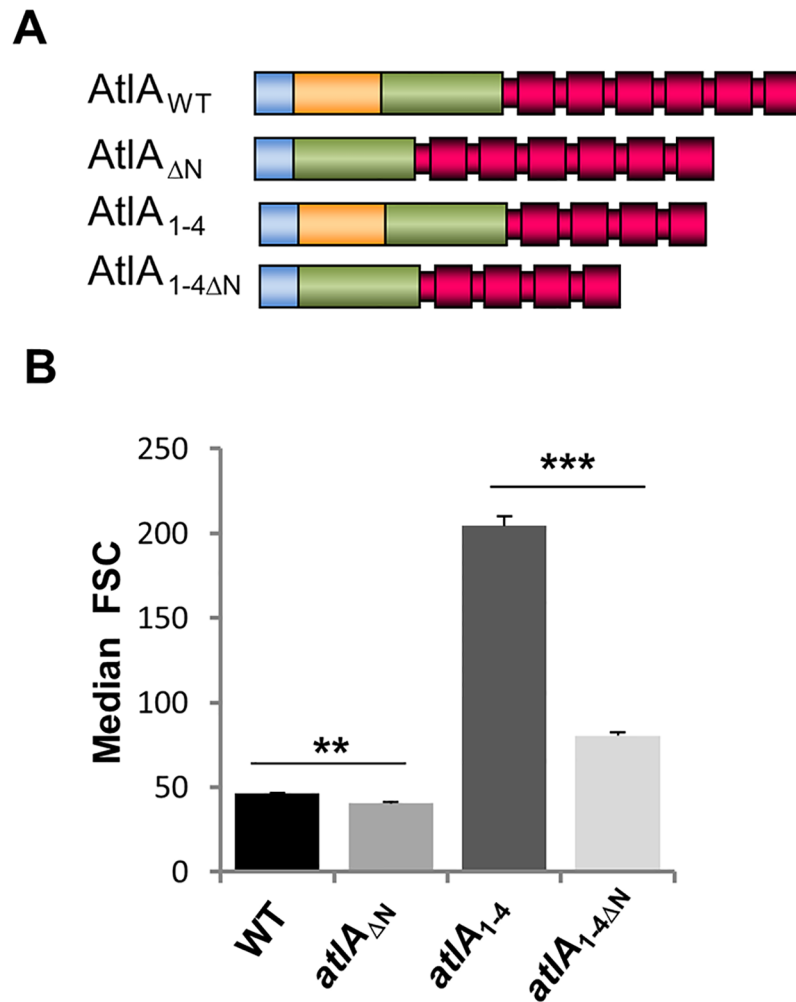
Fig 3. *E. faecalis* **strains expressing N-terminally truncated AtlA form shorter cell chains. A**. Schematic representation of AtlA variants produced by recombinant *E. faecalis* JH2-2 derivatives. $AtlA_{WT}$, full-length AtlA; $AtlA_{\Delta N}$, AtlA truncated from the N-terminal domain; $AtlA_{1-4}$, AtlA truncated from the two C-terminal LysM modules; $AtlA_{1-4\Delta N}$, $AtlA_{1-4}$ truncated from the N-terminal domain. Blue, signal peptide; orange, N-terminal domain; green, catalytic domain; red, LysM domain. **B**. Comparison of median forward scattered (FSC) light values corresponding to the cell chain lengths of WT, $atlA_{\Delta N}$, $atlA_{1-4}$ and $atlA_{1-4\Delta N}$ strains; **$P = 0.0015$; $n = 3$; ***$P = 0.0001$; $n = 3$. See also S2 Fig.

https://doi.org/10.1371/journal.ppat.1006526.g003

Cleavage of AtlA N-terminal domain is required for daughter cell separation during growth

We further explored the contribution of the AtlA N-terminal domain in septum cleavage during growth. We built a recombinant strain producing AtlA with a truncated N-terminal domain ($atlA_{\Delta N}$) (Fig 3A). However, as the parental strain mostly forms diplococci and short chains (2–4 cells), we anticipated only a limited reduction in bacterial cell chain length. To see a more pronounced reduction in bacterial chain length, we analyzed the impact of the N-terminal truncation in a strain forming longer chains. We suspected that truncating the C-terminal domain of AtlA would impair binding of this enzyme to its substrate and its activity, hence leading to the formation of longer chains. We therefore constructed $atlA_{1-4}$, a strain producing an AtlA variant with only 4 C-terminal LysM repeats instead of 6. AtlA proteins produced by

recombinant strains were detected in culture supernatants by Western blot using polyclonal antibodies raised against the catalytic domain of AtlA, indicating that AtlA proteins with the expected molecular weights were produced and secreted in all cases (S1A Fig). The distribution of cell chain lengths measured by flow cytometry was in agreement with our *in vitro* experiments. Truncation of the N-terminal domain led to the formation of shorter chains as indicated by a significant shift towards lower forward scattered light values (Fig 3B). This conclusion was supported by two pairwise comparisons (i) between the cells producing full-length AtlA (WT; FSC = 46.38 ± 0.38) and its N-terminally truncated counterpart ($atlA_{\Delta N}$; FSC = 40.32 ± 0.99) ($^{**}P$ = 0.0015; n = 3) and (ii) between the cells producing AtlA with 4 C-terminal LysM repeats ($atlA_{1-4}$; FSC = 204.45 ± 5.71) and its N-terminally truncated counterpart ($atlA_{1-4\Delta N}$; FSC = 80.33 ± 1.99) ($^{***}P$ = 0.0001; n = 3). The reduction of cell numbers per chain in the mutants producing a truncated AtlA protein was confirmed by light microscopy (S1B and S1C Fig) Altogether, these results showed that the N-terminal domain of AtlA negatively controls the septum cleavage activity of this enzyme.

AtlA N-terminal domain glycosylation inhibits septum cleavage

The N-terminal domain of AtlA contains a high proportion of threonine and serine residues (28% and 12%, respectively; S1D Fig). This property prompted us to test whether this domain can be *O*-glycosylated. To purify AtlA produced by *E. faecalis*, a recombinant strain expressing a C-terminally 6His-tagged AtlA protein and a TEV site between the N-terminal and catalytic domains was constructed by allele exchange (Fig 4A). Cell surface proteins were extracted with 8M urea and His-tagged AtlA protein was purified by metal affinity chromatography. Two major bands of 75 kDa and 62 kDa matching the expected molecular weights of the full-length and N-terminally truncated AtlA, respectively, were detected (Fig 4B, lane 1). A carbohydrate moiety was detected on the full-length AtlA protein, but absent on the truncated AtlA (Fig 4B, lane 2), suggesting that glycosylation occurred at the N-terminal domain of AtlA. To confirm this hypothesis, exponentially growing cells were harvested and incubated in the presence of TEV protease. This treatment released a glycosylated polypeptide matching the apparent molecular weight of the N-terminal domain (Fig 4C, lanes 2 and 3 and Fig 2A, lane 3). No glycosylated polypeptide was detected when the protease was omitted, therefore indicating that the N-terminal domain of AtlA is glycosylated. In Gram-positive bacteria, two glycosyl transferases named GtfA and GtfB have been shown to be essential for surface protein glycosylation [11–13]. We used allele exchange to inactivate two putative glycosyl transferase homologs (*gtfA* and *gtfB*; EF2891 and EF2892 in *E. faecalis* V583) sharing the same glycosyl transferase domain (PFAM PF00534). Following incubation of cells harboring an in-frame deletion of the *gtfAB* locus in the presence of TEV protease, no glycosylated peptide could be detected (Fig 4C, lanes 4–6). Altogether, these results show that the N-terminal domain of AtlA is glycosylated and that this posttranslational modification requires the glycosyltransferases *gtfAB*. Next, we explored the impact of AtlA glycosylation on septum cleavage during growth by measuring the bacterial chain length of *gtfAB* mutants by flow cytometry (Fig 4D) and light microscopy (S2 Fig). We compared the cell chain lengths of *E. faecalis* JH2-2 (WT) forming mostly diplococci and short chains (2–4 cells) and $atlA_{1-4}$, producing AtlA$_{1-4}$ lacking two LysM modules (6–12 cells) with the chain length of their $\Delta gtfAB$ counterparts. Pairwise comparisons of cell chain length by flow cytometry revealed that $\Delta gtfAB$ mutants formed shorter chains than parental strains, thus indicating that the lack of glycosylation enhanced AtlA septum cleavage activity. The cell chains of the parental strain (WT; FSC = 46.09 ± 0.43) were longer than those from the $\Delta gtfAB$ mutant (FSC = 42.04 ± 0.66; $^{**}P$ = 0.0017; n = 3). A more pronounced difference was measured
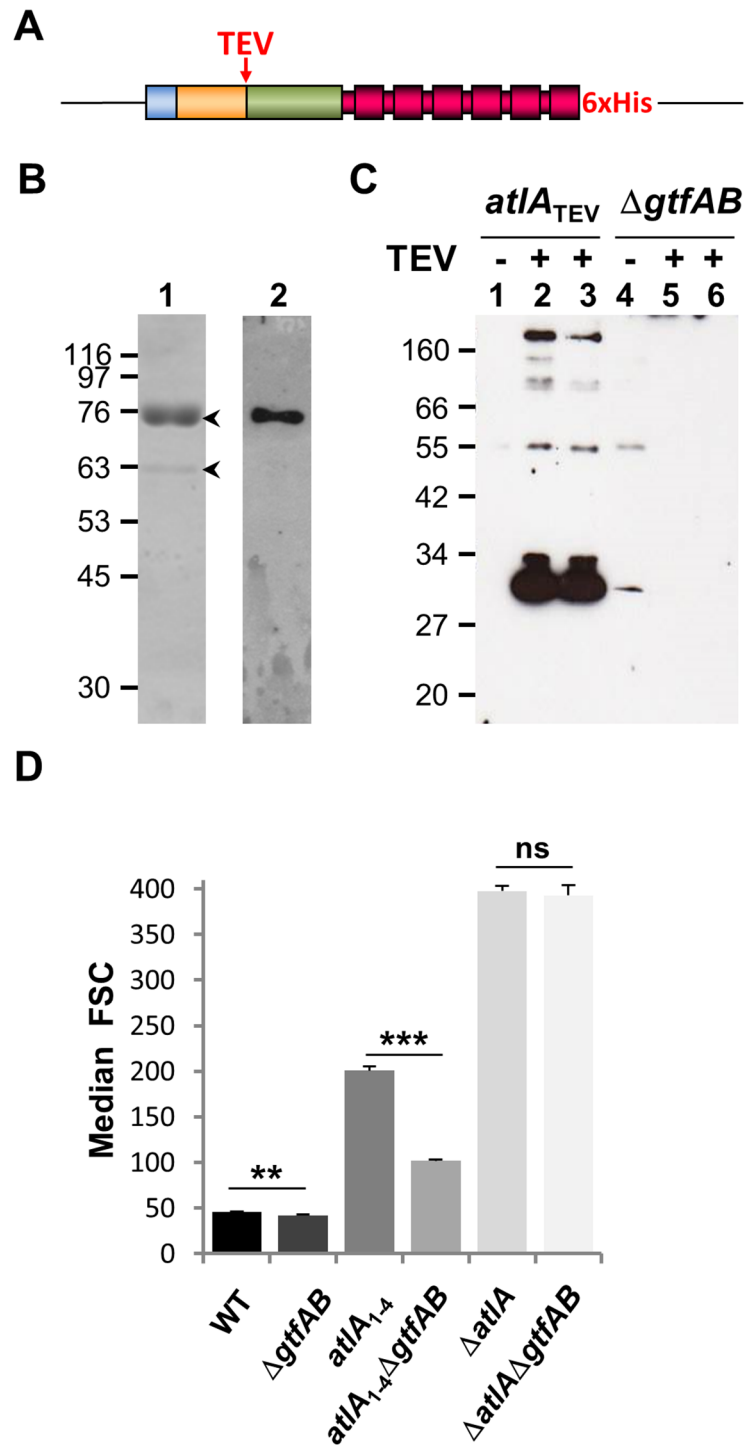
Fig 4. *E. faecalis* strains lacking AtlA glycosylation form shorter cell chains. A. Schematic representation of the *atlA*_{TEV} allele produced by *E. faecalis*. **B**. Metal affinity purification of cell surface associated His-tagged AtlA extracted with 8M urea. Two bands indicated by arrowheads were detected on a Coomassie-stained SDS-PAGE (lane 1); the upper band (72 kDa) corresponds to full-length AtlA proteins and the lower band to AtlA without the N-terminal domain (62 kDa). A clear signal corresponding to glycosylated full length AtlA (lane 2) was detected using the ECL glycoprotein detection kit (GE Healthcare). **C**. Exponentially growing cells from a culture expressing AtlA_{TEV} were resuspended in buffer in the absence (-) or presence (+) of TEV protease to cleave the N-terminal domain of AtlA. Solubilized proteins were recovered by centrifugation, loaded on an SDS-PAGE and transferred on nitrocellulose to detect glycosylated proteins. Two independent cultures treated

with the TEV protease were analysed in parallel. In both cases, a glycosylated polypeptide with the expected molecular weight for the N-terminal domain (see Fig 2A) was detected while no signal was observed in the negative control. When a similar experiment was repeated with protein extracts from a Δ*gtfAB* mutant, no glycosylated protein was detected, indicating that this operon is involved in the post translational modification of AtlA. **D**. Comparison of median forward scattered (FSC) light values corresponding to the cell chain lengths of WT, Δ*gtfAB*, *atlA*$_{1-4}$, *atlA*$_{1-4}$Δ*gtfAB*, Δ*atlA* and Δ*atlA*Δ*gtfAB* strains.

https://doi.org/10.1371/journal.ppat.1006526.g004

between the strain expressing the glycosylated C-terminally truncated AtlA (*atlA*$_{1-4}$; FSC = 200.87 ± 5.71) and its non-glycosylated counterpart (*atlA*$_{1-4}$Δ*gtfAB*; FSC = 101.66 ± 1.47) (***P = 0.0002; n = 3). When introduced to the Δ*atlA* genetic background, the deletion of the *gtfAB* operon did not significantly reduce the bacterial chain length (FSC = 397.68 ± 5.37 versus 392.95 ± 11.37, respectively; P>0.05). Together with light microscopy analyses (S2C and S2D Fig), these results indicate that AtlA glycosylation mediated by *gtfAB* impairs septum cleavage.

Swapping AtlA *N*-acetylglucosaminidase domain for other hydrolase domains cleaving distinct peptidoglycan bonds does not abolish septum cleavage in *E. faecalis*

Substrate recognition by the catalytic domain of peptidoglycan hydrolases is an important factor modulating enzymatic activity [14]. The fact that AtlA is dedicated to septum cleavage can therefore be underpinned by the recognition and cleavage of a specific peptidoglycan structure present at the septum. We hypothesized that if such is the case, the *N*-acetylglucosaminidase activity of AtlA should be essential for septum cleavage. To explore this possibility, we constructed a gene replacement vector encoding an allele of *atlA* with a catalytic domain flanked by two restriction sites (NcoI and BglII). These two sites were used to swap the *N*-acetylglucosaminidase domain of AtlA for the catalytic domains of *E. faecalis N*-acetylmuramidase AtlB [8], *Staphylococcus aureus N*-acetylmuramoyl-L-Alanine amidase Atl [15] or *Streptococcus thermophilus* D,L endopeptidase Cse [16] (Fig 5A and S3 Fig). AtlA alleles encoding variants with distinct peptidoglycan cleavage specificities (Fig 5B) were introduced on the chromosome by gene replacement and expressed as a single copy under the *atlA* promoter. Western blot analyses indicated that all AtlA variants were expressed at similar levels, except AtlA$_{Cse}$, which was subject to proteolysis (S3C Fig) The septum cleavage activity in each strain was analyzed using flow cytometry. Cell chain length of the Δ*atlA* deletion mutant was used as a reference to define the forward scattered light value corresponding to maximal (100%) chain length. Introduction of the NcoI and BamHI restriction sites had a limited impact on the size of the cell chains (11.68 ± 1.35% of the Δ*atlA* mutant chains versus 10.59 ± 1.36% of the Δ*atlA* mutant for the parental JH2-2 strain). All strains expressing AtlA variants with altered enzymatic specificity formed shorter chains than the Δ*atlA* mutant in exponential phase (Fig 5C). This result indicated that the peptidoglycan cleavage specificity of AtlA is not an essential property of the enzyme for septum cleavage. The forward scattered light measurements corresponding to the strains expressing AtlA variants compared to the Δ*atlA* mutant ranged from 28.71 ± 5.38% of the Δ*atlA* mutant for the strain expressing AtlB with a muramidase activity to 53.63 ± 1.3% of the Δ*atlA* mutant for the strain expressing AtlA with an endopeptidase activity. The relatively higher forward scattered light values associated with this strain could be due to the proteolysis of the chimeric protein (S3C Fig). The chain lengths of strains expressing chimeric proteins were all significantly shorter than those of the Δ*atlA* mutant (**P<0.01; n = 3).

A
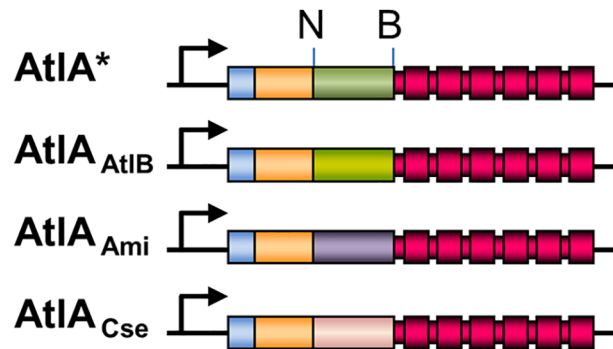
B
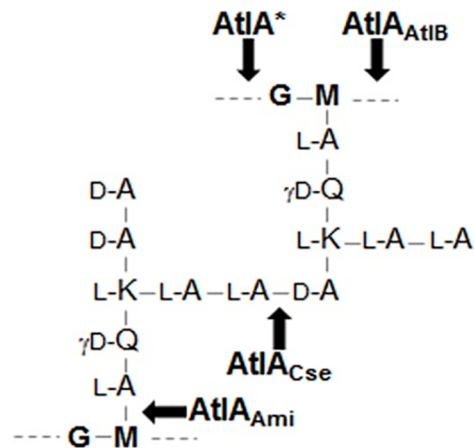
C

Strain	Median FSC	% FSC Δ*atlA*
WT	43.35 ± 0.59	10.59 ± 1.36
*atlA**	47.83 ± 0.65	11.68 ± 1.36
atlA~Ami~	122.68 ± 4.52	29.97 ± 3.68
atlA~AtlB~	117.35 ± 6.32	28.71 ± 5.38
atlA~Cse~	219.57 ± 2.66	53.63 ± 1.21
Δ*atlA*	409.38 ± 24.52	100.00 ± 5.99

Fig 5. AtlA *N*-acetylglucosaminidase activity is not essential for septum cleavage. A. Schematic representation of AtlA variants expressed by recombinant *E. faecalis* JH2-2 derivatives. All strains were constructed by allele exchange to express AtlA variants under the control of the *atlA* promoter (arrow). Two restriction sites (NcoI, N and BglII, B) flanking the region encoding the catalytic domain were introduced by site-directed mutagenesis. The resulting allele in strain *atlA** encodes an AtlA protein with eleven modified amino-acids (see supplementary S3 Fig). The NcoI-BglII fragment encoding AtlA *N*-acetylglucosaminidase activity was replaced with a fragment encoding the *N*-acetylmuramidase activity of *E. faecalis* AtlB to generate strain *atlA*~AtlB~, the amidase activity of *S. aureus* Atl to generate strain *atlA*~Ami~ or the endopeptidase activity of *Streptococcus thermophilus* Cse to generate strain *atlA*~Cse~. **B**. *E. faecalis* peptidoglycan bonds cleaved by the

catalytic domains of *E. faecalis* AtlA and AtlB, *S. aureus* AtlA and *S. thermophilus* Cse. **C**. Comparison of median forward scattered (FSC) light values corresponding to the cell chain lengths of WT, *atlA**, *atlA*$_{AtlB}$, *atlA*$_{Ami}$, *atlA*$_{Cse}$. and Δ*atlA*. All median FSC values were significantly different from the median FSC value from the Δ*atlA* strain (**P<0.01; n = 3).

The multimodular LysM domain of AtlA is a major determinant for septum cleavage

To test the contribution of the LysM domain of AtlA (LysM$_A$) to septum cleavage, we compared the septum cleavage activity of proteins containing this domain or the LysM domain from AtlB (LysM$_B$) using flow cytometry. Four recombinant proteins were produced in *E. coli* and purified: the full-length AtlA and AtlB proteins (without a signal peptide) and derivatives containing a swapped LysM domain (AtlAB and AtlBA; Fig 6A and 6B; S4 Fig). In agreement with our previous work, AtlA septum cleavage activity was much higher than that of AtlB. Whilst 4.6 ± 1.3 pmoles of AtlA reduced the cell chain length of a Δ*atlA* mutant by 50% in 15 minutes at 37˚C, 100-fold more AtlB was not sufficient to produce the same effect. When AtlA LysM$_A$ was replaced by LysM$_B$, the septum activity of the enzyme decreased 17-fold indicating
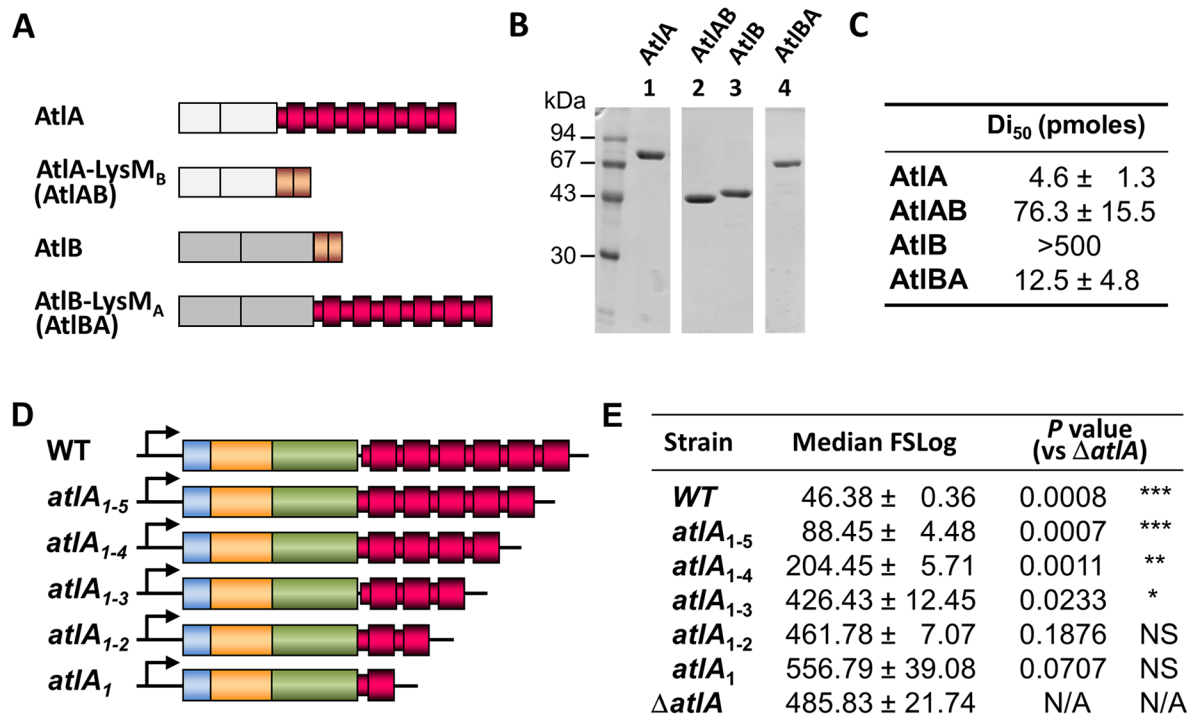
Fig 6. Contribution of the LysM domain to septum cleavage. A. Schematic representation of AtlA and AtlB derivatives expressed and purified to test their septum cleavage activity. Full-length AtlA and AtlB (without signal peptides), as well as their counterparts with LysM$_B$ (AtlAB) or LysM$_A$ (AtlBA) domains, were expressed in *E. coli*. **B**. SDS-PAGE of AtlA (lane 1), AtlAB (lane 2), AtlB (lane 3) and AtlBA (lane 4) samples showing that all proteins were purified to homogeneity. **C**. Flow cytometry analysis of septum cleavage activity of recombinant proteins *in vitro* using OG1RF Δ*atlA* cell chains as a substrate (see materials and methods). The Di$_{50}$ (Dechaining index) value corresponds to the amount of enzyme in pmoles that is able to decrease the median FSC value of Δ*atlA* cell chains by 50% in 15 minutes at 37˚C. **D**. Schematic representation of *atlA* locus in *E. faecalis* JH2-2 and isogenic derivatives producing AtlA with a C-terminal LysM domain containing a variable number of LysM repeats (6 in WT; 5 in *atlA*$_{1-5}$; 4 in *atlA*$_{1-4}$; 3 in *atlA*$_{1-3}$; 2 in *atlA*$_{1-2}$; 1 in *atlA*$_1$). **E**. Comparison of median forward scattered (FSC) light values corresponding to the cell chain lengths of WT, *atlA*$_{1-5}$, *atlA*$_{1-4}$, *atlA*$_{1-3}$, *atlA*$_{1-2}$, *atlA*$_1$ and Δ*atlA* strains. *P* values and significance corresponding to comparisons with the Δ*atlA* strain are indicated.

that LysM$_A$ is critical for optimal septum cleavage. Swapping LysM$_B$ for LysM$_A$ in AtlB led to a septum cleavage activity comparable to that of AtlA ([Fig 6C]).

The contribution of individual LysM repeats to the septum cleavage activity was investigated. A set of strains expressing AtlA with 1 to 5 LysM repeats (henceforth referred to as *atlA$_1$* to *atlA$_{1-5}$* strains) was constructed by allele exchange ([Fig 6D]). Western blot and zymogram analyses ([S4A and S4B Fig]) showed that all strains produced AtlA proteins with the expected size and in similar amounts, except for the *atlA$_1$* strain in which lower amounts were detected. AtlA activity decreased as LysM repeats were truncated. Next, we measured the impact of LysM truncations on the septum cleavage activity by measuring the cell chain length. Flow cytometry analyses revealed that sequential truncation of LysM modules led to a stepwise increase of cell chain length ([Fig 6E] and [S4C Fig]). This result indicated that optimal septum cleavage requires the full-length LysM domain, each module providing an additive contribution to AtA enzymatic activity.

Cell separation defects abolish *E. faecalis* virulence in the zebrafish model of infection

We investigated whether the formation of long chains in *E. faecalis* has an impact on virulence using the zebrafish model of infection [17]. We compared the lethality induced by the wild-type OG1RF strain to that of an in-frame *atlA* deletion mutant OG1RF (Δ*atlA*) forming long chains. In the Δ*atlA* mutant, each chain (equivalent to 1 CFU) can contain several viable cells. To eliminate this bias, Δ*atlA* chains were sonicated to mechanically separate cells ([S5A and S5B Fig]) [18] and establish the number of cells per CFU. This information was then used to inject the same number of cells (but different CFU numbers) for each strain. Zebrafish embryos were infected 30h post fertilization (hpf) and survival was monitored over the following 90h. One of three independent experiments is shown in [Fig 7A] whilst the results for three biological replicates are shown in [S5C and S5D Fig]. Injection of *ca.* 1,000 OG1RF cells killed between 60% and 77% of larvae (n = 79) depending on the experiment. In contrast, the Δ*atlA* mutant only killed 4% to 20% of larvae (n = 88), showing a significant reduction in virulence (***P<0.001 for the experiment shown in [Fig 7A]). At this stage, we envisaged that this difference could be attributed to several factors: (i) the increased chain length of the Δ*atlA* mutant, (ii) (an)other alteration(s) in cell surface properties (like in the *Streptococcus mutans atlA* mutant; [19]) or (iii) a defect in biofilm formation [20]. To specifically investigate the contribution of bacterial chain length to virulence, we subjected the Δ*atlA* mutant to mild sonication. This treatment is dispersing bacterial chains ([S5A Fig]) whilst it does not alter viability (Dubee et al., 2011), virulence ([S6 Fig]) or subsequent bacterial growth rate ([S7 Fig]). Sonication of the Δ*atlA* mutant thus allowed us to compare cells with an identical genetic background, differing only by the size of their cell chains. This treatment restored the virulence of the mutant to similar levels as the wild-type strain (P = 0.455; [Fig 7A]), killing between 46% and 59% of larvae (n = 90).

Previous work revealed that phagocyte evasion is a critical step for *E. faecalis* pathogenesis in the zebrafish [17]. We therefore quantified phagocytosis in zebrafish larvae infected with bacteria expressing the green fluorescent protein (GFP) ([Fig 7B]). Confocal microscopy images were used to measure bacterial uptake by phagocytes labelled with anti L-plastin antibodies. To specifically investigate the impact of the chain forming phenotype on phagocytosis, we compared the uptake of long and short bacterial chains formed by the Δ*atlA* mutant before and after sonication (Δ*atlA^S*). The ratio between green fluorescence area inside to outside phagocytes was significantly higher for the Δ*atlA* mutant (**P = 0.0098; n = 7). A significant difference was also measured when we compared the uptake of the Δ*atlA* mutant to that of
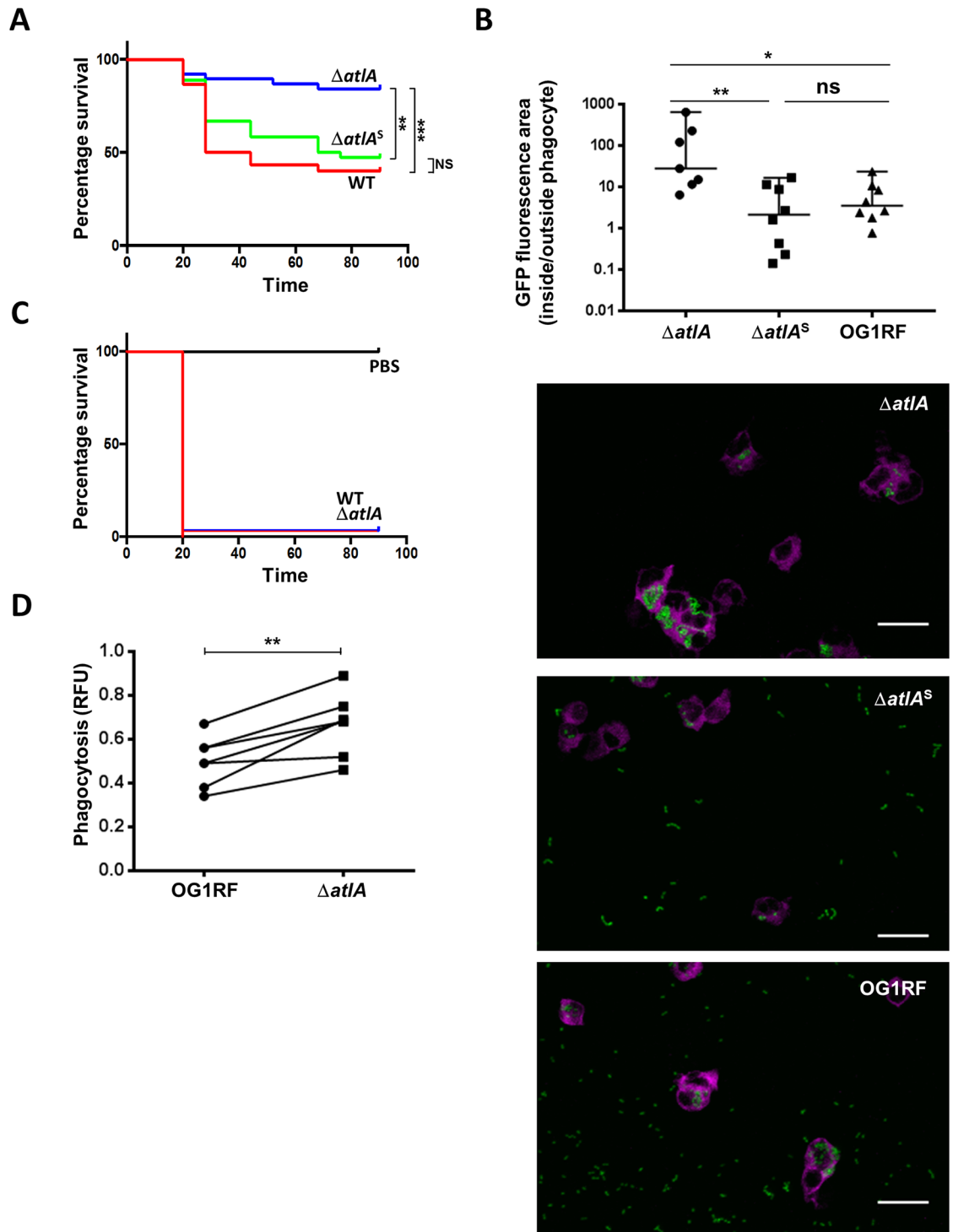
Fig 7. *E. faecalis* long cell chains are less virulent in the zebrafish model of infection and more prone to phagocytosis than diplococci. A. Survival of zebrafish larvae (n>20) following infection with *E. faecalis* OG1RF (WT) and *atlA* isogenic deletion mutant before (ΔatlA) and after (ΔatlA^S) sonication to disperse long chains. Statistical significance was determined by Log-rank test; **P = 0.0011; *** P = 0.0002; NS, P>0.05. **B**. Quantification of *E. faecalis* uptake by zebrafish phagocytes. Embryos were infected with 1,200 *E. faecalis* cells expressing GFP and fixed in 4% paraformaldehyde 1.5h post infection. Phagocytes were immunolabelled using rabbit anti L-plastin antibodies and detected with goat anti-rabbit antibodies conjugated to Alexafluor 647. Fluorescent bacteria and phagocytes were imaged by scanning confocal microscopy. The area of GFP fluorescence signal outside and inside phagocytes was measured

using a dedicated Fiji plugin. The ratio of GFP fluorescence area outside to inside phagocytes was used to quantify bacterial uptake. Phagocytosis was significantly higher for long chains (Δ*atlA*) when compared to their sonicated counterparts (Δ*atlA*^S) (**P = 0.0098) or the wild-type cells (*P = 0.0438). No difference in uptake was found between short chains corresponding to the wild-type or sonicated Δ*atlA* mutant (NS, *P*>0.05). Representative images of phagocytes (magenta) following infection with Δ*atlA*, sonicated Δ*atlA*^S and wild-type OG1RF cells shown. Phagocytes labeled with L-plastin appear in magenta, GFP-producing bacteria in green. Scale bar is 20μm. **C**. Survival of phagocyte-depleted zebrafish larvae (n>20) following injection with *E. faecalis* OG1RF (WT) or Δ*atlA*. **D**. Pairwise comparisons of phagocytosis indexes corresponding to *E. faecalis* OG1RF and Δ*atlA* uptake by human monocyte-derived macrophages (MDM). Statistical significance was determined by paired t-test; Δ*atlA* cells were more efficiently phagocytosed by MDM than WT cells (**P = 0.0024; n = 7).

wild-type (*P = 0.0438; n = 8). As expected, no difference was detected between wild-type and Δ*atlA*^S cells. Representative images used to quantify uptake are shown as an example (Fig 7B). Bacteria forming long chains were mostly found inside phagocytes (96% of total fluorescence area) as opposed to diplococci and short chains corresponding to wild-type and Δ*atlA*^S cells (75% and 60% respectively).

Death rates were the same when immunocompromised zebrafish (n>20 per group) were infected with the wild-type OG1RF strain or with the Δ*atlA* mutant. In both cases, injection of 1250 cells in *pu.1* morphants led to more than 90% mortality within 20h post infection (Fig 7C and S5E Fig). This result suggested that the impaired virulence of the long chain-forming Δ*atlA* mutant is due to the fact that this strain is unable to evade phagocytosis during infection. To make a direct comparison of the uptake of wild-type and Δ*atlA* cells by phagocytes, an *in vitro* assay was performed using monocyte-derived macrophages obtained from peripheral blood mononuclear cells from healthy volunteers (Fig 7D). Phagocytic uptake was quantified following labeling of bacterial cells with pHrodo-S-ester, a pH-sensitive dye displaying increased fluorescence in low-pH compartments of phagosomes [21]. In each pairwise comparison, Δ*atlA* long chains were more efficiently phagocytosed (*P* = 0.0024 over 7 biological replicates) (Fig 7D). Collectively, our results indicate that formation of short chains by *E. faecalis* is a critical property enabling this bacterium to evade phagocytosis during pathogenesis.

Discussion

The formation of diplococci and short chains is a distinctive property of *E. faecalis* that was originally reported over a century ago [22]. This typical morphology results from the separation of daughter cells by the *N*-acetylglucosaminidase AtlA [8]. Here, we show that multiple mechanisms are in place to control septum cleavage by AtlA. We further demonstrate that the formation of diplococci and short chains is crucial for the virulence of this opportunistic pathogen. Cells with impaired cell separation are more prone to phagocytosis and can no longer cause infection. We propose that the control of cell chain length is a novel virulence factor that links cell division and pathogenesis in *E. faecalis*.

Using a specific assay to measure septum cleavage by flow cytometry, we showed that two post-translational modifications, both occurring on the N-terminal domain of AtlA contribute to down-regulate the activity of this enzyme. Our hypothesis is that the N-terminal domain, predicted to be disordered (http://prdos.hgc.jp), sterically hinders the catalytic activity of AtlA. By extension, glycosylation of the N-terminal domain is expected to further impair PG recognition and cleavage by the catalytic domain. Truncation of the N-terminal domain by extracellular proteases thus ensures optimal activity of the enzyme once it has reached its substrate at the cell surface. N-terminal truncation of the N-terminal domain occurs during growth and can be detected by zymogram [8, 10]. It is tempting to assume that the proteolytic cleavage of the AtlA N-terminal domain is primarily mediated by the metalloprotease GelE, which has been associated with formation of short chains in *E. faecalis* [23]. However, the diplococcal

state of *E. faecalis* is not restricted to strains producing GelE, indicating that other proteases can process AtlA. An example is *E. faecalis* JH2-2: although this strain is deficient for the production of GelE, it forms diplococci and very short chains.

Interestingly, the genes essential for AtlA glycosylation were previously shown to catalyze the production of diglucosyl-diacylglycerol [24]. This implies that (an)other glycosyl transferase(s) mediate(s) the direct glycosylation of AtlA. Further investigations are required to identify the corresponding enzyme(s). This task appears relatively difficult given the functional redundancy of glycosyl transferases. The *E. faecalis* V583 genome encodes 15 putative enzymes that could be responsible for AtlA glycosylation. Our results showed that in the absence of AtlA, the *gtfAB* deletion has no impact on septum cleavage. Although we cannot formally rule out that glycosylation of other surface proteins can modulate cell separation, this effect (if any) is limited. The identification and characterization of GtfAB substrates awaits further analysis. Another open question deals with the degree of AtlA glycosylation. It is possible that the extent of AtlA glycosylation varies during growth or in response to environmental cues.

Recent studies have explored the impact of PG structure on substrate recognition and cleavage by the catalytic domain of PG hydrolases. The *N*-acetylglucosaminidase LytB, the *S. pneumoniae* functional homolog of *E. faecalis* AtlA, requires fully acetylated GlcNAc moieties for cleavage. A substrate-assisted catalytic mechanism involving anchimeric assistance by the C2-acetamido group of the GlcNAc moiety is likely to underpin this requirement [25]. Another example is the pneumococcal autolysin LytA, in which several amino acids in the vicinity of the catalytic residues contribute to positioning of the substrate in the catalytic cleft so that the scissile bond is at an optimal distance from the catalytic residue [26]. Our work revealed that the *N*-acetylglucosaminidase domain of AtlA is not essential for septum cleavage. However, swapping the AtlA catalytic domain for another domain results in a lower septum cleavage activity. One possibility is that in *E. faecalis*, AtlA has evolved to optimally recognize and cleave the local PG structure at the septum. Recent work in *E. coli* and *B. subtilis* suggested that septal PG is enriched in "denuded" glycan strands resulting from *N*-acetylmuramoyl-L-alanine amidase activity [27]. Whether denuded glycan strands represent an optimal substrate for AtlA remains to be tested. It is expected that the lack of peptide stems will increase the binding activity of the LysM domain [28]. Thus, measurements of the *N*-acetylglucosaminidase activity of AtlA against glycan chains and chains substituted by peptide stems should be carried out with the catalytic domain in isolation to uncouple binding of the AtlA enzyme to its substrate from catalysis.

Our previous work revealed that AtlA LysM motifs can fold independently and do not interact, thus suggesting that they behave as "beads on a string" [28]. This model implied that instead of forming a quaternary structure, LysM repeats bind PG in a cooperative manner. Here, we showed that septum cleavage increases with the number of LysM motifs, with the formation of diplococci requiring the presence of all six repeats. The model strain V583 encodes twelve proteins with LysM domains; four contain two repeats, seven contain a single repeat, AtlA being the only one with six repeats. Bearing in mind that the formation of diplococci or short chains by *E. faecalis* is critical for virulence, our results suggest that the lifestyle of this organism as a commensal has favored the emergence of multimodular LysM domains in AtlA.

During infection, the size of bacterial cells has a major impact on recognition by the immune system. One example is the cording morphology of mycobacteria, which correspond to snake-like structures formed by the end-to-end and side-to-side aggregation of bacilli [29]. The formation of large bacterial aggregates impairs phagocytosis and is required for virulence [30]. Another well-documented strategy to escape host immunity is the formation of filaments after invasion of epithelial cells by uropathogenic *E. coli* (UPEC) [31].

Inhibition of septation enhances resistance to phagocytosis and increase survival rates of UPEC and other pathogens in the host [32]. The exact mechanism by which filamentation inhibits uptake and killing by phagocytes is unclear. *In vitro* experiments using anisotropic polystyrene particles and alveolar macrophages revealed that the point of contact between phagocytes and particles is critical for phagocytosis initiation [33]. It has therefore been proposed that the increased cell length in filamentous bacteria reduces the probability of macrophages to encountering the cell poles that stimulate the formation of the phagocytic cup [34]. This early step in the uptake by immune cells appears to be a limiting factor, the internalization speed of filaments itself being similar to that of smaller particles [34]. In contrast, minimization of bacterial cell chains has been described as a strategy to overcome host immunity in *Streptococcus pneumoniae* [35]. The effect of cell chain length in *S. pneumoniae* involves subversion of complement-mediated opsonophagocytosis. Interestingly, our assay using monocyte-derived macrophages indicated that in the absence of complement, cell chains can be recognized and readily engulfed by phagocytes. Unlike UPEC filaments, the long chains of enterococci are pretty flexible and often form turns (S5B Fig). This is expected to generate a contact point with phagocytes that will favor cytoskeleton remodeling to form the phagocytic cup [34]. Impaired septum cleavage is primarily expected to restrict the capacity of the bacteria to disseminate and multiply in the host and is not expected to have any impact on clearance by phagocytes. In the context of a systemic infection in zebrafish larvae, diplococci are circulating in the bloodstream. The formation of long chains limits the dissemination of the bacteria, hence increasing their probability of encountering immune cells. We propose that the sequestration of *E. faecalis* inside the phagocytes prevents cell multiplication and release of the metalloprotease GelE that is essential to cause tissue damage and host death [17].

E. faecalis is a common nosocomial pathogen associated with a wide range of infections that can be life-threatening. It was recently shown to promote the growth of other microorganisms during polymicrobial infections [36]. This study suggests that targeting the enzymatic activity of AtlA, the autolysin dedicated to septum cleavage, represents a novel therapeutic strategy to eradicate *E. faecalis*.

Methods

Ethics statement

Monocyte-derived macrophages (MDM) were isolated from whole blood from healthy volunteers at the Sheffield Royal Hallamshire hospital with written informed consent prior to inclusion in the study, as approved by the South Sheffield Research Ethics Committee (07/Q2305/7) [37]. All samples were anonymised. Animal work was carried out according to guidelines and legislation set out in UK law in the Animals (Scientific Procedures) Act 1986 under Project License PPL 40/3574. Ethical approval was granted by the University of Sheffield Local Ethical Review Panel.

Bacterial strains, plasmids and growth conditions

Bacterial strains and plasmids used in this study are described in Table 1. *E. coli* was grown at 37˚C in Brain Heart Infusion (BHI) broth or agar 1.5% (w/v) supplemented with 200ug/ml erythromycin (for pGhost9 derivatives) and 100ug/ml ampicillin (pET derivatives). *E. faecalis* strains were grown in BHI broth or agar at 37˚C, unless otherwise stated. When necessary, the medium was supplemented with 30 µg/ml erythromycin.

Zebrafish strains and maintenance

London wild type (LWT) zebrafish [38] were provided by the aquarium facility at the University of Sheffield. Embryos were maintained in E3 medium at 28°C according to standard procedures previously described [39]. Phagocyte-depleted embryos were obtained following injection of phosphorodiamidate morpholino oligomers against *pu.1* as previously described [40].

Microinjections of *E. faecalis* in zebrafish embryos

Cells were grown to mid-exponential phase (OD_{600}~0.3) and harvested by centrifugation (5,000 x *g* for 10 min at room temperature). Bacteria were resuspended in filtered phosphate buffer saline (150 mM Na_2HPO_4, 20 mM KH_2PO_4, 150 mM NaCl [pH 7.5], PBS) and transferred to microcapillary pipettes. Embryos at 30 hours post fertilization (hpf) were anaesthetized, dechorionated, embedded in 3% (w/v) methylcellulose and injected individually with 2nl of a cell suspension corresponding to *ca*. 1,000 cells as previously described [40]. The number of cells injected was checked before and after each series of injections with a given strain. Zebrafish embryos were monitored at regular intervals until 90 h post infection (hpi).

Immunostaining of phagocytes in zebrafish

Zebrafish larvae were fixed 1.5h post infection with 4% paraformaldehyde (m/v) at 4°C overnight and washed four times in PBS supplemented with 0.4% (v/v) TritonX 100 and 1% (v/v) DMSO (PBS-TxD). Samples were blocked in 5% (v/v) sheep serum in PBS-TxD for 1h at room temperature followed by one wash in PBS-TxD. Cells were incubated at 4°C overnight with primary antibodies (anti-L-plastin 1:400, gift from Paul Martin, University of Bristol). After four washes in blocking solution, embryos were incubated with secondary antibodies (goat anti-rabbit IgG, Alexa Fluor 647 conjugate, Life Technologies) for 2h at room temperature. Larvae were washed four times with PBS-TxD and fixed again with 4% paraformaldehyde (m/v) for 30 min at RT. Immunolabelled embryos were mounted using 0.8% (m/v) agarose in E3 medium and imaged with a confocal microscope.

Imaging of infected larvae by confocal microscopy and quantification of uptake by phagocytes

Immunolabelled embryos were immersed in 0.8% (w/v) low melting point agarose in E3 medium and mounted flat on FluoroDish™ (World Precision Instruments Inc.). Images were collected using a DMi8 confocal microscope (Leica). Image acquisition was performed with the Volocity software and the images were processed with ImageJ 1.49v software. Bacterial phagocytosis was quantified using an ImageJ custom script called Fish Analysis v5 which can be obtained from http://sites.imagej.net/Willemsejj/ or via ImageJ updater. All bacteria were identified based on their (GFP, Channel 1) fluorescence. Subsequently, the fluorescence intensity of the phagocytes (Alexa 647, Channel 2) surrounding the phagocytosed bacteria was measured. The phagocytosed bacteria had high fluorescence intensity of Channel 2 and the cut off of 2 was used to discriminate the phagocytosed from non-phagocytosed bacteria. The area of phagocytosed bacteria was compared with the area of non-phagocytosed bacteria and their ratio was calculated.

Macrophage isolation and culture

Monocyte-derived macrophages (MDM) were isolated from whole blood from healthy volunteers. Peripheral blood mononuclear cells were isolated by Ficoll Plaque (GE Healthcare)

density centrifugation. To differentiate PBMC into monocyte-MDM 2×10^6 PBMC/ml were plated in RPMI 1640 media (Lonza) with 2 mmol/l L-glutamine (Gibco BRL) containing 10% human AB serum (First Link (UK) LTD) in 24-well plates (Costar). After 24h, non-adherent cells were removed, and adherent cells were cultured in RPMI with 10% heat-treated fetal bovine serum (FBS; Lonza) in 5% CO_2 at 37°C to give a final concentration of approximately 2×10^5 MDM/ml at day 14 [37].

In vitro phagocytosis assay

E. faecalis strains were grown to $OD_{600} = 0.6$ and stored in frozen aliquots at -80°C. Viable counts were determined upon thawing and used to calculate volumes necessary to give desired multiplicity of infection (MOI). Bacteria were labelled with pHrodo dye (pHrodo Red, succinimidyl ester, Invitrogen) as previously described [41]. Briefly, bacteria were washed in phosphate-buffered saline before being incubated with 10.2 μM pHrodo in 0.1M sodium bicarbonate pH8.3 for 30min at 37°C protected from light. Excess dye was washed off before MDM were challenged with pHrodo labelled bacteria at MOI = 100 for 4 hours at 37°C. Cells were then fixed in 2% paraformaldehyde and fluorescence (Ex/Em 560/585nm) measured on a Varioskan Flash multimode reader (Thermo Scientific). Relative fluorescence values (RFU) of cell only wells were subtracted from readings to control for autofluorescence.

Construction of pGhost derivatives for allele replacement

A similar strategy was followed to construct all plasmids for allele replacement except pGAB-his, for which the whole insert was synthesized and cloned into pGhost9 using XhoI and EcoRI restriction sites. For pGAAhis, pGBBhis, pGDN, pGtfAB, pGAtlA1, pGAtlA1-2, pGAtlA1-3, pGAtlA1-4, pGAtlA1-5, two homology regions were amplified and fused by overlap extension using PCR [42]. A 5' homology region (referred to as H1) was amplified with oligonucleotides H11 (sense) and H12 (antisense). It was fused to a 3' homology region (referred to as H2) amplified with oligonucleotides H21 (sense) and H22 (antisense). The assembled PCR fragment flanked by two restriction sites was digested and cloned into pGhost9 similarly digested. Oligonucleotide sequences and restriction sites used for cloning are described in S1 Table.

For pGAtlA*, three homology regions (H1, H2, H3) were fused by overlap extension. The resulting plasmid contains a catalytic domain flanked by NcoI and BamHI sites. The NcoI-BamHI fragment encoding the *N*-acetylglucosaminidase activity of AtlA was swapped for NcoI-BamHI fragments encoding catalytic domains with distinct catalytic activities to produce pGAtlA-Cse, pGAtlA-AtlB and pGAtlA-Ami generated by PCR (see Supplemental Experimental Procedures for oligonucleotide sequences). The sequences of the chimeric proteins encoded by these plasmids are described in S3 Fig.

Construction of *E. faecalis* mutants

Isogenic derivatives of *E. faecalis* JH2-2 were constructed by allele exchange using the procedure previously described [8]. Briefly, pGhost derivatives were electroporated into JH2-2 and transformants were selected at a permissive temperature (28°C) on BHI plates with erythromycin. To induce single crossover recombination, transformants were grown at a non-permissive temperature (42°C) in the presence of erythromycin. The second recombination event leading to plasmid excision was obtained after 5 serial subcultures at 28°C without erythromycin. The last overnight subculture was plated at 42°C without erythromycin. A clone harboring a double crossover mutation was identified by PCR and Southern blot hybridization.

To construct double mutants JH2-2 $atlA_{1-4\Delta N}$ and JH2-2 $atlA_{1-4}\Delta gtfAB$, the deletion of two LysM repeats was introduced in JH2-2 $atlA_{\Delta N}$ and JH2-2 $\Delta gtfAB$ backgrounds using the pG*atlA*$_{1-4}$ plasmid (Table 1).

Construction of pET derivatives for protein expression in *E. coli*

pET2818 was used as an expression vector to produce C-terminally His-tagged recombinant proteins. To construct pET-AtlA$_{TEV}$, a cleavage site recognized by the Tobacco Etched Virus (TEV) protease was introduced by PCR by fusing two amplified products (named H1 and H2). For pET-AtlAB and pET-AtlBA, a DNA fragment encoding the N-terminal domain of AtlA or AtlB (referred to as H1) was fused to a DNA fragment encoding the LysM domain of AtlA or AtlB (referred to as H2). The resulting fragments were cut by NcoI and BamHI and cloned into pET2818 that had been similarly digested. Specific oligonucleotides used for each construct are described in S1 Table. The sequences of recombinant proteins expressed in *E. coli* are described in S3 Fig.

Production and purification of his-tagged recombinant proteins produced in *E. coli*

E. coli BL21(DE3) cells harboring pET-derivatives were grown to an optical density at 600 nm (OD$_{600}$) of 0.7 and production of recombinant proteins was induced by addition of 1 mM isopropyl-β-D-thiogalactopyranoside. The cells were harvested 4h after induction, resuspended in buffer A (50 mM Tris-HCl [pH 8.0] containing 300 mM NaCl) and sonicated (5 times 30 sec at 20% output using a Branson Sonifier 450). Soluble proteins were recovered after centrifugation (45,000 x *g*, 20 min at 4˚C), loaded onto Ni^{2+}-nitrilotriacetate agarose resin (Qiagen GmbH, Hilden, Germany), washed with 10 mM imidazole in buffer A and eluted with 300 mM imidazole in buffer A. Recombinant his-tagged proteins were further purified by size exclusion chromatography on a Superdex75 HR 26/60 column (Amersham biosciences, Uppsala, Sweden) equilibrated with PBS. The fractions were analyzed by SDS-PAGE and pooled. Protein concentration was estimated by measuring the absorbance, using a theoretical extinction coefficient at 280 nm (http://www.expasy.org). Proteins were kept frozen at -80˚C in PBS supplemented with 25% glycerol. AtlB stocks were available from previous studies [8].

Protein preparation from *E. faecalis* cultures

Proteins from supernatants were prepared from exponentially growing cultures (OD$_{600}$~0.4). Supernatants were precipitated by addition of TCA (10% v/v final). After 10 min on ice, proteins were recovered by centrifugation (15,000 x *g*, 10 min at room temperature), washed in 100% acetone, dried and resuspended in SDS-PAGE loading buffer (1ml/equivalent OD$_{600}$ = 50).

For the detection of His-tagged AtlA and AtlB produced under the control of the *atlA* promoter, proteins were prepared from cultures in late exponential phase (OD$_{600}$~1). One ml of culture (containing both cells and supernatant) was transferred to a tube containing 250μL of glass beads (100μm in diameter, Sigma). Cells were mechanically disrupted using a FastPrep device (six cycles of 40 sec at maximum speed with 5 min pauses between cycles). Loading buffer was added to the protein samples and equivalents of 40, 20 and 10 μl of the cultures were separated on a 10% SDS-PAGE.

Table 1. Bacterial strains and plasmids used in this study.

Strains, plasmids	Relevant properties or genotype[a]	Source or reference
Strains		
Enterococcus faecalis		
OG1RF	Plasmid-free, virulent laboratory strain isolated from the oral cavity	[43]
OG1RF *gfp*	OG1RF producing the GFP encoded by pMV158	[17]
OG1RFΔ*atlA*	OG1RF mutant harboring a deletion in *atlA*	This work
OG1RFΔ*atlAgfp*	OG1RF Δ*atlA* derivative producing the GFP encoded by pMV158	This work
JH2-2	Plasmid-free laboratory strain	[44]
Δ*atlA*	JH2-2 mutant harboring an in-frame deletion of *atlA*	[8]
P*atlA*::*atlB-his*	JH2-2 producing a C-terminally his-tagged AtlB under the *atlA* promoter; In this strain, the *atlA*- open reading frame is replaced by that of *atlB*	This work
P*atlA*::*atlA-his*	JH2-2 producing a C-terminally his-tagged AtlA (native locus)	This work
P*atlB*::*atlB-his*	JH2-2 producing a C-terminally his-tagged AtlB (native locus)	This work
atlA$_{\Delta N}$	JH2-2 producing AtlA without its N-terminal domain	This work
atlA$_{1-4\Delta N}$	JH2-2 *atlA*$_{\Delta N}$ derivative producing AtlA lacking 2 C-terminal LysM repeats	This work
Δ*gtfAB*	JH2-2 derivative with an in-frame deletion of the *gtfAB* operon	This work
Δ*atlA*Δ*gtfAB*	JH2-2 Δ*atlA* derivative with an in-frame deletion of the *gtfAB* operon	This work
atlA$_{1-4}$Δ*gtfAB*	JH2-2 *gtfAB* derivative producing AtlA lacking 2 C-terminal LysM repeats	This work
*atlA**	JH2-2 producing AtlA with a catalytic domain flanked by NcoI and BamHI sites	This work
atlA$_{Cse}$	JH2-2 *atlA** derivative producing AtlA with endopeptidase activity	This work
atlA$_{AtlB}$	JH2-2 *atlA** derivative producing AtlA with *N*-acetylmuramidase activity	This work
atlA$_{Ami}$	JH2-2 *atlA** derivative producing AtlA with amidase activity	This work
atlA$_{1-5}$	JH2-2 producing AtlA lacking the last C-terminal LysM repeat	This work
atlA$_{1-4}$	JH2-2 producing AtlA lacking the last 2 C-terminal LysM repeats	This work
atlA$_{1-3}$	JH2-2 producing AtlA lacking the last 3 C-terminal LysM repeats	This work
atlA$_{1-2}$	JH2-2 producing AtlA lacking the last 4 C-terminal LysM repeats	This work
atlA$_1$	JH2-2 producing AtlA lacking the last 5 C-terminal LysM repeats	This work
Escherichia coli		
TG1	Host for plasmid propagation	Lab stock
TG1(RepA)	TG1 derivative producing RepA for pGhost propagation at 37˚C	P. Serror
BL21(DE3)	BL21 derivative for protein expression	Novagen
Plasmids		
pGhost9	Thermosensitive plasmid for gene replacement in *E. faecalis* (Erm^R)	[45]
pMV158	Replicative plasmid for constitutive *gfp* expression	[46]
pGHH0799	pGhost9 derivative used to construct strain OG1RF Δ*atlA*	[8]
pGABhis	pGhost9 derivative used to construct strain P*atlA*::*atlB-his*	This work
pGAAhis	pGhost9 derivative used to construct strain P*atlA*::*atlA-his*	This work
pGBBhis	pGhost9 derivative used to construct strain P*atlB*::*atlB-his*	This work
pGDN	pGhost9 derivative used to construct strain *atlA*$_{\Delta N}$	This work
pGgtfAB	pGhost9 derivative used to construct strain Δ*gtfAB*	This work
pGatlA1-5	pGhost9 derivative used to construct strain *atlA*$_{1-5}$	This work
pGatlA1-4	pGhost9 derivative used to construct strain *atlA*$_{1-4}$	This work
pGatlA1-3	pGhost9 derivative used to construct strain *atlA*$_{1-3}$	This work
pGatlA1-2	pGhost9 derivative used to construct strain *atlA*$_{1-2}$	This work
pGatlA1	pGhost9 derivative used to construct strain *atlA*$_1$	This work
pGatlA*	pGhost9 derivative used to construct strain *atlA**	This work
pGatlA-Cse	pGhost9 derivative used to construct strain *atlA*$_{Cse}$	This work

(*Continued*)

Table 1. (*Continued*)

Strains, plasmids	Relevant properties or genotype[a]	Source or reference
pGatlA-AtlB	pGhost9 derivative used to construct strain *atlA*AtlB	This work
pGatlA-Ami	pGhost9 derivative used construct strain *atlA*Ami	This work
pET2818	pET28a derivative for overexpression of His-tagged proteins (Amp[R])	[10]
pET-AtlA$_{TEV}$	pET2818 encoding AtlA with a TEV site upstream of the catalytic domain	This work
pET-AtlB	pET2818 encoding AtlB	This work
pET-AtlAB	pET2818 encoding AtlA with a LysM domain replaced by that of AtlB	This work
pET-AtlBA	pET2818 encoding AtlB with a LysM domain replaced by that of AtlA	This work

[a] Amp[R], resistant to ampicillin; Erm[R], resistant to erythromycin

https://doi.org/10.1371/journal.ppat.1006526.t001

Western blot detection of AtlA and AtlB

Proteins were transferred to a nitrocellulose membrane. After a blocking step for 1h at room temperature in Tris buffer saline (TBS, 10mM Tris-HCl pH7.4, 150mM NaCl) supplemented with tween-20 (0.025%, v/v) and milk (2%, m/v), the membrane was incubated with rabbit polyclonal anti-AtlA antibodies raised against the catalytic domain of AtlA (1:1,000 dilution) or polyclonal anti-His antibodies (1:2,000 dilution; Ebioscience). Proteins were detected using goat polyclonal anti-rabbit antibodies conjugated to horseradish peroxidase (Sigma) at a dilution of 1:20,000 and clarity Western ECL Blotting Substrate (BioRad).

Detection of AtlA activity by zymogram

Proteins from the supernatant were separated on a 10% SDS-PAGE containing *Micrococcus luteus* autoclaved cells as a substrate (final OD_{600} = 2). After electrophoresis the gel was rinsed in distilled water and proteins were renatured at 37°C in a buffer containing 50mM Tris-HCl (pH7.5) and 0.1% (v/v TritonX-100).

Flow cytometry analysis of cell chain length

Cells were grown overnight without agitation at 37°C. Cells were diluted 1:100 into fresh broth (OD_{600} ~0.02) and grown in standing cultures to mid-exponential phase (OD_{600}~0.2 to 0.4). Bacteria were diluted 1:100 in phosphate buffer saline filtered on a 0.22μm pore size membrane (Millex-GV syringe filter unit, Millipore) to eliminate salt crystals which could interfere with measurements and analyzed by flow cytometry using Millipore Guava Easy Cyte system. Light scatter data were obtained with logarithmic amplifiers for 20,000 events.

To measure the septum cleavage activity of recombinant proteins, the OG1RF Δ*atlA* mutant was grown to exponential phase (OD_{600} = 0.2), collected by centrifugation, and bacterial chains were resuspended in filtered PBS containing various concentrations of recombinant proteins. Cell size distribution was determined by flow cytometry after 15 min of incubation at 37°C. Relative logs of forward scattered light values (FS log) were collected for 5,000 events and expressed as a percentage of the control strain incubated in the absence of enzyme.

Light and fluorescent microscopy analysis of bacteria

Cells were grown to mid-exponential phase (final OD_{600}~0.3) and fixed with 1.6% paraformaldehyde in PBS for 30min at RT. After fixation, bacteria were washed twice in distilled water and mounted onto poly-L-lysine coated slides and imaged using a DeltaVision deconvolution microscope equipped with an UplanSApo 100x oil (NA 1.4) objective and a Photometrics

Coolsnap HQ CCD camera. ImageJ software was used to optimize contrast and to count the numbers of cells per chain.

Statistical analyses

All experiments reported in this study correspond to at least three biological replicates. Statistical analyses were performed using GraphPad Prism version 6.0e. Comparisons between survival curves were made using the log rank (Mantel-Cox) test. Median FSC values were compared using a two-tailed, unpaired Student's t test with Welch's correction. Comparison of OG1RF and Δ*atlA* derivative uptake *in vitro* by MDM was carried out using a paired Student's t test. Comparison of uptake by zebrafish macrophages was carried out using an unpaired non-parametric Dunn's multiple comparisons test. The number of cells per chain was compared using a non-parametric Mann-Whitney U test. Statistical significance was assumed at P values below 0.05.

Supporting information

S1 Fig. Analysis of *E. faecalis* strains producing an N-terminally truncated AtlA. A. Western blot detection of AtlA proteins in culture supernatants. Supernatant proteins from exponentially growing cells were recovered by centrifugation, precipitated with 10% (m/v) TCA, washed with acetone and resuspended in PBS. Following SDS-PAGE and transfer on a nitrocellulose membrane, AtlA proteins were detected using an anti-AtlA polyclonal serum against the catalytic domain of AtlA. WT, *E. faecalis* JH2-2; $atlA_{\Delta N}$, derivative expressing AtlA truncated from the N-terminal domain; $atlA_{1-4}$, derivative expressing AtlA truncated from the two C-terminal LysM modules; $AtlA_{1-4\Delta N}$, $AtlA_{1-4}$ truncated from the N-terminal domain WT; A strain with an in-frame deletion of *atlA* (Δ*atlA*) was used as a negative control. **B**. Average numbers of cells per chain formed by WT (3.0 ± 1.6; n = 427 cells); $atlA_{\Delta N}$ (2.6 ± 1.4; n = 534 cells); $atlA_{1-4}$ (9.4 ± 4.8; n = 442 cells) and $atlA_{1-4\Delta N}$ (5.9 ± 3.4; n = 610 cells) strains; ****P<0.0001. **C**. Light microscopy images showing cell chain lengths of the mutants. **D**. Sequence of AtlA N-terminal domain (residues 54 to 172). S/T/E residues are indicated in red.
(TIF)

S2 Fig. Analysis of *E. faecalis* strains lacking AtlA glycosylation. A. Western blot detection of AtlA proteins in culture supernatants (as described in S1 Fig). WT, *E. faecalis* JH2-2; $atlA_{1-4}$, derivative expressing AtlA truncated from the two C-terminal LysM modules; Δ*gtfAB*, derivative with an in-frame deletion of the Δ*gtfAB* operon; $atlA_{1-4}$Δ*gtfAB*, Δ*gtfAB* derivative with the truncation of the two C-terminal LysM modules of *atlA*. A strain with an in-frame deletion of *atlA*, Δ*atlA* was used as a negative control. **B**. Average numbers of cells per chain formed by WT (3.0 ± 1.6; n = 427 cells); Δ*gtfAB* (3.0 ± 1.3; n = 364 cells); $atlA_{1-4}$ (9.4 ± 4.8; n = 442 cells); Δ*gtfAB* $atlA_{1-4}$ (6.5 ± 3.7; n = 298 cells); NS, P>0.05; ***, P = 0.0005. **C**. Light microscopy images showing cell chain lengths of the mutants.
(TIF)

S3 Fig. Description of AtlA derivatives expressed in *E. faecalis* and *E. coli*. A. Schematic representation of the amino acid modifications introduced on either side of the catalytic domain for cloning purposes. **B**. Sequence of the AtlA variants with a swapped catalytic domain. Sequences in red correspond to catalytic domains of chimeric proteins expressed by recombinant *E. faecalis* strains analyzed in Fig 6. **C**. Western blot detection of chimeric proteins. Protein samples corresponding to crude extracts were run on an SDS-PAGE, transferred on a nitrocellulose membrane and probed with an anti-LysM polyclonal serum. The

arrowheads indicate unspecific signals. **D**. Sequences in blue correspond to LysM domains used to construct the chimeric recombinant proteins expressed in *E. coli* (see Fig 5).
(TIF)

S4 Fig. Characterization of *E. faecalis* strains producing a LysM domain with a variable number of LysM repeats. A. Western blot detection of AtlA proteins in culture supernatants. Cells were grown until exponential phase (OD_{600} = 0.2–0.5) and spun down. Supernatants were precipitated with 10% (m/v) TCA prior to detection of AtlA as described in supplementary Fig 1. Bands with the expected molecular weights were detected in all the strains. **B**. Zymogram analysis of AtlA activity in culture supernatants. Samples analyzed in (**A**) were loaded on an SDS-PAGE containing autoclaved *M. luteus* cells (OD_{600} = 2). After migration, the gel was rinsed and incubated in renaturing buffer to detect AtlA activity. Truncation of LysM repeats was associated with a decrease in AtlA activity. **C**. Light microscopy images showing cell chain lengths of the mutants.
(TIF)

S5 Fig. Analysis of the virulence of *E. faecalis* Δ*atlA* mutants forming long chains. A. Comparison of median forward scattered (FSC) light values corresponding to the cell chain lengths of WT (OG1RF), Δ*atlA* and sonicated Δ*atlA* (Δ*atlA*^{S}) strains. **B**. Light microscopy images showing cell chain lengths of WT and Δ*atlA* derivatives expressing cytoplasmic GFP. **C**. Survival of zebrafish larvae (n>20) following infection with *E. faecalis* OG1RF (WT) and *atlA* isogenic deletion mutant before (Δ*atlA*) and after (Δ*atlA*^{S}) sonication to disperse long chains. The results corresponding to three independent experiments are shown. For each experiment, the number of cells injected (determined after sonication) is indicated. **D**. *P* values resulting from pairwise comparisons using the log rank test. **E**. survival of phagocyte-depleted zebrafish larvae following injection with 1250 cells of *E. faecalis* OG1RF (WT) or Δ*atlA*.
(TIF)

S6 Fig. Analysis of the impact of mild sonication on *E. faecalis* OG1RF virulence. A. Survival of zebrafish larvae (n>20) following infection with *E. faecalis* OG1RF (WT) and OG1RF sonicated (WT^S) cells. The results corresponding to three independent experiments are shown. For each experiment, the number of cells injected (determined after sonication) is indicated. **B**. *P* values resulting from pairwise comparisons using the log rank test.
(TIF)

S7 Fig. Analysis of bacterial growth rates of *E. faecalis* Δ*atlA* and Δ*atlA*^{S}. Cells from an overnight culture in BHI were diluted to an OD_{600} of 0.01 in 25ml BHI and growth of standing cultures were monitored over 7 hours. The growth rate of each strain was determined using the OD values between 60 and 240 minutes (exponential growth). The data presented are the average of 3 independent cultures. OD values of individual growth curves are presented.
(TIF)

S1 Table. Oligonucleotides used in this study.
(DOC)

Acknowledgments

Author Contributions

Conceptualization: Bartłomiej Salamaga, Stéphane Mesnage.

Formal analysis: Bartłomiej Salamaga, Tomasz K. Prajsnar, Joost Willemse, Stéphane Mesnage.

Investigation: Bartłomiej Salamaga, Tomasz K. Prajsnar, Ana Jareño-Martinez, Martin A. Bewley, Françoise Chau, Tassadit Ben Belkacem, Stéphane Mesnage.

Methodology: Bartłomiej Salamaga, Joost Willemse, Martin A. Bewley, Stephen A. Renshaw, Stéphane Mesnage.

Project administration: Stéphane Mesnage.

Resources: Joost Willemse, Annemarie H. Meijer, David H. Dockrell, Stephen A. Renshaw.

Software: Joost Willemse.

Supervision: Stéphane Mesnage.

Validation: Bartłomiej Salamaga, Ana Jareño-Martinez, Martin A. Bewley, Françoise Chau, Stéphane Mesnage.

Visualization: Bartłomiej Salamaga, Stéphane Mesnage.

Writing – original draft: Bartłomiej Salamaga, Stéphane Mesnage.

Writing – review & editing: Bartłomiej Salamaga, David H. Dockrell, Stephen A. Renshaw, Stéphane Mesnage.

References

1. Arias CA, Murray BE. The rise of the *Enterococcus*: beyond vancomycin resistance. Nature reviews Microbiology. 2012; 10(4):266–78. Epub 2012/03/17. https://doi.org/10.1038/nrmicro2761 PMID: 22421879

2. Bradley CR, Fraise AP. Heat and chemical resistance of enterococci. J Hosp Infect. 1996; 34(3):191–6. PMID: 8923273

3. Chang S, Sievert DM, Hageman JC, Boulton ML, Tenover FC, Downes FP, et al. Infection with vancomycin-resistant *Staphylococcus aureus* containing the *vanA* resistance gene. The New England journal of medicine. 2003; 348(14):1342–7. Epub 2003/04/04. https://doi.org/10.1056/NEJMoa025025 PMID: 12672861

4. Noble WC, Virani Z, Cree RG. Co-transfer of vancomycin and other resistance genes from *Enterococcus faecalis* NCTC 12201 to *Staphylococcus aureus*. FEMS microbiology letters. 1992; 72(2):195–8. Epub 1992/06/01. PMID: 1505742

5. Sievert DM, Ricks P, Edwards JR, Schneider A, Patel J, Srinivasan A, et al. Antimicrobial-resistant pathogens associated with healthcare-associated infections: summary of data reported to the National Healthcare Safety Network at the Centers for Disease Control and Prevention, 2009–2010. Infection control and hospital epidemiology. 2013; 34(1):1–14. Epub 2012/12/12. https://doi.org/10.1086/668770 PMID: 23221186

6. de Been M, Pinholt M, Top J, Bletz S, Mellmann A, van Schaik W, et al. Core genome multilocus sequence typing scheme for high-resolution typing of *Enterococcus faecium*. Journal of clinical microbiology. 2015; 53(12):3788–97. Epub 2015/09/25. https://doi.org/10.1128/JCM.01946-15 PMID: 26400782

7. Guzman Prieto AM, van Schaik W, Rogers MR, Coque TM, Baquero F, Corander J, et al. Global emergence and dissemination of Enterococci as nosocomial pathogens: attack of the clones? Frontiers in microbiology. 2016; 7:788. Epub 2016/06/16. https://doi.org/10.3389/fmicb.2016.00788 PMID: 27303380

8. Mesnage S, Chau F, Dubost L, Arthur M. Role of *N*-acetylglucosaminidase and *N*-acetylmuramidase activities in *Enterococcus faecalis* peptidoglycan metabolism. The Journal of biological chemistry. 2008; 283(28):19845–53. Epub 2008/05/21. https://doi.org/10.1074/jbc.M802323200 PMID: 18490448

9. Emirian A, Fromentin S, Eckert C, Chau F, Dubost L, Delepierre M, et al. Impact of peptidoglycan *O*-acetylation on autolytic activities of the *Enterococcus faecalis N*-acetylglucosaminidase AtlA and *N*-acetylmuramidase AtlB. FEBS Lett. 2009; 583:3033–8. Epub 2009/08/19. https://doi.org/10.1016/j.febslet.2009.08.010 PMID: 19686739

10. Eckert C, Lecerf M, Dubost L, Arthur M, Mesnage S. Functional analysis of AtlA, the major *N*-acetylglucosaminidase of *Enterococcus faecalis*. Journal of bacteriology. 2006; 188(24):8513–9. https://doi.org/10.1128/JB.01145-06 PMID: 17041059

11. Lee IC, van S, II, Tomita S, Morsomme P, Rolain T, Hols P, et al. GtfA and GtfB are both required for protein *O*-glycosylation in *Lactobacillus plantarum*. Journal of bacteriology. 2014; 196(9):1671–82. Epub 2014/02/18. https://doi.org/10.1128/JB.01401-13 PMID: 24532775

12. Li Y, Huang X, Li J, Zeng J, Zhu F, Fan W, et al. Both GtfA and GtfB are required for SraP glycosylation in *Staphylococcus aureus*. Current microbiology. 2014; 69(2):121–6. Epub 2014/03/25. https://doi.org/10.1007/s00284-014-0563-2 PMID: 24658735

13. Wu R, Zhou M, Wu H. Purification and characterization of an active *N*-acetylglucosaminyltransferase enzyme complex from Streptococci. Applied and environmental microbiology. 2010; 76(24):7966–71. Epub 2010/10/26. https://doi.org/10.1128/AEM.01434-10 PMID: 20971868

14. Reste de Roca F, Duche C, Dong S, Rince A, Dubost L, Pritchard DG, et al. Cleavage specificity of *Enterococcus faecalis* EnpA (EF1473), a peptidoglycan endopeptidase related to the LytM/lysostaphin family of metallopeptidases. Journal of molecular biology. 2010; 398(4):507–17. Epub 2010/03/30. https://doi.org/10.1016/j.jmb.2010.03.033 PMID: 20347848

15. Oshida T, Sugai M, Komatsuzawa H, Hong YM, Suginaka H, Tomasz A. A *Staphylococcus aureus* autolysin that has an *N*-acetylmuramoyl-L-alanine amidase domain and an endo-beta-*N*-acetylglucosaminidase domain: cloning, sequence analysis, and characterization. Proc Natl Acad Sci U S A. 1995; 92 (1):285–9. PMID: 7816834

16. Layec S, Gerard J, Legue V, Chapot-Chartier MP, Courtin P, Borges F, et al. The CHAP domain of Cse functions as an endopeptidase that acts at mature septa to promote Streptococcus thermophilus cell separation. Molecular microbiology. 2009; 71(5):1205–17. Epub 2009/01/28. https://doi.org/10.1111/j.1365-2958.2009.06595.x PMID: 19170887

17. Prajsnar TK, Renshaw SA, Ogryzko NV, Foster SJ, Serror P, Mesnage S. Zebrafish as a novel vertebrate model to dissect enterococcal pathogenesis. Infection and immunity. 2013; 81(11):4271–9. Epub 2013/09/05. https://doi.org/10.1128/IAI.00976-13 PMID: 24002065

18. Dubee V, Chau F, Arthur M, Garry L, Benadda S, Mesnage S, et al. The *in vitro* contribution of autolysins to bacterial killing elicited by amoxicillin increases with inoculum size in *Enterococcus faecalis*. Antimicrobial agents and chemotherapy. 2011; 55(2):910–2. Epub 2010/11/26. https://doi.org/10.1128/AAC.01230-10 PMID: 21098238

19. Ahn SJ, Burne RA. The atlA operon of Streptococcus mutans: role in autolysin maturation and cell surface biogenesis. Journal of bacteriology. 2006; 188(19):6877–88. https://doi.org/10.1128/JB.00536-06 PMID: 16980491

20. Thomas V, Hiromasa Y, Harms N, Thurlow L, Tomich J, Hancock LE. A fratricidal mechanism is responsible for eDNA release and contributes to biofilm development of *Enterococcus faecalis*. Molecular microbiology. 2009; 72(4):1022–36. Epub 2009/04/21. https://doi.org/10.1111/j.1365-2958.2009.06703.x PMID: 19400795

21. Miksa M, Komura H, Wu R, Shah KG, Wang P. A novel method to determine the engulfment of apoptotic cells by macrophages using pHrodo succinimidyl ester. Journal of immunological methods. 2009; 342(1–2):71–7. Epub 2009/01/13. https://doi.org/10.1016/j.jim.2008.11.019 PMID: 19135446

22. Thiercelin ME. Sur un diplocoque saprophyte de l'intestin susceptible de devenir pathogene. CR Soc Biol. 1899; 5:269–71.

23. Waters CM, Antiporta MH, Murray BE, Dunny GM. Role of the *Enterococcus faecalis* GelE protease in determination of cellular chain length, supernatant pheromone levels, and degradation of fibrin and misfolded surface proteins. Journal of bacteriology. 2003; 185(12):3613–23. https://doi.org/10.1128/JB.185.12.3613-3623.2003 PMID: 12775699

24. Theilacker C, Sanchez-Carballo P, Toma I, Fabretti F, Sava I, Kropec A, et al. Glycolipids are involved in biofilm accumulation and prolonged bacteraemia in *Enterococcus faecalis*. Molecular microbiology. 2009; 71(4):1055–69. Epub 2009/01/28. PMID: 19170884

25. Rico-Lastres P, Diez-Martinez R, Iglesias-Bexiga M, Bustamante N, Aldridge C, Hesek D, et al. Substrate recognition and catalysis by LytB, a pneumococcal peptidoglycan hydrolase involved in virulence.

Scientific reports. 2015; 5:16198. Epub 2015/11/06. https://doi.org/10.1038/srep16198 PMID: 26537571

26. Sandalova T, Lee M, Henriques-Normark B, Hesek D, Mobashery S, Mellroth P, et al. The crystal structure of the major pneumococcal autolysin LytA in complex with a large peptidoglycan fragment reveals the pivotal role of glycans for lytic activity. Molecular microbiology. 2016; 101(6):954–67. Epub 2016/06/09. https://doi.org/10.1111/mmi.13435 PMID: 27273793

27. Yahashiri A, Jorgenson MA, Weiss DS. Bacterial SPOR domains are recruited to septal peptidoglycan by binding to glycan strands that lack stem peptides. Proc Natl Acad Sci U S A. 2015; 112(36):11347–1152. Epub 2015/08/26. https://doi.org/10.1073/pnas.1508536112 PMID: 26305949

28. Mesnage S, Dellarole M, Baxter NJ, Rouget JB, Dimitrov JD, Wang N, et al. Molecular basis for bacterial peptidoglycan recognition by LysM domains. Nature communications. 2014; 5:4269. Epub 2014/07/01. https://doi.org/10.1038/ncomms5269 PMID: 24978025

29. Julian E, Roldan M, Sanchez-Chardi A, Astola O, Agusti G, Luquin M. Microscopic cords, a virulence-related characteristic of *Mycobacterium tuberculosis*, are also present in nonpathogenic mycobacteria. Journal of bacteriology. 2010; 192(7):1751–60. Epub 2010/01/26. https://doi.org/10.1128/JB.01485-09 PMID: 20097851

30. Bernut A, Lutfalla G, Kremer L. [Looking through zebrafish to study host-pathogen interactions]. Medecine sciences: M/S. 2015; 31(6–7):638–46. Epub 2015/07/15. https://doi.org/10.1051/medsci/20153106017 PMID: 26152168

31. Justice SS, Harrison A, Becknell B, Mason KM. Bacterial differentiation, development, and disease: mechanisms for survival. FEMS microbiology letters. 2014; 360(1):1–8. Epub 2014/09/18. https://doi.org/10.1111/1574-6968.12602 PMID: 25228010

32. Justice SS, Hunstad DA, Cegelski L, Hultgren SJ. Morphological plasticity as a bacterial survival strategy. Nature reviews Microbiology. 2008; 6(2):162–8. Epub 2007/12/25. https://doi.org/10.1038/nrmicro1820 PMID: 18157153

33. Champion JA, Mitragotri S. Role of target geometry in phagocytosis. Proc Natl Acad Sci U S A. 2006; 103(13):4930–4. Epub 2006/03/22. https://doi.org/10.1073/pnas.0600997103 PMID: 16549762

34. Möller J, Luehmann T, Hall H, Vogel V. The race to the pole: how high-aspect ratio shape and heterogeneous environments limit phagocytosis of filamentous *Escherichia coli* bacteria by macrophages. Nano letters. 2012; 12(6):2901–5. Epub 2012/05/18. https://doi.org/10.1021/nl3004896 PMID: 22591454

35. Dalia AB, Weiser JN. Minimization of bacterial size allows for complement evasion and is overcome by the agglutinating effect of antibody. Cell host & microbe. 2011; 10(5):486–96. Epub 2011/11/22. https://doi.org/10.1016/j.chom.2011.09.009 PMID: 22100164

36. Keogh D, Tay WH, Ho YY, Dale JL, Chen S, Umashankar S, et al. Enterococcal metabolite cues facilitate interspecies niche modulation and polymicrobial infection. Cell host & microbe. 2016; 20(4):493–503. Epub 2016/10/14. https://doi.org/10.1016/j.chom.2016.09.004 PMID: 27736645

37. Dockrell DH, Lee M, Lynch DH, Read RC. Immune-mediated phagocytosis and killing of *Streptococcus pneumoniae* are associated with direct and bystander macrophage apoptosis. The Journal of infectious diseases. 2001; 184(6):713–22. Epub 2001/08/23. https://doi.org/10.1086/323084 PMID: 11517432

38. Bojarczuk A, Miller KA, Hotham R, Lewis A, Ogryzko NV, Kamuyango AA, et al. *Cryptococcus neoformans* intracellular proliferation and capsule size determines early macrophage control of infection. Scientific reports. 2016; 6:21489. Epub 2016/02/19. https://doi.org/10.1038/srep21489 PMID: 26887656

39. Nusslein-Volhard C. Zebrafish. A practical approach. New York, NY: Oxford Universty Press; 2002.

40. Prajsnar TK, Cunliffe VT, Foster SJ, Renshaw SA. A novel vertebrate model of *Staphylococcus aureus* infection reveals phagocyte-dependent resistance of zebrafish to non-host specialized pathogens. Cellular microbiology. 2008; 10(11):2312–25. Epub 2008/08/22. https://doi.org/10.1111/j.1462-5822.2008.01213.x PMID: 18715285

41. Jubrail J, Morris P, Bewley MA, Stoneham S, Johnston SA, Foster SJ, et al. Inability to sustain intraphagolysosomal killing of *Staphylococcus aureus* predisposes to bacterial persistence in macrophages. Cellular microbiology. 2016; 18(1):80–96. Epub 2015/08/08. https://doi.org/10.1111/cmi.12485 PMID: 26248337

42. Ho SN, Hunt HD, Horton RM, Pullen JK, Pease LR. Site-directed mutagenesis by overlap extension using the polymerase chain reaction. Gene. 1989; 77(1):51–9. Epub 1989/04/15. PMID: 2744487

43. Dunny GM, Brown BL, Clewell DB. Induced cell aggregation and mating in *Streptococcus faecalis*: evidence for a bacterial sex pheromone. Proc Natl Acad Sci U S A. 1978; 75(7):3479–83. Epub 1978/07/01. PMID: 98769

44. Jacob AE, Hobbs SJ. Conjugal transfer of plasmid-borne multiple antibiotic resistance in *Streptococcus faecalis* var. zymogenes. Journal of bacteriology. 1974; 117(2):360–72. PMID: 4204433

45. Maguin E, Duwat P, Hege T, Ehrlich D, Gruss A. New thermosensitive plasmid for gram-positive bacteria. Journal of bacteriology. 1992; 174(17):5633–8. PMID: 1324906

46. Nieto C, Espinosa M. Construction of the mobilizable plasmid pMV158GFP, a derivative of pMV158 that carries the gene encoding the green fluorescent protein. Plasmid. 2003; 49(3):281–5. PMID: 12749839